Measurement of Film Thickness in Lubricated Components using Ultrasonic Reflection

Phil Harper

January 2008

Thesis submitted for the degree of Doctor of Philosophy

Department of Mechanical Engineering
University of Sheffield

Summary:

Many everyday objects are used without consideration of the fact that they rely on a tiny layer of lubricant as thin as $1/1000^{th}$ of the thickness of a human hair in order to operate correctly. However, without the lubricant, problems are quickly noticed: door hinges squeaking, wear in engines or failure of hip implants.

This layer of lubricant that is so critical to so many applications is remarkably difficult to measure, firstly because it is so thin, and secondly because it is embedded between two other materials.

This thesis documents the application of ultrasound to the measurement of this layer of lubricant. The concepts of ultrasonic reflection are explained and the equations governing the acoustic response of a thin layer of lubricant are described. The equipment used to generate and receive ultrasound is discussed and the developments made in creating an ultrasonic measurement system are described.

Key highlights of this work are the developments in the use of low frequency ultrasound (~0.5MHz), methods of calibration for high temperature applications, the use of piezo elements in generating and receiving ultrasound and software for online, post-processed and modelled film thickness.

The technology was applied to three real world applications – journal bearings, piston rings and prosthetic hip joints. Measurements are shown to agree with published literature. The use of ultrasound in the measurement of lubricant film thickness is shown to be a viable technique for research and condition monitoring.

Table of Contents:

Chapter 8: Hydraulic Motor Piston Ring Film

Thickness

Two cats are on a roof. Which one falls off first?

The one with the smallest μ

Acknowledgements

It is often not what you know but who you know that is significant in life. So it is with this PhD. There have been too many people to mention who have helped out in various ways over the course of this project. I would like to especially thank the following:

Supervisor – Prof. Rob Dwyer-Joyce – Thanks for all your enthusiasm for this project and the help you have given over the years.

Technician – Mr Dave Butcher – Thanks for all your help in making components and putting up with my constant requests at the last minute for urgently required work.

The Tribology Group, University of Sheffield – Being part of a group of people who are excited about research and the practical application of technology has been a brilliant and inspiring experience. Thanks for all the fun and putting up with my quirks over the years. Special thanks to Tom, Dave, Robin, Matt, and Neil for your help.

Product Suppliers – During my time at the university I have often exploited the goodwill of companies to send me samples and provide me with information. Thanks especially to Ferroperm Ltd, Morgan Electro Ceramics Ltd, and Holdtite Ltd.

Fellow Researchers – Over the course of my time at the University of Sheffield I have conducted tests on a wide range of components in a wide range of academic and industrial settings. Thanks especially to Dave Horner (Michell Bearings Ltd), Andre Van-Der-Ham (SKF, Netherlands), Goran Anderberg (Hunhnseal AB, Sweden), Claire Brocket and John Fisher (University of Leeds), Ulf Olaffson and Ulf Sjödin (KTH University, Stockholm), Sashi Balakrishnan (Loughborough University).

Friend and Mentor – Tim Chester – This thesis would probably not have been written without your constant prods! Thank you for not giving up on me.

My Wife – Janelle Harper – Thank you for putting up with my passion, preoccupation, and dreams for this work. I love you.

Sol Gloria Dei

Nomenclature:

All symbols also defined in the text

Symbol	Description	Units
A	amplitude of reflected pulse	V
A_0	amplitude of reference pulse	V
B	bulk modulus of a lubricant	Pa
c	speed of sound	ms^{-1}
C	radial clearance in a journal bearing	m
C_0	clamped capacitance	farad
d	distance	m
dB	logarithmic unit of measurement	dimensionless
D	distance	m
D	transducer element diameter	m
D	diameter	m
E	Young's modulus	Pa
f	frequency	Hz
f_r	free resonating frequency	Hz
f_{ns}	resonant frequency	Hz
F	transducer focal length	m

F_C	focal spot size	m
h	film thickness	m
h_L	film thickness of layer	m
Hz	hertz	cycles/second
i	incident angle	rad
i	the imaginary number (square root of -1)	
k	stiffness of an interface (per unit area)	Nm^{-3} or GPa/μm
L	inductance	webers per ampere
L	length	m
m	distance	meters
m	mode number of f_{nt}	dimensionless
MHz	megahertz	Hz E+10^6
N	frequency constant of piezo materials	Hz/m
nm	nanometers	m^{-9}
ns	nanoseconds	s^{-9}
p	pressure	Pa
P	applied load	N
P	sound pressure	dimensionless
PW	pulse width	s^{-9}
R	radius	m
R	reflection coefficient	dimensionless
R_a	average roughness	μm
S	Sommerfeld number	dimensionless
t	time	s
T	thickness	m
T	transmission coefficient	dimensionless
V	volume	m^3

W	load	N
x	distance	arbitrary
z	acoustic impedance	kg/s.m^2
a	attenuation coefficient	nepers/m
γ	diversion angle from the transducer centre line	rad
ε	eccentricity ratio	dimensionless
η	dynamic viscosity	Pa s
θ	angle of a wave to an interface	radians
λ	wavelength	m
μm	microns	m^{-6}
μ	coefficient of friction	dimensionless
ν	Poisson's ratio	dimensionless
ρ	material density	kgm^{-3}
Φ	attitude angle	radians
ω	angular velocity	radians
ω	frequency (=2πf)	Hz
∞	infinity	dimensionless

Abbreviations and Acronyms

1-D	one dimensional
2-D	two dimensional
AFG	arbitrary function generator
BNC	bayonet Neill-Concelman type connector
CPU	central processing unit
dll	dynamic linked library
DAQ	data acquisition
DSP	digital signal processing

EHL	elastrohydrodynamic lubrication
FFT	fast Fourier transform
FPGA	field programmable gate array
GPIB	high speed data transfer cable, hardware and protocol
HVPZT	high voltage lead zirconate titanate
IC	internal combustion
LabVIEW®	graphical programming language
LVPZT	low voltage lead zirconate titanate
NDT	non destructive testing
PC	personal computer
PCI	peripheral component interconnect computer bus
PZT	lead zirconate titanate
UHF	ultra high frequency
UPR	ultrasonic pulser receiver
UPVC	unplasticised polyvinyl chloride
USM	ultrasonic model

Chapter 1:
Introduction

No surface is perfectly smooth. At a microscopic level surfaces are like landscapes (in fact the earth is a surprisingly smooth object – similar to a snooker ball. We experience it as rough because we exist on a smaller scale than the roughness of mountains). When two of these surfaces are against one another and in relative motion to one another the high points (or asperities) touch and friction and wear can result. The purpose of lubrication is to separate these surfaces by a thin layer of lubricant so that the surfaces do not come into contact, thus reducing friction and preventing wear.
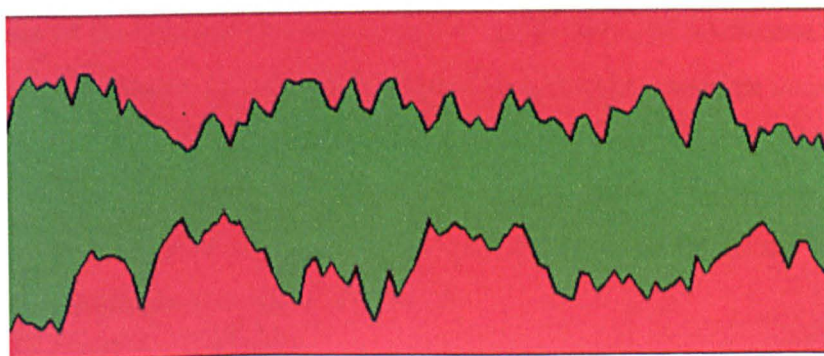
Figure 1.1. Two surfaces (in red) separated by a lubricant (in green). Vertical axis not to scale.

1.1. Lubrication

The role of a lubricant is to

- Cool the components

- Carry away debris from the fluid film

- Prevent corrosion

- Separate surfaces to reduce or prevent wear and friction.

Fluid film lubrication can be divided into two main areas, hydrodynamic and elastohydrodynamic (ignoring for the purpose of this study hydrostatic). Hydrodynamic lubrication is found in low to moderate pressure conformal contacts such at journal bearings, thrust bearings, and piston rings. Elastohydrodynamic lubrication is found in high pressure non-conformal contacts such as gear teeth and rolling element bearings. The lubricant film area in gear teeth and rolling element bearings is normally very small and presents some considerable obstacles to the measurement of lubricant film thickness using ultrasound. Hydrodynamically lubricated components, on the other hand, normally have a large lubricant film area making it simpler to apply the use of ultrasound to measure the film thickness.

This thesis considers the challenge of hydrodynamic lubrication only.

1.2. Nature of the Problem

The thickness of the lubricant layer is crucial to the correct and continued operation of any lubricated component. If the layer is too thin then friction and wear increases. Failure eventually results (in real engineering components failure may occur virtually instantaneously). At the other end of the spectrum if the lubricant film is too thick there can be significant energy losses due to churning of the lubricant, or, in the case of piston rings, leakage resulting in a decrease in efficiency.

The design and development of lubricated components (bearings, artificial joints, mechanical seals etc) can be something of a 'black art'. An understanding of the behaviour of these components has been developed over many decades, helped by computational modelling in recent years. The computational models by necessity rely on assumptions in order to calculate film thicknesses. The accuracy of these assumptions

(e.g. thermal effects, stiffnesses, surfaces roughnesses, Newtonian fluids, dynamic forces etc) determines to a large extent the accuracy of the model. Significantly however, many components are designed, made and tested without an in depth understanding of what is actually happening at the lubricant film. This is primarily due to a lack of technology to monitor what is happening in real engineering components.

The primary reason for the lack of technology is the difficulty in taking measurements. The lubricant films are very thin. They are inaccessible (trapped between two metallic components). Strain gauges and displacement sensors may give a global picture of a problematic component without providing local information on film thickness. Optics, often used in the lab, are restricted to optically translucent components or optical windows, and haven't made it outside the research laboratory. Electrical methods either require electrical isolation of one or more parts or disrupting the lubricant film to insert a sensor, both of which is problematic.

Many bearings are monitored using temperature (there is virtually no monitoring of piston rings or mechanical seals in the industrial environment) as it is the best available technology. However while temperature may show that there is a change in operation, it may not indicate why that change is occurring.

A technology is required that can accurately measure film thickness non-invasively in a wide range of components in a wide range of applications. This thesis presents such a technology.

1.3. Aims and Objectives of the Project

The aim of this project is to take a laboratory based concept for measuring lubricant films using ultrasonic reflection and develop it into a robust industrial measurement system.

In order to accomplish this, the following objectives were pursued:

- Research existing methods for condition monitoring and identify strengths and weaknesses of existing systems.
- Develop sensors that are 1) Small, 2) Low cost, and 3) easily applicable to real world engineering components.

- Develop the 'system' for application in real world engineering applications (i.e. sensors, adhesives, solder, cables, connectors, computer hardware etc).

- Develop a robust method that can work in real industrial situations (e.g. no adverse effects from the surrounding environment).

- Develop a method that can work at high speed for monitoring dynamic events.

- Develop software for controlling hardware and calculating film thickness in real-time.

- Demonstrate the technology via case studies on real engineering components.

1.4. Layout of Thesis

This thesis is a record of the work carried out by the author in developing a robust industrial measurement technique.

- Chapter 2 - Background. This chapter reviews existing methodologies for condition monitoring of bearings and also looks at techniques for the measurement of lubricant film thickness.

- Chapter 3 - Principles of Ultrasonic Reflection. This chapter reviews the physics behind ultrasound and the equations that govern reflection of ultrasound. The equations are expanded to consider thin liquid layers and the measurement of fluid film thickness.

- Chapter 4 - Generation of Ultrasound. This chapter reviews the individual generic parts of an ultrasonic system including sensors, pulsers, digitisers and hardware.

- Chapter 5 - Measurement System Development. This chapter falls into two main parts – hardware and software, and charts the developments that were implemented over the course of the research in both of these areas. Details are given of 1) the specific individual hardware components that were used, 2) software for hardware control and real-time film thickness measurements, and 3) software modelling.

- Chapter 6 – Implementing Measurements. This chapter looks at several issues in the application of this technology to real world components. Issues such as material properties, reference signals are discussed. Some consideration is given to the issue of calibration (where there is an external influence affecting the measurement) and validation (confirming that the measured value is the actual

one). Finally an example measurement is shown demonstrating the steps that are gone through in order to measure film thickness.

- Chapter 7 - Journal bearings. Tests were conducted on two separate journal bearings. Firstly a test rig in the Tribology lab at the University of Sheffield was used. Measurements were made over a range of loads and speeds. The transducer position was also rotated around the bearing circumference. Secondly, tests were conduced on an industrial journal bearing in a test rig at Michell Bearings Ltd. Measurements were again made over a range of loads and speeds and results were compared with a computational model.

- Chapter 8 - Piston Ring. Tests were conducted on a hydraulic motor piston ring test rig at KTH University, Stockholm, Sweden. These tests were technically more difficult due to a small moving component and needed to be conducted at higher speed. A focusing transducer was also used.

- Chapter 9 - Artificial Hip Joint. These tests were conducted in collaboration with the Bio-Engineering Lab at the University of Leeds. Measurements were made on a metal-on-metal hip joint in a Hip Joint Simulator. Measurements were taken over a range of loads and actuation speeds. This work developed the sensor technology as well as high speed measurements.

- Chapter 10 - Future Work. Consideration is given to potential future work that could be carried out to further develop this research.

- Chapter 11 - Conclusions. This chapter surveys the work carried out as discussed in this thesis.

Chapter 2: Background

The health of any system relies on the health of the individual components that make up that system. In engineering this is no less true. Complex engineering systems depend on a wide range of individual components, or machine elements. The correct operation of each individual element is usually required for the correct operation of the whole system. This is especially so in the case of bearings – their failure normally results in the complete failure of the system they are part of. This may result in expensive repairs and loss of production time.

As a result there is great interest in evaluating the condition of bearings. Several condition monitoring methodologies will be considered in this chapter. These methodologies fall into three main groups – acoustic, temperature and displacement measurements. Some are widely used in industry to protect expensive machinery. Despite this they have major drawbacks and are often not suitable approaches to condition monitoring. Others don't exist outside the research lab.

In addition, current methods of measuring oil film thickness will be outlined and evaluated. It will be demonstrated that current technology is not suitable for online condition monitoring. Thus a new method for the measurement of oil film thickness is needed.

An improved concept in bearing condition monitoring will be suggested. This is based on measuring the oil film thickness in bearings and machine elements.

2.1. Bearing Condition Monitoring

Davies et al [1998] suggest a framework for understanding condition monitoring as shown in figure 2.01 below. This framework has six main categories – Aural, Vibration, Visual, Operational Variables, Temperature and Wear Debris (including oil analysis). These categories, however, are do not have sharp delineations between them. For example the categories of Aural and Vibration are overlapping categories that differ in terms of order of magnitude (10kHz as compared to 100kHz), or the categories of Visual and Temperature overlap when considering a FLIR camera monitoring system that provides a visual picture of temperature. In this study, when considering condition monitoring of hydrodynamic bearings, the subject has been broken down into three main branches: acoustic, temperature and displacement.
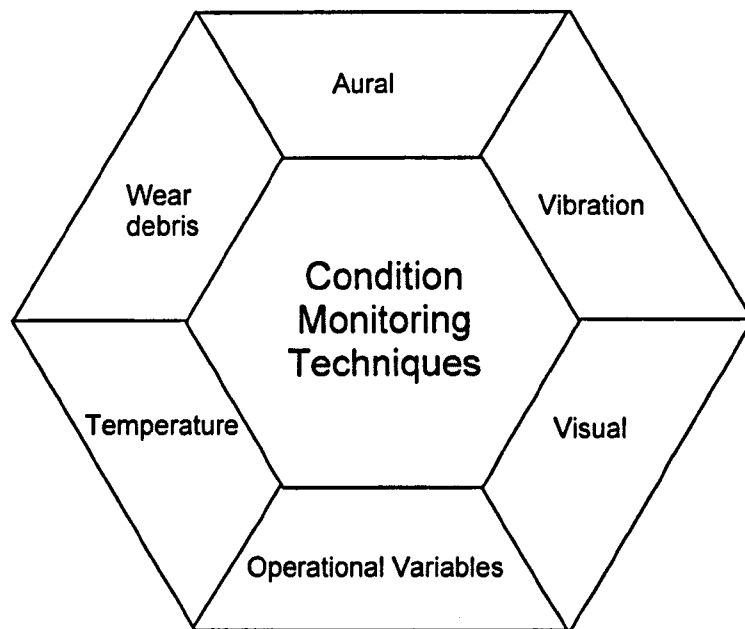
Figure 2.01. Condition Monitoring Techniques (taken from Davies [1998]).

2.1.1. Acoustic Techniques

There are a wide variety of acoustic techniques on the market for monitoring bearings. They are mostly 'passive techniques' in that they just 'listen' and pick up machine noise. By interpreting this 'noise' one can deduce the state of a bearing.

2.1.1.1. Shock Pulse Method (SPM)

When two materials strike each other two things normally happen:

- a shock (pressure) wave is produced and propagates through the materials
- vibration is caused and occurs after the initial impact.

Figure 2.02 below illustrates both of these effects.
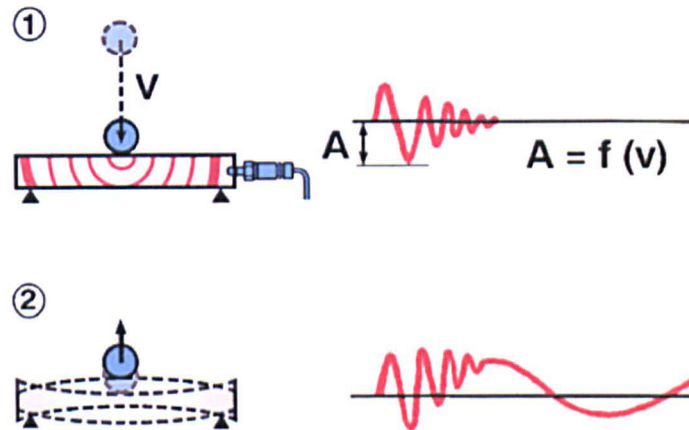
Figure 2.02[1]. Shock wave due to impact (1) and bulk vibration occurring afterwards due to impact (2).

Shock pulse is a method of measuring this initial shock wave (that typically occurs around the 36kHz mark). When there is adequate lubrication the amplitude at this frequency is low due to a damping effect of the lubricant layer. Where there is inadequate lubrication there is little damping and thus an increase in shock pulse energy emission. (see Morando [1996]).

This method does not measure oil film thickness. It is possible to correlate the amplitude of the shock pulse to film thickness although this has not been used as an oil film measurement technique. The primary reason for this is because it is very difficult to independently measure the oil film thickness to provide calibration. However, SPM does give a very good indication of lubricant health. If there is adequate lubrication then the

---

[1] Taken from http://www.spminstrument.com/data/images/methods/SPM_1.gif accessed on 17th December 2007

8

ball and raceway are separated thus minimising shock pulse emissions. See figure 2.03 for an example of a simulated response.
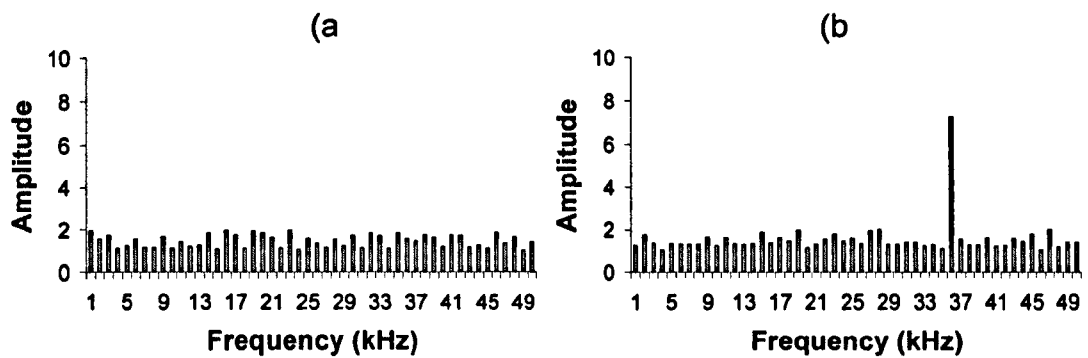
Figure 2.03. A simulated shock pulse measurement from a) a well lubricated bearing, and b) a poorly lubricated bearing.

This method, due to its dependency on metal to metal impact, is not used to monitor hydrodynamic bearings.

2.1.1.2. Acoustic Emissions (AE)

Acoustic emission strictly speaking, does not measure oil film thickness. When a structure is stressed a whole variety of events occur within the microstructure that each emit acoustic energy. For example, during cyclic loading cracks may open and close. This opening and closing results in the emission of acoustic waves which may then monitored. Through monitoring it is possible to detect the growth of these cracks (generally seen as an increase in acoustic emission). See figure 2.04 for more details of the sources of acoustic emissions.

9
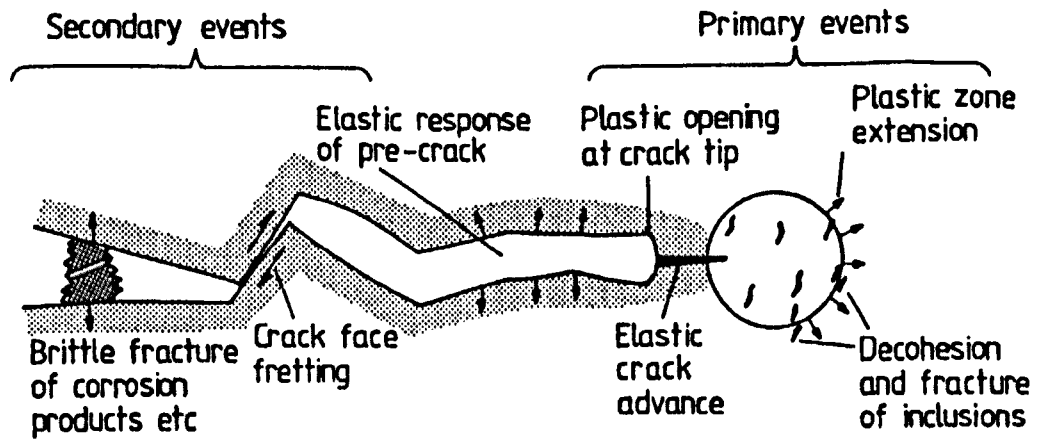
Figure 2.04. Picture showing the primary and secondary events that produce acoustic emissions (Scruby [1987]).

Generally when there is adequate lubrication the effect of many of these sources of acoustic emissions are minimised. In the absence of lubrication, however, the growth of AE is noticeable, see figure 2.05 for example.
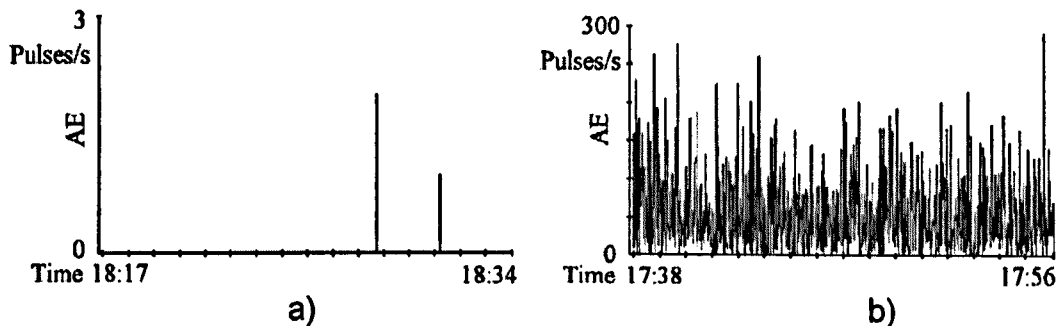
Figure 2.05. A sample measurement from an acoustic emission sensor showing a) a lubricated bearing, and b) an unlubricated bearing (Miettinen [2000]).

This technique suffers from the problem of interpretation. It is very difficult do identify what is causing a spike in an AE signal. The growth in amplitude of a signal may be due to vibration, misalignment, a lubrication issue or some other problem.

Additionally this technique requires damage to occur in order to generate acoustic signals. In most bearings systems, however, the onset of damage results in immediate failure of the component.

2.1.1.3.   Rolling Element Bearing Activity Monitor (REBAM)

A highly sensitive eddy current sensor is placed in close proximity to the bearing race way (rolling element bearing) in the loaded region (see figure 2.06). The eddy current sensor does not touch the outer race way that is unsupported above it. As a ball passes over the unsupported region there is a deflection of the race way towards the REBAM sensor. In a healthy bearing this is in the region of 0.25 to 1.3μm. In a damaged bearing this can rise to between two and five times this value.
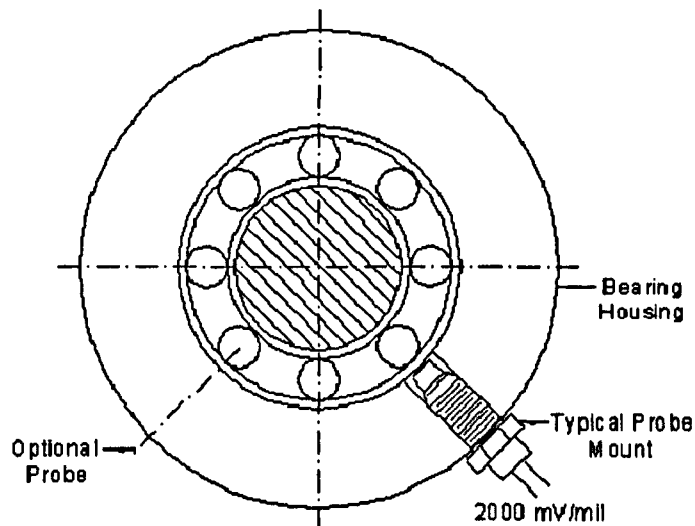
Figure 2.06. Schematic showing the positioning of a REBAM sensor (Bently [2005].

This method is used exclusively in rolling element bearings and does not have applications in hydrodynamic bearings. However, it does give some indication of the scope of eddy current probes and their sensitivity.

2.1.2. Temperature Techniques

Often machinery is operated in a steady state condition, i.e. continuous running over a long period of time. In this situation it is often possible to detect problems in bearings by monitoring their temperature. Normally an increase in bearing temperature is an indication that something is wrong. Temperature measurement falls into two categories: Direct and Indirect monitoring.

2.1.2.1.   Direct Online Bearing Temperature

Direct temperature measurement is made through permanently installed thermocouples in the bearing, normally as close as possible to the oil film. This is then fed into a

condition monitoring system that measures, evaluates and records temperatures from all the bearings.

Measurement is made through thermocouples or thermistors that are located within the bearing housing. Figures 2.07 and 2.08 show an example of thermocouple installation positions.
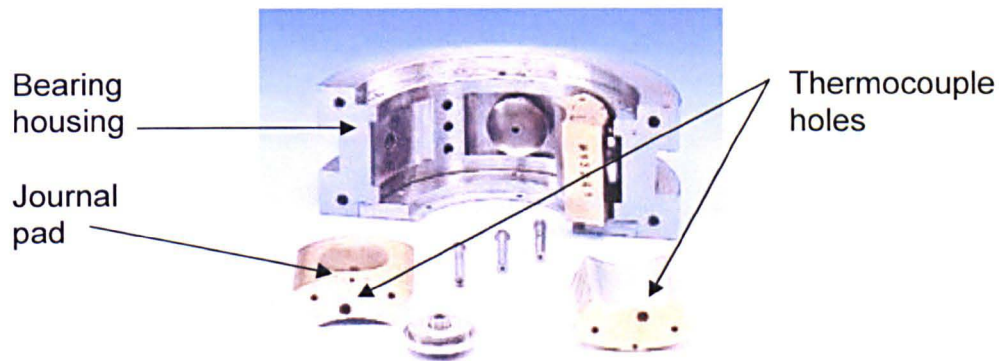
Figure 2.07. A tilting pad journal bearing showing holes for thermocouples (Sartorius [2005]).
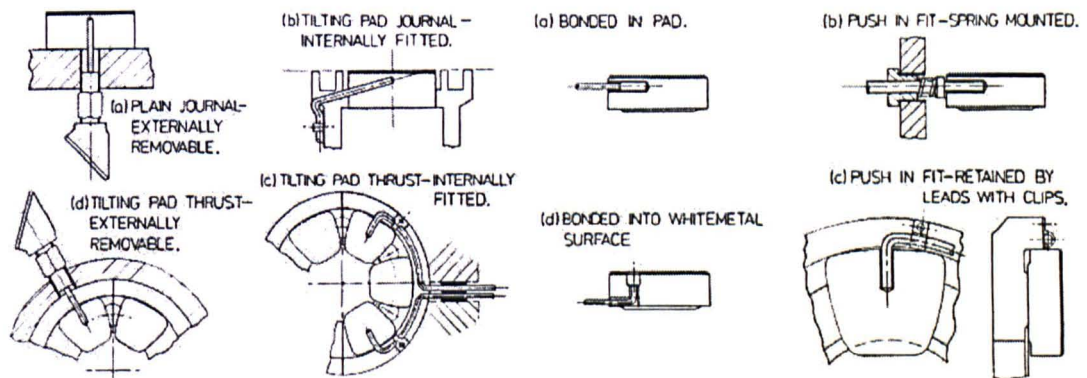
Figure 2.08. Various arrangements for installing thermocouples in thrust and journal bearings (Garner et al [2005]).

In an online temperature monitoring system alarms are normally set to warn of any changes in bearing temperature. Garner et al [2005] suggest a setting of 10°C for alarm and 15°C for trip above the steady state temperature.

There are several problems associated with this technique:

- Whilst this method is well established and convenient, it does not provide any information on what has gone wrong. The temperature rise may be due to several

factors. For example a ship propeller main bearing may rise 2°C every week over two months (Horner [2003]). Why this was happening was not be clear and neither was the best remedy for this problem. The only solution in this situation is to take the bearing out of commission for inspection.

- This method is not suited to bearings that have a thermally insulating sacrificial surface such as PTFE coated thrust pads. For example, in a hydro-electric power station, thermocouples were installed below the PTFE surface. Failure of the bearings occurred and was discovered, not by high temperature readings, but by PTFE particles clogging the filters! The thermocouples read a normal operating temperature (from personal communication with David Horner, Michell Bearings).

2.1.2.2. Indirect Investigative Bearing Temperature

In some situations it is not suitable to install an extensive condition monitoring system. In these applications an infrared thermal camera may be used to detect areas of over heating. This is an indirect method as it normally measures the temperature of the bearing housing rather than the bearing itself. Figure 2.09 shows example output from equipment using this technique.
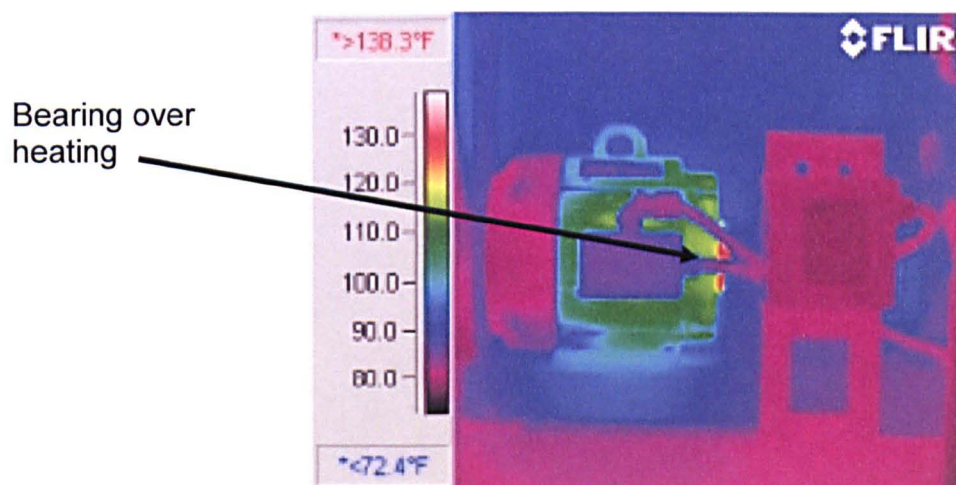
Figure 2.09. Picture from a FLIR camera showing a bearing over heating (FLIR Systems [2005]).

Whilst this is a useful technique, especially in exposed rolling element bearings, this technique suffers from the following:

- Many hydrodynamic bearings support a large load and thus have a considerable cross section to prevent excessive mechanical deformation. This results in a large

thermal inertia. Thus it can take a considerable time for excessive heat generation at an oil film to be observable at the bearing housing.

- Bearings may fail in a very short period of time. As this technique is a random or periodic measurement, failure may occur between sampling intervals.

- FLIR cameras are very expensive and other technologies are more economically viable.

2.1.3. Displacement Techniques

Some bearings are monitored using a method of shaft displacement to determine when the oil film is too thin. The techniques may be Eddy current, Laser Back Reflection or LVDT. Whilst some of these techniques can monitor shaft displacements down to 1μm, it must be remembered that this is not equivalent to oil film thickness as there may be considerable distortion of the shaft, bearing or both.

2.1.3.1. Linear Variable Differential Transformer (LVDT)

LVDT's are a method of measuring displacement. A mechanical displacement moves a push rod that moves an armature resulting in a change in the electrical signal. Figure 2.10 shows some example LVDTs. The housing, spring loaded push rod and connecting cable can be seen.
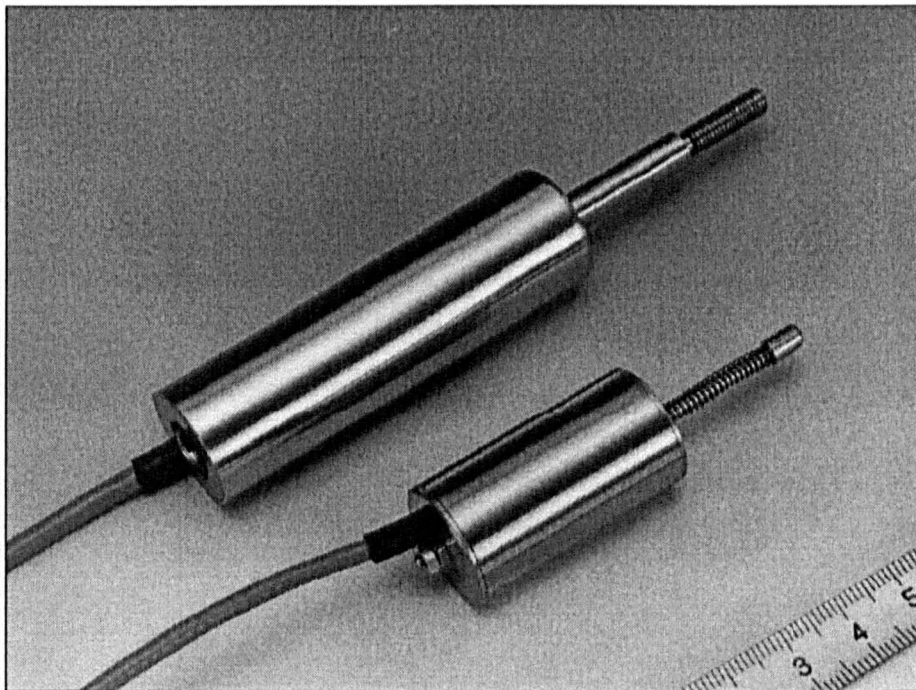
Figure 2.10. Examples of LVDT's from Applied Measurements Ltd [2005].

Usually a LVDT consists of three coils and an armature. The armature is usually made from a magnetic material and is electrically isolated from the attached push rod. The primary coil is excited with an AC signal from between 1 and 30kHz. If the armature is in the centre, between coils 1 and 2 (see figure 2.11) then the resulting signals from 1 and 2 are exactly out of phase (figure 2.11 A)) and the net signal is zero. When the armature moves however, there is a shift in the frequencies between 1 and 2 and the resulting signals from 1 and 2 are almost in phase. The degree to which they are in phase or out of phase is a measurement of distance of the armature.
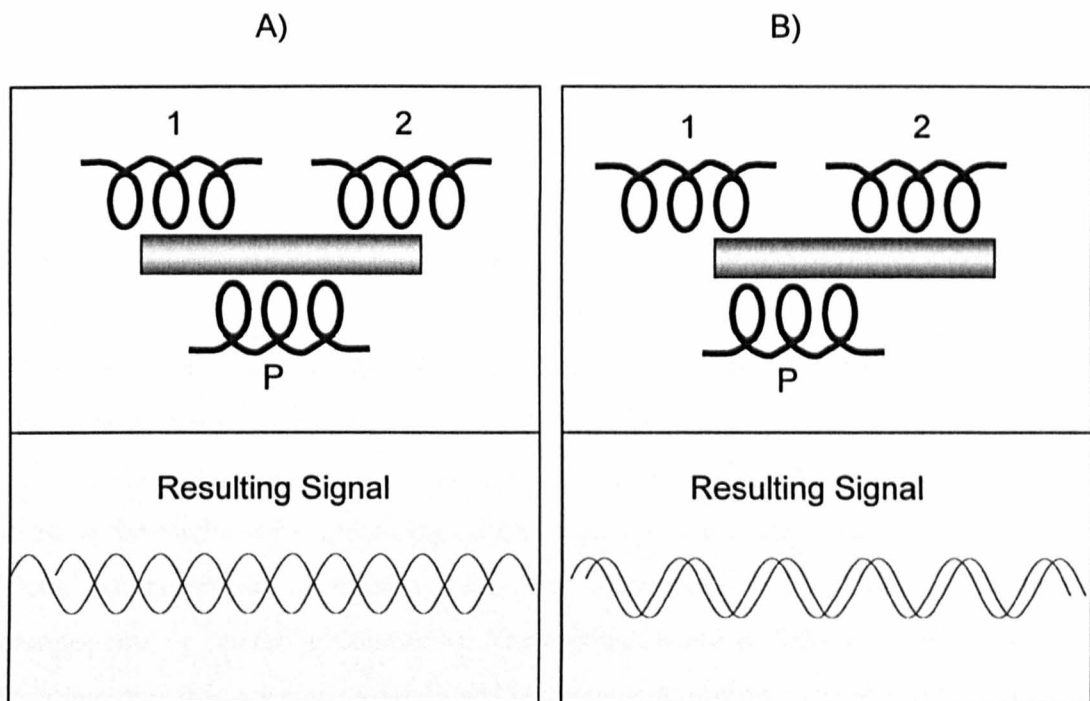
Figure 2.11. Schematic of the operation of a LVDT. A) shows the armature in the central position. The resulting signal from 1 and 2 is exactly out of phase with each other. B) shows when the armature has moved a distance. The resulting signal from 1 and 2 is now almost in phase.

This method of film thickness has the following disadvantages:

- This is not, strictly speaking, a method of oil film thickness measurement, but rather a measure of displacement. From this displacement it can be inferred what the oil film thickness is. The obvious problem is that in many hydrodynamic applications there is significant distortion due to loading and thermal bending/stressing (Allen [1971]). Thus an oil film may be measured on the

outside of a thrust pad, but an entirely different oil film may be present at the centre of the pad.

- Most LVDT systems suffer from a lack of vertical resolution. In a hydrodynamic bearing 5μm may be critical, but the best a commercial LVDT system can repeatedly measure is approximately 15μm.

2.1.3.2. Eddy Current

Wakuri [1993] used eddy current displacement sensors to measure film thickness in an experimental arrangement looking at lubrication between a simulated piston ring and optically translucent pyrex.

Section 2.2.1.3 below describes the operation of an eddy current sensor.

2.2. Measuring Oil Film Thickness

Measuring oil film thickness provides a clear indication of the health of a bearing. Too thin an oil film (or too thick) can lead to further related problems. Methods of measuring oil film thickness may be broadly grouped in two main areas: electrical techniques and optical techniques.

Most of the methods for measuring oil film thickness are limited to use in the laboratory. These measurement techniques have the advantage of not using real bearings, components or operating conditions. For example some techniques have requirements for operation that are unrealistic in real bearings (e.g. optically translucent 'windows' or components, see section 2.2.2 below, or electrical isolation of bearing components). However, laboratory conditions do not fully replicate real world conditions (e.g. loads, speeds, vibrations, temperatures etc) and give a 'general' picture rather than a specific one.

2.2.1. Electrical Techniques

These techniques utilise the electrical properties of the lubricant or the bearing to deduce the thickness of the oil film.

2.2.1.1. Resistive technique

The electrical resistance across an oil film is related to its thickness. This principle has been extensively used to measure oil film thickness. Popinga [1941] used this technique as early as 1941 to determine the breakdown of the lubricating film between a piston and

cylinder. Other contributors include Chu et al [1967], Dyson [1966], El-Sisi et al [1960]. Furuhama et al [1961], Lane et al [1952], MacConochie et al [1960] and Tallian et al [1965]. With the exception of Furuhama et al [1961], none of these applications have considered hydrodynamic applications but rather focus on non conformal contacts (such as gear teeth and rolling element bearings). Furuhama et al [1961] considered piston ring lubrication which may be considered hydrodynamic.

There are several draw backs with this technique:

- Electrical isolation. The rotating and stationary parts of the bearing need to be adequately insulated from each other or erroneous measurements will be made. This is often not practical in the field.

- Quantitative measurement. This technique relies on calibration with known lubricants and known distances.

- Average measurements. Unless a surface mounted sensor is used, this method will provide an average reading over the measurement area.

- Temperature fluctuation. As the temperature of a lubricant changes then so will the resistance and thus there is a need for temperature calibration

- Oil degradation and alteration. The electrical properties may fluctuate with the addition of anti-wear or anti-friction additives, the increase of metallic particles due to wear in the system, or the build up of other particles such as soot. Additionally as oil degrades over time the electrical properties will change.

2.2.1.2. Capacitive technique
The distance between two objects can be obtained by measuring the capacitance of the gap between them. Through calibrating the sensor to know distances and measured capacitances film thickness measurements may be made.

Hamilton et al [1967] and Mann [1995] applied the technique to large metal disks, the latter using thin film capacitive sensors. Astridge [1967] applied the technique to elastohydrodynamic contacts. New [1974] and Hopf et al [1989] have used a capacitive approach to measure oil films in hydrodynamic bearings. Irani et al [1997] used a capacitive approach to measure film thickness in the main bearing of a fired engine. All the above publications comment on the difficulty of maintaining a calibration during testing.
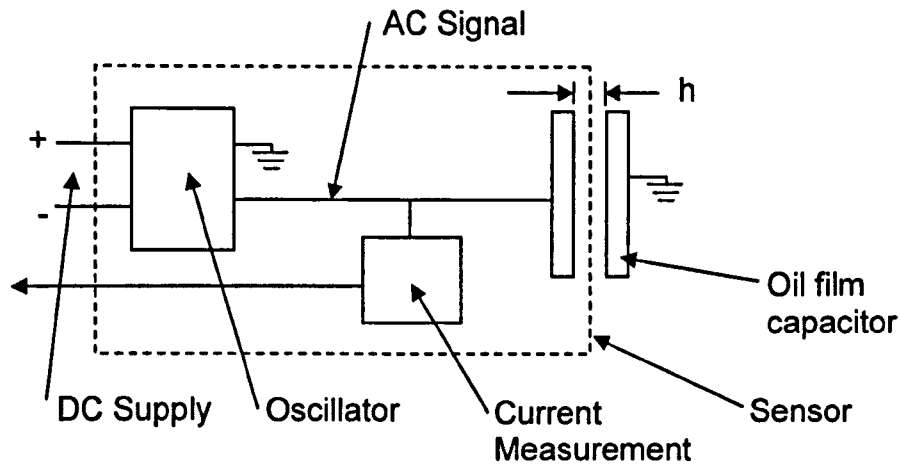
Figure 2.12. A schematic of a capacitance film thickness sensor.

The main drawbacks with a capacitive measurement of film thickness are:

- The requirement for a sensor to be mounted in the fluid film. This can disrupt the film locally and introduces a weak point in the bearing surface.

- knowing what the capacitance of the lubricant is during operation. This problem is further complicated by the fact that the capacitance of the lubricant can change with time (due to degradation of the lubricant), temperature, shear rate and contamination of the lubricant. Irani et al [1997] found this to be a significant problem during testing.

2.2.1.3. Inductive technique

Inductive devices, otherwise known as eddy current transducers, use a generated electro magnetic field to calculate distance. Eddy current transducers are used widely in NDT for crack and defect detection[2].

The principle of operation is that an alternating current flowing through a coil will induce circulating swirling (eddy) currents in any magnetic material in close proximity to the coil. In NDT, a crack in the material results in a change (interruption) in the eddy current flow resulting in an increase in the coils impedance. Through monitoring the voltage across the coil, changes in the material being investigated can be monitored.

---

2 See http://www.ndt-ed.org/EducationResources/CommunityCollege/
EddyCurrents/Introduction/presentstateofET.htm accessed on 18th December 2007

For film thickness monitoring the eddy current decreases with increasing separation between the coil and the surface. Thus by measuring the voltage across the coil and comparing to a reference the separation can be calculated.
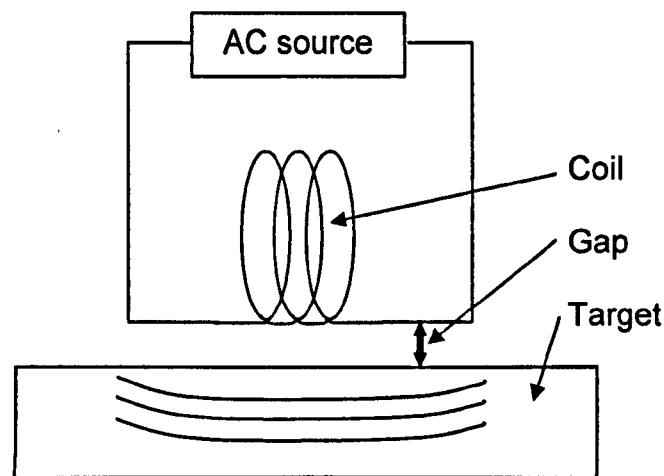
Figure 2.13. An example of an eddy currant inductance probe.

This technique has probably the most extensively used technique for measuring film thickness in hydrodynamic applications. Kim et al [1995], Gustafson [1967], Tanaka et al [1985] and Glavatskikh et al [2001] have used this technique to measure the oil film thickness in thrust pad bearings. Tonnesen et al [1981] and Read et al [1987] have used this technique in journal bearings.

This technique suffers from the following problems:

- The sensor has to be mounted in the pad surface (see figure 2.14 below). Usually the sensor is recessed slightly into the surface to protect it in the event of a bearing wipe, or in the case of Glavatskikh et al [2001], to account for differning rates of thermal expansion. This has the effect of disrupting the bearing surface by having a different material in the loaded region, but also by having a change in the local oil film thickness (due to the recess).

- Temperature fluctuation. The sensor output drifts significantly with temperature. Therefore some sort of temperature compensation is needed to remove this effect from the results.
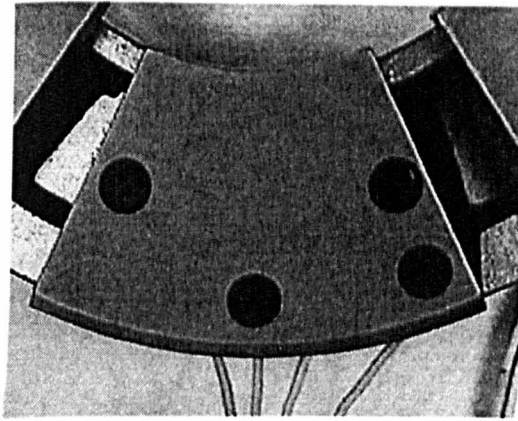
Figure 2.14. Four eddy current sensors mounted on a tilting thrust pad, backfilled with black epoxy (Glavatskikh et al [2001]).

2.2.2. Optical techniques

There are several techniques that can be employed using light to give an optical measurement of oil film thickness.

2.2.2.1. Optical Interferometry

This method used the interference (constructive and destructive) between two light beams to determine oil film thickness. The two primary approaches are the fringe colour method and the dark band fringe method.

2.2.2.1.1. Fringe Colour Method

Optical Interferometry is where a light beam is split and the beam is recombined after going through an oil film. The presence of a thin layer delays one part of the beam. When the beam is recombined there is an interference pattern produced (see figure 2.15). By measuring the number of fringes and the colours formed the film thickness can be obtained. This method is widely used for measuring oil film thickness in EHD contacts (see Spikes [1999]). Wakuri et al [1981] used this technique to measure film thickness between reciprocating slider with a circular profile and an optical flat.
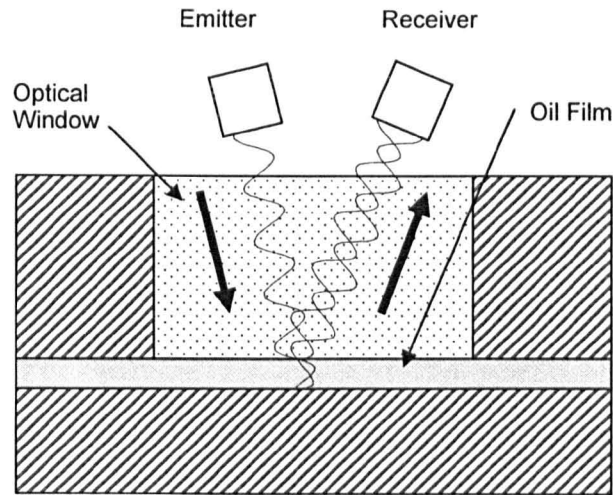
Figure 2.15. A light source emits light through an optical window through an oil film. The received light is constructively or deconstructively interfered depending on the thickness.

Fringe colour optical interference disadvantages:

- This method has an upper limit of about 1 μm. Since most hydrodynamic bearings operate well above this, it is suitable only for elastrohydrodynamic (EHD) lubrication regimes.

- Due to using light as the measurement tool the bearing, or part thereof must be optically translucent. Given that most optically translucent materials are not suitable as real bearing materials this method is restricted to research applications.

2.2.2.1.2. *Dark Band Fringe Method*

A second method of optical interferometry uses the condition for dark bands to measure oil film thickness. Higginson et al [1967] used this technique to measure oil film thickness in a journal bearing. A white light source produces a range of wavelengths. Using this range of wavelengths it is possible to produce fringes of equal chromatic order. Using an arrangement such as figure 2.16, certain wavelengths are destructively interfered with to produce black lines that correspond to the thickness of the oil layer.
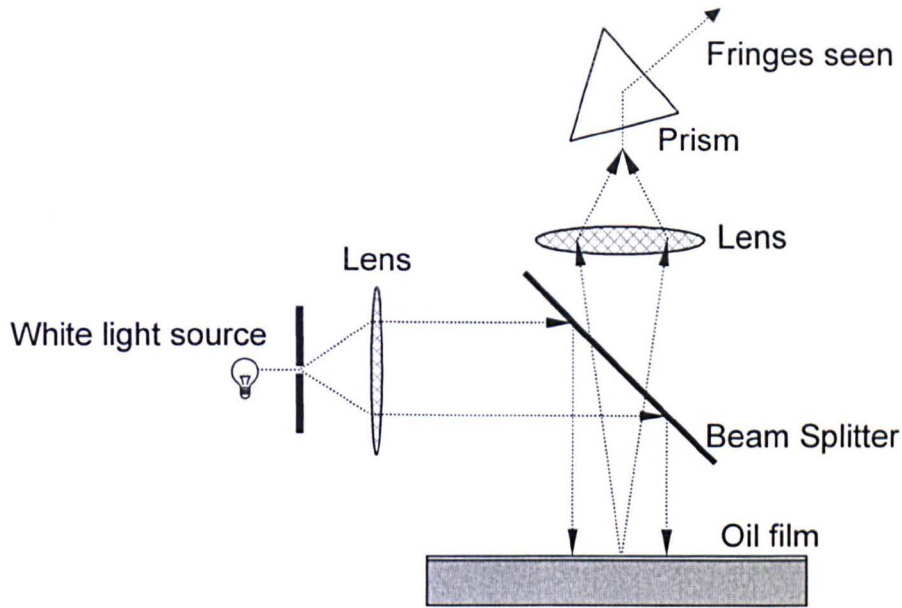
Figure 2.16. Schematic arrangement for generating dark bands from an oil film.

This method has a big advantage over the fringe colour method in that its measurable range of film thicknesses is from 0.25μm to 100μm. However, this methods major disadvantage is the same as the fringe colour method: the need for an optically translucent bearing.

2.2.2.2. Back Reflection Technique

This technique is based on triangulation between a laser emitter (or a white light emitter as used in the optic lever technique demonstrated by Glavatskikh et al [2000]) and one or two single or multiple receivers. Figure 2.17 shows a schematic of a single emitter and receiver.
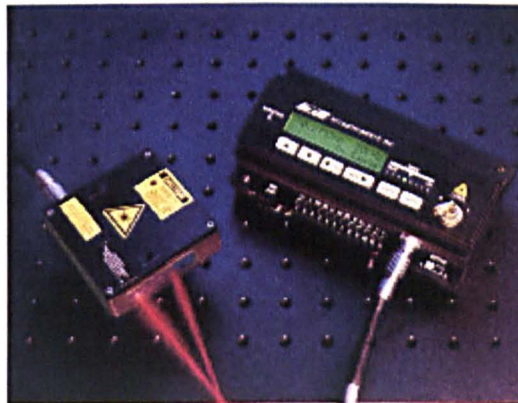
Figure 2.17. An example product using the laser back reflection technique from MTI Inc [2005]. The laser and receiver angles may be observed.

In figure 2.18 the central optic fibre emits a laser light. Receiver 1 consisting of six optic fibres receives some of the signal. Receiver 2, also consisting of six optic fibres also receives some of the signal. The output from receiver 1 and receiver 2 are divided to give a signal ratio. The use of six optic fibres improves the measured signal and removes spurious measurements due to surface inhomogeneities. As the distance between the sensor and the target increases (from zero) the received amplitude of receiver two (see figure 2.18) increases in proportion to the distance. At a certain point it reaches a maximum value before tailing off as the separation increases beyond the range of the sensor.
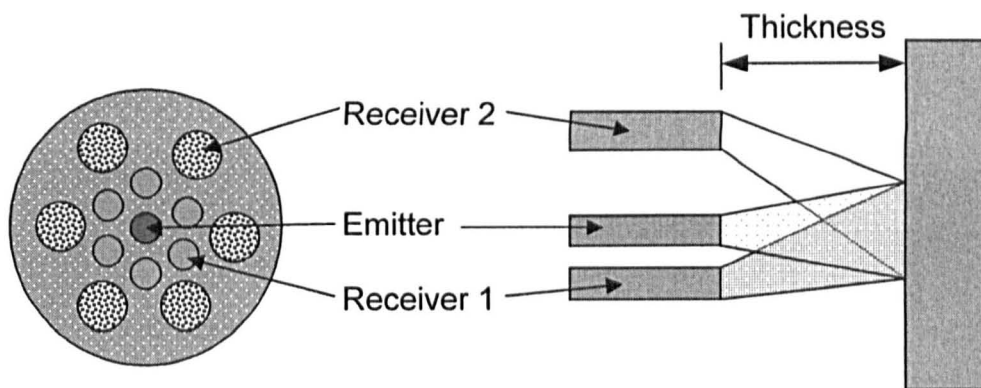
Figure 2.18. Back reflection method of oil film thickness measurement.

Hobel et al [1999] and Glavatskikh et al [2000] have applied this technique to thrust pad bearings. In the former a sensor was mounted in the collar of the bearing to measure the oil film thickness circumferentially in the bearing. In the latter a sensor was mounted in the thrust pad.

This technique has been successfully in a few applications but the following problems presented themselves:

- This method is dependent on the reflectivity of the target. Hobel et al [1999] quoted that measurements on Babbitt targets were two orders of magnitude higher due to higher reflectance when compared to PTFE. Whilst it may be possible to set the system up for specific materials it is not clear what may happen over time. For example, in the event of lacquer build up the reflectivity will decrease. This will manifest itself as a thicker oil film when in fact the oil film may be thinner!

- This method necessitates the position of a sensor/optical window in the bearing surface. This will change the bearing structure and possibly the local oil film formation.

2.2.2.3. Laser Induced Fluorescence (LIF)

This technique uses the principle that when a laser strikes a lubricant film doped with a fluorescent dye, the film will fluoresce, the intensity of which is related to the fluid film thickness. Smart et al [1997] describe a fluorescense technique using a mecury lamp to measure free surface film thickness. Richardson et al [1991] and Shaw et al [1992] describe the application of laser induced fluorescence to the measurement film thickness in the piston ring/liner interface. A small optical fibre was inserted into the cylinder wall (Shaw et al [1992] used an optical fibre that was 50μm diameter).
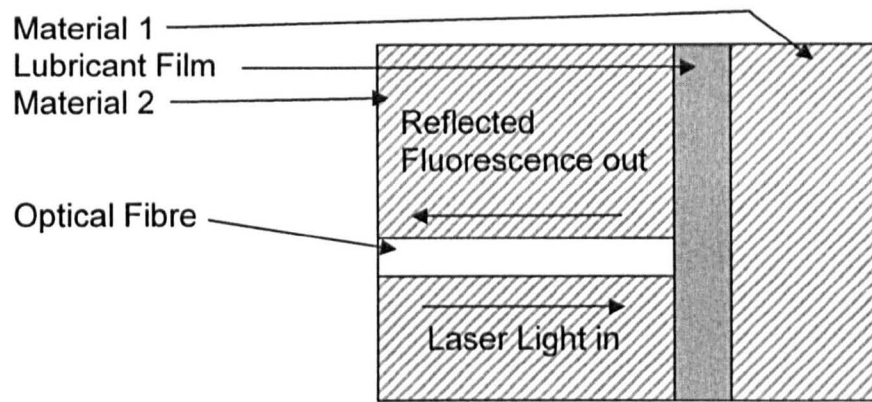
Figure 2.19. Schematic of application of Laser Fluorescence technique using an optical fibre.

Sanda et al [1997] and Baba et al [2006] both use an optically transparent cylinder and the LIF technique to measure film thickness.

Whilst this technique has been used in a number of applications, particularly where a small measurement area is required, it does suffer from serious drawbacks:

- the requirement for an optically translucent component or part of component in order to get the light in and out.
- The technique relies heavily on correct calibration. Smart et al [1997] describe the measurement of a surface film on two different substrates giving two different (non-linear) results.

- The technique can suffer from a degradation of fluorescence intensity due to either temperature or all of degradation. Having said this, Baba et al [2006] have demonstrated a linear relationship between film thickness and fluorescence intensity using Rhodamine B in the temperature range 25 to 125°C (long term tests were not conducted however).

- A change in the surface reflectivity of the surfaces either side of the oil film can have a significant impact on the calibration. However, Hidrovo et al [2001] developed an Emission Reabsorption Laser Induced Fluorescence (ERLIF) using two different doping dyes that removed the effect of surface reflectivity, although with in the literature it does not seem to be used for measuring film thicknesses in bearings

2.3. Conclusions

In this chapter several methods for condition monitoring have been outlined. Some of these methods are used within industry to monitor hydrodynamic bearings, principally temperature monitoring and displacement measurement. These techniques tend to be used in large safety critical or production critical equipment, often where there is an existing problem.

This chapter has considered other methods of measuring oil film thickness. All of the methods suffer from major constraints such as measurement range, measurement resolution, measurement speed, temperature limits, local film thickness, cost, application to 'real' bearings.

None of the electrical techniques directly measures oil film thickness, but rather measures a value of capacitance, potential or resistance and using a calibration procedure calculates an oil film thickness. The value of film thickness changes with a change in the lubricant.

Whilst optical techniques have many benefits in terms of resolution, speed, accuracy, there remains one major drawback: optical translucency. Using an optical technique necessitates that there is a window through which light may enter the oil film and be received back again. This is often not feasible in many engineering applications (either to build a component with an optical window or made the whole component of an optically translucent material such as glass). The presence of a window in a bearing changes the

mechanical properties of the bearing (such as strength, thermal distortion, resonant frequency etc). Often it also changes the local film formation (for example a recess in the bearing surface).

In conclusion, there is no existing non-invasive condition monitoring technology on the market that monitors film thickness in real engineering components under real operating conditions.

Chapter 3:

Principles of Ultrasonic Reflection

3.1. What is Ultrasound

The human capacity to sense sound is limited. We are unable to 'hear' sound with a frequency below about 20Hz and above 20kHz (some authors define the upper limit at 16kHz, Filipczynski et al [1966]). Generally humans are unable to 'hear' sound above and below these frequencies although we may be able to perceive them.[1] Sound which is above the human audible range is classed as ultra-sound.

Ultrasound can vary from 20kHz well into the GHz range depending on the application. For Non Destructive Testing (NDT) the range of ultrasonic frequencies that is commonly used is much smaller. For air coupled applications the testing frequencies are from 50kHz up to 1MHz. Below 50kHz the resolution is so poor to be of virtually no practical use, and above 1MHz the attenuation in air becomes too great. For generic NDT field testing, frequencies from 2-20 MHz are often used with a high proportion of testing in the 3-7 MHz range. This frequency range gives a good compromise between attenuation in the test material and resolution for flaw detection or material thickness. Higher frequencies are generally reserved for acoustic microscopy, with frequencies from 2MHz up to 8GHz being used (Kino [1987]).

---

[1] An example of this is the assertion of many record buffs that records 'sound' much better than compact discs. We seem to have some 'sense' of sound below and above these frequencies.

3.2. Motion and Modes of Ultrasonic Waves

A sound wave can be simulated by a sine wave (see figure 3.01) with alternating areas of compression and expansion. The wavelength is the distance that is taken to complete one cycle for given material properties. The frequency is the number of cycles per second (otherwise known as Hertz, Hz).
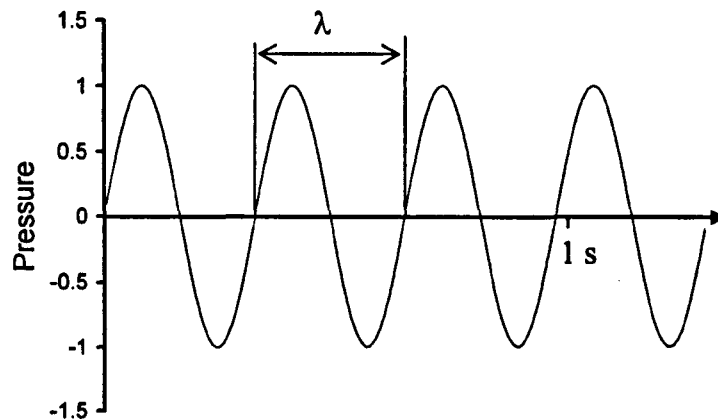
Figure 3.01. A sine wave showing wavelength λ, with a frequency of 3 Hz (cycles per second)

A sound wave travels with an associated speed, depending on the material it passes through (see 3.3.2), and also depending on its mode, to which we now turn our attention.

3.2.1. Longitudinal Waves

Sound waves can propagate through a material longitudinally (also known as pressure or compression waves). This is analogous to a stretched light spring (for example the kids toy called a Slinky Spring) being given a sharp impact in the direction of its length. A resulting compressive area (surrounded by expansion areas on either side) will travel up the length of the spring (see figure 3.02). This is by far the most common type of sound wave encountered in ultrasonic NDT and will be the subject of this work.

28
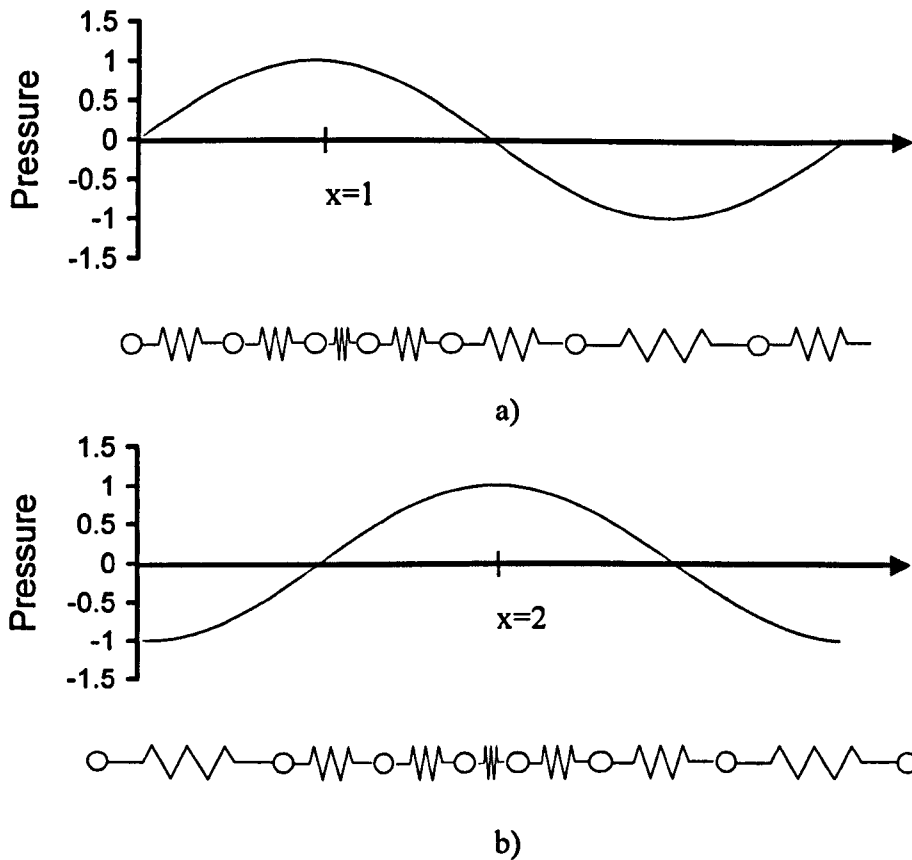
Figure 3.02. Propagation of a wave through an elastic solid represented by discreet particles separated by springs. In a), the peak of compression is at x=1. In b), the peak of compression has moved a distance to x=2.

Direction of propagation
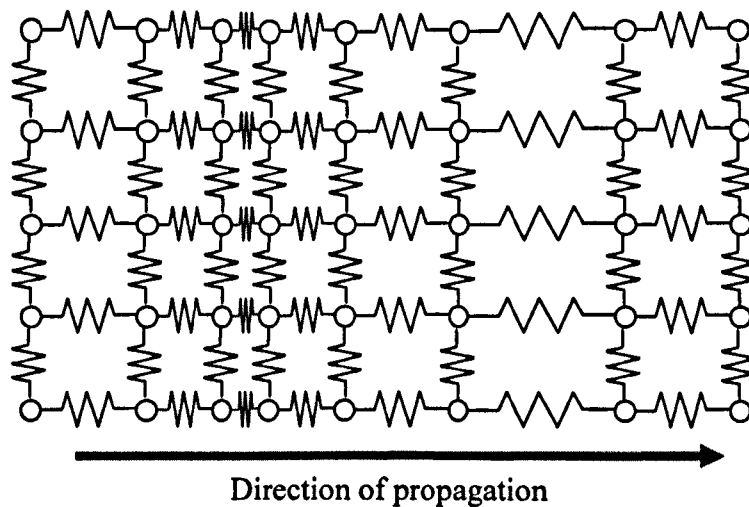
Figure 3.03. Schematic representation of a longitudinal wave propagating through a solid represented by particles separated by springs with associated stiffness and damping.
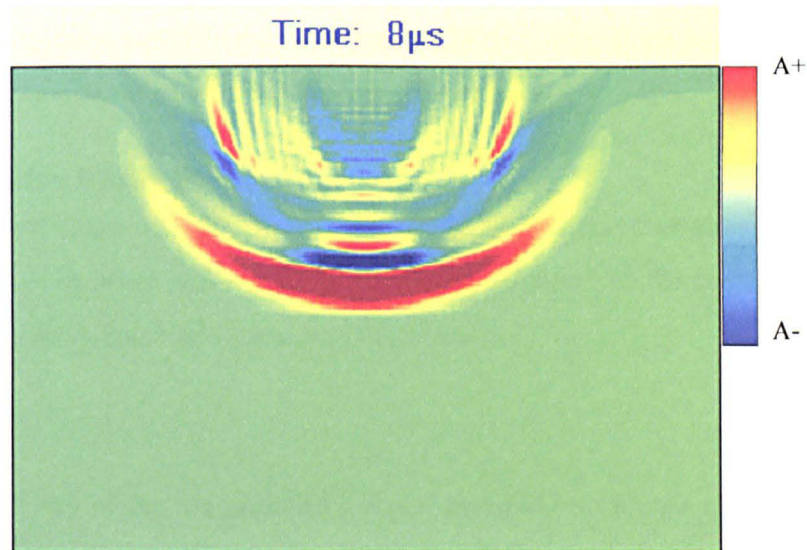
Figure 3.04. Simulation of a three cycle 10 MHz longitudinal sound wave propagating through steel 8μs after it started. The colours represent the amplitude of the sound wave at that point in 2-D space (Lee [2003]).

3.2.2. Shear, Raleigh and Lamb Waves

Shear waves oscillate perpendicular to the direction of propagation. It is analogous to a light spring (e.g. the Slinky as previously mentioned) being given an impact perpendicular to its length. An oscillation from side to side will propagate along the length of the spring (i.e. a wave oscillation perpendicular to the direction of propagation). Shear waves will not propagate through liquids due to their inability to support a shear force. The speed of sound of a shear wave, c_S through a material is approximately half of the longitudinal speed of sound, c_L.

Raleigh waves exist on the surface of a material and are a combination of longitudinal and shear waves interacting.

Lamb waves (or plate waves) exist in thin plates where the whole plate oscillates in a specific manner.

Shear, Raleigh and Lamb waves have not been used in this study to measure oil film thickness due to their unsuitability in terms of either application or ability of detection (Shear waves do not travel across a liquid, Raleigh waves only travel on the surface of a material and not through it, and Lamb waves only exist in thin plates).

3.3. Material Properties

Before considering ultrasound further it is important to define some material properties that affect the transmission of ultrasound through materials.

3.3.1. Acoustic Impedance

Acoustic impedance can be described as the resistance to the transmission of sound through a material. In other words it is the "acoustic stiffness" of the material. Acoustic impedance, z, can be defined by equation (3.01) below:

$$z = \rho c \tag{3.01}$$

where ρ is the density of the material and c is the speed of sound in a material. Units of acoustic impedance are kg/s.m², otherwise known as Rayls.

This resistance to the transmission of sound becomes important when a sound wave travels from a material with one value of z to a material with a different value of z. If the values of z in each material are different then the sound wave will be split into transmitted and reflected components. See table 3.01 for some sample values of acoustic impedance. See section 3.4 for more details on waves at boundaries.

3.3.2. Speed of Sound

The speed of sound in a material is the speed at which a sound wave will propagate through that material. This is dependent on the Young's modulus and Poisson's ratio (for a solid) or the Bulk modulus (for a liquid), and the density of the material according to equations (3.02) and (3.03) below. Equation (3.02) is valid for waves travelling through a bulk material. The speed of sound can be easily acquired by measuring the time it takes for a pulse of sound to travel a fixed known distance. Typical values of speed of sound for various materials are shown in table 3.1.

$$c_{solid} = \sqrt{\frac{E}{\rho} \frac{1-\upsilon}{(1+\upsilon)(1-2\upsilon)}} \tag{3.02}$$

$$c_{liquid} = \frac{B}{\rho} \tag{3.03}$$

Where c is the speed of sound, E is the Young's modulus, B is the bulk modulus of the material, and ρ is the density of the material.

	Speed of Sound, m/s	Density, kg/m^3	Acoustic Impedance
Aluminium	6320	2700	17.1 e+6
Brass	4280	8560	36.7 e+6
Steel	5900	7700	45.4 e+6
Water	1480	1000	1.48 e+6
Oil	1740	870	1.51 e+6

Table 3.01. Speed of sound, density and acoustic Impedance for five materials[2]

3.3.3. Attenuation

Attenuation of a sound wave is defined as the loss of energy of a sound wave passing through a material. This happens in two principle ways (not counting geometric effects):

- Scattering as a result of boundaries within the material (e.g. grain boundaries, imperfections, inclusions etc). This can be readily seen where the grain size or defect size is much larger than the wavelength and the wave is split into reflected and transmitted waves. Both the reflected wave and the transmitted wave is further split into reflected and transmitted waves at the next boundary that is encountered. Thus an incident wave can quickly be subdivided into tens or hundreds of waves.

Where the grain size is small when compared to the wavelength (especially for 0.001λ to 0.01λ) scatter is not significant. However, when the grain size is large compared to the wavelength (0.1λ and upwards) there can be significant effects on the scattering of the signal, so much so that transmission of sound is impossible. Figure 3.05 shows the relationship between wavelength and frequency and how at high frequencies (e.g. 50 MHz) the wavelength is very small and thus is susceptible to scattering in coarse grained materials.

[2] Accessed on 16/11/07 at
http://www.ndt-ed.org/GeneralResources/MaterialProperties/UT/ut_matlprop_index.htm
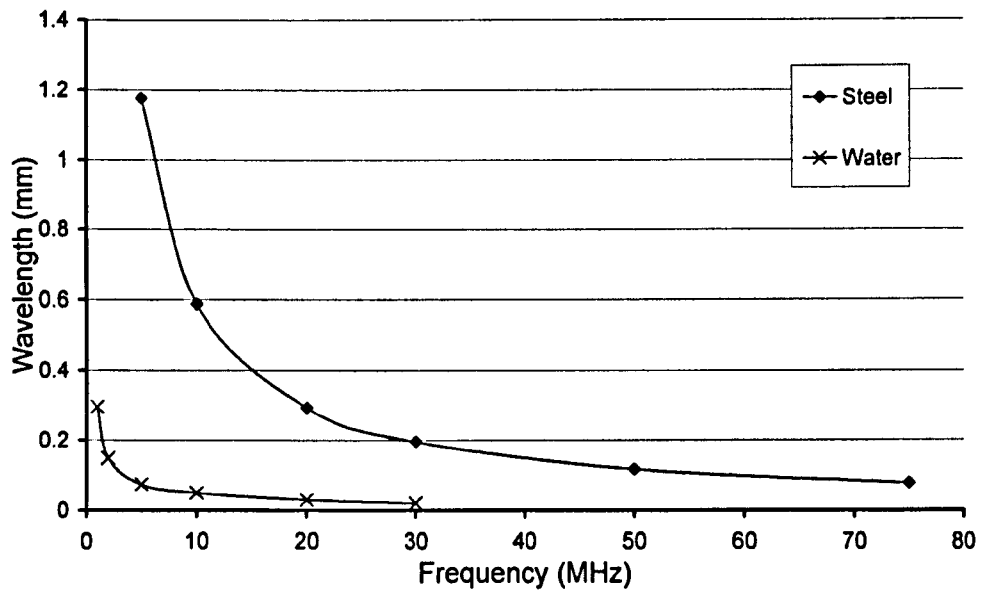
Figure 3.05. Wavelength versus frequency for a sound wave travelling through mild steel and water.

Grain size varies considerably for different materials and also different manufacturing processes. It can range from several hundred microns to a few microns. One producer[3] specifies annealed tempers in terms of grain size. Table 3.02 shows the associated maximum frequency that could be used for each grain size.

Quoted Temper (mm)	Grain Size(μm)	Maximum Frequency(MHz)
0.015	15	40
0.025	25	25
0.035	35	15
0.050	50	12
0.070	70	8
0.100	100	6

Table 3.02. Grain sizes for various tempers and associated approximate maximum frequencies.

- Absorption, or the conversion of sound energy into heat energy. This reduces the amplitude of the sound waves that is transmitted through a material. This can be

---

[3] Busby Metals, http://www.busbymetals.com/docs/glossary_t.htm accessed 16/11/07

overcome by increasing the amplitude of the incident wave to thereby increase the reflected wave to an acceptable level. Absorption also increases with an increase in frequency.

When looking at steels with a frequency above 10 MHz attenuation is mostly due to scattering and absorption is not significant. However, when looking at plastics absorption dominates the attenuation.

As both scattering and absorption are properties of the material, the quantity of material that the sound wave travels through will determine the overall attenuation. In some instances it may be possible to look through highly attenuative material if it is a thin test specimen. The attenuation of a material can be expressed by equation (3.04)

$$A = A_0 e^{-\alpha d} \tag{3.04}$$

Where A is the received amplitude of the ultrasonic signal, A_0 is the amplitude of the incident ultrasonic signal, d is the distance that the ultrasonic wave has travelled, and α is the attenuation coefficient. α is measured in nepers/m where nepers are a dimensionless quantity. Nepers/m can be converted to decibels/m using equation (3.05)

$$\alpha / m = 0.1151 dB / m \tag{3.05}$$

3.4. Waves at boundaries

Boundaries are very important when considering ultrasound as every ultrasonic wave has to cross a boundary at some point (for example, from the wave source into the component).

3.4.1. Reflection Coefficient

The reflection coefficient, R, is the fraction, A_r, of the amplitude of an incident wave, A_i, that is reflected from a boundary according to equation (3.06) below:

$$R = \frac{A_r}{A_i} \tag{3.06}$$

A sound wave travelling through a medium will be reflected at a boundary according to equation (3.07).

$$R = \frac{z_1 - z_2}{z_1 + z_2} \qquad\qquad\qquad (3.07)$$

Where R is the reflection coefficient and z_1, z_2 are the acoustic impedances of material 1 and 2 respectively. This may be illustrated by considering a compressive pulse travelling along a light spring. When the pulse reaches the end of the spring (the spring/air interface) it 'reflects' and travels back along the spring to the point of origin. This 'complete' reflection is due to the fact that the spring is very stiff when compared to air. Thus the pulse will be fully reflected ($z_1 >> z_2$ in equation (3.07)). For a sound wave travelling through steel and being reflected at a steel/air interface, R=0.999.

At an interface between two bodies with the same acoustic impedance a sound wave will be fully transmitted (i.e. R=0). This is for perfect contact between the bodies. The relationship between the signal transmitted across the interface, T (the Transmission Coefficient), and the signal reflected from the interface, R (the Reflection Coefficient) is given in equation (3.08).

$$|R| = 1 - T \qquad\qquad\qquad (3.08)$$

A pulse will be partially reflected and partially transmitted at an interface between two acoustically different materials. This is especially obvious when one material has z of approximately half the z in the other material (in contrast to steel/air). Table 3.03 shows some sample reflection coefficients for various material combinations.

	z_1	z_2	R
Aluminium/Steel	17.06	45.63	-0.46
Steel/Oil	45.63	1.51	0.94
Water/Steel	1.48	45.63	-0.94
Steel/Brass	45.63	37.3	0.1
Brass/Rubber	37.3	1.4	0.93

Table 3.03. Acoustic impedances and reflection coefficients for various combinations

In Table 3.03 some of the reflection coefficient values are negative. This indicates that there is a phase reversal at the boundary and the reflected wave is inverted. In practice the modulus of the reflection coefficient is used.

It can be seen that equation (3.07) is frequency independent. This is valid for a 'perfect' interface between two materials. However, where the interface is 'imperfect' (i.e. the surfaces are not completely conformal) the interface may be described by a spring model. Tattersall [1973] derived equation (3.09) to describe this imperfection.

$$R = \frac{z_1 - z_2 + i\omega\left(\frac{z_1 z_2}{k}\right)}{z_1 + z_2 + i\omega\left(\frac{z_1 z_2}{k}\right)}$$

(3.09)

Where k is the stiffness of the interface. It can be seen that equation (3.09) reduces to equation (3.07) for a perfect interface ($k=\infty$). Unlike equation (3.07), equation (3.09) is frequency dependent for $k<<\infty$.

3.4.2. Snells Law

A sound wave incident to a boundary will be reflected according to the angle that the incident wave makes to that boundary. Equation (3.10) shows the relationship between the incident and transmitted waves and the angles that they have to vertical. For a wave incident at 90° to a boundary, $\sin\theta_1=1$ and the reflection and transmission is controlled by equations (3.07) and (3.09).

$$\frac{\sin\theta_1}{\sin\theta_2} = \frac{c_i}{c_t}$$

(3.10)

Where θ_i and θ_t are the angles of the incident and transmitted waves respectively and c_i and c_t are the speed of sound in materials 1 and 2 respectively. Figure 3.06 shows this graphically.
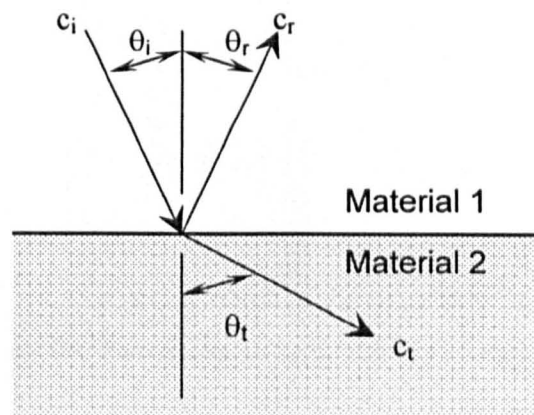
Figure 3.06. Snells law, showing the relationship between an incident signal in material 1, a reflected signal in material 1 and a transmitted signal in material 2.

3.4.3. Mode conversion

Upon striking a boundary waves can change mode (e.g. a longitudinal wave striking an oblique surface will be split into longitudinal and shear components). This can result in extra signals being detected and erroneously recorded. This is usually only a problem where either the incident ultrasonic wave is not perpendicular to the interface or there are geometry effects. Figure 3.07 shows two examples of mode conversion.
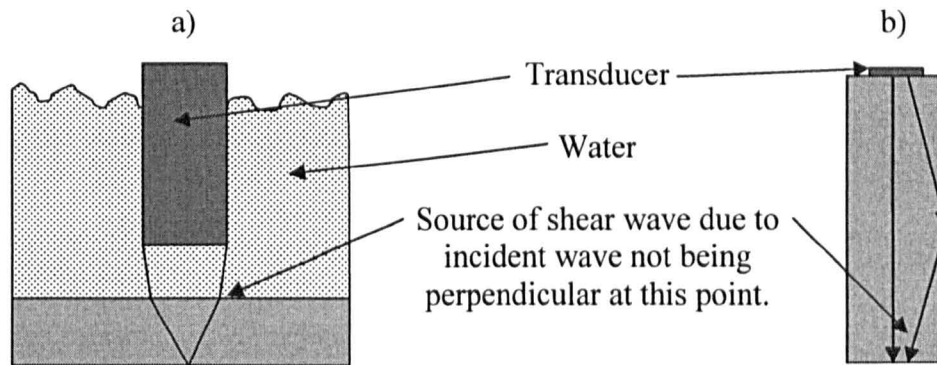
Figure 3.07. Examples of mode conversion in ultrasonic applications. a) a focused transducer in water, and b) a longitudinal sensor bonded onto a component.

3.5. Waves through Layers

Many engineering components are made up of layers of different materials. A bearing is simply two materials in relative motion to one another separated by a lubricating material, or in other words, an embedded layer. When a sound wave travelling through a material meets an embedded layer it reflects in a manner uniquely dependent on the layer. Figure 3.08 shows a diagram of two materials separated by an embedded layer.
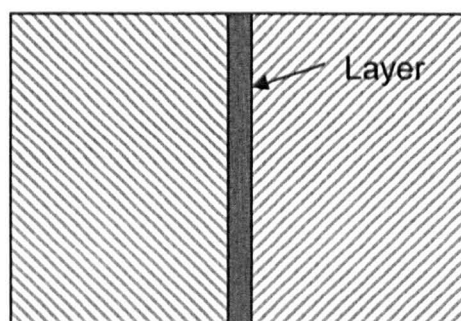
Figure 3.08. Two materials separated by an embedded layer.

The response of a sound wave to a thin imbedded layer depends on the acoustic properties of the layer and its thickness according to equation (3.09). Assuming that the acoustic properties are known the thickness can be calculated using a sound wave.

3.5.1. Layer thickness greater than λ

Where the interfaces of a layer are not in close proximity (i.e. a thick layer, greater than 100μm apart) each interface will give a separate reflection (see figure 3.09). These reflections can be received and the time between each reflection can be measured to give the time of flight. If the speed of sound of the layer is known then the thickness can easily be calculated using equation (3.11)

$$c = \frac{D}{t}$$ (3.11)

Where c is the speed of sound in the layer, D is the thickness of the layer and t is the time taken for a sound wave to travel through the layer.

This technique is known as the time of flight technique and is used extensively in thickness gauging. Figure 3.09 shows the simulated reflection from a thick layer of a 30MHz pulse showing the front face and back face echoes. Notice the change in phase of the signal from the front and back face as expected from equation (3.07) using acoustic properties for steel and oil appropriately. Wittig et al [1994] used this technique to measure the free surface film thicknesses in the range 0.5 – 5mm on the inside of the bearing chamber.
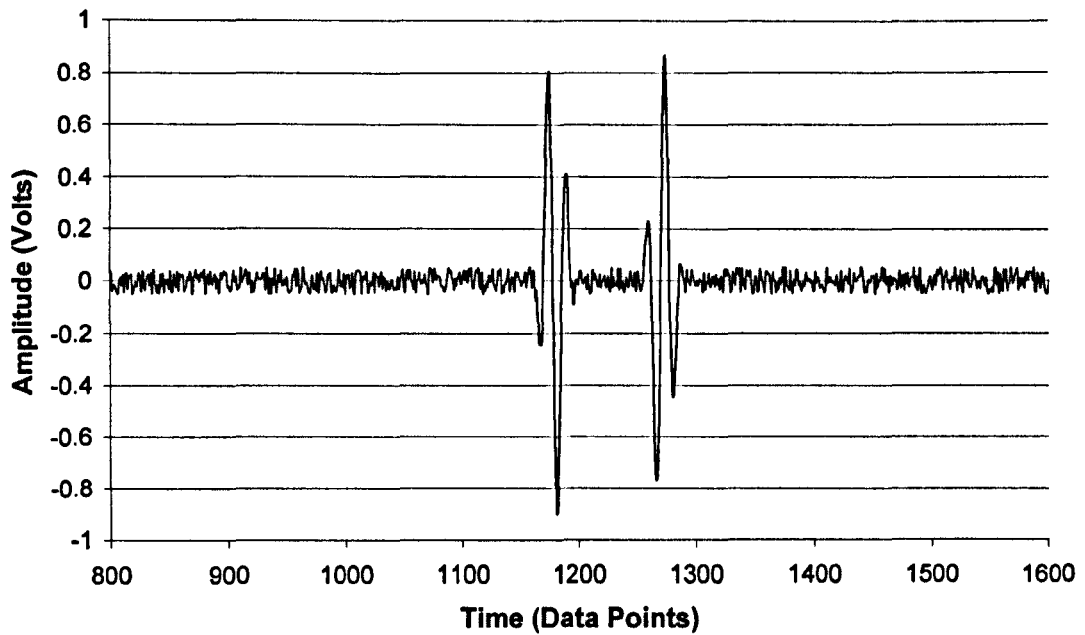
Figure 3.09. Simulated reflected pulses from a 200μm oil layer.

3.5.2. Layer thickness equal to λ

Where the interfaces on either side of a layer are in close proximity (i.e. a thin layer thickness, approximately λ) all the sound of a single frequency will be reflected except at $h=\lambda$, 2λ, 3λ, ... where all the sound will be transmitted (for $z_1=z_3>>z_2$). For short duration pulses there is a corresponding frequency spectrum (see section 4.3.1.4 for more details). The frequency spectrum contains many frequencies and thus there will be a point in the frequency spectrum where the reflection coefficient drops from one at $h<\lambda$ to zero (assuming $0<R<1$) at $h=\lambda$ and then recovers back to one again at $h>\lambda$. Figure 3.10 shows the response of the reflected amplitude for given frequencies.
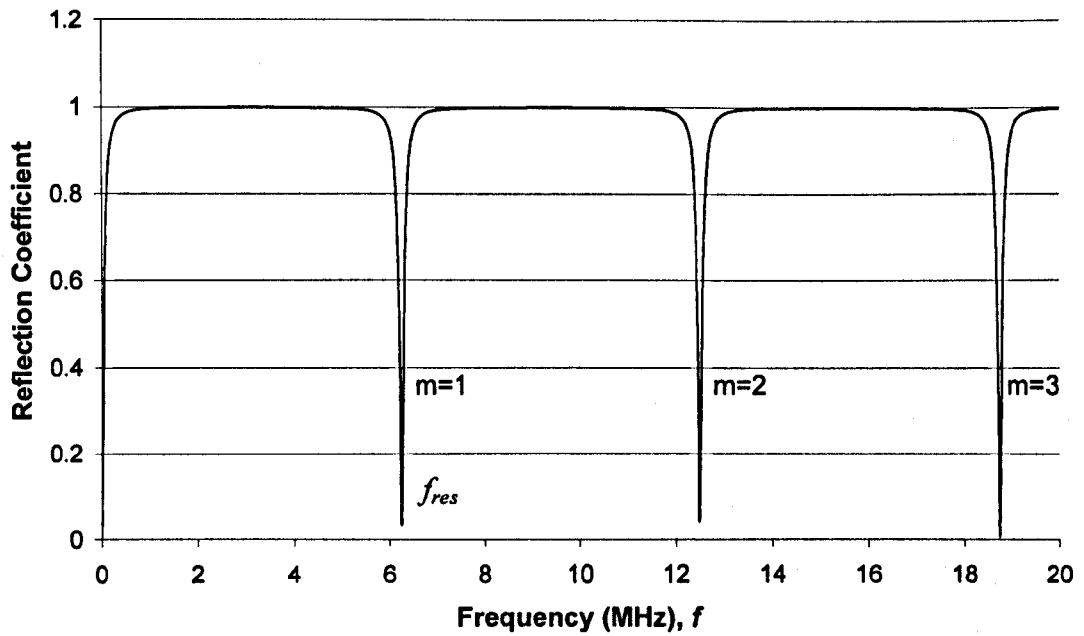
Figure 3.10. Predicted relationship between reflection coefficient and frequency for a 100μm oil layer.

Equation (3.12) shows the relationship between layer thickness, speed of sound in the layer and the frequency at which the amplitude decreases.

$$h = \frac{cm}{2f_{res}}$$ (3.12)

Where h is layer thickness, c is the speed of sound in the layer, m is the mode number of λ and f_{res} is the frequency.

This method, known as the resonant dip technique (see Dwyer-Joyce et al [2002]), is suitable for measuring films in typical bearing applications down as thin as 50μm. Below this the frequency required becomes too high for practical use.

3.5.3. Layer thickness less than λ

Where the interfaces on either side of a layer are in very close proximity (i.e. a very thin layer, $h<<\lambda$) the layer acts as a single reflector (i.e. it behaves as a single interface rather than two discreet interfaces) according to equation (3.09). At each frequency a proportion of the wave is transmitted and reflected depending on the layer thickness and the speed of sound of the layer. Thus at lower frequencies less is reflected and at higher frequencies more is reflected. Thus for a short duration pulse with a specific frequency content, the proportion of the wave reflected will be lower at lower frequencies and higher at higher frequencies.

The stiffness of a material is described as its resistance to deformation with an applied force. Where the applied force is perpendicular to a thin layer, the stiffness of the layer may be described as the required change in pressure, p, to give a certain change in the thickness of that layer, h.

$$k=-\frac{\mathrm{d}p}{\mathrm{d}h_L}$$

(3.13)

For a fluid the stiffness is described by the bulk modulus, B, its resistance to compressibility. Thus B is the change in pressure required to give a certain change in volume.

$$B=-\frac{\mathrm{d}p}{\mathrm{d}V/V}$$

(3.14)

Generally the area over which a sound wave acts is large in relation to the thickness of the layer. Thus the fluid in the layer is constrained to only deform across the layer (i.e. a deformation of its thickness, h_L) and not spread out. Therefore:

$$-\frac{dV}{V} = \frac{dh_L}{h_L}$$ (3.15)

In other words, the stiffness of a thin liquid layer is equal to the normal stiffness of that layer ($k=k_N$).

Applying (3.14) to (3.15) gives:

$$B = -\frac{d\,p}{d\,h/h}$$ (3.16)

Combining (3.13) and (3.16) gives:

$$k = \frac{B}{h_L}$$ (3.17)

The bulk modulus of a liquid is related to the density, ρ and the speed of sound, c of the liquid according to (3.03) rewritten here as,

$$B = \rho c^2$$ (3.18)

Combining (3.17) and (3.18) for a thin layer ($\rho = \rho_L$ and $c=c_L$).

$$k_L = \frac{\rho_L c_L^{\,2}}{h_L}$$ (3.19)

Thus it can be seen that the stiffness of a thin layer is related to its thickness, density and speed of sound. This definition of stiffness can be combined with (3.09) for two cases, $z_1=z_2$ and $z_1 \neq z_2$.

3.5.3.1. Spring Model for $z_1=z_2$

In some applications the material on either side of an interface is the same such as in a artificial hip joint or a piston ring on liner (steel/serum/steel and steel/oil/steel respectively).

Where $z_1=z_2$ equation (3.09) simplifies down to equation (3.20).

$$R = \frac{1}{\sqrt{1 + \left(\frac{2k_L}{\omega z}\right)^2}}$$

(3.20)

Where z is the acoustic impedance of the material on either side of the layer. Figure 3.12 below show the graphical representation of equation (3.20) above.

Applying equation (3.19) to equation (3.20) gives a relationship between layer thickness and reflection coefficient.

$$h = \frac{2\rho_L c_L{}^2}{\omega z} \sqrt{\frac{R^2}{1-R^2}}$$

(3.21)

Thus by measuring the reflection coefficient from a thin layer the thickness of that layer may be determined by using equation (3.21).
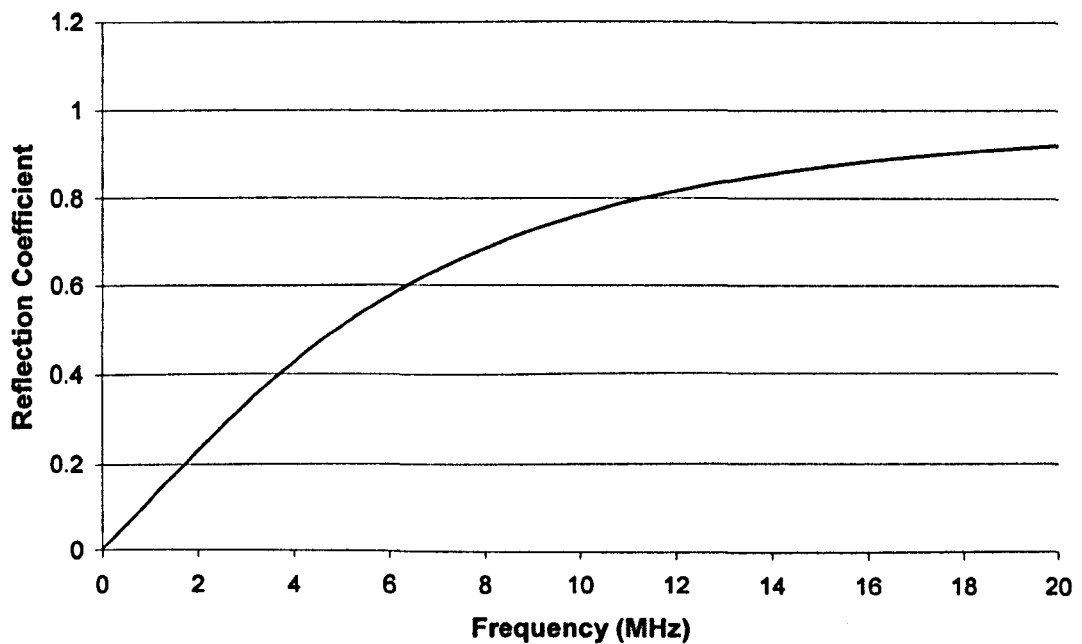
Figure 3.12. Plot of R vs. f for steel/oil/steel for a 1μm oil film. Notice that R_{min} is zero.

3.5.3.2. Spring model for $z_1 \neq z_2$

In most hydrodynamic bearings the materials on either side of the lubricant layer are different. In this case the acoustic impedances on either side of the layer are different and must be taken into account.

Where $z_1 \neq z_2$, equation (3.09) can be represented by equation (3.22) below.

$$R = \sqrt{\frac{(\omega z_1 z_2)^2 + k^2(z_1 - z_2)^2}{(\omega z_1 z_2)^2 + k^2(z_1 + z_2)^2}} \qquad (3.22)$$

for $z_L << z_1$, z_2. For most bearing systems this is true and the equation above holds. Figure 3.13 below shows the graphical representation of equation (3.22) above.

Applying (3.19) to (3.22) gives

$$h = \frac{\rho_L c_L^2}{\omega z_1 z_2} \sqrt{\frac{R^2(z_1 + z_2)^2 - (z_1 - z_2)^2}{1 - R^2}} \qquad (3.23)$$

Thus equation (3.23) gives the thickness of a layer by measuring the reflection coefficient (provided the other variables are known).
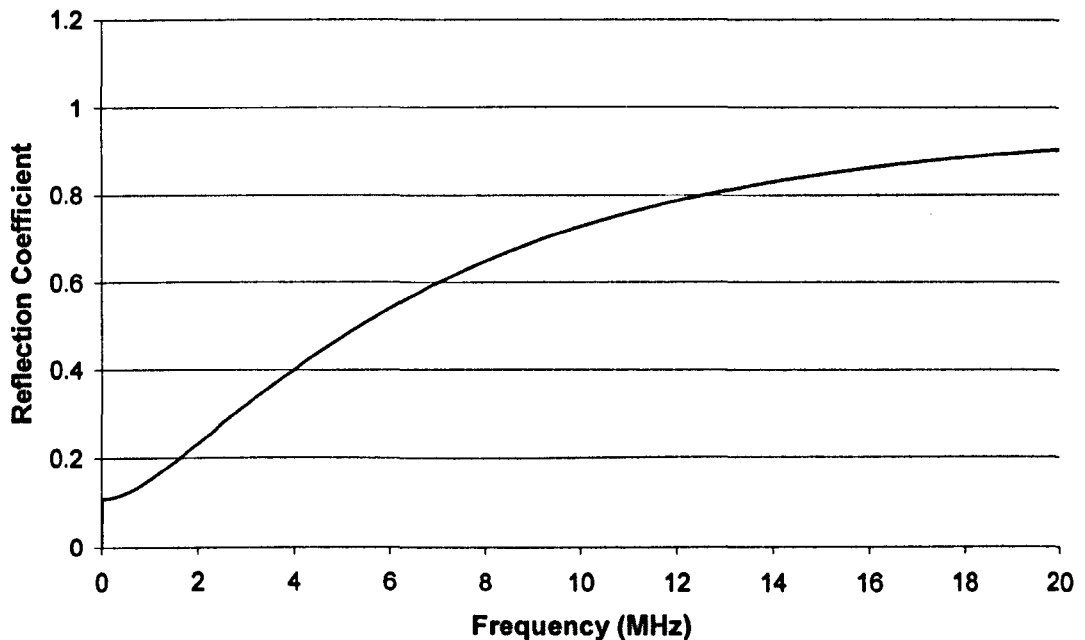
Figure 3.13. Plot of R vs. f for Brass/Oil/Steel for a 1 μm oil film. Note that R_{min} is non zero at zero frequency.

3.5.4. Evaluation of Methods

With each of the layer thickness/wavelength ratios there are corresponding methods of measuring layer thickness. Each of these methods has associated advantages and disadvantages as shown in table 3.4.

Method	Min	Max	Advantages	Disadvantages
Time of Flight	~100μm	∞	• Not effected by temperature. Temperature affects only the amplitude. • No need for a reference. • No upper limit.	• Can only measure thick layers. This technique has a lower limit of approximately 100μm using high frequencies and thus is not suitable for measuring oil film thicknesses in engineering components.
Resonant Dip	~30μm	∞	• Not effected by temperature. This technique measures the frequency that the resonant dip occurs and this is not affected by temperature. • No need for a reference. Again the resonant dip frequency can be measured independent of any reference. • No upper limit.	• Can only measure thick layers (down to about 30 μm using high frequencies). This limits this technique to applications where there are very thick lubricant films.
Spring Model	~10nm	~50μm	• Can measure very thin layers. Theoretically using this technique layers as thin as 10nm can be measured.	• A reference signal is required. • Temperature dependant. • Small measurement bandwidth.

Table 3.4. Comparison of the various techniques

3.5.5. Focus of Research

This research will be primarily focusing on the third of these techniques, the spring model. This is because the majority of the lubricant films found in real engineering components are in the 0.1-50 μm range.

3.5.6. Modelling - Time1

Pialucha [1992] developed an algorithm to accurately predict the response of a layer to an ultrasonic wave. The incident wave from an ultrasonic transducer was considered. When it struck an interface the plane wave was divided up into wave components, each with the same frequency but varying directions of propagation (decomposition). Evaluation of the reflected field was then performed using the global matrix reflection coefficient algorithm to give the magnitude and phase of each reflected plane wave. Each individual reflection coefficient was then summed using an inverse Fourier transform to give the total reflection coefficient. This is then performed for a multi layer system to give a global reflection coefficient from the intermediate layer.

This model was written into a computer program to solve the equations and provide modelling software, Pialucha [1992]. A version of this software (called Time1) has been used in this present work to model the experimental systems that were investigated.

3.6. Conclusions

This chapter has looked at ultrasound and the physical principles behind it. Material properties have been defined and explained and their effect on ultrasound has been discussed. The equations governing ultrasound have been stated and expanded to consider the reflection from thin layers. The physical basis for measuring film thickness using ultrasound has been explained.

Chapter 4:

Generation of Ultrasound

4.1. Introduction

This chapter looks at the generic system required for generating, receiving and processing ultrasonic waves. This includes the sensors, coupling, cabling, pulsing/receiving equipment, digitisers and signal processing/storage.

4.2. Generating Ultrasound

There are several methods of generating ultrasound. These include laser, EMAT and piezo. Piezo induced ultrasound is the most widely used although the others are used in specialist areas. This chapter focuses on the use of piezo to generate ultrasound.

A piezo material is defined as a material that undergoes a physical change in one or more dimensions upon the application of a voltage. Piezo materials also emit a voltage when they undergo a physical deformation. This makes them ideal as sensors where they can emit a voltage proportional to the deformation they experience.

The most commonly used piezo materials are piezo ceramics, but piezo polymers may also used. Piezo polymers have the advantage of low acoustic impedance and can be used in situations where there are acoustic matching difficulties when using ceramic materials (i.e. transmitting ultrasound into skin in medical applications). Piezo polymers also have an advantage of being flexible. This can have advantages in situations where, for example, there is a curved surface (AEA Technology's Fleximat System is an example of

a piezo polymer transducer). The primary restriction in the use of piezo polymers is the maximum temperature that they can withstand – approximately 50°C.

Piezo materials can vary considerably and can have very different properties, both inherent in the material and as a response to external conditions. For this reason a piezo material should be chosen according to the desired response for given conditions.

Piezo ceramic material can come in several forms such as sheets, disks, cylinders, rings, or concave 'lenses' (see figure 4.01 below). It is also possible to coat a material with a piezo ceramic coating (Lee et al [2004]).
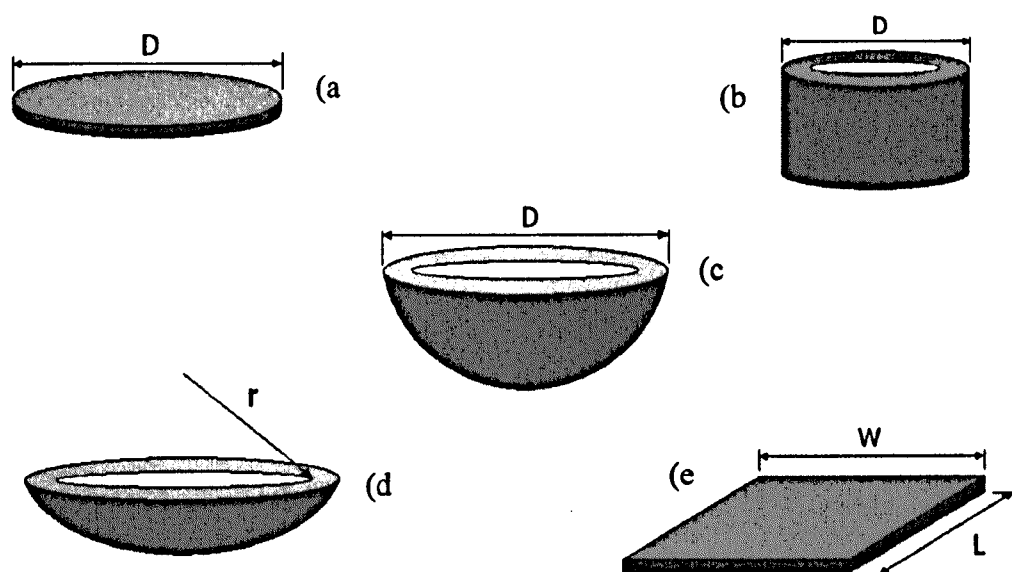
Figure 4.01. Standard piezo shapes used in ultrasound: a) Disc, b)Tube, c)Hemisphere, d)Focal Bowl, e)Plate

4.3. Sensors

In this work piezo materials were used exclusively for generating and receiving ultrasound. The sensors that were used, however, took a variety of forms. Generic NDT sensors are discussed below. Developments made in the used of non standard sensors and piezo elements are discussed in Chapter 5: Measurement System Development.

4.3.1. NDT Sensors

Ultrasound is extensively used in NDT and many sensors have been developed for the wide range of applications that use ultrasonic NDT. NDT sensors vary in size, shape,

bandwidth and frequency but they are essentially similar in construction. Figure 4.02 shows a typical NDT sensor.
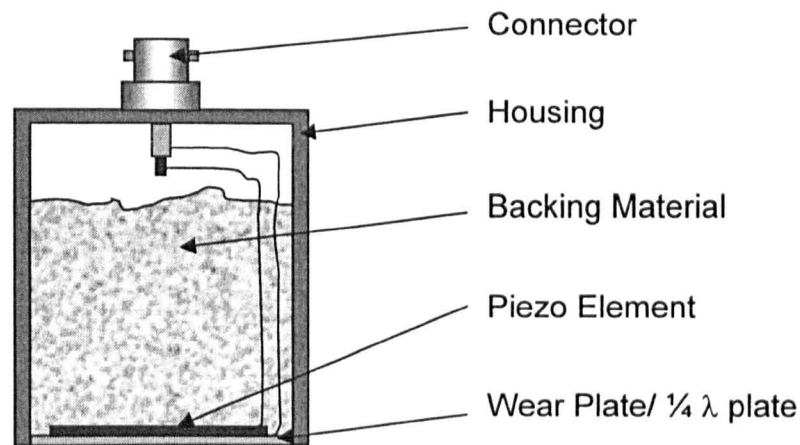
Figure 4.02. The construction of a typical NDT sensor.

4.3.1.1. Coupling

In order to transmit a longitudinal wave from a sensor to the test piece a couplant must be used. The function of the couplant is to transmit the sound wave to the test piece. It must be able to do this in all test conditions without 'conditioning' the incident or reflected wave (or by conditioning either the incident or reflected wave in the same manner for all test conditions).

Typical couplants are water, water-based gel, treacle and adhesive.

- Water is generally used in situations where the sensor has to be focused and the couplant length is expected to vary. It is also used in very high temperature applications where the ultrasonic signal is transmitted along a jet of water. This allows the sensor to remain at a low temperature whilst looking at a high temperature specimen.

- Water-based gel is used with contact NDT sensors. Using a gel allows movement of the sensor whilst maintaining adequate coupling. This method has a disadvantage in terms of signal transmission being dependant on the thickness of the couplant layer. This is because the thickness of the couplant layer is extremely hard to control.

- Treacle, due to its high viscosity, is used to transmit a shear wave from a sensor to the test piece.

- Adhesives are also used to permanently bond sensors to test pieces. The obvious disadvantage with this method is that the sensors have to be sacrificed unless the bond line can be broken non-destructively.

4.3.1.2. Focusing

A sound wave created by a planar NDT sensor tends to 'spread' with distance. That is to say that the spatial resolution increases with distance from the transducer. However, it is possible to a focus a planar piezo (i.e. a flat disc) element by using the refractive effect (see Snell's law in section 3.4.2). This can be done by attaching a piezo element to a 'lens' that will cause the sound wave to be refracted in such a way as to induce focusing. Figure 4.03 shows an arrangement to focus a sound wave from a planar piezo element.
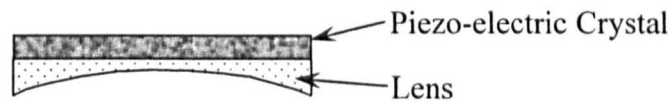
Figure 4.03. Attaching a planar piezo element to a concave lens.

This method is not as efficient as using a concave lens shaped piezo element due to refraction losses (for example see (d in figure 4.01).

In many applications it is desirable to reduce the spatial resolution of the sound wave. The reason for doing this is to look at features that are smaller than the piezo element. The method of reducing the spatial area of maximum sound power is called focusing. This is usually done through having a concave 'lens' shaped piezo element. This has the effect of concentrating the sound energy at the focal point.

The position of the focal point is a function of the frequency of the piezo element, the radius of curvature of the piezo element, the diameter of the piezo element and the material that the sound wave is travelling through. Equation (4.01), quoted in Panametrics [2006], expresses the relationship between these.

$$FS(-6dB) = \frac{1.02Fc}{fD} \qquad (4.01)$$

Where FS is the focal spot size

F is the Focal Length

c is the speed of sound in the material

f is the frequency

D is the diameter of the Element

It can be noted that the size of the focal spot is fundamentally a function of the frequency of the piezo element. Figure 4.04 shows the relationship between frequency of the piezo element and the focal spot diameter.
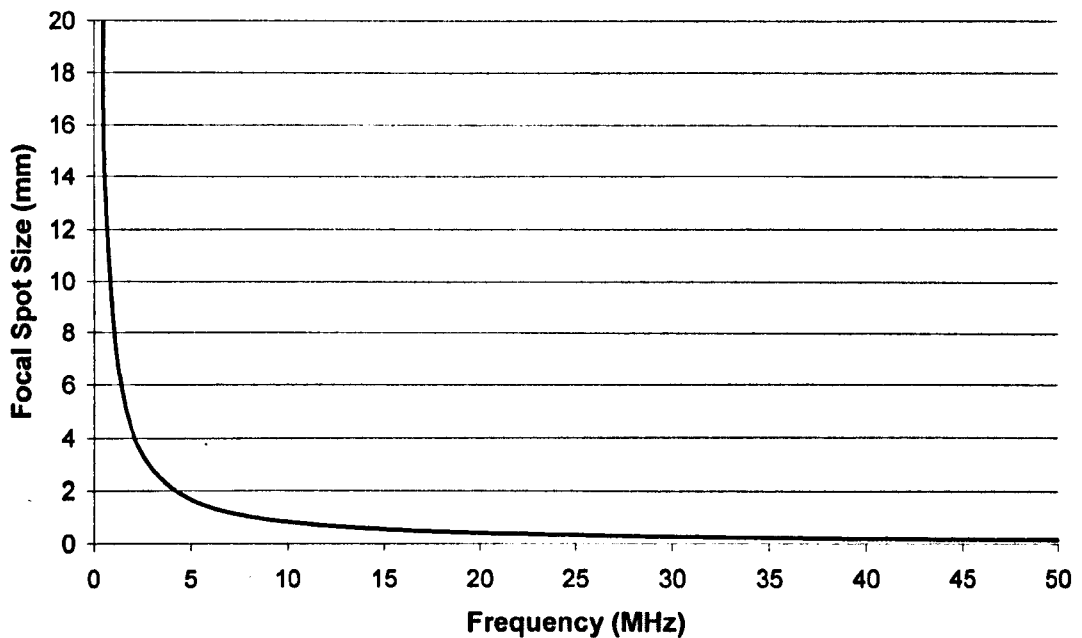
Figure 4.04. The relationship between the centre frequency of the piezo element and the focal spot size for a piezo element of 6mm diameter.

If a focused sound wave travels through an interface having different values of acoustic impedance then the sound wave will be refracted at the interface. This refraction results in the focal length changing as described in equation (4.02), quoted in Panametrics [2006].

$$h_1 = F_t - h_2 \left(\frac{c_2}{c_1} \right) \qquad (4.02)$$

Where: h_1 is the distance of material 1

h_2 is the distance of material 2

F_t is the focal length of the transducer

c_1 is the speed of sound in material 1

c_2 is the speed of sound in material 2

This refraction has the effect of shortening the focal distance as shown in figure 4.05.
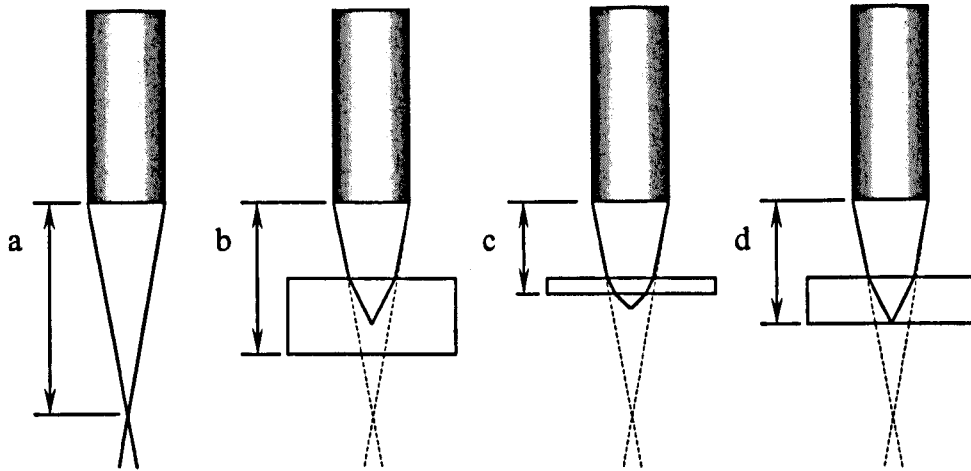
Figure 4.05. Effect on focal distance due to refraction at an interface. Shown are distances a) focal length in water, b) distance to bottom under focused, c) distance to bottom over focused, d) distance to bottom correctly focused.

As a result of this refractive effect, most focusing immersion NDT sensors are quoted as having a specified focal length in water.

4.3.1.3. Temperature Effects

As piezo materials are, on the whole, temperature dependent (see section 5.1.3.2.2), NDT sensors are also temperature dependant. Due to the multi-layer construction of these sensors, they have a particular response to temperature. Each layer in the sensor has a different coefficient of thermal expansion. This limits their maximum operating temperature due to the stresses that can occur in the layers. Exceeding the maximum operating temperature can result in disbonding of one or more of the layers. Usually NDT sensors are rated to a maximum temperature (often around the 60°C mark). It is possible to get NDT sensors that are rated to a higher continuous operating temperature, but generally not above 100°C.

It can be very difficult to quantify the response of a NDT sensor as an increase in temperature can affect the sensor along with other variables such as couplant thickness, couplant contact area and couplant speed of sound. Figure 4.06 shows the temperature response of a 1 MHz transducer with temperature.
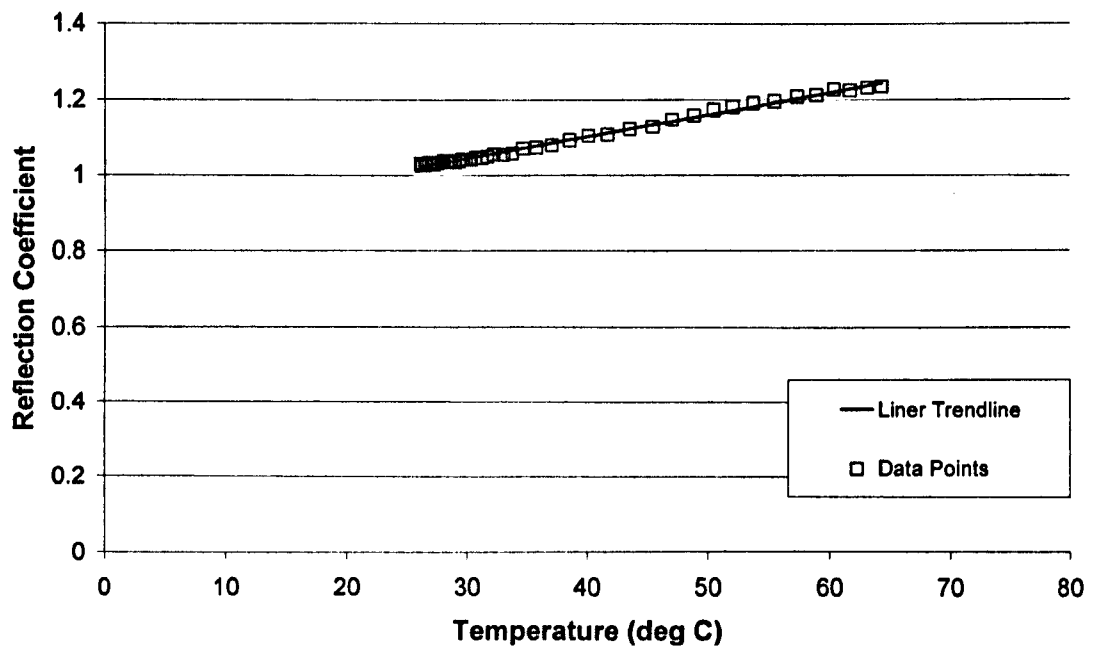
Figure 4.06. Reflection Coefficient Vs Temperature for a 1MHz Ultrasonic Transducer

4.3.1.4.   Frequency Response

NDT sensors are usually constructed to produce a specific frequency response. Generally it is desirable to have as short a pulse as possible (i.e. to minimise the number of cycles in a signal) as the shorter the signal the smaller the defect that can be detected. This is done by damping the piezo crystal to minimise the number of cycles in a signal. This results in a wide band of frequencies that are excited in the sensor. Thus a heavily damped sensor is said to have a wide bandwidth. Figure 4.07 shows a typical frequency response from a NDT sensor.
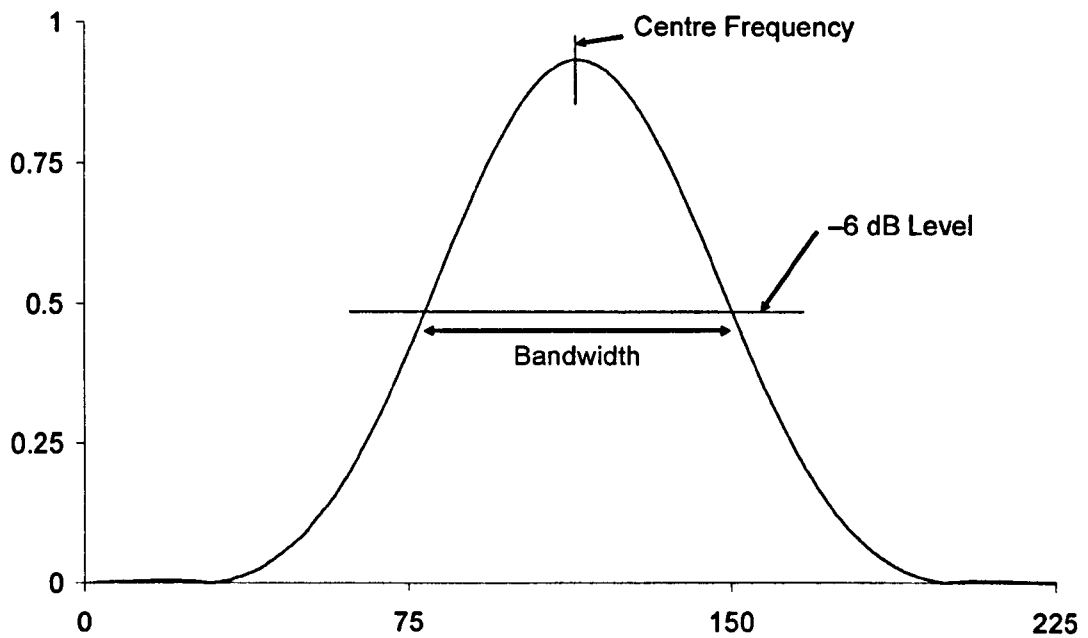
Figure 4.07. Frequency response from a NDT Sensor showing the band width at –6dB.
The bandwidth is about 62%.

Bandwidth is often expressed as a percentage ratio where

$$Bandwidth(\%) = \frac{Bandwidth}{CentreFrequency}$$

(4.03)

For NDT sensors, a bandwidth >90% is regarded as a wide bandwidth sensors. It is possible to get sensors with up to 150% bandwidth, although usually they have 50-70% bandwidth.

Damping has the effect of decreasing the number of cycles in the signal whilst increasing the frequency spectrum, see figure 4.08 for example. Note the decrease in number of cycles in the time domain plot from a) to b) and also the decrease in amplitude in the frequency spectrum plot from a) to b).
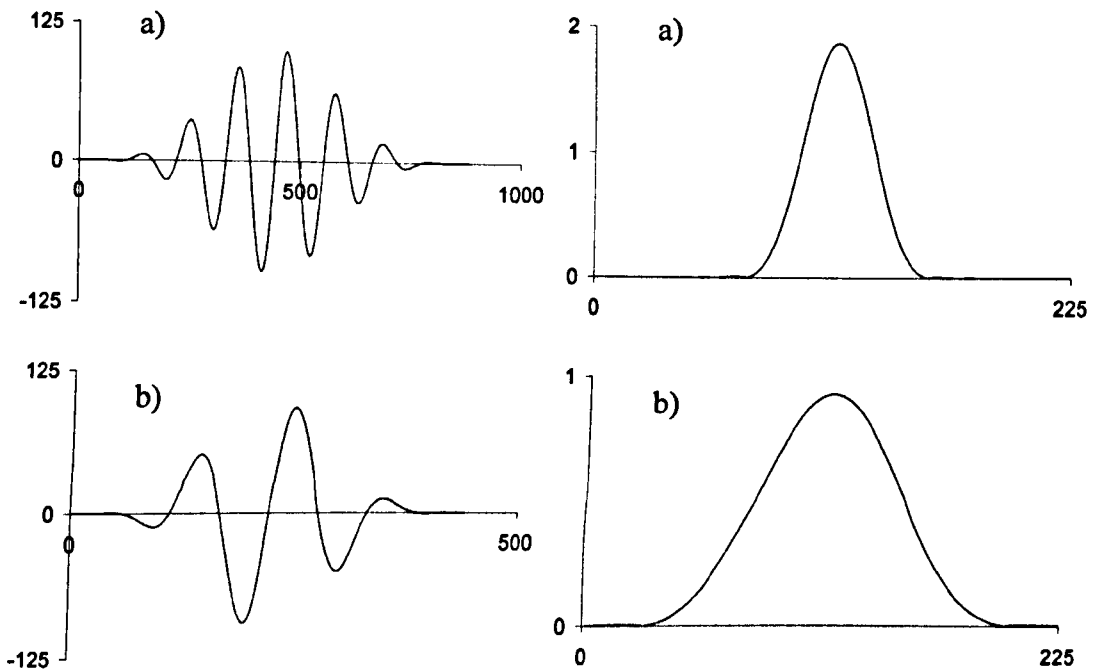
Figure 4.08. a) A relatively undamped ideal signal and its corresponding frequency spectrum, and (b) a highly damped ideal signal and its corresponding frequency spectrum.

In most NDT situations, operators are more interested in the time domain response of the sensors. As has been shown, this is linked to the frequency response of the sensor, the piezo material and the damping in the sensor. NDT sensors usually have a damping material bonded to the back of the piezo element to improve bandwidth.

4.4. Connectors and Cables

Commercial NDT sensors have connectors attached to allow the fitting of a suitable cable for pulsing and receiving the ultrasonic signals. The connectors on the sensors encountered in this project were either industry standard Microdot or UHF. For both of these types of sensors commercial cables were purchased with the required specification in terms of frequency attenuation and capacitive properties.

Microdot cables normally have a small diameter due to the small size of the actual connector. Typically they are 50Ω, 2.5mm diameter. This small size can be beneficial in situations where there is a limitation in the space within a test rig for getting a cable in. Additionally smaller cables have a smaller allowable radius of curvature.

UHF connectors and cables are normally used on larger sensors. A typical cable diameter is 5mm, usually to allow a BNC connector on the other end (BNC connectors are widely used within industry and are standard on most ultrasonic and DAQ devices). These connectors are often found on larger immersion style sensors.

4.5. Hardware

The hardware in an ultrasonic system comprises Pulser/Reciever, Digitiser and PC.

4.5.1. Pulser/Receiver

As the measurement of film thicknesses uses active ultrasound, this requires both pulsing and receiving of high frequency pulses. Figure 4.08 below shows the typical functional blocks within a UPR.
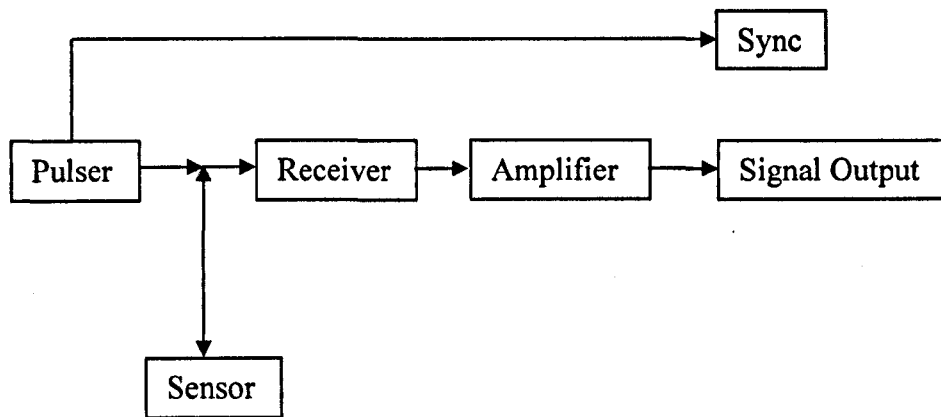
Figure 4.08. Schematic of a pulser/receiver.

4.5.1.1. Pulsing

The pulser generates and sends a configurable pulse to the sensor. Usually the pulse is configurable in the following ways:

- Pulse amplitude, in other words the voltage that is sent to the sensor. This controls the amplitude of the signal that will get sent from the sensor and hence the amplitude of the signal that is received by the sensor.

- Pulse width, in other words the length of the pulse (in time) that is sent to the sensor. This controls the frequency of excitation of the sensor (the wider the pulse, the lower the frequency)

    It is usual to excite a piezo crystal at its natural frequency, or Centre frequency (see figure 4.06). This is a function of the thickness of the crystal. Equation (4.05) describes the relationship between the thickness and the centre frequency.

$$f_p = \frac{c_p}{h_p} \qquad\qquad (4.05)$$

Where f_p is the centre frequency of the piezo element, c_p is the speed of sound in the piezo element (generally around 2000 m/s), and h_p is the thickness of the piezo element. Thus a 10 MHz crystal made from PZT5A1, 0.2mm thick will have a centre frequency of 10 MHz.

Pulsing a sensor to excite it at a specific frequency is achieved by setting the pulse width according to equation (4.06).

$$PW = \frac{1}{2f} \qquad\qquad (4.06)$$

Where PW is the pulse width and f is the desired centre frequency of the transmitted pulse.

Other features of the pulser (that are not generally configurable) that affect the way the sensor is excited are:

- Pulse shape. Common pulse shapes are a spike, a top-hat function and a sine wave as shown in Figure 4.09.
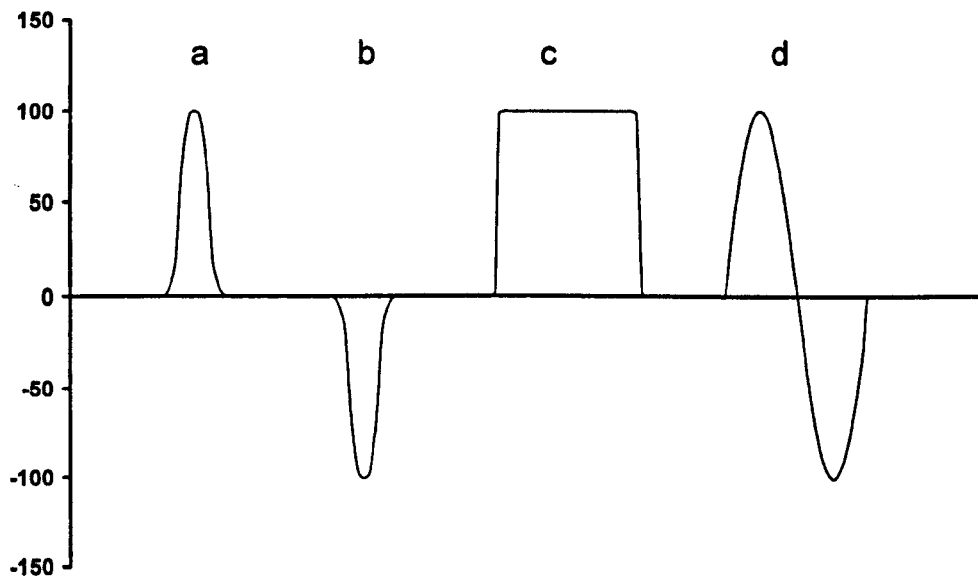
Figure 4.09. Various pulse shapes A) Positive Spike, B) Negative Spike, C) Top Hat, and D) Sine Wave

Of these pulse shapes the negative spike is the most common (especially in older NDT equipment). The top-hat is also popular due to the ease of controlling the

pulse amplitude and width. Some equipment uses an arbitrary function generator (AFG) to input a specific user defined pulse (Indeed an AFG can be used on its own as a pulser for ultrasound except that AFG's tend to have lower voltages of about 10 V and they normally are not able to receive on the same cable as they pulse) before amplifying to a voltage needed to drive NDT sensors. This can be useful in applications where specific sensor excitation at specific frequencies is desired.

- Pulse rise time. This is the time taken for the pulser to go from 0 volts to the specified voltage (i.e. the squareness of the top-hat in figure 4.09). If this is very fast, less than about 5 ns, high frequency oscillations can be initiated in the sensor. Higher frequencies can be filtered out, but may be detrimental to signal quality. This is the reason that the ultrasonic sensor must be matched to the pulsing (and receiving) equipment.

4.5.1.2. Receiving

As the receiver is on the same line as the pulser (in a pitch catch arrangement) a switch is normally used to stop the high voltage pulsing signal (up to several hundred volts in some applications) entering the receiving circuitry and thus swamping the amplifier. Rather, once the high voltage signal has been sent out to the sensor, the receiver switches to 'listen' to the incoming reflected signal from the sensor. This allows the receiver to have a high sensitivity to received pulses without being swamped by the pulsing signal.

As a result of the requirement for pulsers to pulse at high speeds (up to 20kHz) the switching circuitry becomes very complex and costly as very high quality switches are needed if there is to be no degradation of either the pulsing signal or the received signal.

The receiving circuitry consists of an amplifier and a variable gain amplifier. The received signal (of the order of 1mv) is amplified to the order of 1V. The variable gain amplifier then amplifies the signal (the quantity of amplification is specified by the user) ready for digitisation.

4.5.2. Digitiser

The received signal is digitised so that it can be processed in a computer. Digitisation can either occur in a digital oscilloscope, a dedicated digitiser or in a computer on a PCI card. In order to capture enough information to accurately represent the analogue wave form

the digitiser needs to be ten times faster than the signal. This will give ten data points per cycle (see figure 4.10). Thus a 20 MHz signal needs a 200 MHz digitiser. It is possible to work with lower frequency digitisers using sophisticated techniques for analysis.
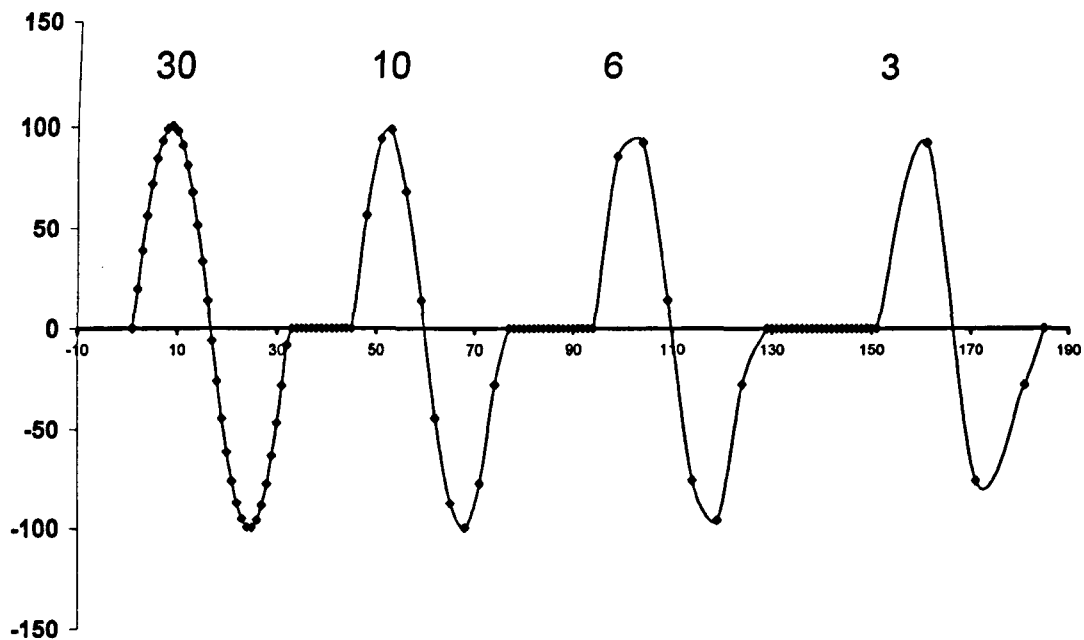
Figure 4.10. Sine waves with 30, 10, 6, 3 data points respectively.

4.5.3. Computer

The purpose of the computer in the system is to provide signal processing capability for the signals received. This signal processing can be simple (for example peak detection to measure the time between two peaks) or complex (for example Joint Time-Frequency Analysis for examining time dependent frequency responses of pulses). It is not essential to have a PC for data processing as many of today's FPGA's and DSP chips are capable of being programmed for specific signal processing. However, given the low cost and flexibility offered by using a PC with customisable software, this is generally the most attractive option.

4.5.4. Combined systems

There are several combined solutions on the market for pulsing, receiving and processing ultrasonic signals. These range from purpose built boxes housing all the separate relevant components to custom made PCI cards with pulser, receiver and digitiser all on board. Currently the PCI based systems are very popular due to several factors: compact units, lower cost than individual units, ability to fit into existing computing hardware and the

ease of building a multi channel system. NDT Solutions Ltd is an example of a supplier of this type of equipment.

4.6. Conclusions

This chapter describes the various components in an ultrasonic system required for measuring film thicknesses. NDT sensors have been discussed with considerations such as temperature, bandwidth and focusing explained. The main connectors and cables used to connect NDT sensors have been mentioned. The operation and configuration of ultrasonic pulser/receivers has been described. The key points in digitising the ultrasonic signal have been discussed. Finally, computers and combined systems have been explained.

Chapter 5:

Measurement System Development

Chapter 4 detailed the generic details for generating and receiving ultrasound and some of the physical principles to be considered. This chapter deals with the key achievements in the development of the lubricant film thickness measurement system. There are two primary areas in the development: Hardware and Software. These are dealt with in turn in the following pages.

This chapter only details the generic developments and apparatus used in the following measurement experiments in chapters 7-9. Each experiment required some specific modifications in order to implement the technology. These developments are discussed with the experiment in the relevant chapter.

5.1. Hardware

In Chapter 4 the various parts of the measurement system were described in principle. In this section the actual equipment used is specified, steps in development are described, and the reasoning behind hardware decisions is discussed.

5.1.1. UPR

A NDT Solutions Ltd UPR (ultrasonic pulser receiver – a discontinued product at time of writing) was used exclusively in the experiments for pulsing and receiving. Figure 5.01 below shows a picture of the UPR. The instrument is designed for the research environment with a receiver bandwidth of 0.1MHz to 70MHz. It has an excellent signal to noise ratio, high speed pulse repetition rate (up to 10kHz), high frequency pulsing

(configurable up to 35MHz and a high frequency setting above 35MHz), and two software selectable channels (available as pitch-catch or pulse-echo). The UPR came with software (WinUPR) for controlling it over a parallel port. During experimental work a LabVIEW® driver was developed and written to allow control of the UPR within the LabVIEW® envrioment.

Figure 5.01. NDT Solutions Ltd UPR (with Laptop on top).

5.1.2. Digitiser

High speed digitising equipment is invariably expensive (although prices are coming down) and so there were some restrictions in the options available for digitisation. Initial research used the available equipment in the lab.

5.1.2.1. LeCroy Digital Oscilloscope

In some of the initial experiments a LeCroy WaveRunner LT342 (see figure 5.02) was used to capture and digitise the signal from the UPR. The Oscilloscope had a 500MHz digitiser on board. The signal was shown on screen before part of it was selected and transferred via GPIB to the PC. The only function that the oscilloscope served was in digitisation.
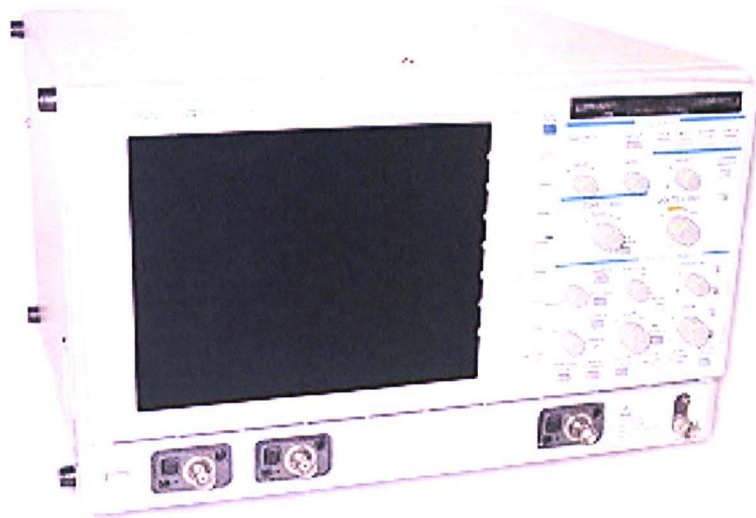
Figure 5.02. The LeCroy LT342 Digital Oscilloscope[1].

In order to acquire data from the oscilloscope programmatically, software was written in LabVIEW® to control the hardware settings on the oscilloscope, capture data and download over GPIB. Example software is included in appendix 4.

5.1.2.2. Gage Digitiser PCI Card

One of the disadvantages in using the oscilloscope mentioned in section 5.1.2.1 is its size and weight. This becomes troublesome when testing in a confined space or travelling in an aeroplane. For this reason a 500MHz Gage Digitiser PCI card (shown in figure 5.03 below) was purchased and used as an alternative in some of the experiments to capture the data. This was mounted in a compact PC to provide a compact instrument for ease of transport. The PCI card was supplied with existing software for operation as a standard oscilloscope. In order to use this hardware for film thickness measurements specific software was written to control the hardware and acquire the data. The software was written in LabVIEW® and an example is included in appendix 5.

---

[1] Taken from http://www.atecorp.com/Equipment/Lecroy/LT342.jpg on 25/01/08
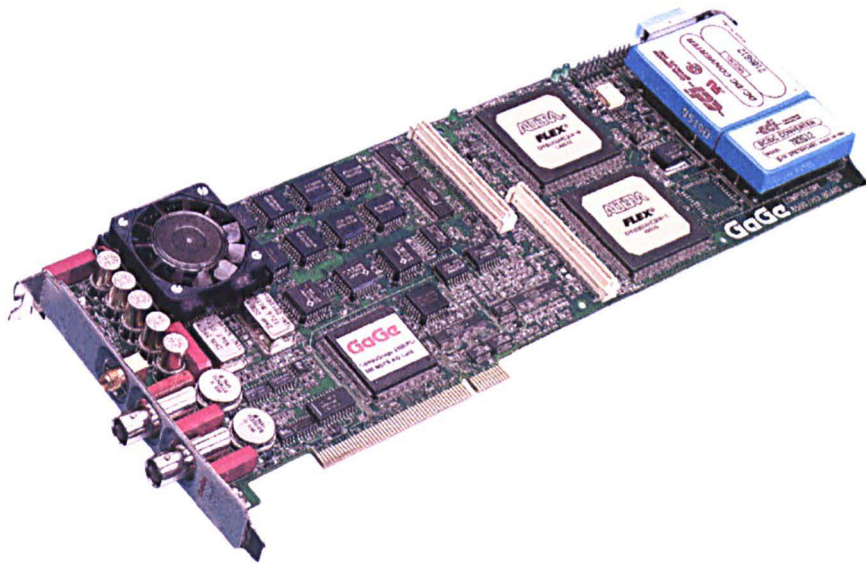
Figure 5.03. Gage PCI digitiser card[2].

5.1.3. Sensors

There were two major contributions in the area of sensors over the course of this project. Firstly the use of low frequency sensors, and secondly the use of piezo elements as sensors.

5.1.3.1. Low Frequency

During the first investigation into fluid films in journal bearings it was discovered that there was a range of film thicknesses associated with the bandwidth of the ultrasonic transducer. Figure 5.04 below shows the predicted response of a range of lubricant films to an ultrasonic wave. Typical simulated bandwidths of two transducers are shown on the graph in grey. The lower bandwidth is approximately 0.5-1.5MHz. Assuming a centre frequency of 1MHz the bandwidth is 100%. The upper bandwidth is approximately 4.5-10.5MHz. Assuming a centre frequency of 7MHz the bandwidth is 86%. These are in the range of standard commercial NDT transducers of these centre frequencies.

---

2 Taken from http://www.gage-applied.com/Products/PDF/compuScope_8500.pdf on 25/01/08
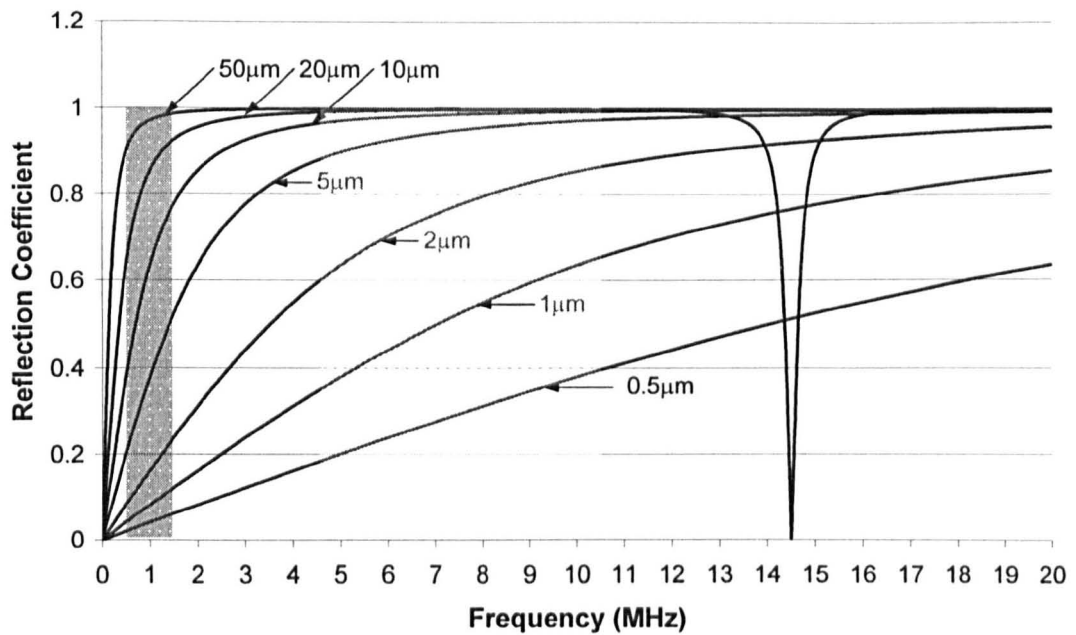
Figure 5.04. Reflection coefficient vs frequency for a range of film thicknesses. Two transducer bandwidths are shown in grey.

It will be noted from figure 5.04 that the sensor with the lower frequency bandwidth will be able to measure films from approximately 1μm to 50μm. The sensor with the higher frequency bandwidth will be able to measure films from approximately 0.1μm to 8μm. Both of these examples assume a noise limit of 0.05<R<0.98. This means that a sensor with a lower frequency will be able to measure a range of thick films whilst not being able to measure very thin films. The sensor with the higher frequencies will be able to measure a range of thinner films whilst not being able to measure very thick films.

This development in the matching of sensor bandwidth with the expected films in a particular application, and in particular of using low frequency sensors for monitoring a wide range of applications, resulted in the application of this technology to a wider range of applications than had previously been considered.

5.1.3.2. Piezo Elements

During the project the need for permanent bonding of the transducers to the substrate led to the use of bare piezo elements. This was driven by the risk of damage to expensive NDT sensors (typically £400+ each) and the low cost of bare piezo elements (typically

£2 each). Some samples were obtained from Morgan Electroceramics Ltd[3] (see figure 5.05) and tested for their suitability in the application of measuring oil films. The crystals are sliced from a rod of ceramic, where the thickness corresponds to the free resonating frequency, f_r according to

$$fr = \frac{N}{t}$$
(5.01)

Where N is the frequency constant of the piezo material

T is the thickness of the piezo material

For many standard ceramics N is approximately 2000kHz/m, giving a value of f_r of 10MHz for a piezo element 0.2mm thick.

Figure 5.05. A picture of bare piezo element beside a pencil tip.

After the ceramic disk is sliced from the ceramic rod, it is entirely coated in a thin layer of silver to act as an electrode. In order to provide positive and negative terminals, a track is burned using laser ablation in the top surface in the shape of a 'D'. This then allows for the connection of the positive and negative cable on only one side of the sensor. These type of electrodes are known as 'wrap around electrodes'.

5.1.3.2.1. *Coupling*
Bare piezo elements can be very small, contain negligible internal damping, require attachment of connecting wires and have a low unit cost. Due to these factors adhesive bonding is the most satisfactory method of coupling (as opposed to mechanical clamping or soldering). Adhesive bonding provides the following:

---

[3] See http://www.morganelectroceramics.com/ accessed 23/01/08

- Support and mechanical strength to an otherwise frail and brittle material

- Damping of the element

- Minimal variation in transmission of sound due to variable coupling.

The method of coupling is very important when considering the frequency response of the piezo ceramic sensors. If the bond line is too thick then there will be less mechanical damping and a narrower frequency bandwidth as well as poor transmission of sound energy into the component. If the bond line is thin then there is good damping, a wide frequency bandwidth and good transmission of energy into the component.

A range of adhesives were tested over the course of the project to determine their suitability for use in sensor bonding. Two primary adhesives were identified - Resist200 (a cyanoacrylate adhesive) from Holdtite Ltd for low temperature work (up to 90°C), and MBond 600(+610) (a two part epoxy adhesive) from Vishay Measurements Group UK Ltd for higher temperature work (up to 200°C).

5.1.3.2.2. *Temperature Effects*

Piezo materials undergo both a change in dimensions with temperature (themal expansion/contraction) and a change in the piezo effect with temperature. Both of these need to be considered when looking at the effect of temperature on the output of piezo sensors. The coefficient of thermal expansion for piezo materials can vary anywhere between -4 E-06 K^{-1} to +11 E-06 K^{-1}.
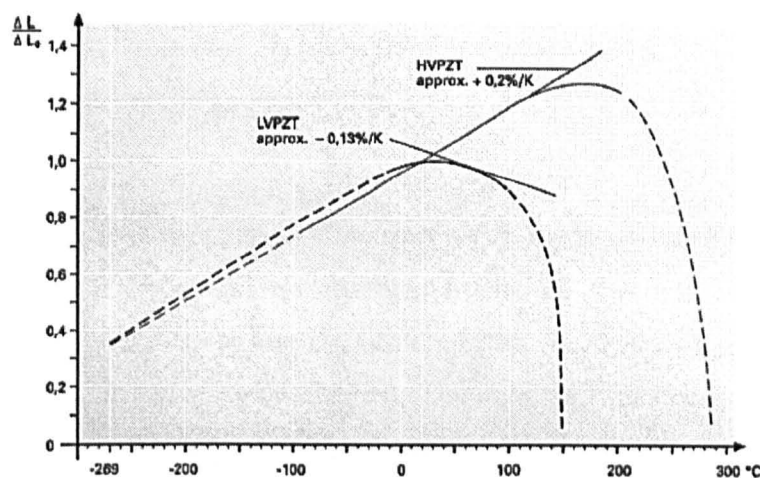
Figure 5.06. Piezo effect against temperature for high voltage lead zirconate titanate (HVPZT) and low voltage lead zirconate titanate (LVPZT)[4].

---

[4] Taken from http://www.physikinstrumente.com/tutorial/4_36.html on 07/10/2007

Due to these changes with temperature, a method of temperature calibration is required for using these sensors in applications with higher temperatures. Section 6.3 details some approachs used to auto calibrate for temperature.

5.1.3.2.3. *Frequency Response*

Due to no external damping, piezo elements have a very narrow bandwidth. However, when a piezo element is bonded onto a machine element the front face of the sensor is constrained and damping is introduced. Figure 5.07 below shows the predicted response of a piezo ceramic that has been bonded to various substrates with different acoustic impedances.
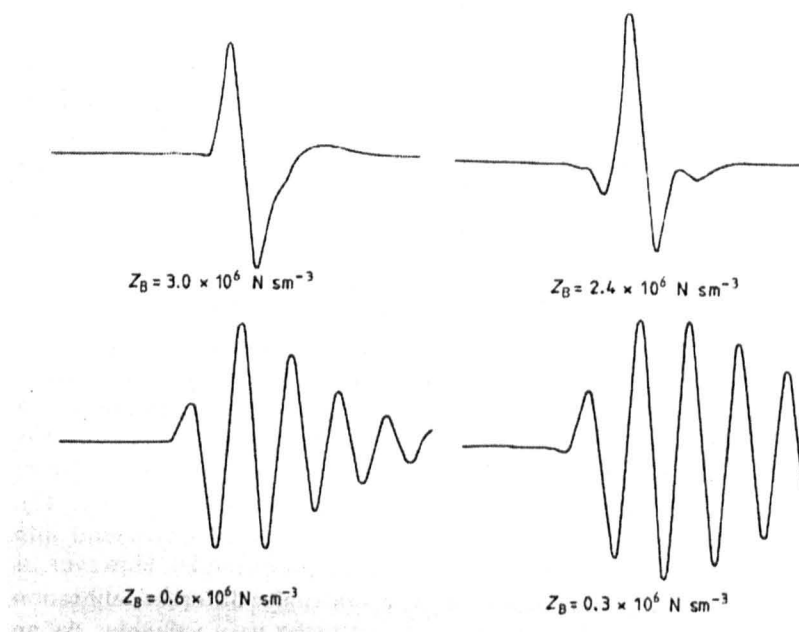
Figure 5.07. Predicted response of a piezo ceramic bonded to various backing materials with varying acoustic impedances (Silk [1984], p44).

5.1.4. Cables

In addition to the cables mentioned in section 4.4, a range of other cables were used during testing which depended on the constraints of the test rig, any required modifications to a component or test rig, and the effect on the transducer. The range of cables was linked to the use of piezo elements. The lack of connectors on piezo elements removed any restriction on the type of cable used.

It was found that the type, size, length and electrical properties significantly affected the operation of the sensor. These effects can be understood by modelling the sensor and

cable as a resonant electric circuit. Mason [1948] formulated a model that has been widely used to understand the behaviour of piezo sensors.

When introducing a cable into the modelled circuit capacitance, inductance and resistance are introduced into the circuit. Silk [1984] describes equation 5.02 below for considering the effect on the resonant frequency of a sensor circuit from the introduction of an inductance L:

$$F_T = 1/2\pi\sqrt{LC_o} \qquad\qquad (5.02)$$

Where F_T is the resonant frequency

L is the introduced inductance

C_o is the clamped capacity of the sensor

This led to the careful selection of cables to maximise the sensitivity of the sensor by setting its resonant frequency.

5.1.5. Computer

Two experimental setups of the apparatus were used during the experiments carried out in chapters 7-9.

In the first case, a personal computer was used to receive the data from the oscilloscope control the settings on the UPR and process the data. A National Instruments GPIB PCI card was installed on the PC to control and receive data from the oscilloscope across the GPIB interface.

In the second case, a compact industrial computer was used to house the Gage digitiser card, control the settings on the UPR and process the data.

5.1.6. Tachometer

In most engineering components that have a lubricant film, the film thickness is a function of external parameters such as speed and load. In order to monitor speed a laser tachometer (manufactured by Compact Instruments Ltd) was used to read revolutions per minute (rpm) of a shaft. This was recorded and saved to file with the film thickness to give film thickness vs speed for the experiment. The laser tachometer is non-

contacting and uses reflective tape on the shaft as the trigger the rpm reading. This results in one trigger per revolution. The hardware in the tachometer converted this trigger to a rpm reading.

The laser tachometer was supplied with a windows driver and application for reading film thicknesses. In order to correlate measurements of film thickness with speed a separate LabVIEW® driver was written to incorporate the speed measurement into the online film thickness measurement software. An example of the driver developed is shown in appendix 2.

5.2. Software

5.2.1. Labview Environment

LabVIEW® (by National Instruments Inc.) is a versatile software package that allows the user to quickly and easily build customised software to both control hardware and manipulate data. Sophisticated building blocks for signal processing are included within the program to speed up programming time and reduce debugging time. A program that runs in the LabVIEW® environment is called a Virtual Instrument (from here on called a Vi). Vi's can use other Vi's as building blocks as shown in figure 5.08. This allows the programmer to create reusable code that can quickly be swapped in or out for another piece of code.
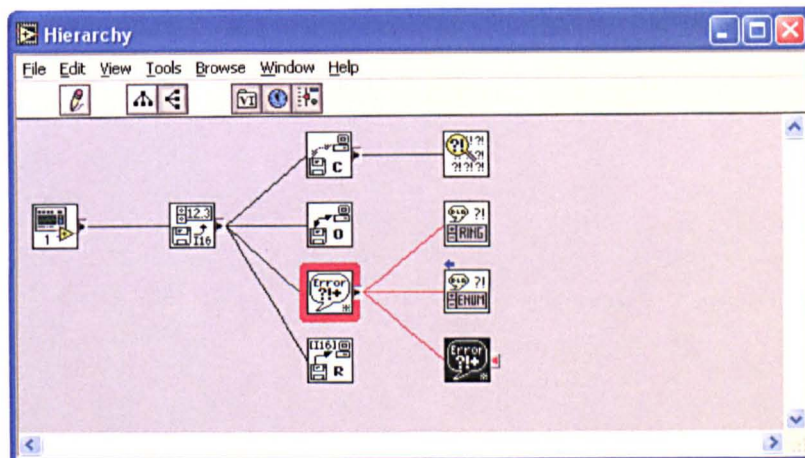
Figure 5.08. The hierarchy within a Vi made up from other subVi's.

5.2.2. Control Software

The UPR is controlled via windows software (WinUPR.exe) over the parallel port on the computer. In order to streamline the control of hardware and software signal processing, LabVIEW® vi's were written to interface with the windows dll file for controlling the UPR. Appendix 3 contains the code for the control of the UPR.

5.2.3. On-line Film Thickness Calculation

The software for signal processing and calculation of film thickness in real time was written in LabVIEW®. Signal processing tools within LabVIEW® such as the FFT algorithm were utilised along side bespoke LabVIEW® algorithms for calculating film thicknesses. The bespoke LabVIEW® algorithms that were created were based upon the equations governing ultrasonic reflection at a thin layer as described in section 3.5. Figure 5.09. below shows the flow of data within the code from oscilloscope initialisation right through to film thickness calculation. Appendix 4 contains example code for online film thickness measurement.
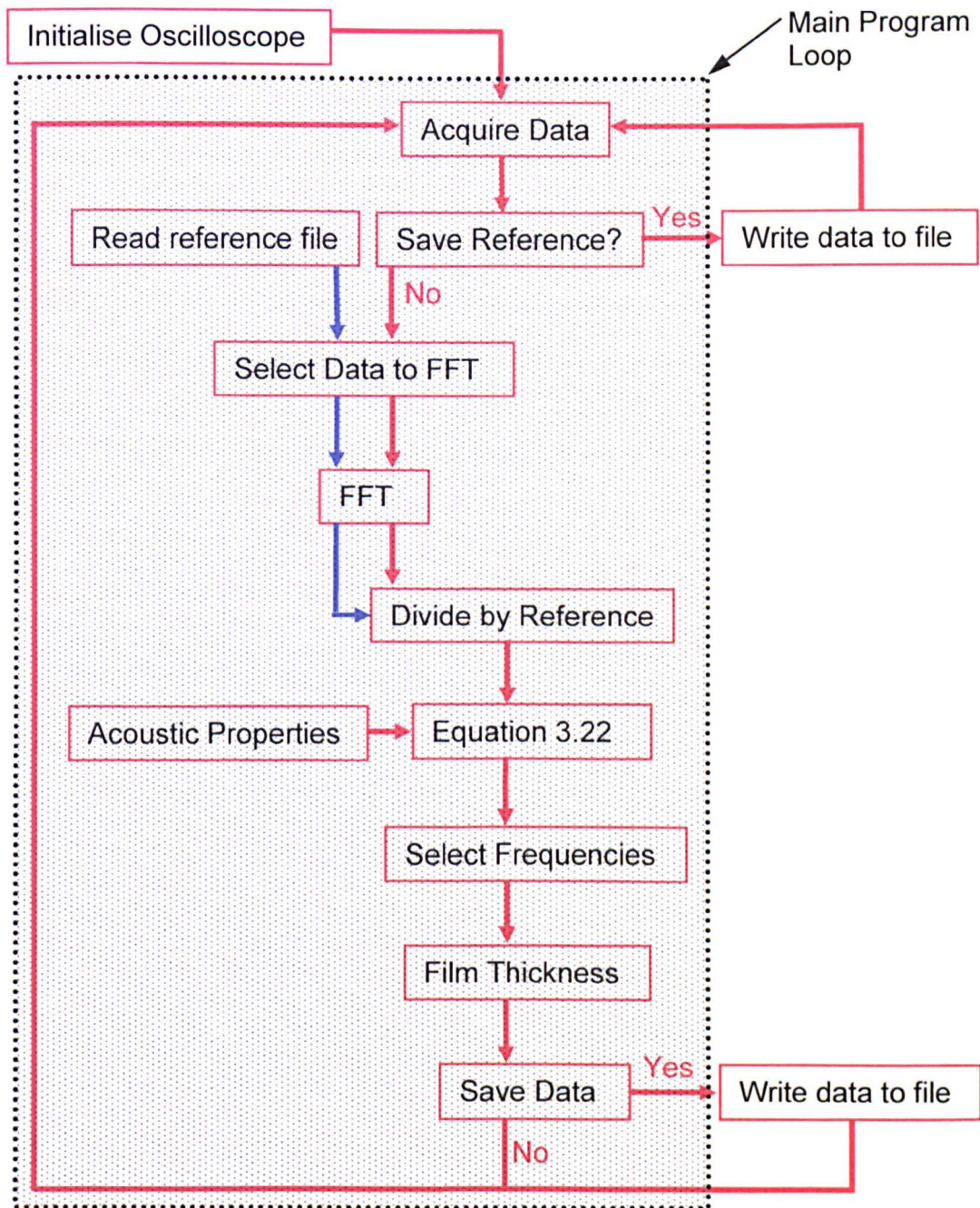
Figure 5.09. Flow diagram of software for calculating film thickness.

5.2.4. Post-Processing Film Thickness Calculation

Software was written in LabVIEW® to handle the data that was captured. Due to the high rate of data capture in some applications, the data files were very large, typically 400 to 600MB (for a recording lasting approximately 1 minute). The software firstly had to open these files one line at a time (attempting to open files of this size into memory resulted in the computer crashing, unsurprisingly). Each line of the file consisted of approximately 200 pulses, each with 1002 data points. Each pulse was extracted from this data stream, converted to the frequency domain, put through the spring model algorithm converted to film thickness. Figure 5.10 shows the data flow in the post processing software. Example code is included in Appendix 5.
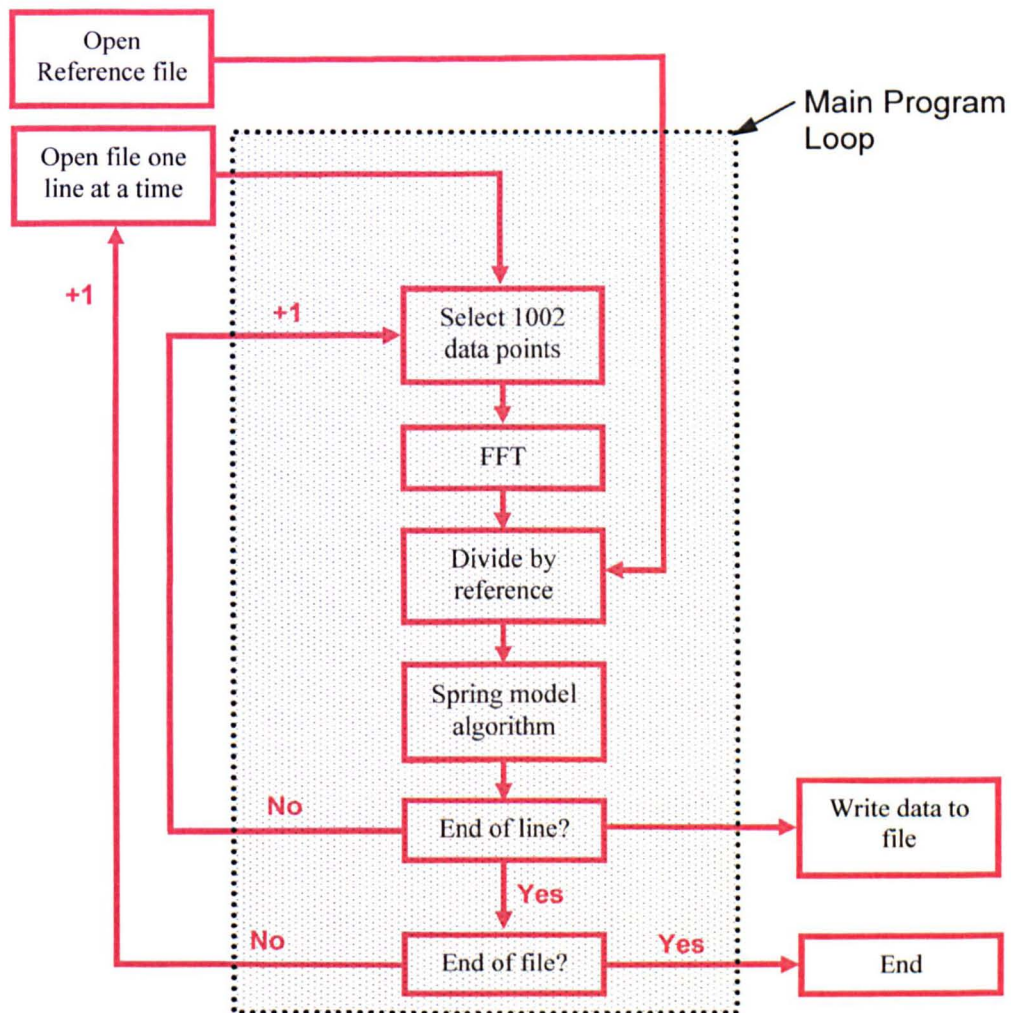
Figure 5.10. Schematic of data flow in post processing software

73

5.2.5. Modelling - LabVIEW®

Using the equations developed by Tattersall [1973], a further computational model to Time1 was written in LabVIEW® (a graphical programming package from National Instruments) called USM. The software modelled an ultrasonic pulse and the response of that pulse in both the frequency and time domains to various lubricant film thicknesses. The software also allows the selection of a real ultrasonic pulse and computes the modelled response of that pulse to selected lubricant film thicknesses. Attenuation parameters, simulated system noise and bandwidth limits can also be added to accurately simulate real world signals and film thickness measurements. Figure 5.11 below shows the user interface of the software and a copy of the software is included in Appendix 6. Figure 5.12 below shows the data flow and schematic of the program.
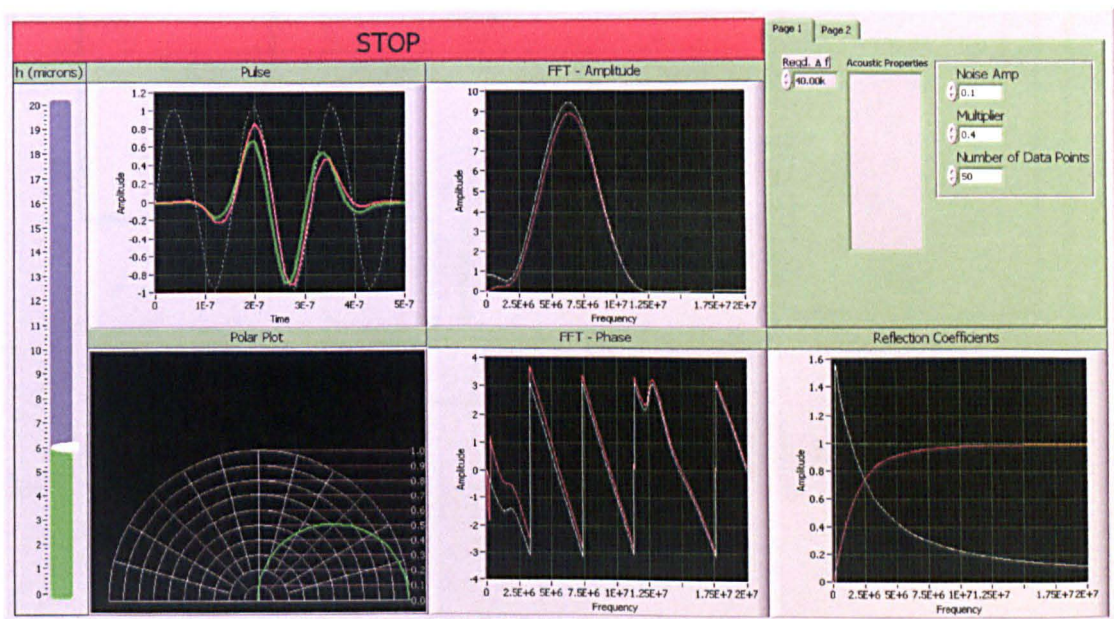
Figure 5.11. Example user interface of the USM software.

The film thickness is set using the slider on the left. The frequency, noise and bandwidth can be defined using numeric inputs. The reflection coefficients for both amplitude and phase of the signal are calculated and shown in the bottom right corner. Using these reflection coefficients the frequency spectra of amplitude and phase are calculated as shown in the top and bottom centre graphs in figure 5.11 respectively. Finally the response in the time domain is calculated via an inverse FFT and shown in the top left-hand corner (red pulse – input, green pulse – calculated output, and dashed line – sine representation of the centre frequency of the input pulse).

74
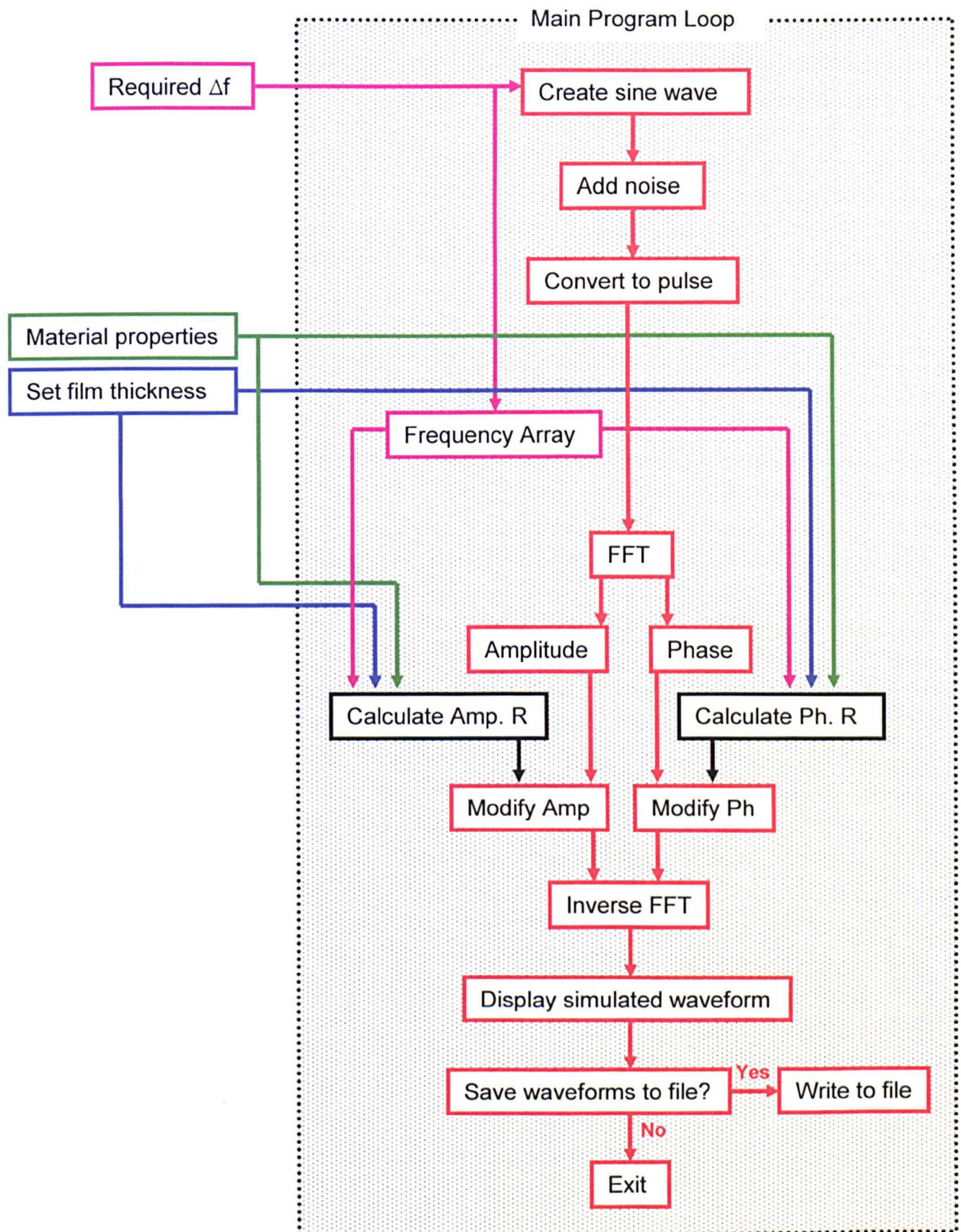
Figure 5.12. Schematic of USM software

5.3. Conclusions

This chapter has described the development of the measurement system. The actual UPR, digitiser, tachometer and computer used during testing has been mentioned. Significant developments in sensors, cable selection and software development have been described and explained.

Chapter 6:

Implementing Measurements

This chapter describes some of the practical issues in applying the theory described in chapter 3 to real engineering components. In the first half of the chapter (sections 6.1-6.2) issues such as material properties and reference signals are discussed. Problems faced in industrial environments are described and methods of measuring material property values are described.

In the second half of the chapter (sections 6.3-6.4) some consideration is given to the issue of calibration (where there is an external influence affecting the measurement) and validation (confirming that the measured value is the actual one).

Finally an example measurement is shown demonstrating the steps that are gone through in order to measure film thickness.

6.1. Material Properties

Implementing sections 3.4 and 3.5 to real engineering components necessitate resolving several experimental issues in determining the various material properties of the components used in a 'bearing system'.

6.1.1. Speed of Sound of Materials

Manufacturers of engineering components often specify the material properties of the material that a component is manufactured from. However, often the speed of sound is

not a property that is often specified. In this situation it is possible to use equations such as 3.02 (or alternatives if a special geometry) to determine the speed of sound.

In some cases the speed of sound is not known and a direct measurement of the speed of sound in the component material is required. Usually the thickness is known (for example measured by a Vernier calliper) and the time it takes for a sound wave to pass through the material is measured, giving the speed of sound.

It should be noted that it is only important to know the speed of sound in the bearing materials if the spring model is being used to measure the oil film thickness. If it is possible to measure the oil film using the resonant dip technique then the speed of sound in the bearing material is not needed.

6.1.2. Density of Materials

The density of materials used in engineering components can be difficult to measure. This is due to the requirement to accurately measure the weight and volume. Fortunately, in the applications considered in this project, manufacturers specified the density of the various materials used.

In applications where the density is not known it is possible to calculate the density by measuring both the reflection coefficient and the phase from a range of oil films between a material with known acoustic properties and the material with the unknown material properties.

6.1.3. Acoustic Impedance of Materials

In some applications the acoustic impedance of a material is not known. It is, however, sometimes possible to measure the acoustic impedance of a material using equation 3.08. If R is measured and one of the acoustic impedances is known then the other acoustic impedance can be calculated. This can be used in situations where the speed of sound, density or both are unknown.

6.1.4. Attenuation of Materials

In most of the applications considered in this project, the materials were highly homogeneous high quality materials. This allows for the transmission of ultrasonic signals with ease. Some bearing materials, however, are designed to have a coarse hard

and soft structure. An example of this is the use of lead chunks in a copper/bronze matrix. The lead acts as a solid lubricant in the event of contact between the stationary and moving parts. The copper/bronze acts as a strong support material. Ultrasonically this material can be highly attenuative. In some applications it can be almost impossible to pass an ultrasonic wave through all but the thinnest sections.

In applications such as these it is possible to insert a plug (see figure 6.01) into the bearing of sufficiently similar mechanical properties, but radically different acoustic properties. This then allows for the transmission of ultrasound into the bearing interface and the measurement of oil films.
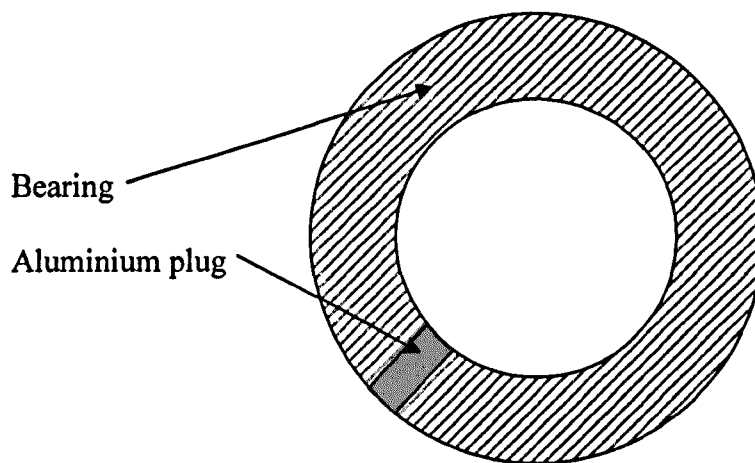
Figure 6.01. Schematic of an aluminium plug inserted into a bearing.

It should be noted that this technique invalidates the non-invasive nature of the ultrasonic technique.

6.1.5. Speed of Sound of Lubricants

To determine the oil film thickness in a bearing according to equation 3.20 it is necessary to know the speed of sound in the lubricant. In general lubricant oils have a speed of sound in the range 1250-1450m/s. Determination of the speed of sound of a lubricant is a relatively straight forward experiment where depth of lubricant is divided by the time it takes an ultrasonic wave to travel through that distance. Examples of a range of liquids is shown in table 6.01 below. It will be seen that there is some variation in the speeds of sound in the various liquids. This is due to the bulk modulus of the liquid and not the viscosity (for longitudinal waves. There is a relationship between viscosity and speed of sound for shear waves).

Oil Type	Speed of Sound (m/s)
Castor Oil	1480
Diesel Oil	1250
Linseed Oil	1770
Motor Oil (SAE 20)	1740
Olive Oil	1430
Paraffin Oil	1420
Paraffin (15° C)	1300
Petroleum	1290
Silicone Oil (25° C)	1350

Table 6.01. Speeds of sound for various oils[1]

During testing the speed of sound in the lubricants was measured using a measurement block similar to that shown in figure 6.09. The use of this measurement device also allowed the acoustic properties of the lubricant to me measured over a range of temperatures by placing the measurement device in an oven.

6.2. Reference signals

In order to calculate film thickness the amplitude of the reflected signal must be compared to the reference signal. The reference is taken when the bearing is disassembled or adjusted to give an air gap in the bearing. This allows the reference to be taken and stored for a bearing/air interface. It is obviously relatively simple in the lab to take a reference. In industry, however, this is a more troublesome task. Machines cannot simply just be stopped and stripped down to obtain a new reference. It is required that the reference be constant at any point in the measurement process. I.e. the reference at the start of the test procedure must be the same as the reference at the end of the test procedure.

---

[1] Taken from http://www.ndt-ed.org/GeneralResources/MaterialProperties/UT/ut_matlprop_liquids.htm on the 01/04/08

In practice during this project, sensors were only be applied to components when they were disassembled. This allows a reference pulse to be taken and recorded. Section 6.3 below deals with situations where the reference pulse (i.e. the amount of acoustic energy being transmitted into a component) may change with operating conditions.

6.3. Calibration

There are several factors that affected the robustness of the measurement system:

- As has previously been discussed, piezo materials are sensitive to temperature.

- The strength of the adhesive joint is affected by temperature.

- The operation of the sensor is sensitive to changes in the electrical properties of the hardware used.

- The acoustic properties of the lubricant may change with varying operating conditions.

In situations where these factors are present a method of calibration is necessary to give confidence in the results. The following four sub-sections 6.4.1-6.4.4 detail several methods of sensor calibration that were used during experimental testing. Section 6.4.5 details a method of calibration for changes in the acoustic properties of the lubricant.

6.3.1. Calibration-Free Resonant Dip

This first method of calibration is, strictly speaking, not a method of calibration, rather a calibration free method. Figure 6.02 shows the FFT response of several pulses from a selection of oil films. It can be noted that the location of the dip is a function of the layer thickness and the speed of sound of the layer. This dip is independent of amplitude (i.e. the ratio of amplitudes is not a function of layer thickness). Thus in the event of a change of amplitude (due to a temperature increase, for example) the measured layer thickness stays constant.
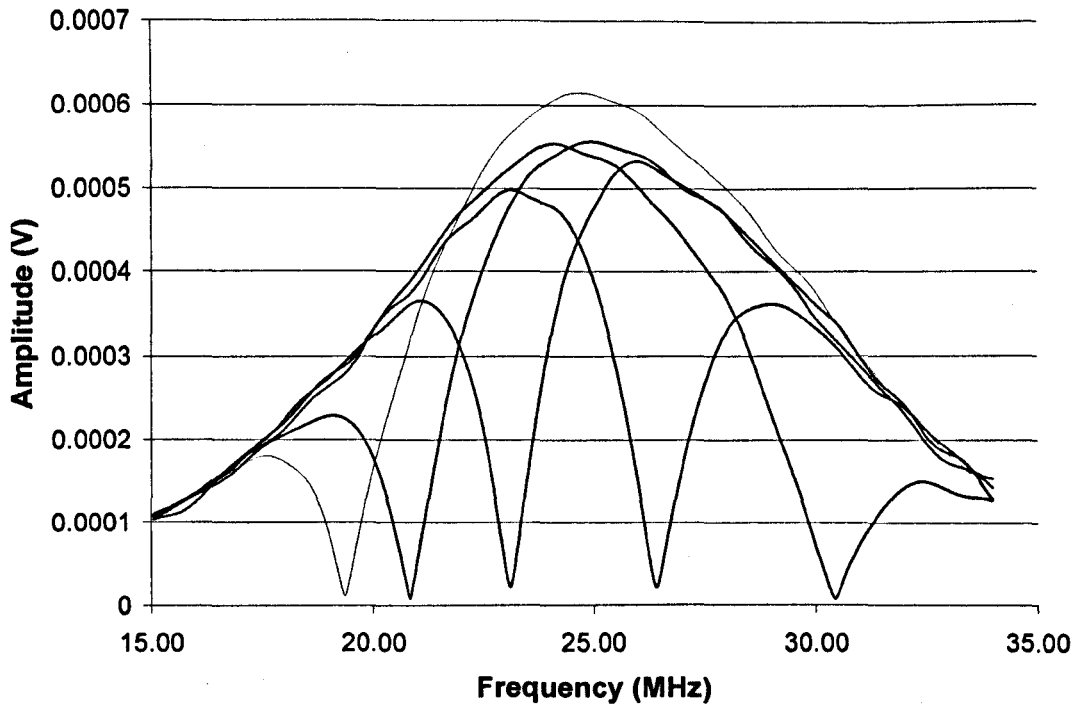
Figure 6.02. Amplitude (V) of the FFT of a received signal versus frequency.

The only disadvantage in using this method is that the resonant dip method is not generally useful for measuring oil films in many hydrodynamic engineering applications as the films are much thinner than can be measured using this technique.

6.3.2. Over Thickness Calibration

This method operates on the principle that each ultrasonic sensor has a certain 'window' in which it can detect oil films. Once the oil film exceeds the upper limit of the sensor the reflection coefficient approaches one (assuming $Z_B>>Z_L$). In figure 6.03 below, a simulated 7.5MHz sensor has a 'window' from 0.1μm to 8μm. It can be seen from figure 6.03 that this sensor will be able to measure an 8μm oil film, but will not be able to measure a 50μm oil film. Indeed the measured response from the transducer at 50μm is the same as an infinitely thick oil film.
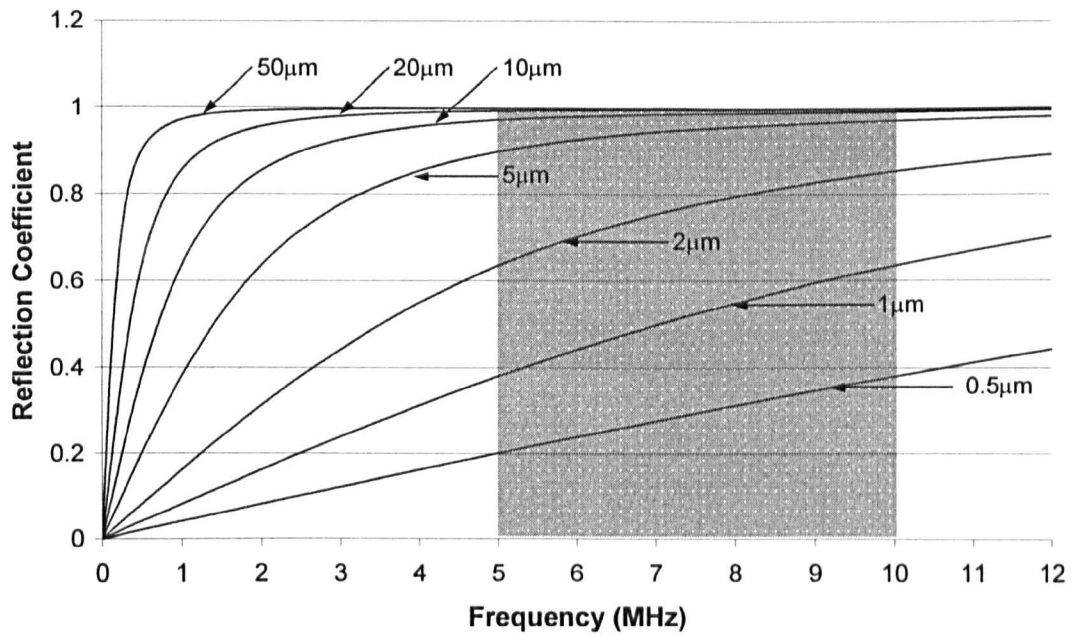
Figure 6.03. Predicted reflection coefficient versus frequency for a range of film thicknesses for a steel/oil/steel interface. Grey area is the bandwidth of a typical sensor.

During the duty cycle of a bearing the oil film may periodically increases beyond the upper limit of the sensor. If this is the case, then the original reference can be compared to this 'new' reference. In this way, this method of calibration can be used to check sensor integrity. Figure 6.04 shows the use of this technique for calibrating an ultrasonic transducer in a bearing.
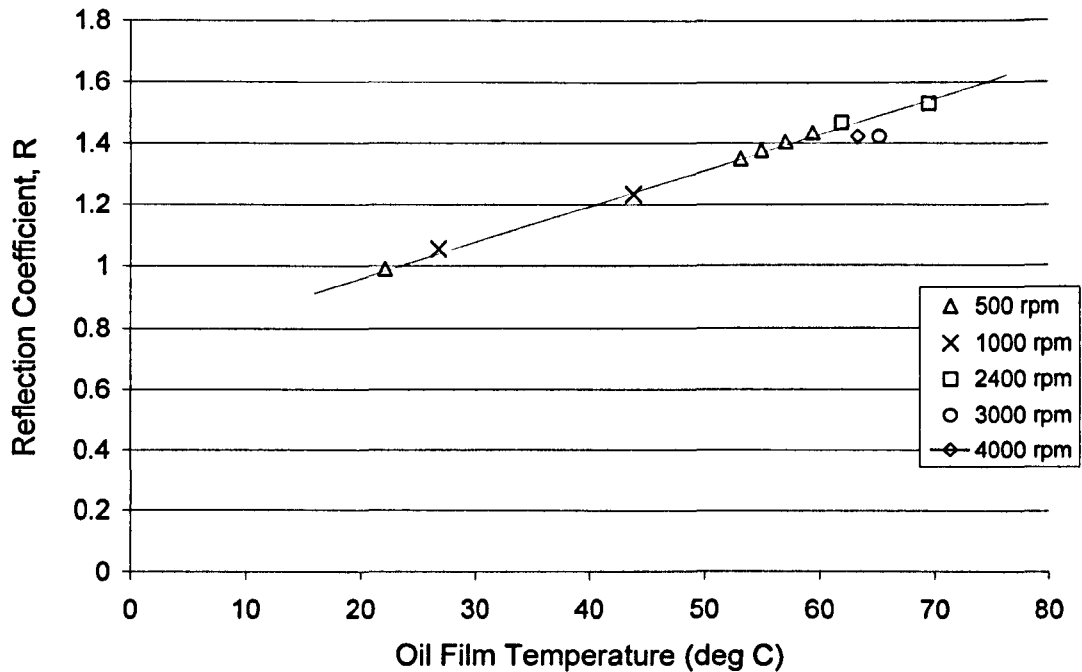
Figure 6.04. Reflection coefficient Vs temperature using the Over Thickness Calibration method.

A slight variation on this method is where in some experimental arrangements (for example a sensor attached to the liner measuring the piston ring lubricant film thickness as it moves past) there is effectively an air reference when the mating component that forms the film is not present during some of the cycle. This allows a reference to be taken when the test setup is fully assembled.

6.3.3. Intermediate Interface Calibration

This method uses interface between the ultrasonic sensor and the oil film. This interface must be made from two sufficiently different materials that an intermediate reflection is produced, but the materials must be sufficiently similar that this reflection is not too great. The portion of the signal that is reflected (according to equation (3.06)) can act as a calibration signal. If the interface is perfect then the reflected wave will not change with changing operating conditions. Thus any change in this intermediate signal is an indication of a change in the sensor. Hence changes in the sensor may be monitored and the film thickness measurement calibrated.

Figures 6.05 shows the acoustic response from a white metal coated journal bearing. Figure 6.06 shows schematically the various reflections within the bearing.
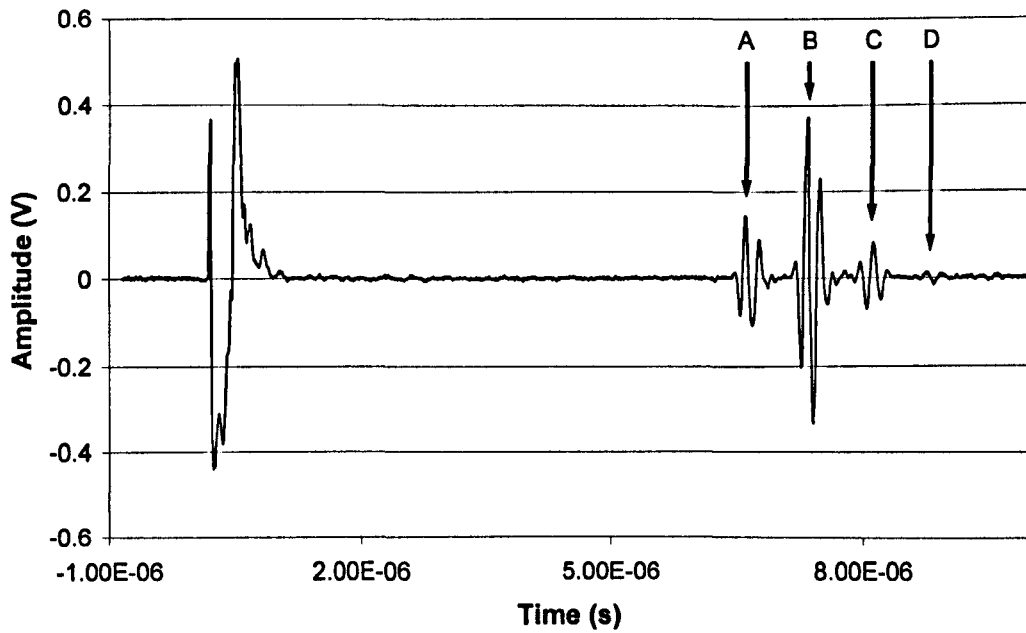
Figure 6.05. Reflected pulse from a journal bearing with a white metal layer. Points A, B, C, and D refer to the corresponding points in figure 6.06
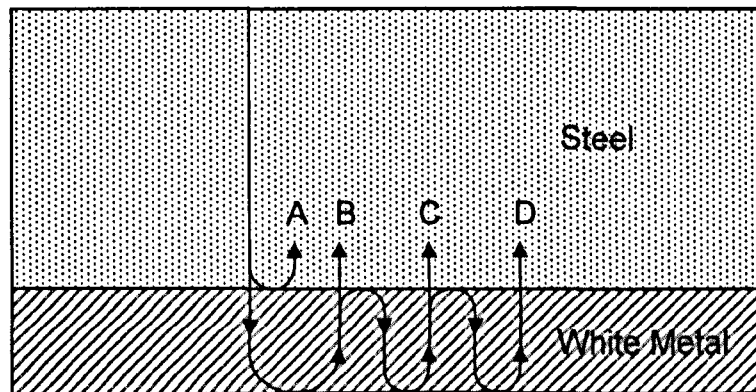
Figure 6.06. Schematic of pulse reflections in a white metal faced thrust pad bearing. Points A, B, C, and D refer to the corresponding points in figure 6.05.

Many components use a sacrificial layer at the sliding surface, but not all (for example piston rings/liners). Where there is no interface between the sensor and the fluid film, it may be possible to artificially create an interface by means of a delay line (to delay the signal) of different material than the component. Figure 6.07 below shows a schematic of one such arrangement.
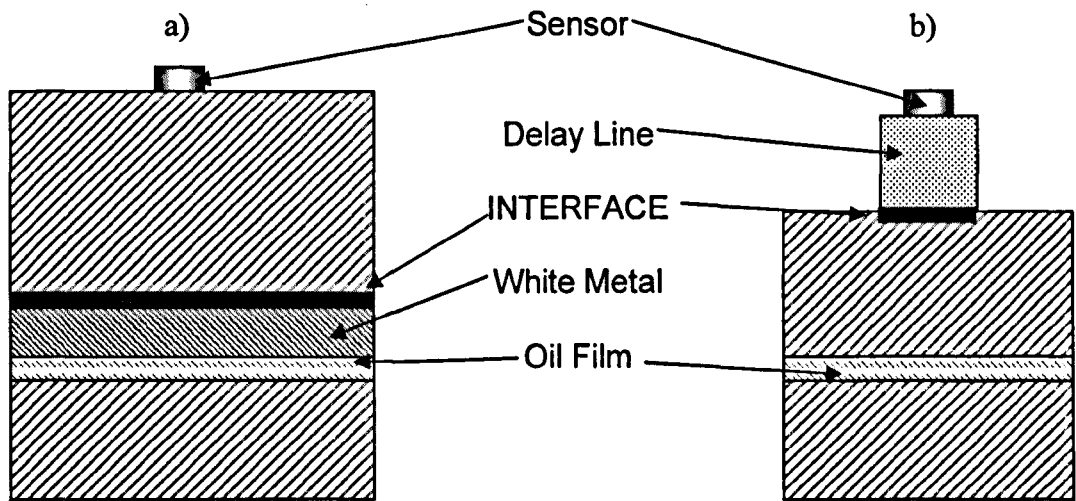
Figure 6.07. Intermediate interface Calibration using a) white metal layer in bearing, b) delay line on back of bearing. The calibration interface is indicated and shown as a thick black line.

6.3.4. Partial Intermediate Interface Calibration

This calibration technique is similar to the intermediate interface calibration technique except that geometry rather than different materials are used to produce a calibration pulse. If part of the sound path of an ultrasonic pulse is abruptly stopped then there will be a partial reflection of the ultrasonic pulse. The proportion of the sound wave that is reflected back is a function of the proportion of the sound path that is cut off. This abrupt stop may be as a result of a slot, notch or step in the sound path.
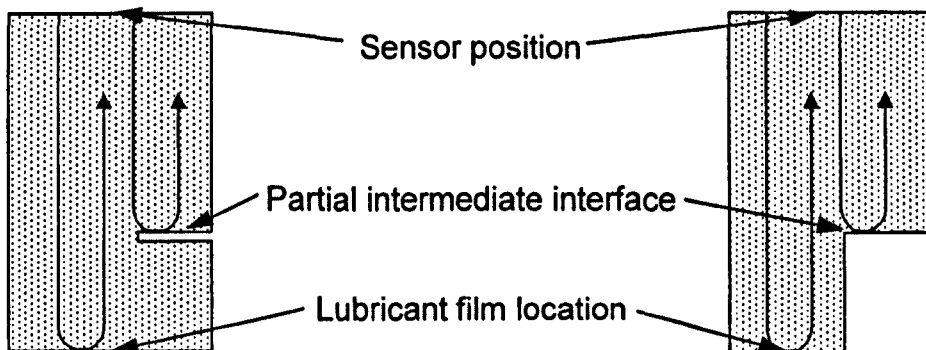
Figure 6.08. Schematic of two possible partial intermediate interface arrangements.

It was discovered that care needed be taken to ensure that the notch does not cause overlapping reflections with the reflection from the oil film. If the notch is positioned at $L/2$ where L is the thickness of the component then the second reflection from the notch will overlap on the first reflection from the lubricant film (i.e. $(L/2)x4 = Lx2$).

6.3.5. Material Property Calibration

As previously mentioned, the acoustic properties of the material in the 'bearing system' may change with operating conditions. Generally the acoustic properties of the materials used in components (e.g. steel) does not change with operating conditions encountered in most 'bearing systems'. However, this is not true of the lubricant. The acoustic properties of the lubricant can change considerably with changing operating conditions such as temperature, pressure, shear rate, degradation and particle inclusion. Figure 6.09 below shows the schematic of a method for calibrating for changes in the acoustic properties of the lubricant.

A feed is taken from the lubricant supply system. The lubricant enters the chamber from the left and flows through the chamber to the right. While the chamber is flooded with lubricant the acoustic properties can be continuously monitored. This method can be used to calibrate the measurement system on-line.
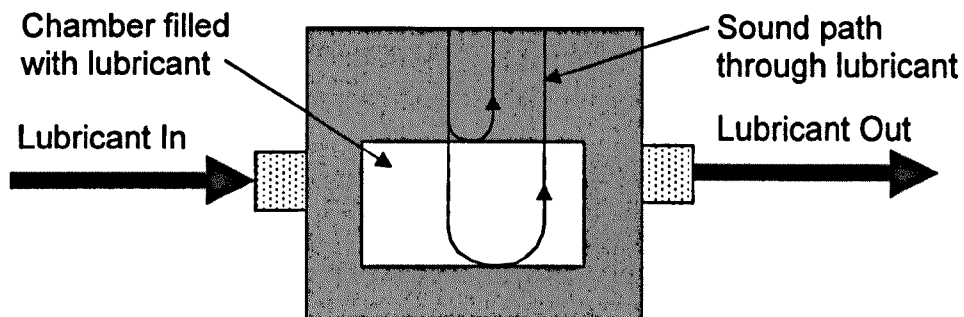
Figure 6.09. Schematic of a chamber for calibration of lubricant during testing.

6.4. Measurement Verification

In order to validate the ultrasonic technique, it was necessary to compare it with other methods of measuring film thickness. However, as has previously been discussed in chapter 2, there is a lack of comparable techniques for measuring fluid film thickness. Therefore two experiments were carried out that utilised physical geometry as a method of comparing film thickness.

6.4.1. Wedge Experiment

A wedge of fluid trapped between two solids provided a method for comparing physical geometry with the ultrasonic technique. Two sheets of 6mm thick float glass were separated by a shim of known thickness at one end. Figure 6.10 below shows a schematic of the test setup. The shim, glass sheets and sensor were immersed in a water tank to

allow for movement of the sensor along the wedge. The sensor was mounted on an arm attached to a lead-screw driven by a stepper motor to control the steps between measurement points.
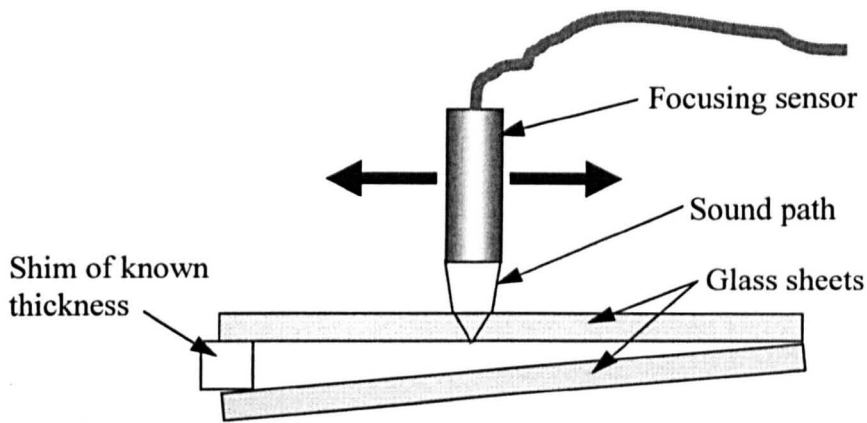
Figure 6.10. Schematic of wedge experiment.

Figure 6.11 below shows the results obtained from this test. The systematic error in figure 6.11 is most likely due to an error in the thickness of the shim used or a film thickness between the shim and the glass on both sides thus distorting the measurement.
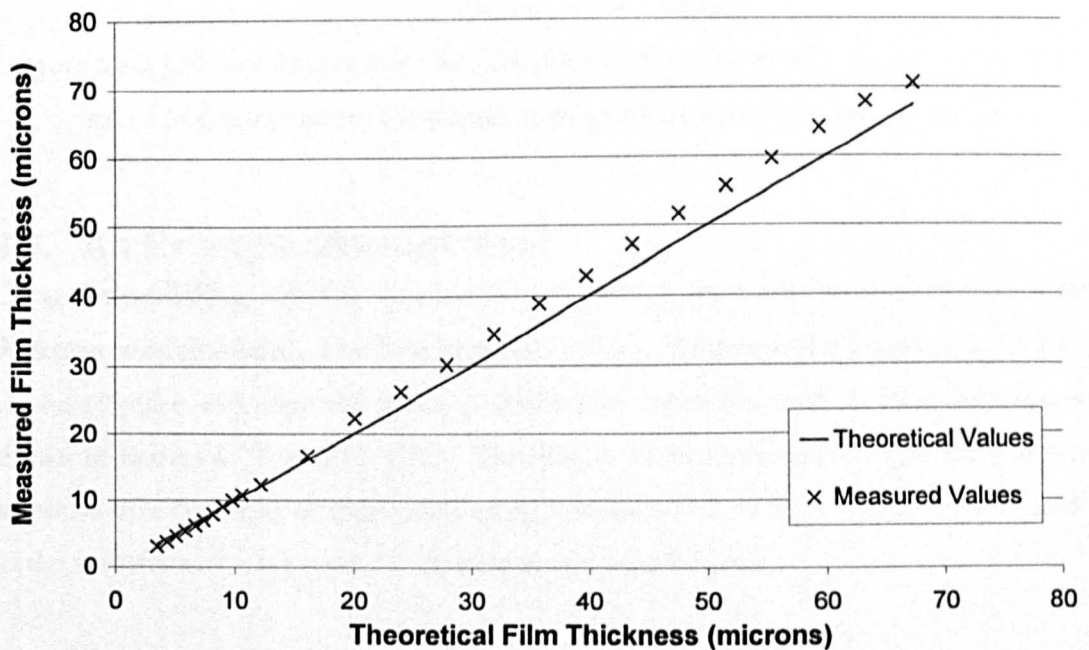
Figure 6.11. Results from wedge experiment showing thickness from geometry and thickness from wedge experiments.

6.4.2. Journal Geometry Experiment

In the Journal Bearing experiments (see chapter 7), the measured oil film round the circumference was compared to the predicted oil film from geometry as calculated from equation 7.05. There was excellent agreement (see figure 6.12) between the measured and actual oil film thicknesses. This experiment thus provided validation of the ultrasonic method for measuring oil film thicknesses.
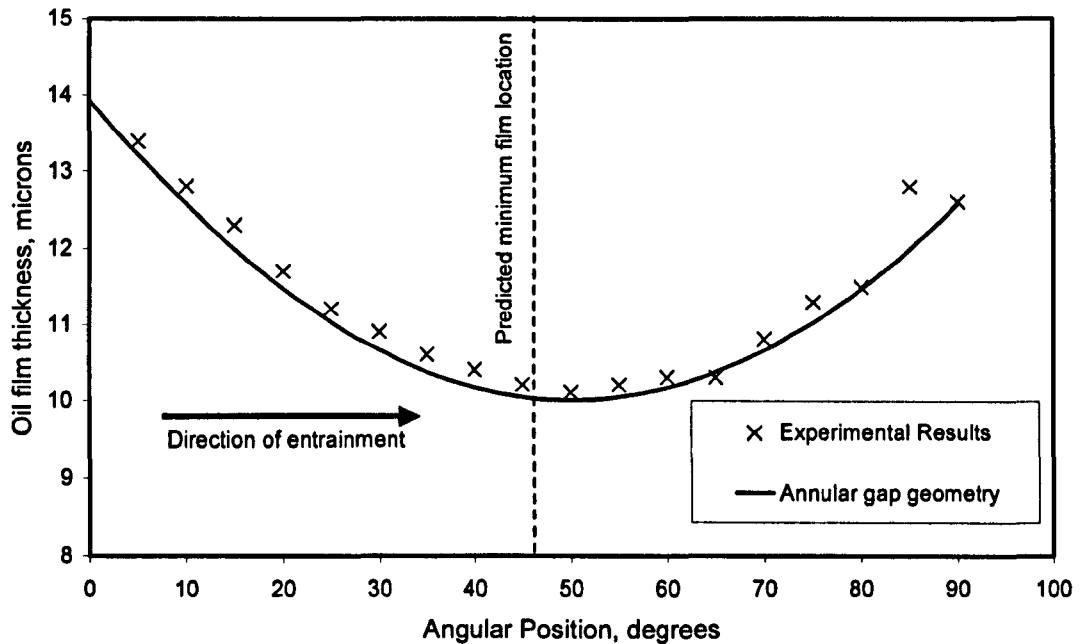
Figure 6.12. Oil film thickness Vs angular position for a journal bearing at a fixed load, speed and temperature for annular gap geometry and experimental results.

6.5. An Example Measurement

Using the modelling software detailed in section 5.2.5, an example measurement of film thickness was simulated. The four steps of 1. Time domain pulse capture, 2. FFT's of reference pulse and captured pulse, 3. Reflection coefficient and 4. Film thickness are shown in figures 6.13 to 6.16 below. The data is entirely simulated and is the predicted response of a thin layer to ultrasound using equations 3.12 to 3.22. Noise has been added to the waveforms to improve the likeness to real world signals.
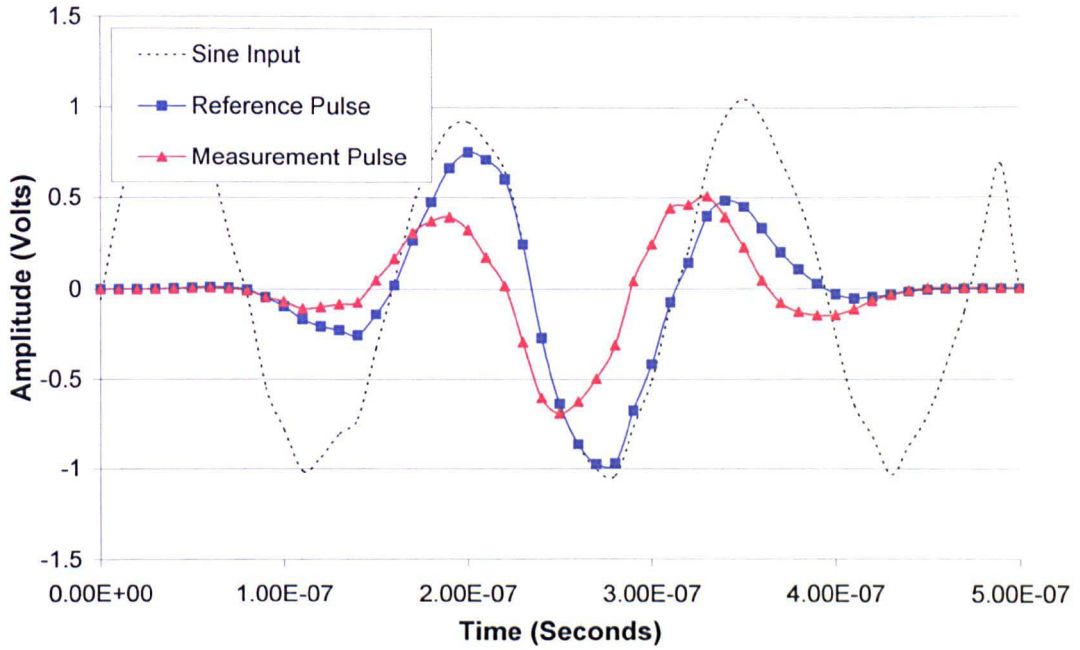
Figure 6.13. Step 1: Time domain pulses. Reference pulse (shown in blue) and measurement pulse (shown in red).
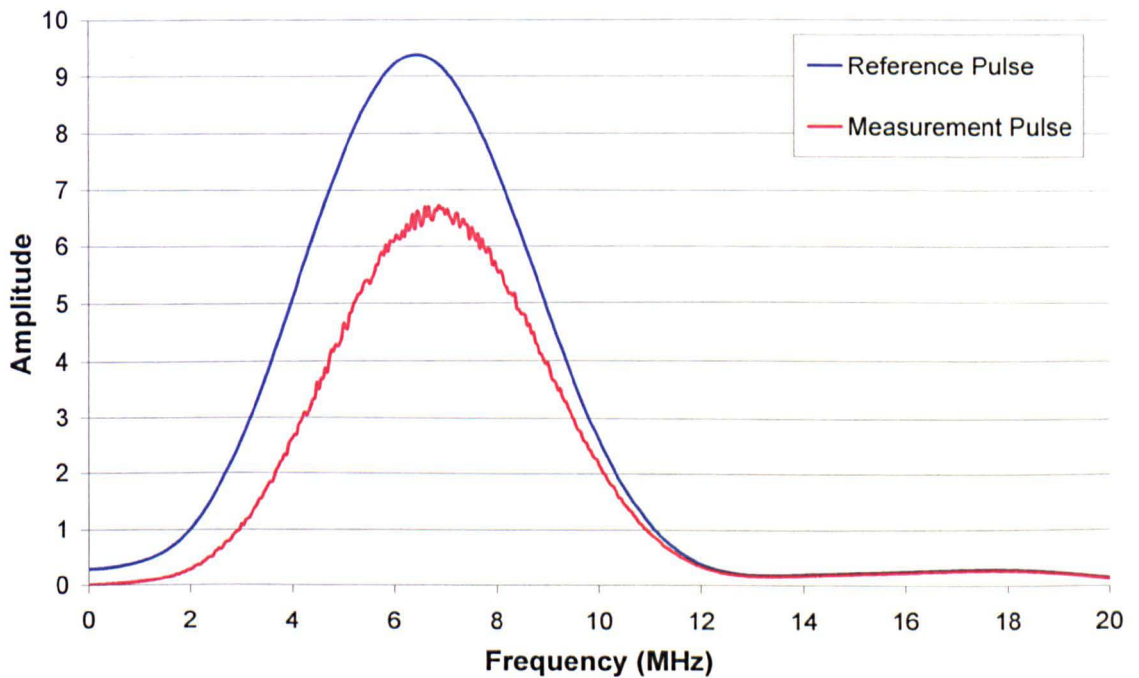
Figure 6.14. Step 2: FFT's of the reference and measurement pulse shown in figure 6.01 above.
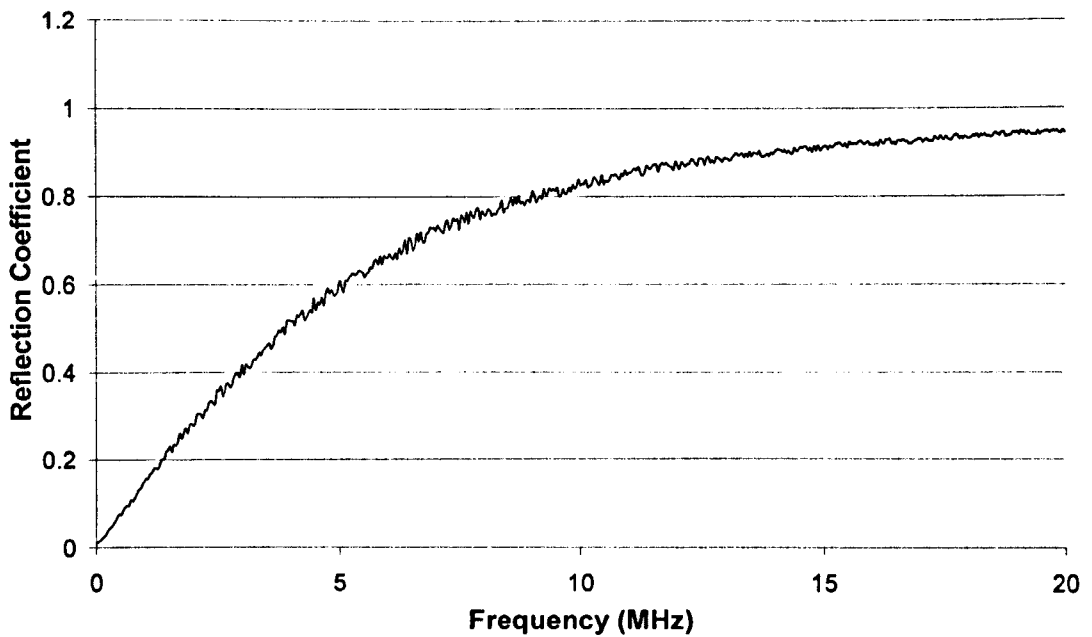
Figure 6.15. Step 3: The Reflection Coefficient obtained by dividing the measurement pulse by the reference pulse as shown in figure 6.02.
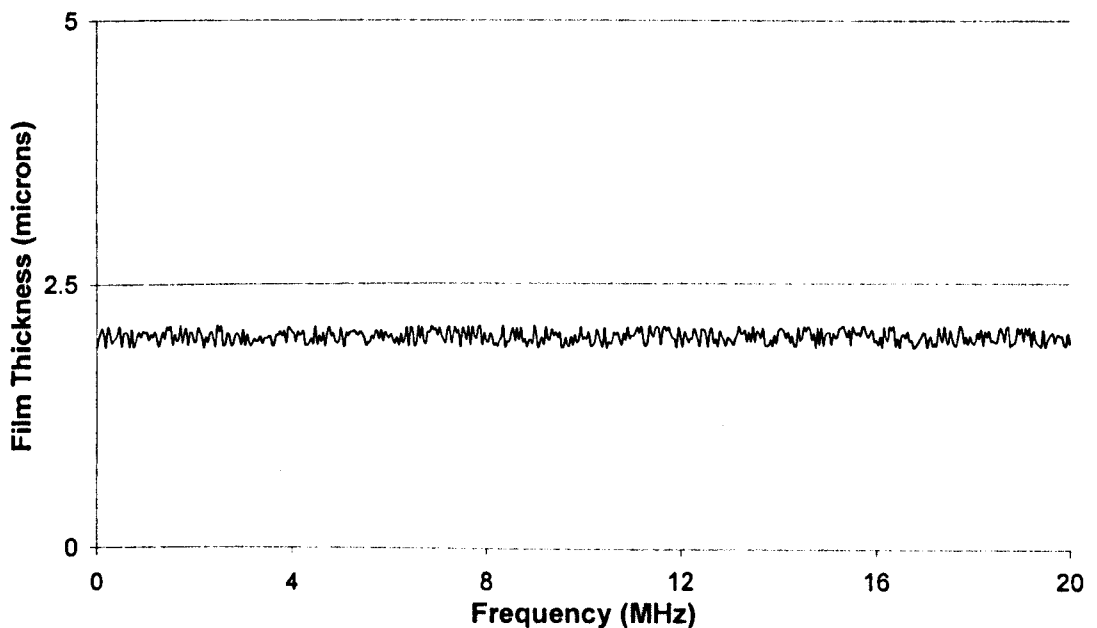
Figure 6.16. Step 4: Film Thickness using the reflection coefficient values in figure 6.15 above and equation (3.22).

6.6. Conclusions

This chapter has discussed experimental issues in implementing measurements. The practicalities of measuring material properties have been described. Techniques for calibration of the ultrasonic method in situations where there is a temperature effect have been explained. Validation experiments and results have been shown for the technique. Finally the steps taken in an example measurement have been graphically represented.

Chapter 7:

Journal Bearing Film Measurement

This chapter describes the application of the measurement system to the measurement of film thicknesses in two journal bearings.

The first bearing test rig was built and assembled at the University of Sheffield. The bearing in this test rig was a simplified journal (low-temperature, low speed, and low load) that allowed the main concepts of film thickness measurement to be proven before moving on to more complex bearings. Measured film thicknesses were compared with Sommerfeld theory and showed good agreement.

The second bearing test rig was owned and run by Michell Bearings Ltd, Newcastle, UK. This test rig, in an industrial environment, was more complex (e.g. the presence of a white metal layer in the bearing) as was the testing (higher temperatures, higher speeds, and higher loads). Temperature effects were found to be significant and methods of temperature compensation were developed and applied to this test rig. Finally comparisons were made between the measured film thicknesses and a computational model.

7.1. Journal Bearing Background

Journal bearings are used in a wide variety of applications to support a radial load. They benefit from a high load capacity, low friction and a wide range of rotational speeds (typically from 10rpm in rock crushing equipment to 20,000rpm in formula one engines and 200,000rpm in automotive turbochargers).

Journal bearings consist of a rotating shaft (journal) that is supported in a conformal cylinder (bearing), lubricated with oil (see fig 7.01 for example).
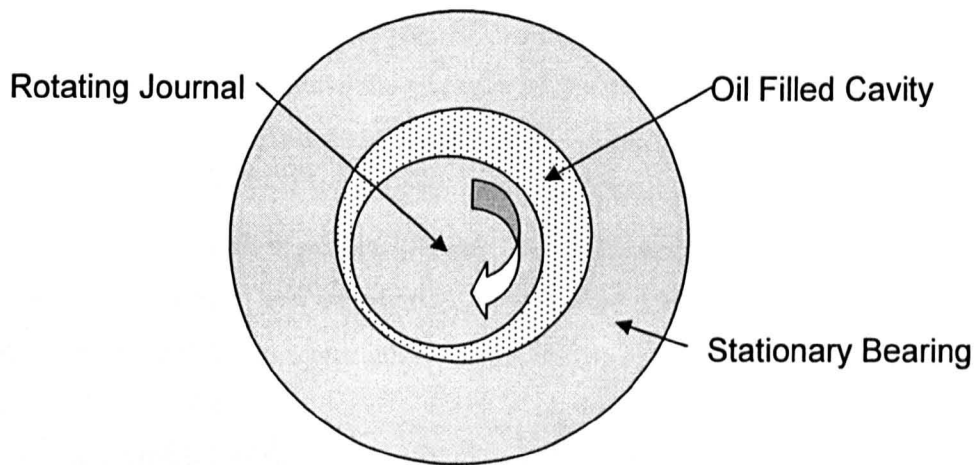
Figure 7.01. Schematic of a journal bearing

When the journal is stationary and a load is acting down in the vertical direction the minimum oil film (for a stationary case h=0mm) is at 0° vertical (see a) in figure 7.02). If there is no lubrication then the journal will tend to 'climb' up the side of the bearing (see b) in figure 7.02). The amount to which it does this is a function of the friction coefficient between the two surfaces. Commonly this change in position is referred to as the attitude angle, ϕ. If there is lubrication then oil will be drawn into the interface between the journal and the bearing. This will result in the journal 'floating' on a layer of oil (see c) in figure 7.02). It can be seen from figure 7.02 that the attitude angles are positive and negative with respect to the vertical for the lubricated and unlubricated cases.
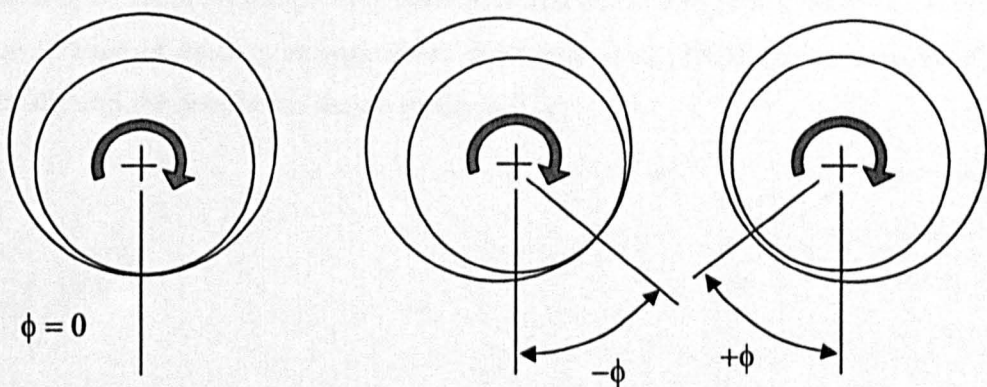
Figure 7.02. Journal positions for three cases: a) stationary, b) unlubricated and c) lubricated.

7.1.1. Sommerfeld Number

The loads and speeds that a journal bearing can support are determined by the dimensions of the bearing and the viscosity of the lubricant. Arnold Sommerfeld [1904 & 1942] did important work solving the Reynolds equation for hydrodynamic lubrication in a one-dimensional journal bearing. He used the Sommerfeld transformation to in order to solve the Reynolds equation [Maday, 2002]. Raimondi et al [1958] proposed the Sommerfeld Number (see equation (7.01)), a non dimensional number based on the solution of the Reynolds equation that describes the operation of a journal bearing.

$$S = \frac{\eta \omega DL}{W} \left(\frac{R}{C} \right)^2 \qquad (7.01)$$

where η is the viscosity of the lubricant

ω is the angular velocity of the journal

D is the diameter of the journal

L is the length of the bearing

R is the radius

C is the radial clearance in the bearing

W is the load

Steady state loading, laminar flow, Newtonian and incompressible lubricant, and no transient events are all assumed.

Raimondi et al [1958] solved the Reynolds equation numerically for a range of L/D radios and for a range of bearing arrangements. Khonarsi et al [2001] solved equation (7.01) numerically and the results are shown in figure 7.03.
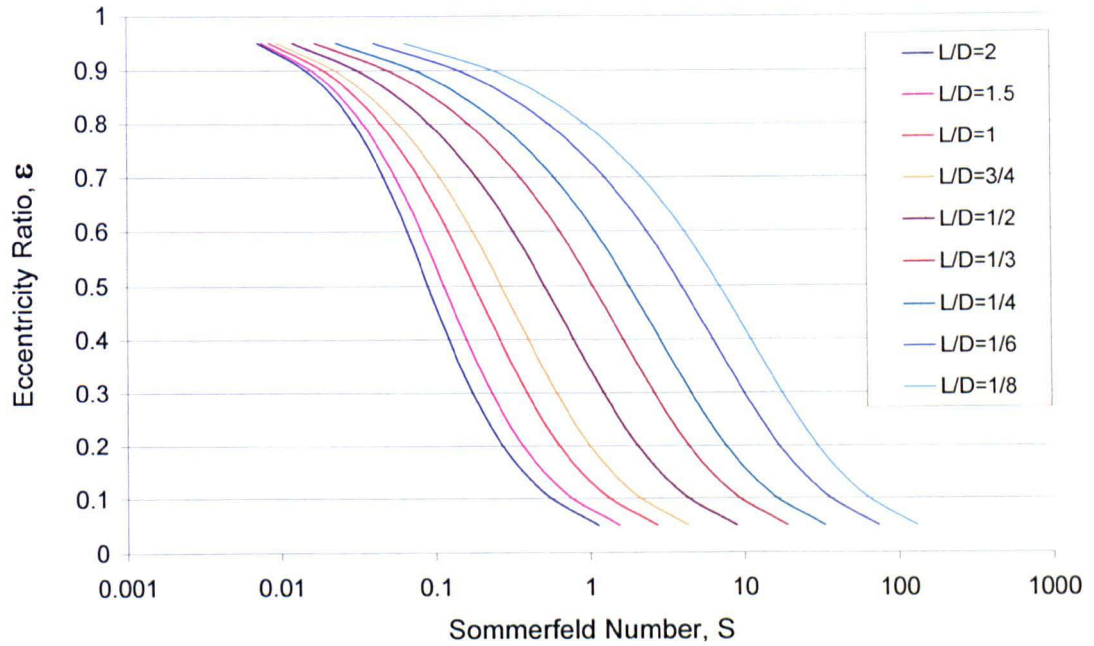
Figure 7.03. Eccentricity ratio Vs Sommerfeld number for a range of different length to diameter ratios (adapted from Khonsari et al [2001]).

The minimum film thickness, h_{min}, for a bearing of known dimensions can be determined from figure 7.03 using equation (7.02).

$$h_{\min} = C(1 - \varepsilon)$$ (7.02)

The minimum oil film thickness is of importance in determining the running characteristics of the bearing, limits of operation, and required dimensions and tolerances.

In order to calculate the minimum film, load vectors and position of the lubricant supply it is also important to determine the attitude angle, ϕ. Figure 7.04 shows the relationship between the attitude angle and the Sommerfeld number.
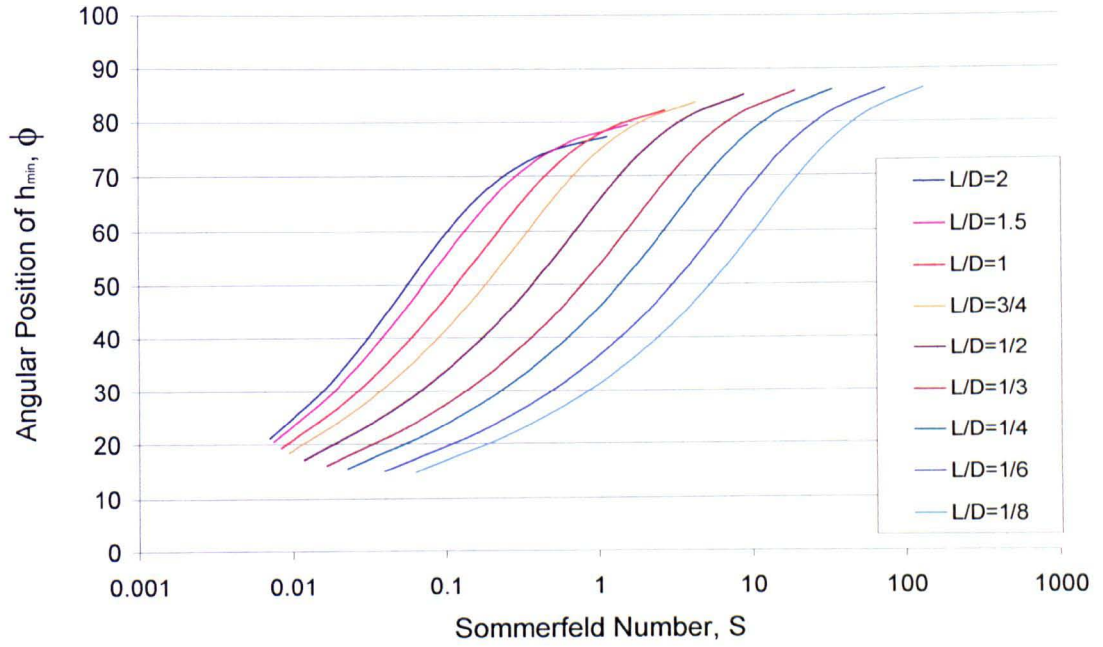
Figure 7.04. Relationship between the attitude angle and the Sommerfeld number for a range of length to diameter ratios (adapted from Khonsari et al [2001]).

The attitude angles in figure 7.04 may be represented by

$$\phi = \tan^{-1}\left[\left(\frac{\pi}{\psi\varepsilon}\right)\sqrt{1-\varepsilon^2}\right] \tag{7.03}$$

where

$$\psi = 4\left[1+\left(\frac{L}{D}\right)\left(1-1.25\varepsilon^\delta\right)\right] \tag{7.04}$$

where $\delta = 0.18$ for a lubricant film starting at h_{max} (i.e. where the oil supply is 90° to the vertical). If the oil film does not start at h_{max} then a different value of δ should be used (see [Martin 1998]).

The film thickness profile may be approximated to (Williams [1994]),

$$h = C + e\cos\theta \tag{7.05}$$

96
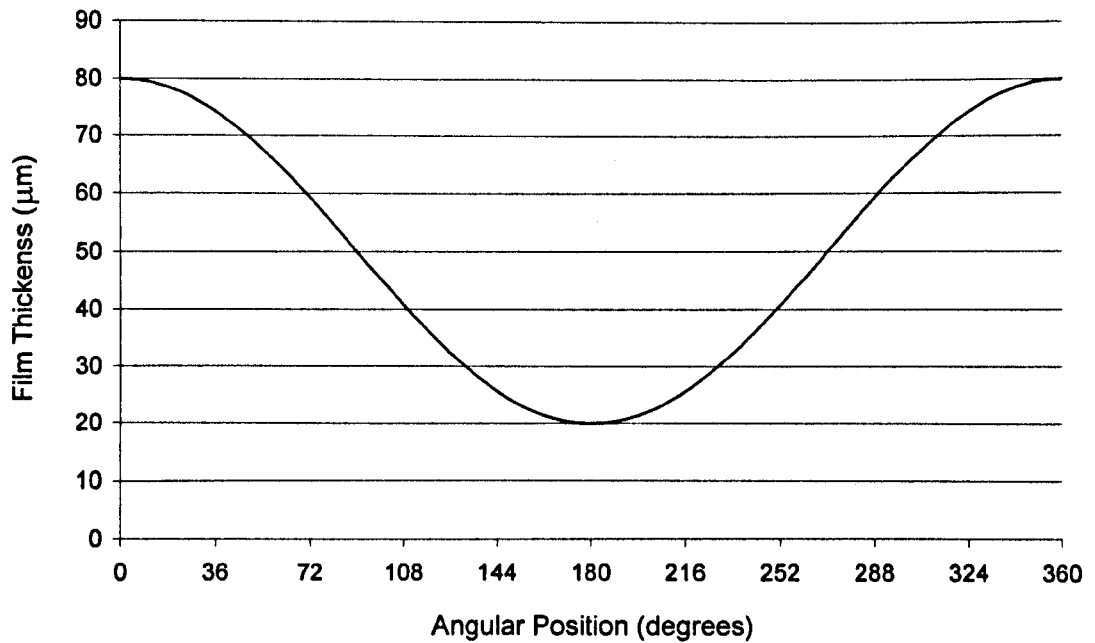
Figure 7.05. Film thickness Vs angular position for a journal bearing having a minimum
oil film of 20 μm

7.1.2. Babbitt layer

In the event of a bearing failure the two surfaces may come into contact whilst at high
load and high speed. For this reason the bearing is often coated with a sacrificial layer.
This sacrificial surface is often called 'white metal' (or Babbitt from its inventor Isaac
Babbitt who discovered it in 1839) due to its appearance on a bearing surface.

If ultrasound is to be used as a technique for measuring the film thickness then it must
be established that the white metal layer does not interfere with the signal. Figure 7.06
shows the response from a Babbitt layer to an ultrasonic signal. Discreet pulses can be
clearly observed from the interfaces from the steel/Babbitt and Babbitt/air. Using time
of flight the thickness of the layer can be calculated.
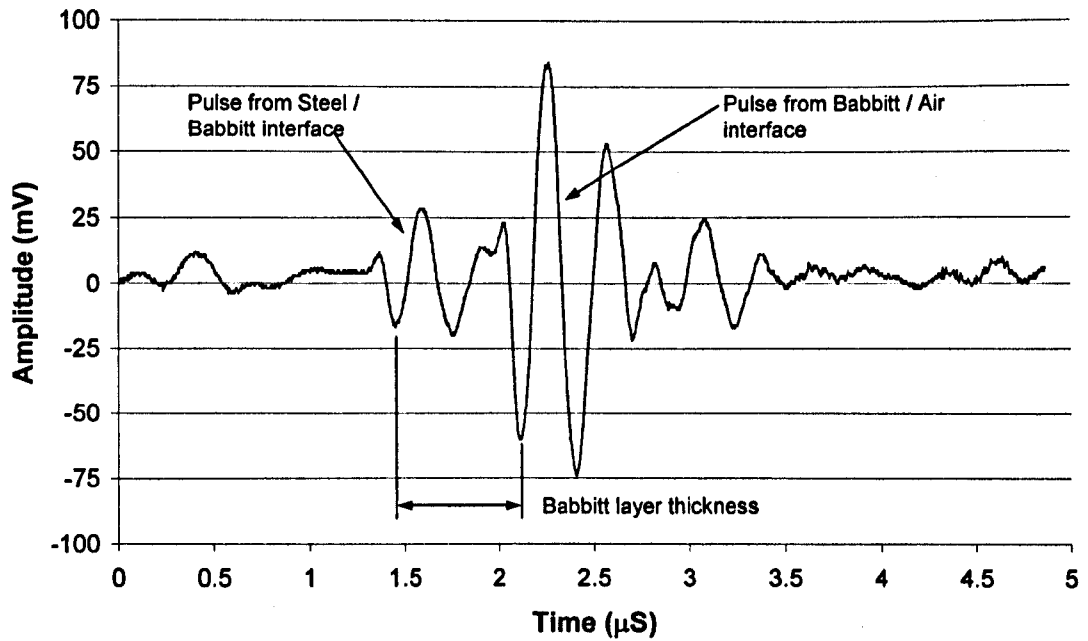
Figure 7.06. Amplitude Vs time for a pulse from a thrust pad with a Babbitt layer.

7.2. Experiments on Sheffield Bearing Apparatus

A rolling element bearing test rig in the Tribology Lab at the University of Sheffield was converted to take a journal bearing. The journal was made from a stepped shaft of EN24 steel with a central journal diameter of 75mm (see figure 7.07). The bearing was made from CZ121 commercial grade leaded brass with a length of 37.5mm to give a diameter to length ratio of ½. The brass bearing was mounted in a steel bearing holder using an interference fit. The diametrical clearance between the journal and the bearing was 50μm.
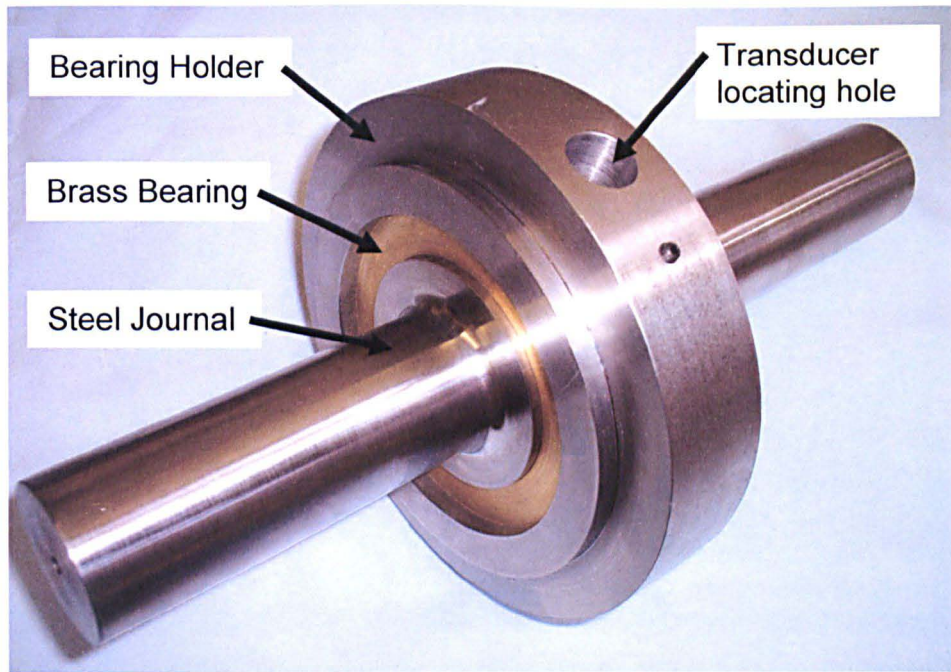
Figure 7.07. Journal bearing used for ultrasonic testing.

The bearing holder was mounted in a loading arm as shown in figure 7.08. Load was applied by means of a hydraulic jack through a pin to minimise lateral forces. The shaft was supported on two spherical roller bearings in pillow block housings. This retained the shaft and applied an opposing force on the loading arm.
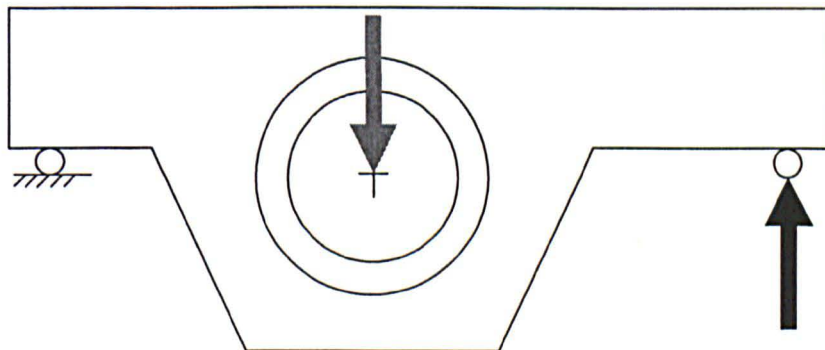
Figure 7.08. Schematic of the loading arm and bearing position. Load from the hydraulic jack was applied in the direction of the black arrow. The opposing force exerted by the journal is shown by the grey arrow.

The rig had a 3kW motor and a variable speed drive from 0-700rpm (see figure 7.09). A toothed belt was used to drive the journal.
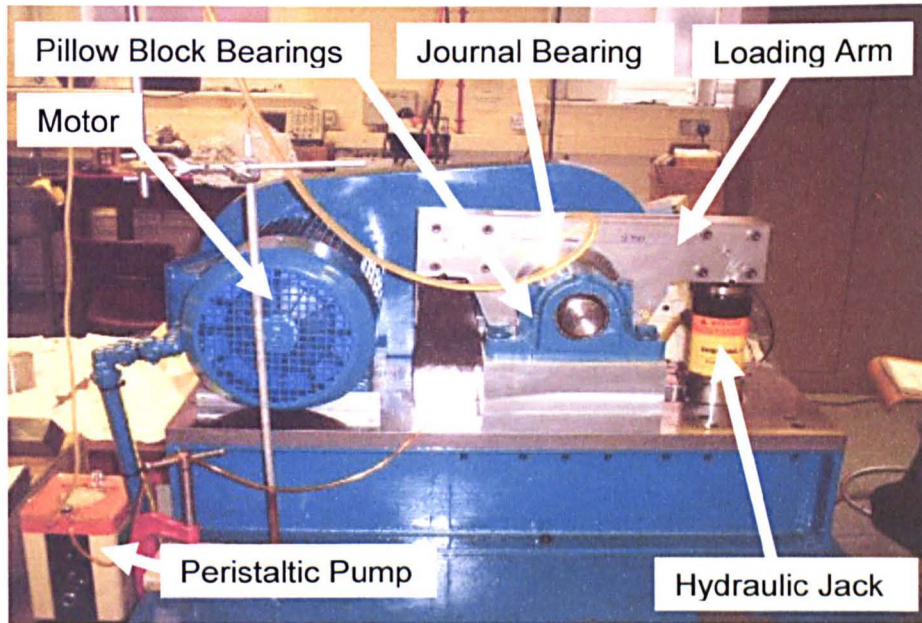
Figure 7.09. Journal bearing test rig showing pump, hydraulic jack, motor, journal bearing, loading arm and retention bearings.

Oil (Shell Tellus T32 – 32 cSt @ 40°C, 5.4 cSt @ 100°C) was supplied to the bearing from a peristaltic pump at a pressure of 0.5 - 2 Bar. A slot was machined in the bearing to supply oil across the full length of the bearing (see figure 7.10).
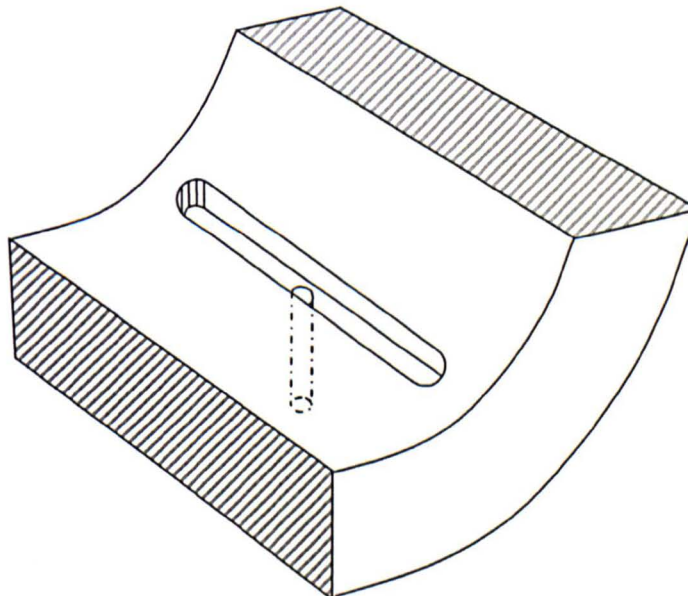
Figure 7.10. Section through the brass bearing showing the oil supply hole and slot.

It will be noted from figure 7.05 that the oil film is not the same the whole way around the circumference. Thus it is necessary to position the sensor where the oil film is to be

measured. The test rig was designed so that the bearing housing (containing the transducer) was able to rotate, with 5° graduations marked off. This allowed the measurement of oil film thickness in the circumferential direction from 0° to 90 °.
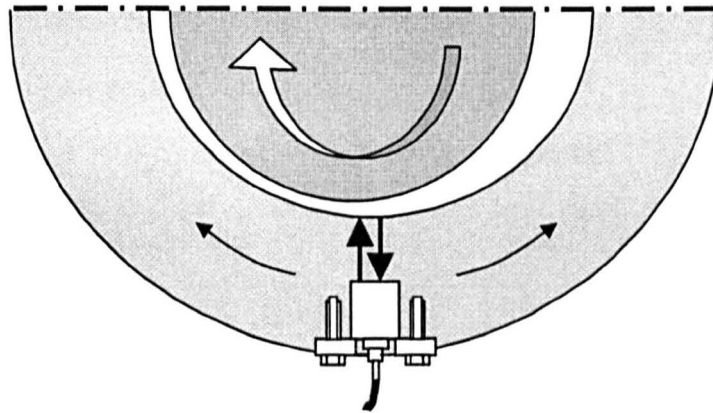
Figure 7.11. Schematic showing position of sensor. Ultrasound transmits and reflects in the directions of the large black arrows. The bearing is able to rotate in the direction of the small black arrows.

In order to ensure that the interface between the transducer and the bearing was consistent, a metal plate was screwed on behind the transducer. This retention plate ensured that the transducer did not move during the testing.

7.2.1. Sensor selection

Using figure 7.03 and equation (7.02) the range of expected film thicknesses was determined. Using the ultrasonic model described in section 3.5.3.2, the range of frequencies was calculated at 0.5 – 1MHz for measuring films in the order 0.2μm to 50μm. In order to measure these frequencies a Panametrics 1MHz NDT transducer was specially purchased for this application.

7.2.1.1. Sensor temperature effects

In order to quantify the effect of temperature on the sensor, the sensor was mounted on a piece of material similar to that used in the bearing and placed in an oven. Figure 7.12 below shows the response of the peak amplitude to temperature. It will be noted that the amplitude increases with temperature which is the opposite to what is expected from a piezo material. The reason that there is an increase in reflection coefficient is because of thermal induced mechanical strain within the layers of the commercial sensor.

During testing the temperature of the oil leaving the bearing was monitored and due to the low speed, low power and low load it was found that there were not significant temperature effects in the bearing. Throughout testing both the oil and sensor temperature was measured but reached a maximum of approximately 45°C.
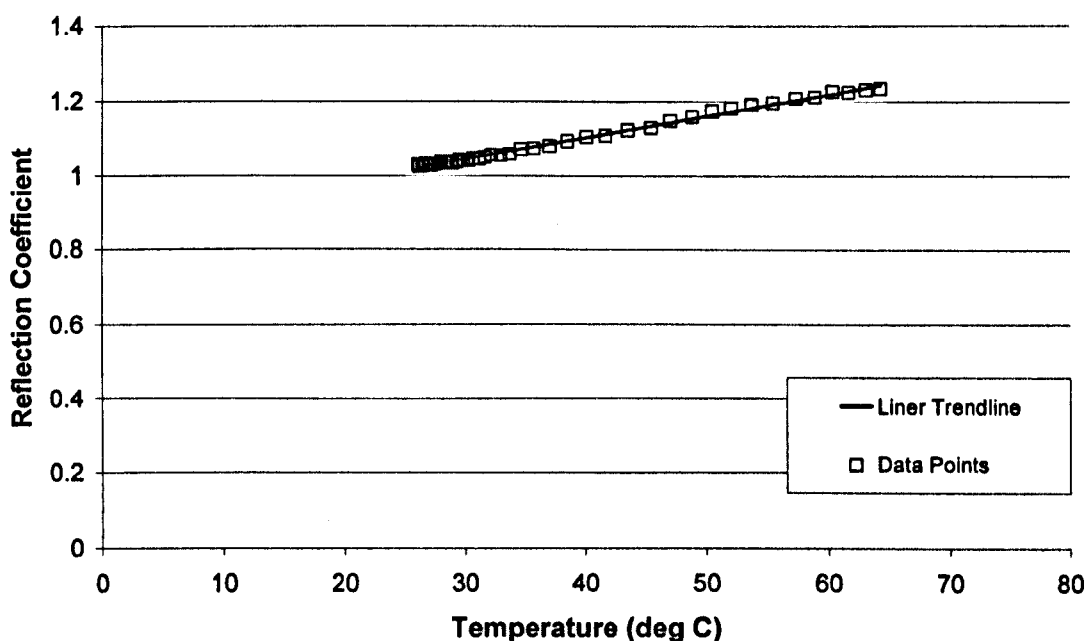
Figure 7.12. Plot of reflected amplitude against temperature for a 1MHz Panametrics NDT Contact Sensor.

7.3. Results

Testing was carried out by varying the load and speed of the journal. The transducer was located at 0° to vertical.

7.3.1. Reflection Coefficient and Determination of Film Thickness

This section shows the steps taken to get from the raw signal to film thickness. Figure 7.13 shows the amplitude frequency spectrum (FFT) of the received pulse from the transducer. It can be seen that the centre frequency of the pulse is approximately 1 MHz.
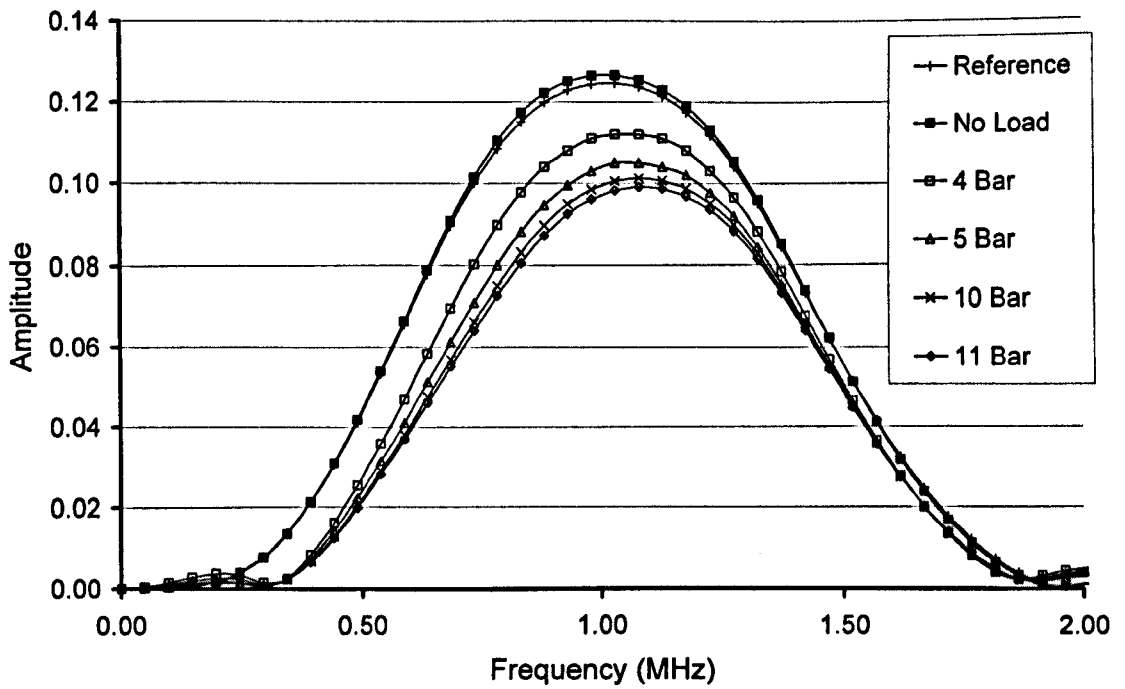
Figure 7.13. Amplitude Vs frequency of received signal for a range of loads

Each set of data points shown in figure 7.13 was divided by the reference, also shown in figure 7.13. This gave reflection coefficient against frequency as shown in figure 7.14.
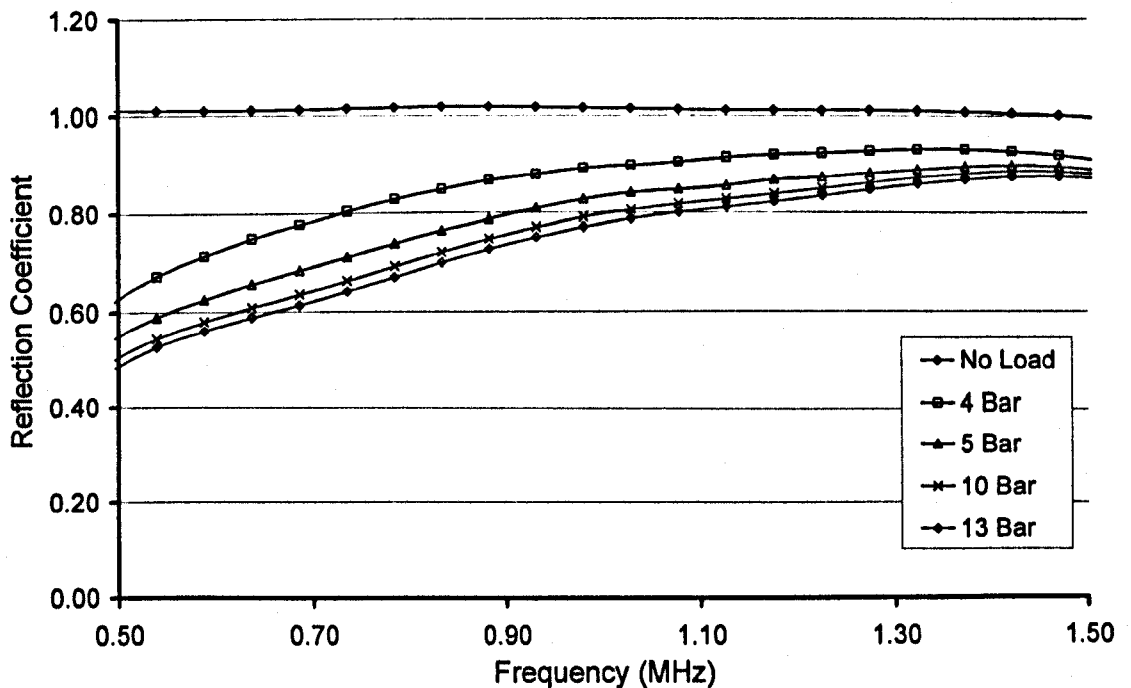
Figure 7.14. Reflection coefficient Vs frequency for the data in figure 6.13.

The data points shown in figure 7.13 were substituted into equation (3.22) to give film thickness against frequency as shown in figure 7.14. It will be noted that the film

thickness is approximately a horizontal line indicating that the film thickness does not vary with frequency. This indicates that equation (3.22) is valid for these cases.
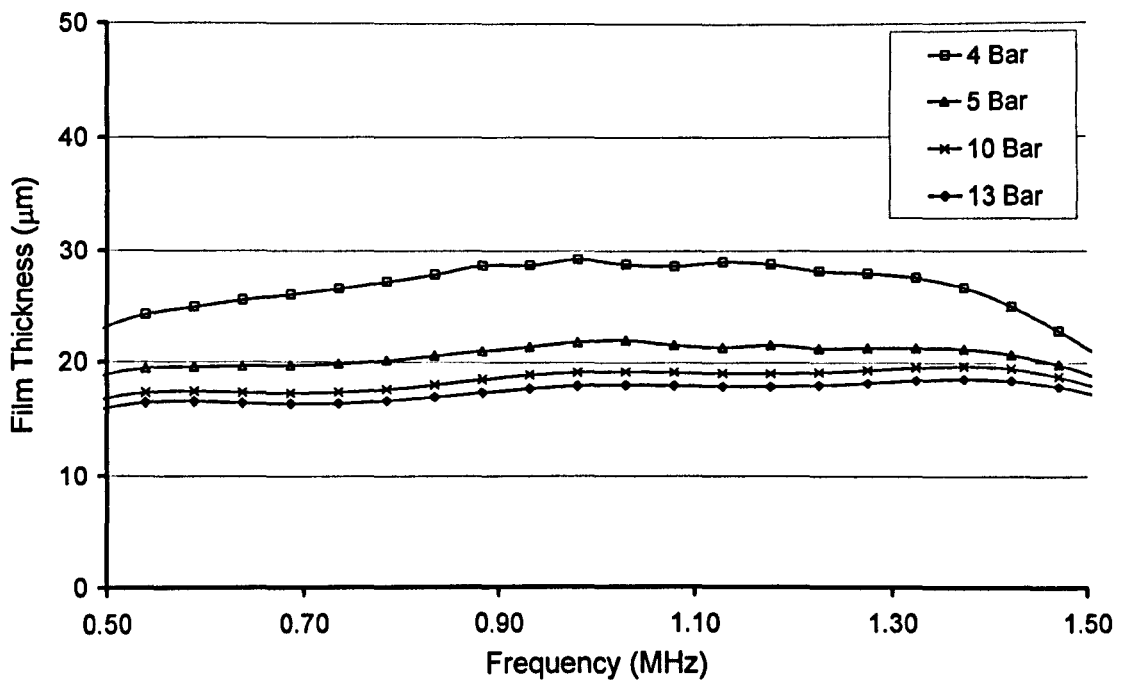
Figure 7.15. Film thickness Vs frequency for the data from figure 7.14.

7.3.2. Variation of Bearing Operating Conditions

Figure 7.16 shows the measured film thickness at the centre frequency of the transducer for a range of loads and speeds.
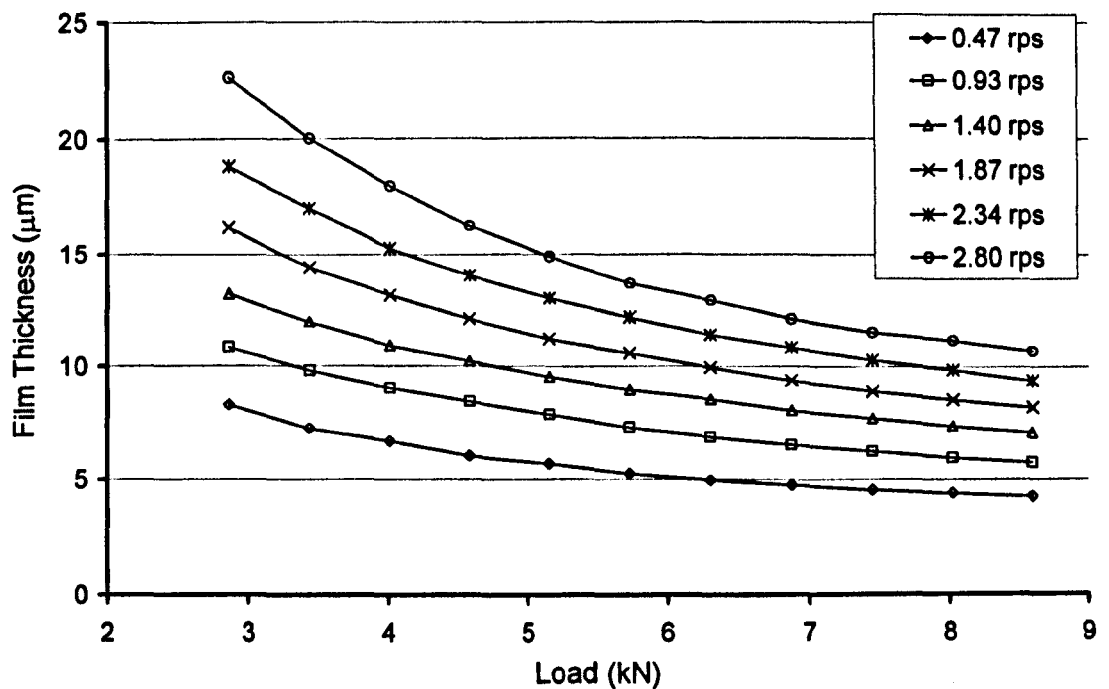
Figure 7.16. Oil film thickness Vs bearing load for a range of speeds.

The Journal bearing was run over a range of loads speeds as shown in figure 7.17. Initially the load was kept constant at 21.5 kN and the speed was increased in 70 rpm steps up to 700 rpm. Then the speed was kept constant at 700 rpm and the load was increased in 4.3 kN steps up to 38.7 kN. Finally the load was kept constant at 38.7 kN and the speed was reduced in 70 rpm steps down to 70 rpm.
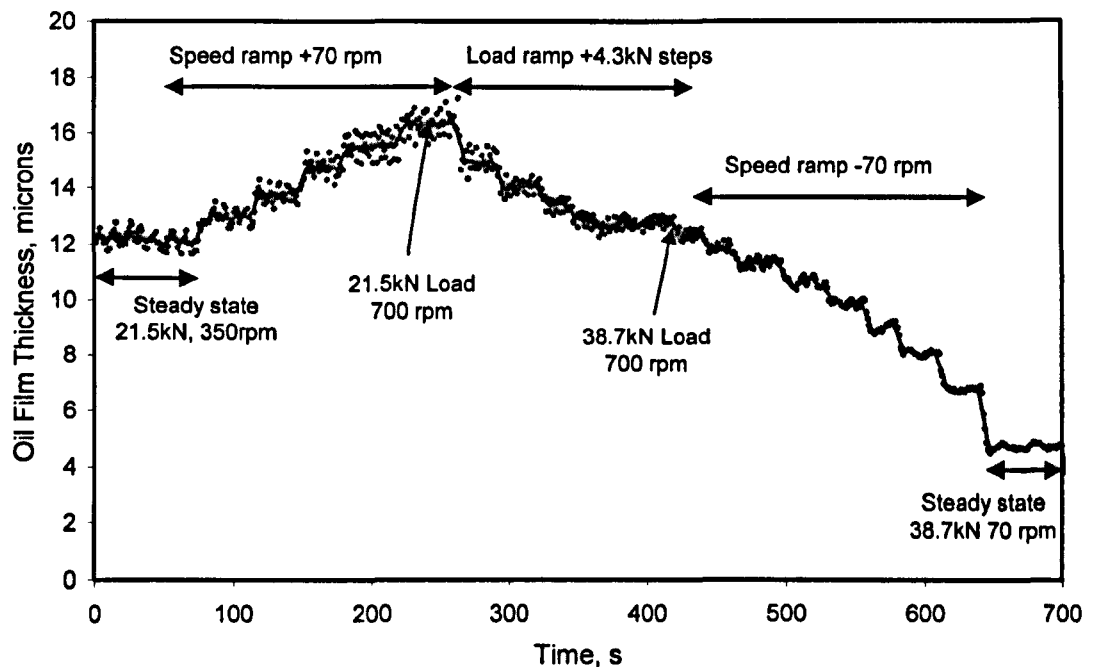
Figure 7.17. Film thickness measured over a range of loads and speeds

The data points from figure 7.16 were substituted into equation (7.01) to give film thickness against Sommerfeld number as shown in figure 7.18. As expected from section 7.1.1 the film thickness load curves from figure 7.16 all collapse down onto one line.

There is some disagreement, however, between the experimental results and the Sommerfeld theory (the sensor was vertical, not at h_{min}). This may be due to a couple of factors:

- the reference pulse was been taken whilst the rig was cold and thus would be slightly lower than expected.

- There may have been some bearing misalignment.

- The exact temperature of the oil in the loaded region was not known and may account for some discrepancy.

Also, above a value of R of approximately 0.95 there is a deviation in the results from the theory. This deviation is due to the fact that as the reflection coefficient approaches one the film thickness tends towards infinity (as shown in equation 3.22). This means that there is a tendency to over-predict film thicknesses where the reflection coefficient is very close to 1 (above 0.95). It can be seen in figure 7.18 that there is only one data set that deviates significantly from the rest of the data and that data set is for very thick films (i.e. R is approaching 1). This systematic error is due to an incorrect reference being used to calculate film thickness, most likely recorded when the test rig was cold.
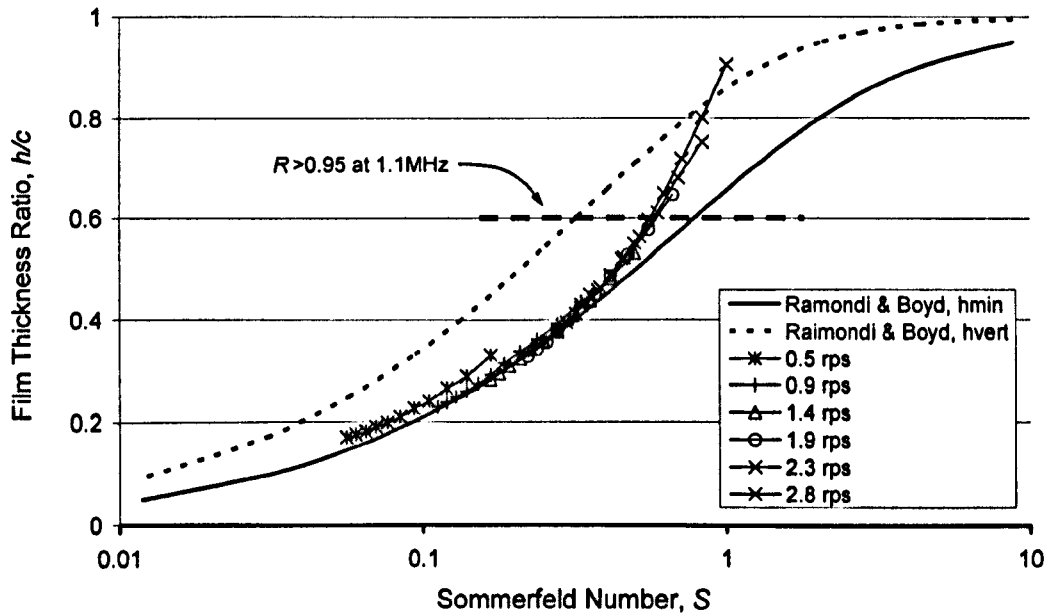
Figure 7.18. Film thickness Vs Sommerfeld number for the range of loads and speeds shown in figure 7.16.

The bearing housing was rotated about the journal to change the transducer location according to section 7.0.2. Figure 7.19 shows the film thickness measured round the circumference of the journal from 0° vertical to -90° in the direction of journal rotation. The predicted position of the minimum oil film was calculated from figure 7.04.

7.3.3. Measurement of Circumferential Film Thickness

Figure 7.11 shows schematically the location of the transducer and the method of rotating the transducer around the circumference of the journal. Experimental results are shown in figure 7.19 below. It can be seen that there is good agreement between the experimental and theoretical results.

There is some deviation in the results in the diverging region (i.e. to the right of the minimum film thickness). This is most likely due to cavitation within the lubricant resulting in changes to the acoustic properties of the lubricant. There was some significant fluctuation in the results in this region that confirms this hypothesis (each data point in figure 7.19 is only one snapshot in time).
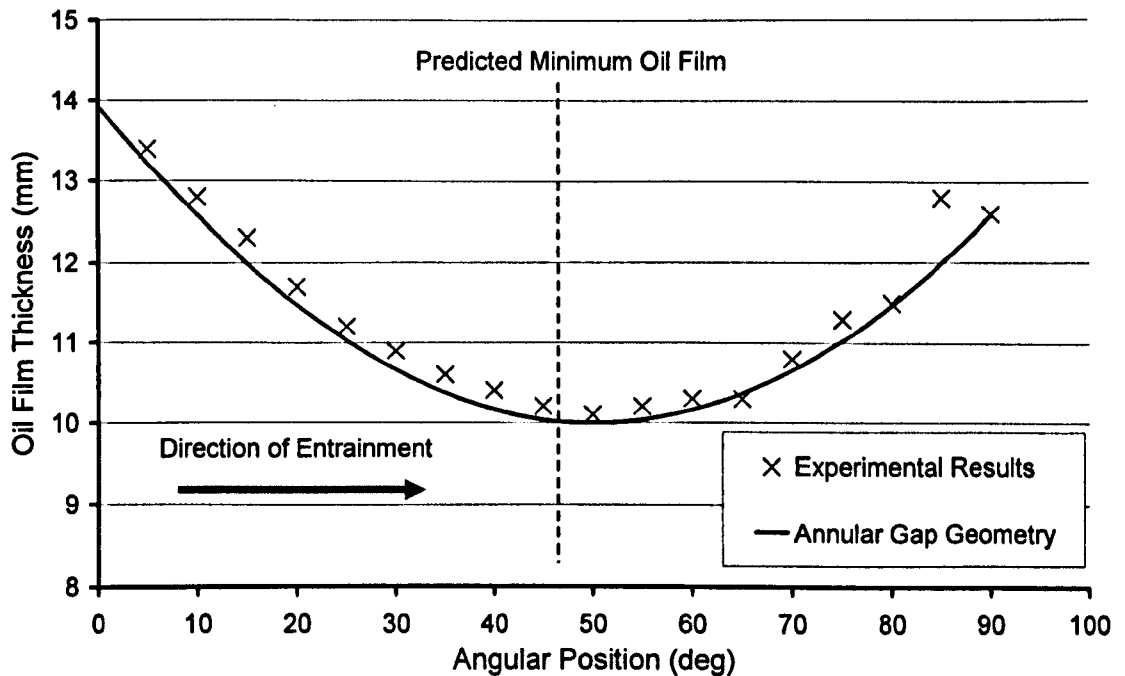
Figure 7.19. Measured oil film thickness round the circumference of a journal bearing for a fixed load and speed.

7.4. Experiments on a Commercial Motor Bearing

In order to prove the viability of this technique in real bearings, measurements were made on a standard hydrodynamic journal bearing.

7.4.1. Bearing Design

Michell Bearings Ltd. is a designer and manufacturer of journal and thrust bearings for a wide range of marine and industrial applications. One of their products, a 90mm diameter, 45mm wide, 50μm clearance white metal faced journal bearing, is used in many industrial applications. The bearing separates in two, a top half and a bottom half, with two thrust faces, one on each side (see figure 7.20).
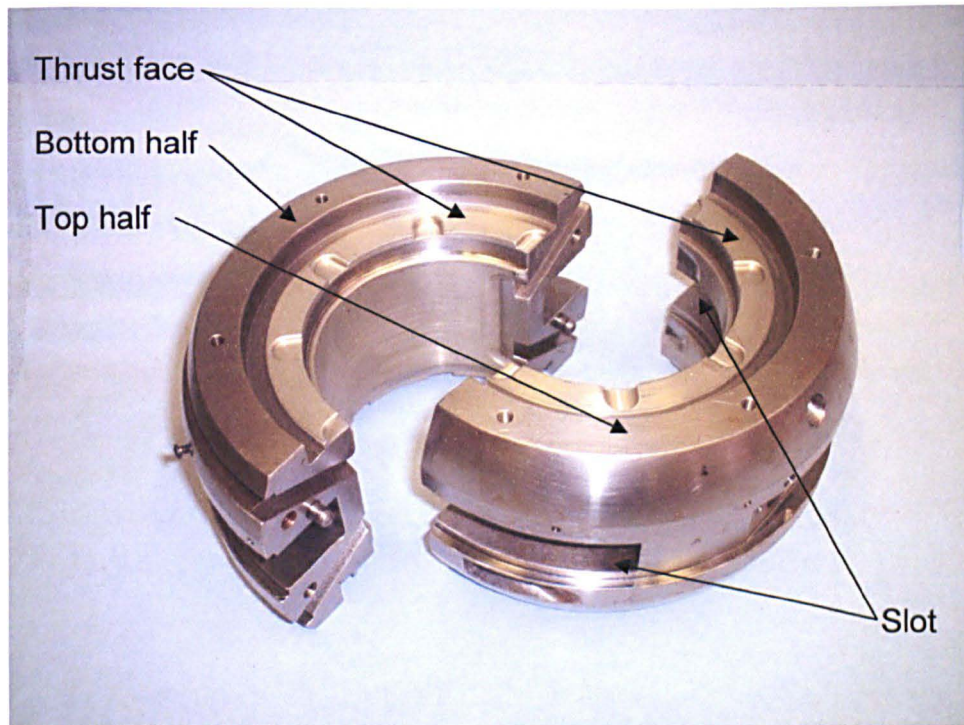
Figure 7.20. Michell Bearings Ltd 90mm journal bearing

Oil (Shell Tellus T68 – 68 cSt @ 40°C, 8.6 cSt @ 100°C) is supplied to the bearing by means of a slip ring. The bottom of the slip ring sits in a reservoir of oil and the top of the ring rests on top of the shaft (see figure 7.21). The top half of the bearing has a slot in it to accommodate the slip ring. As the shaft rotates the friction between the ring and the shaft causes the ring to rotate. The rotating ring carries oil up from the reservoir onto the shaft. This oil is then carried round to the loaded region by the rotation of the shaft.
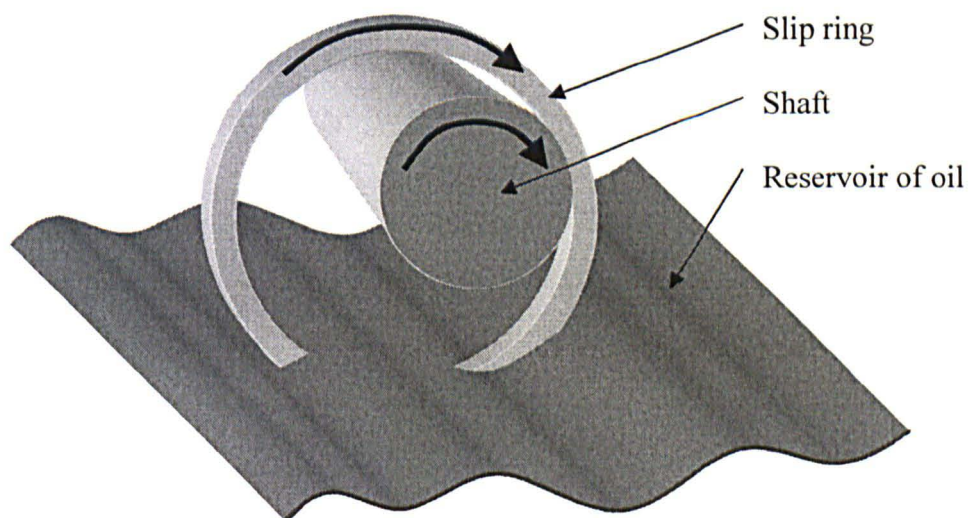
Figure 7.21. Picture showing a slip ring on a shaft for providing lubrication.

7.4.2. Bearing Test Apparatus

The test rig was arranged so that there was a support bearing, a loading bearing and a test bearing (see figure 7.22 and 7.23). The test rig was designed so that a variety of test bearings could be mounted on the end of the rig. Load was applied to the journal by a hydraulic cylinder acting vertically downwards on the loading bearing.
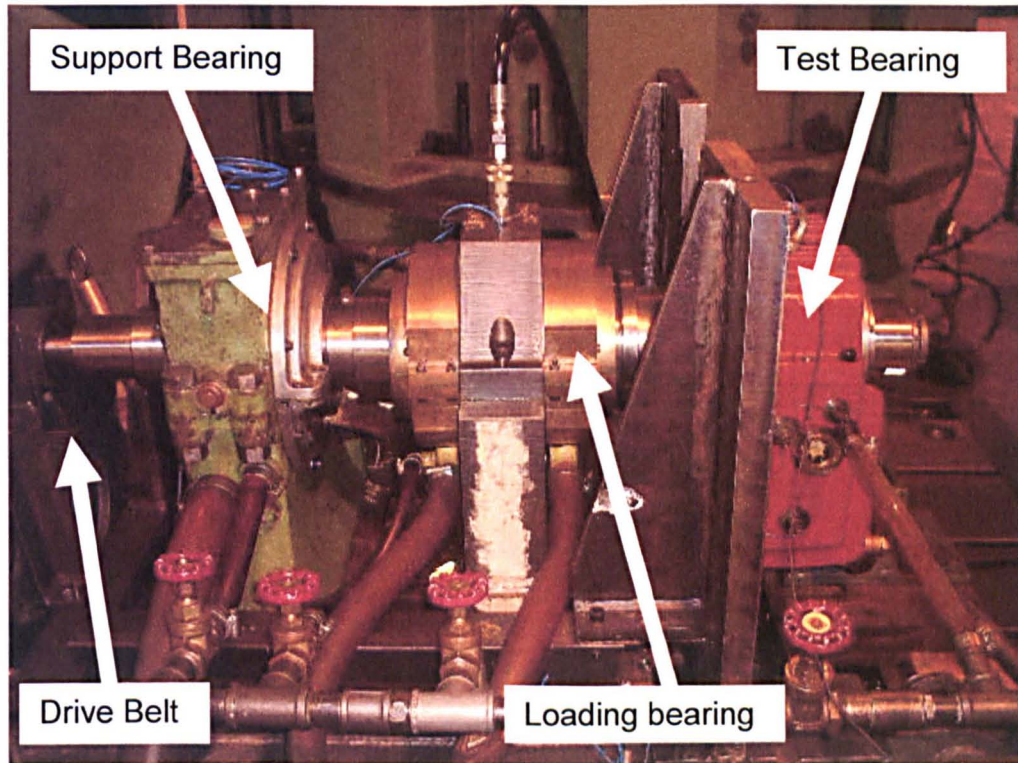
Figure 7.22. Journal bearing test rig.
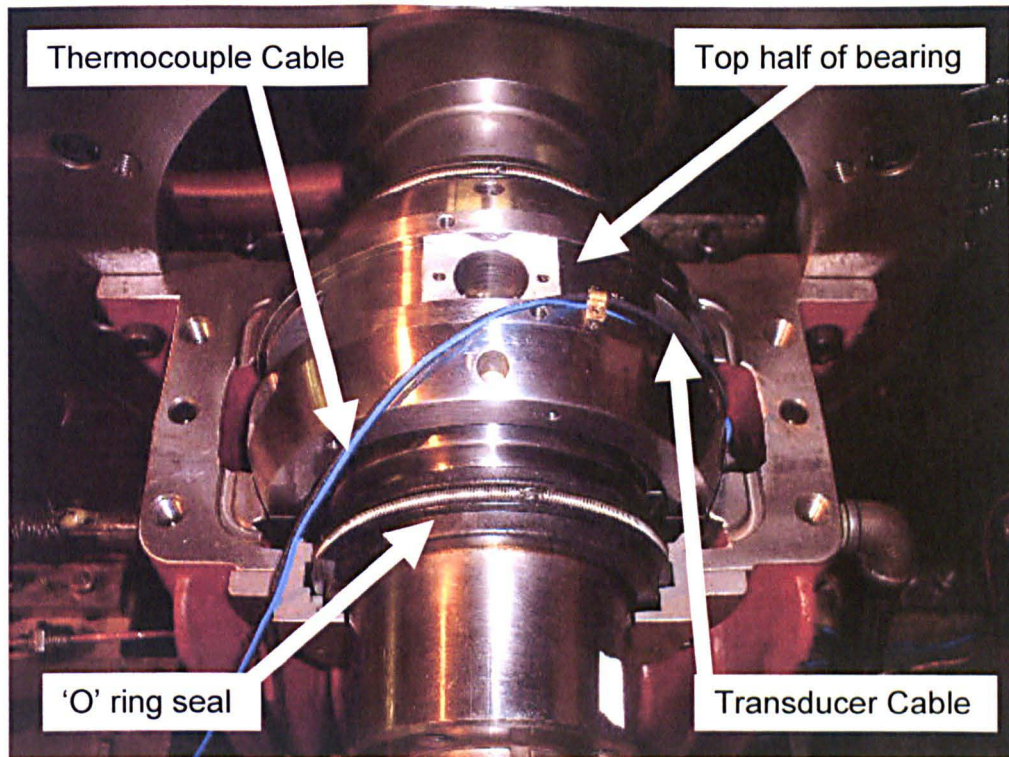
Figure 7.23. Test bearing housing disassembled.

7.4.3. Bearing Instrumentation

7.4.3.1. Sensor Installation

The bearing that was used in this test rig was unable to rotate. The transducer was located at 0° to the vertical (i.e. at the bottom) as this would allow comparison to models that predicted oil film thickness at this position.
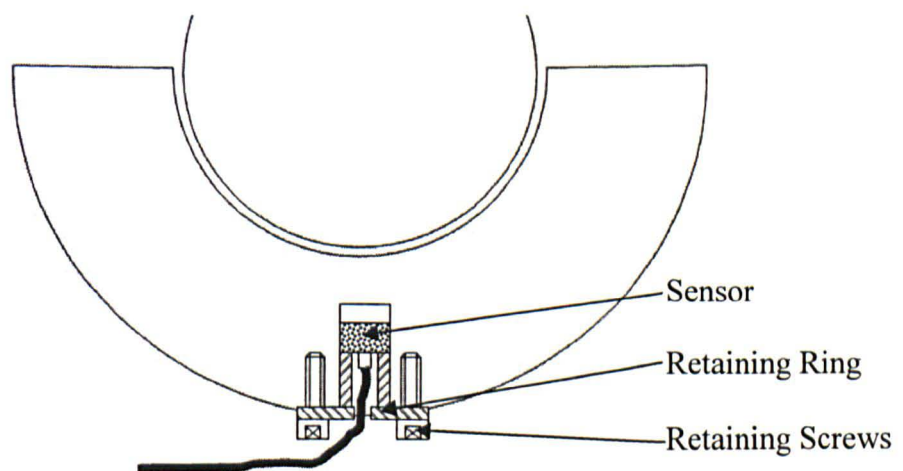
Figure 7.24. Schematic showing position of sensor.

7.4.3.2. Temperature compensation

At the time of testing it was not known that the temperature dependence of the ultrasonic transducer was a significant factor in taking measurements. Once trials commenced in Michell bearings it soon became apparent that the results were being heavily influenced by the running temperature in the bearing.

In order to calibrate the transducer a thermocouple recorded the transducer temperature. From section 6.2.3 it can be seen that the reflection coefficient from a very thick oil film is approximately 1. Therefore when the oil film is thicker than the frequency range of the sensor can measure, the reflected signal is equal to one. Hence a thick film was generated at several temperatures and a relationship was established between reflection coefficient and temperature. Figure 7.25 shows the results of the reflection coefficient at various temperatures using the over thickness calibration technique.
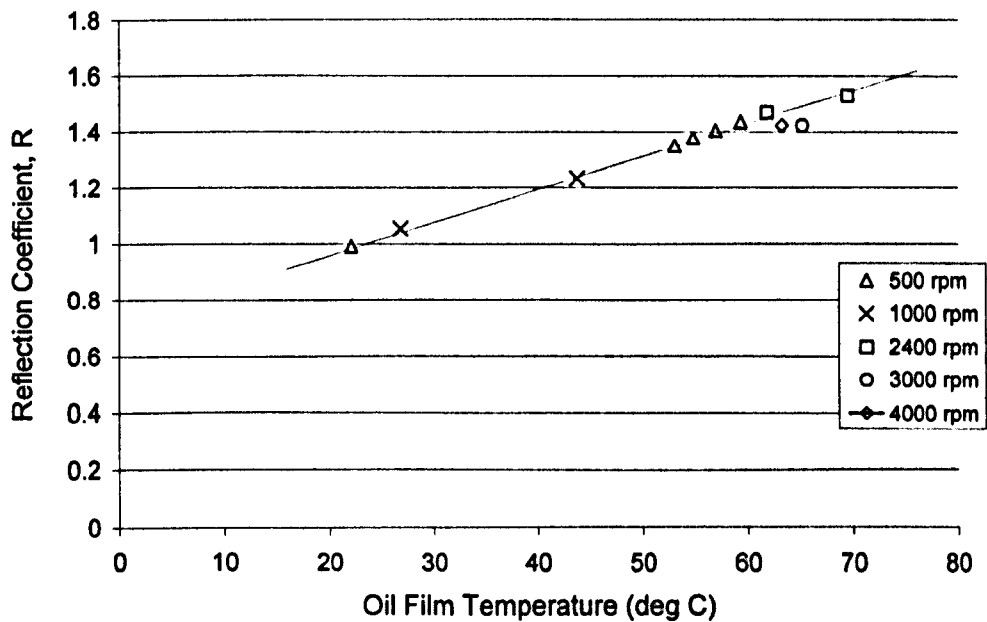
Figure 7.25. Plot of reflected amplitude against temperature for a 1MHz Panametrics NDT contact transducer.

Once a relationship was established between reflection coefficient and temperature the film thickness measurements were calibrated to account for the temperature change of the sensor.

7.5. Results

7.5.1. Reflection Coefficient and Determination of Film Thickness

Figures 7.26 - 7.29 show the steps taken in converting the received ultrasonic signal to film thickness.
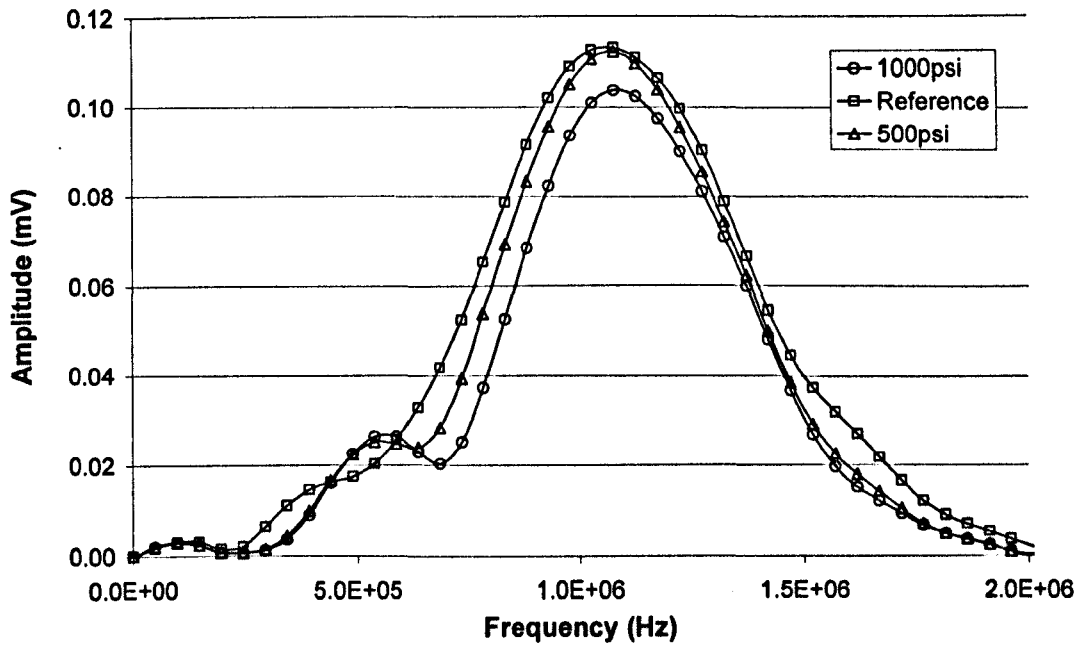
Figure 7.26. FFT's of reference, 1000psi test and 500psi test
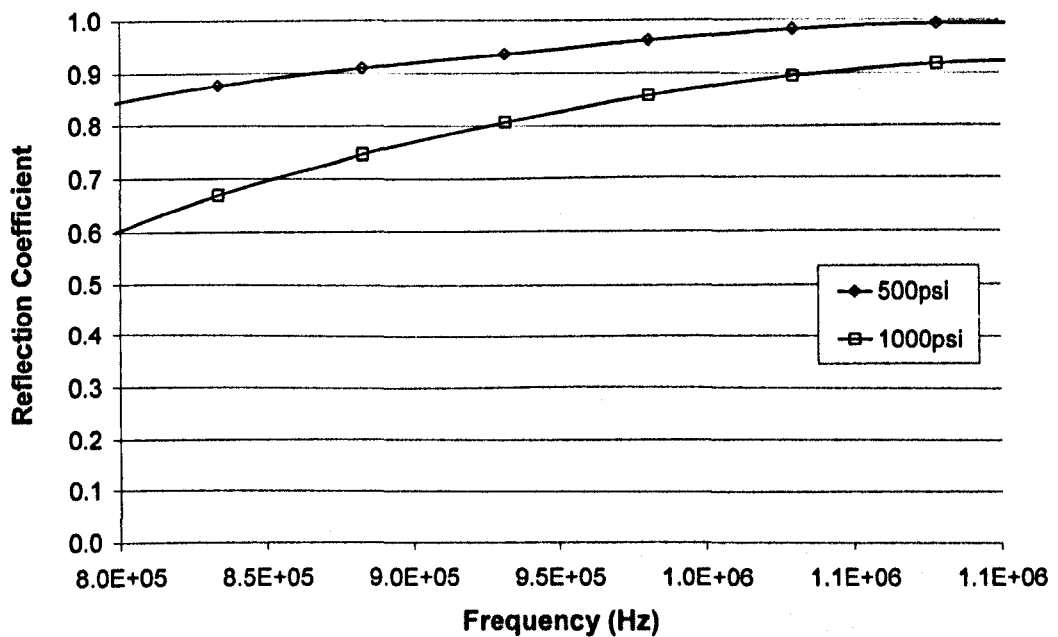
Figure 7.27. Reflection coefficient versus frequency for a range of oil films
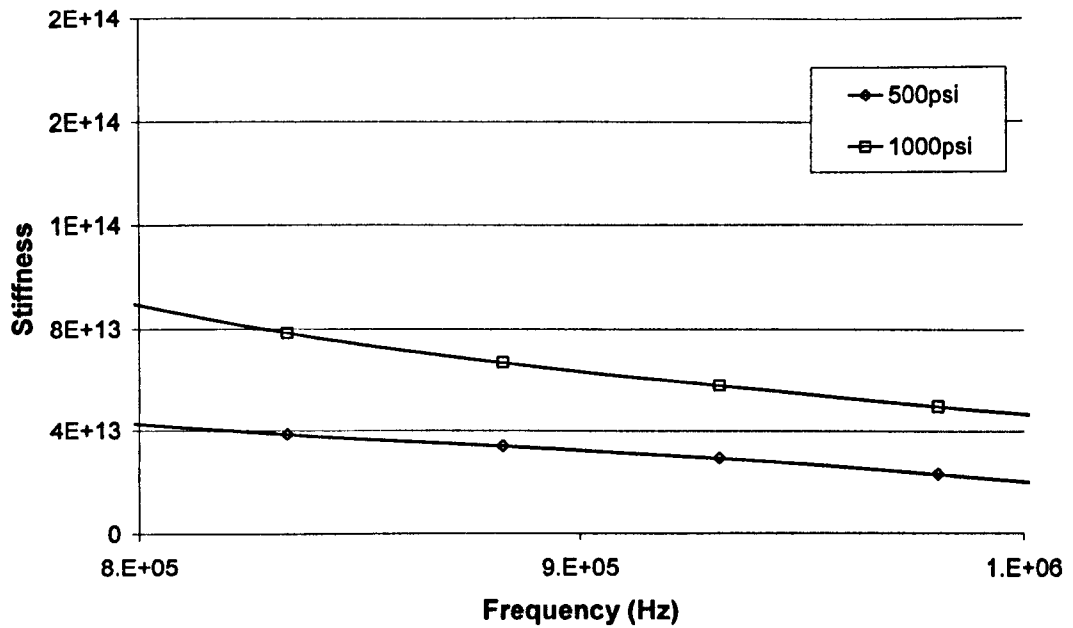
Figure 7.28. Stiffness of the oil film versus frequency for a range of oil films
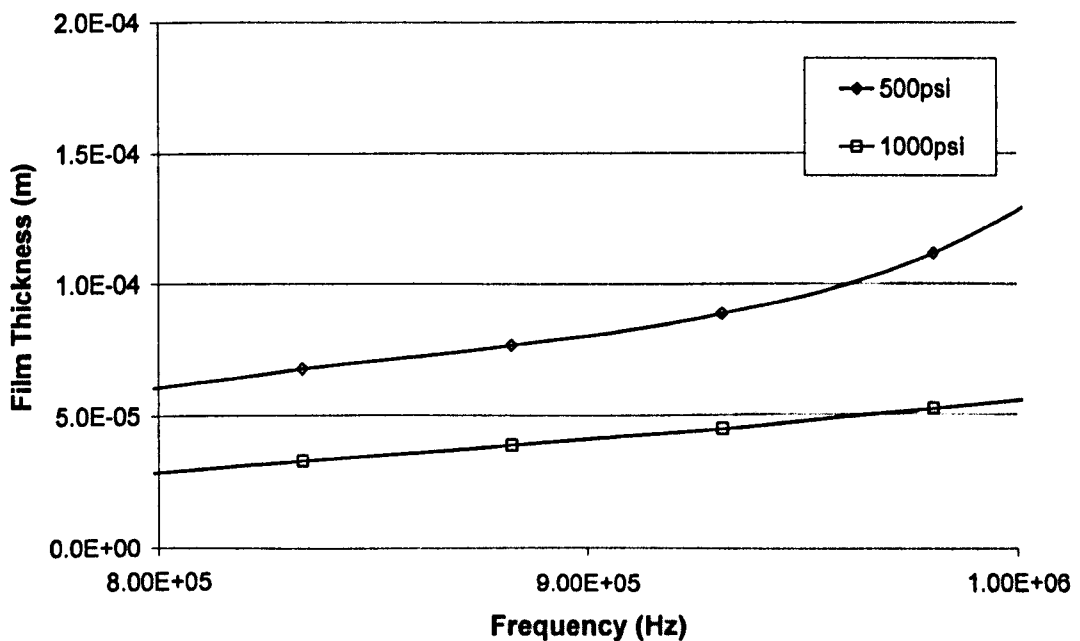
Figure 7.29. Oil film thickness versus frequency for a range of oil films

It can be seen in figure 7.29 that the film thickness is not constant with frequency. According to equation 3.22 the film thickness over the bandwidth of the sensor should be constant (as illustrated in figure 6.16). Intuitively this makes sense; it shouldn't matter what frequency sensor you use to measure the film thickness, the result should always be the same. This frequency dependence was most likely caused by the temperature effect within the sensor. The response of the sensor due to thermal expansion affects the

113

response of the sensor at all frequencies. Crucially though, the sensor response is not the same at all frequencies. Figure 7.25 shows a linear response of the centre frequency of the sensor. Figure 7.30 shows the response of specific frequencies to an increase in temperature (data taken from a 0.5MHz sensor). It can be seen that whilst the centre frequency has an approximately linear increase with frequency, the change in other frequencies is not the same. Thus, whilst it may remain accurate to calibrate the film thickness at the centre frequency this is not the case at other frequencies.
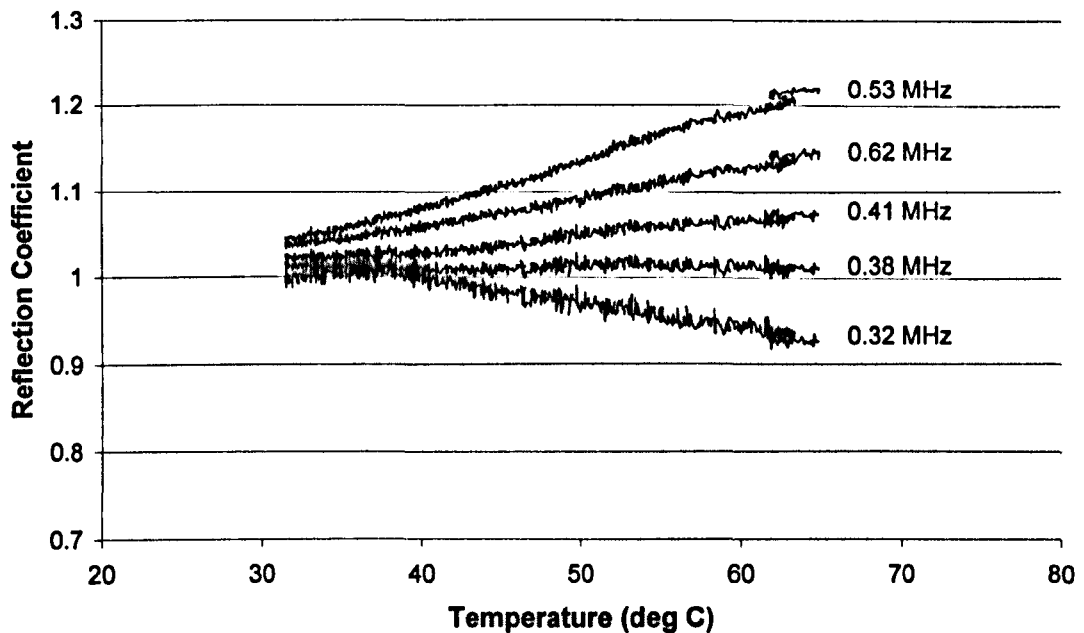
Figure 7.30. Response of individual frequencies to an increase in temperature for a 0.5MHz centre frequency sensor.

7.5.2. Variation of Bearing Operating Conditions

Figure 7.31 show the results from tests running at a range of loads and speeds. The trends observed in the film thickness are what are expected from theory (i.e. thicker films at higher speeds, lower films at lower speeds, thicker films at lower loads and thinner films at higher loads).
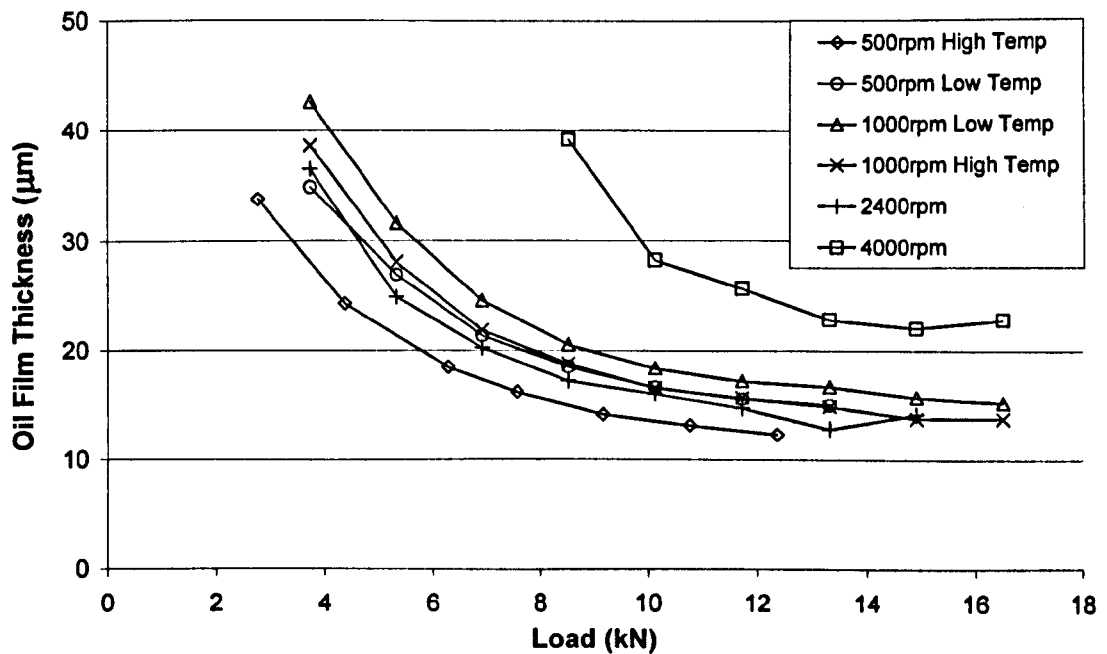
Figure 7.31. Oil film thickness versus load for a range of operating conditions.

7.5.3. Comparison with a Computational Model

Figures 7.32, 7.33 and 7.34 below show a comparison of the ultrasonic measurements with two different computational models. The models are part of Michell bearings' internal propriety design tools and are based upon a solution of the Reynolds equation in both 1-Dimension (only taking into account circumferential film thickness) and 2-Dimensions (taking into account circumferential and transverse film thicknesses). The 1-D model does not take into account temperature variation within the bearing and is based upon the Ocvirk short bearing solution. It assumes parabolic pressure distribution in the axial direction. The 2-D model calculates pressure distribution in the axial direction and is able to model the temperature profile across the film and using that to adjust the predicted film thickness. The model assumes constant shaft temperature and varying circumferential temperature. Output from the 2-D model is shown with and without temperature correction.

Figure 7.32 below shows a rather surprising result in that the 1D model more accurately represents the collected data than the 2D models. This is most likely because the developed pressure distribution in the axial direction is added to the 2D model producing a thicker calculated film.
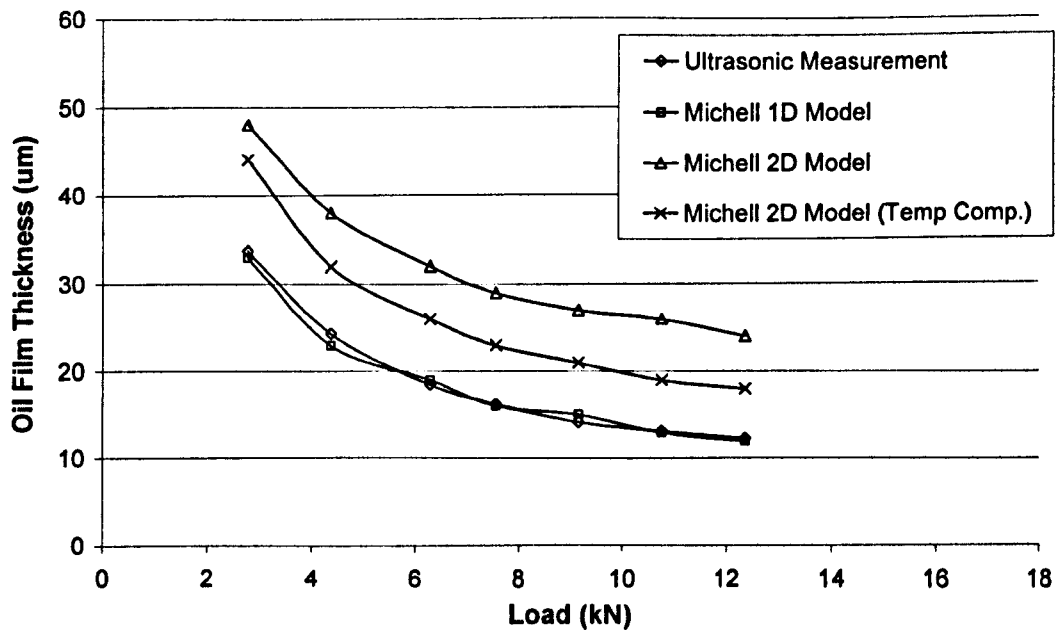
Figure 7.32. Comparison of oil film thickness versus load for ultrasonic measurement and various computational models running at 500rpm

Figure 7.32 above and figures 7.33 and 7.34 below show that the ultrasonic method measures films that are thinner than that predicted by either of the 2D Models. This is most likely because the assumed side leakage rates from the bearing are too low producing thicker calculated films.
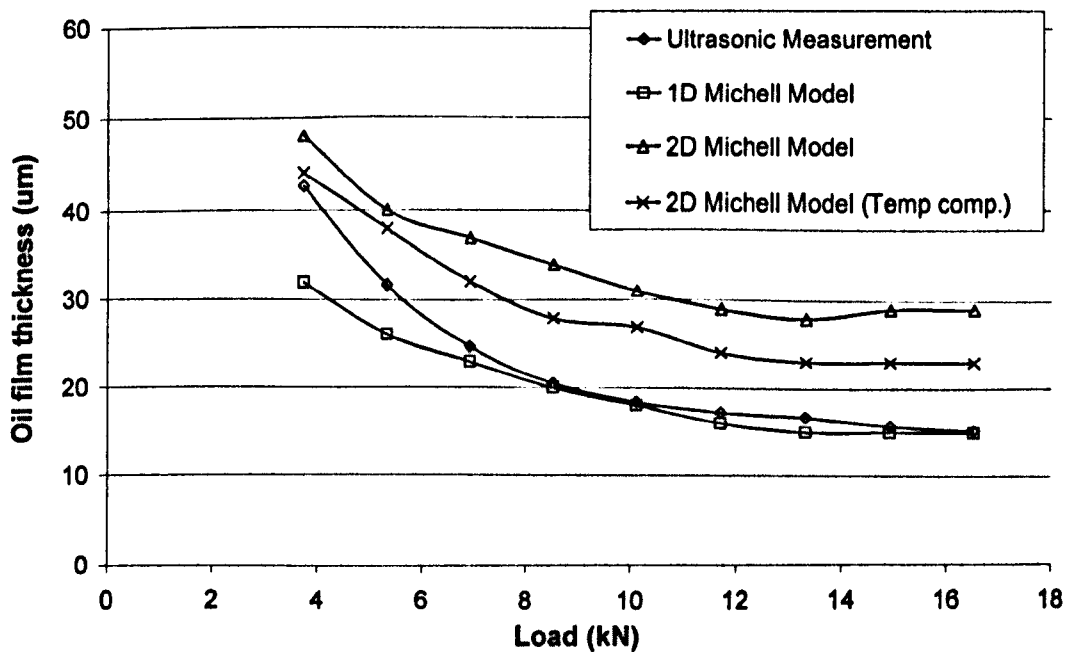
Figure 7.33. Comparison of oil film thickness versus load for ultrasonic measurement and various computational models running at 1000rpm
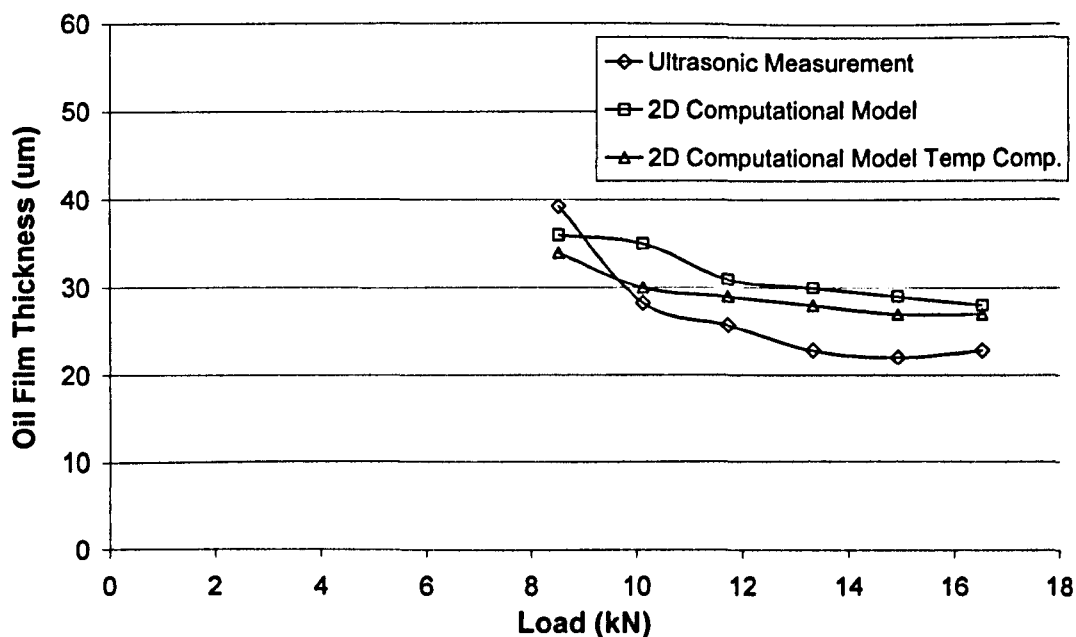
Figure 7.34. Comparison of oil film thickness versus load for ultrasonic measurement and various computational models running at 4000rpm

7.6. Conclusions

This chapter has demonstrated the application of the ultrasonic technique for measuring oil film thickness in two journal bearings. The following bullet points highlight the key points that were learned from these studies:

- Importance of Temperature. It was suspected that temperature would play a role in the stability and accuracy of the sensor. When the results were examined, they were found to be heavily dependent on the temperature of the sensor. This result emphasised the requirement for some sort of temperature calibration technique to be used in real engineering applications.

- Development of Over Thickness Calibration Technique. When the temperature dependent results were examined it was discovered that the reflected amplitude of a film that was too thick was the same as the reflected amplitude of a reference pulse at that temperature. This was used to calibrate the response from the sensor.

- Effect of Cavitation. It was expected that cavitation would occur within the diverging region of the bearing, but it was unclear what effect this would have on the results. It was discovered that it caused some fluctuation in the film thickness. This discovery can be used to detect cavitation in bearings.

- Importance of Selection of Correct Transducer. For this work a special sensor was selected based upon the expected film thicknesses in the bearing. The sensors frequency bandwidth was sufficient for the films encountered during testing.

- Limits on Technique where $R \geq 0.95$. An upper limit for the reflection coefficient was discovered and shown to adversely affect measurements of film thickness above that limit.

- The measurements were compared to theoretical film thicknesses and the trends in the results were very similar.

Chapter 8:

Hydraulic Motor Piston Ring Film Measurement

This chapter details tests that were carried out on a piston ring test rig to measure the oil film thickness between a piston ring and cylinder over a range of loads and speeds. The work was carried out at KTH University, Stockholm, Sweden where the film measurement equipment was attached to a rig that was being used to measure frictional forces for various piston ring designs.

The use of ultrasonic film thickness measurements in this application required the development of several new techniques:

- Focusing of the sound wave onto a small component that was moving back and forth past the measurement point.

- Transmission of ultrasound through a very attenuative material in the piston liner

- Increased speed of capture compared to the work on piston rings

The aim of all this work was to understand the effect of operating conditions on film thickness in order to aid in the design process.

8.1. Piston Ring Background

Pistons are used in a wide range of applications for converting pressure to force or vice a versa. Examples are high pressure combustion gasses in an internal combustion (IC) engine that are converted to a linear force, compressed gas in a linear actuator, and high

pressure oil acting against a piston in a hydraulic motor. In each of these examples a gas or a liquid is used to displace a piston within a cylinder. See figure 8.01 for example.

1: Without Piston Ring   **2: With Piston Ring**
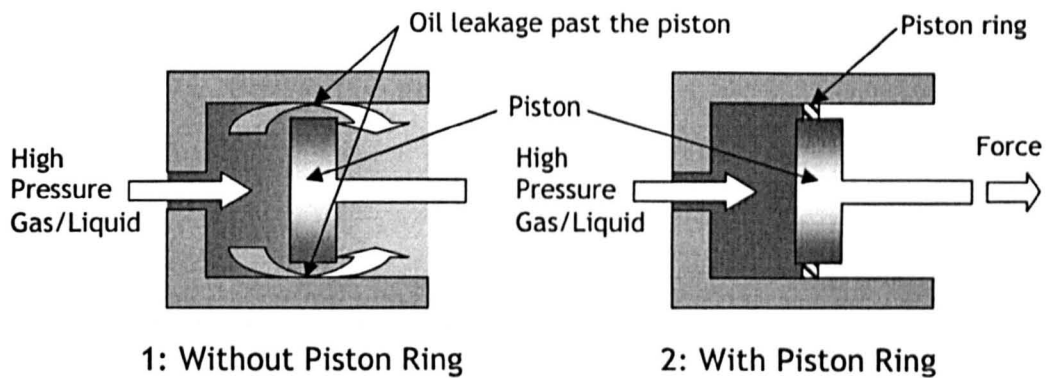
Figure 8.01. 1 - gas/liquid leaking past the piston and thus there is no exerted force.
2 - a piston ring retaining the gas/liquid and producing a force.

Piston rings are used in these situations for the following reasons:

- The piston ring acts as a seal to contain the high pressure gas or liquid on one side of the piston.

- The piston ring is a small part that can be easily and cost effectively replaced in the event of wear or damage.

- In the event of wear to the cylinder resulting in a dimensional change, a new piston ring with larger dimensions can be used to reduce the clearance.

- Due to a small cross section the piston ring can conform under pressure to the cylinder surface and thus improve sealing.

Piston rings are usually made from a material that suits the application. For example in a hydraulic cylinder the 'piston ring' (usually called a seal) is made from a conformal rubber or plastic. This is possible due to the low sliding speed and relatively low number of cycles. In an internal combustion engine the piston rings are usually made from steel or an alloy thereof. These are used due to the high sliding speed and high number of cycles.

In order to achieve a good seal there needs to be a close radial tolerance between the inner bore of the cylinder and the outer diameter of the piston ring. Typically this tolerance is in the range 5-10 μm. The tolerance controls, to a large extent, what the film thickness is at low pressures (if there is a large tolerance then there will be a thick film).

In operation there is also hydraulic pressure acting on the piston ring that forces it to 'open' as shown in figure 8.02. These opening forces affect the film thickness between the ring and the cylinder. This opening force only becomes significant at very high pressures, which are also the conditions where there is likely to be thick films. By careful design of the ring it is possible to balance these effects to control film thickness.
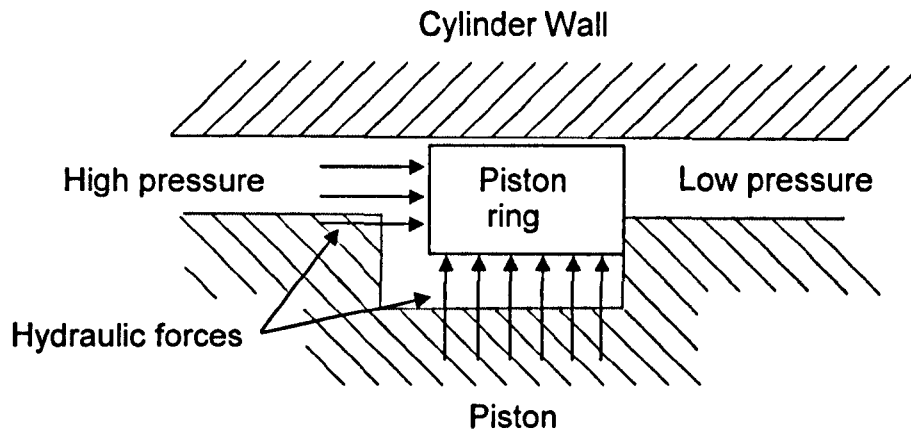
Figure 8.02. Schematic showing the hydraulic forces acting on a piston ring.

In order to benefit from this 'opening' force the piston rings are designed to be wide and thin. The thickness of the ring is related to the expected pressures that the piston is likely to see.

A curved crown shape improves lubrication by creating a convergent wedge between the ring and the cylinder wall. Oil is drawn into the interface between the piston ring and the cylinder wall when the piston moves along the cylinder. As the oil pressure across the width of the ring increases it supports and balances the hydraulic opening force on the ring.

Figure 8.03 shows the position of the piston ring in relation to the piston, cylinder, high pressure region and low pressure region.
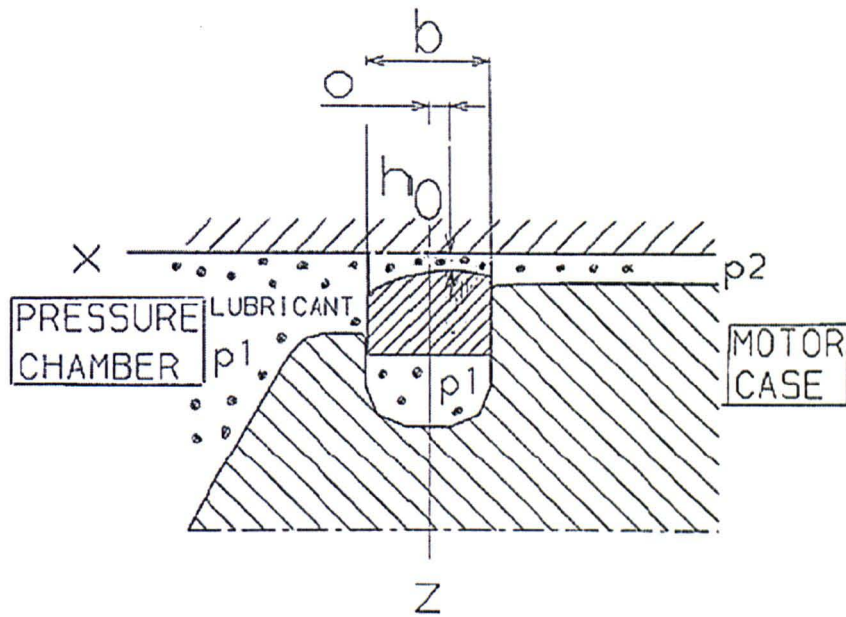
Figure 8.03. Piston, piston ring and cylinder. Also shown is pressure p1 acting in the pressure chamber and also acting on the inner face of the piston ring [Sjodin, 2005].

8.2. Hydraulic Motor

The piston application being studied in this chapter is a hydraulic motor. Hydraulic motors are used in many applications where a high torque low speed shaft rotation is required. Typical examples are shown in figure 8.04.
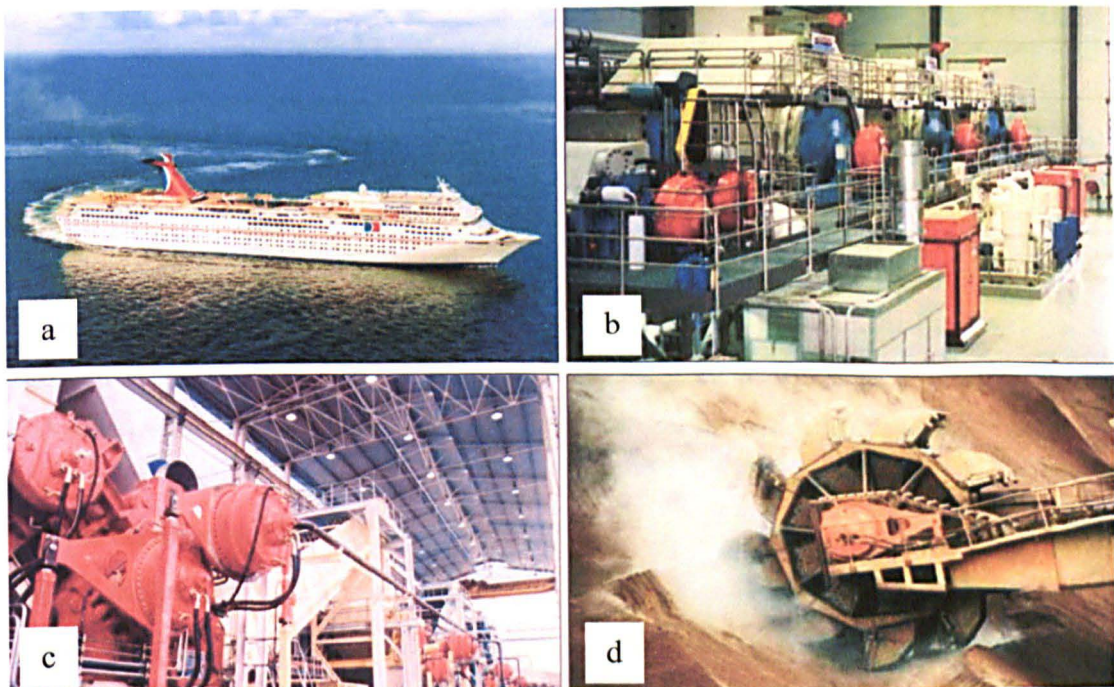
Figure 8.04. Applications where Hägglunds hydraulic motors are used: a) Cruise Ships, b) Sugar Refining, c) Paper Mills and d) bulk materials handling (Skytte af Sätra [2005]).

Radial piston hydraulic motors have radial pistons that move in and out in the radial direction and produce a rotation of a shaft. Figure 8.05 shows a typical with the radial nature of the pistons shown.
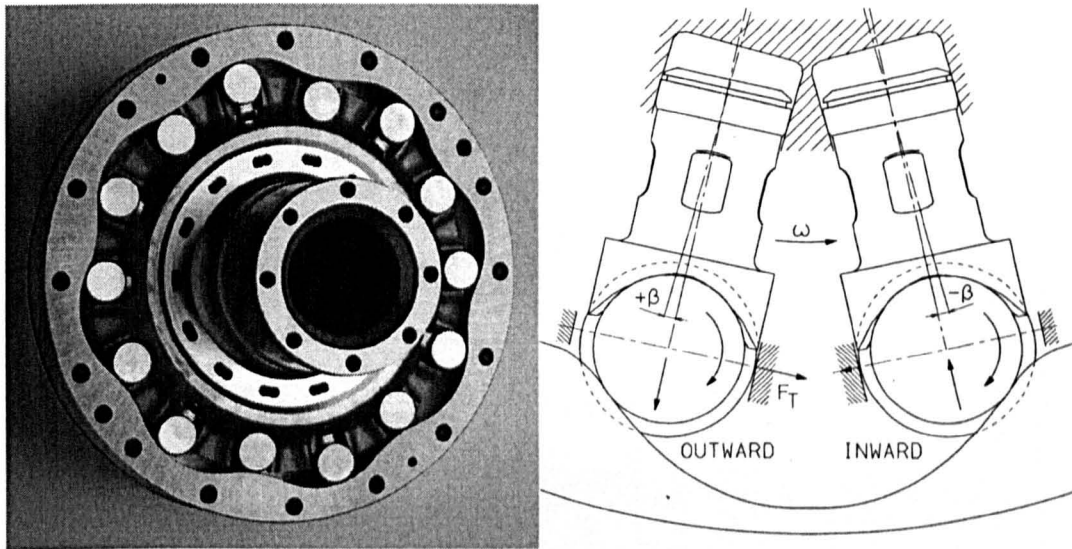
Figure 8.05. The Hägglunds radial piston hydraulic motor. Piston movement during the stroke in driving mode. Working pressure at outward movement and charge pressure at inward movement.

The efficiency of this motor is linked to the piston ring/cylinder oil film. If there is very thick oil film a considerable quantity of oil can leak from the high pressure side of the piston to the low pressure side of the piston. This results in a decrease in efficiency. If there is a very thin oil film then there may be an increase in friction and also wear of the piston ring and/or cylinder. For both of these reasons it is important to know the oil film thickness between a piston ring and the cylinder.

The piston rings used in the hydraulic motor shown in figure 8.05 are complete rings (rather than split rings as in IC engines) with a specific profile that runs against the cylinder. In contrast to IC engines, there is only one piston ring per piston in the hydraulic motor. Thus the job of the single ring is critical for correct, efficient operation.

The piston rings in a hydraulic motor are designed to seal a pressure in one direction. As a result the piston rings may have an anti-symmetrical profile across their sealing face as shown in figure 8.06. The profile, or crown shape, is designed to improve lubrication in one direction between the piston ring and the cylinder.
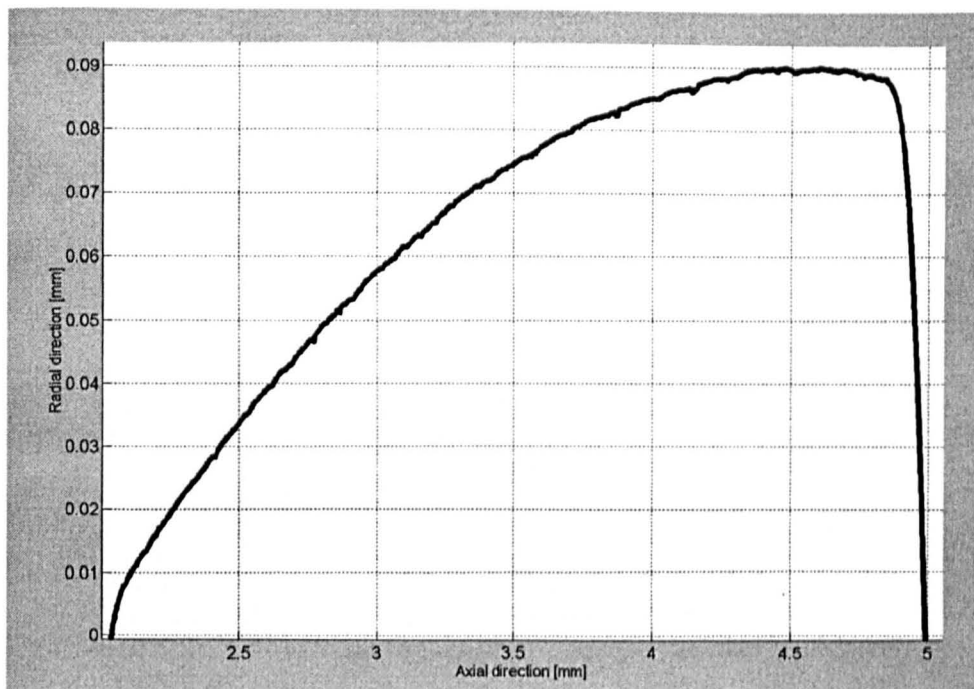
Figure 8.06. Example profile of a piston ring designed for uni-directional sealing (Sjodin, [2005]).

In testing a range of different tolerance rings were tested to examine their effect on film thickness. Some of these rings, however, produced film thicknesses that were outside the range of the sensor (see figure 6.03). This was due to either an excessive clearance in the radial direction (too small a ring for the cylinder) or an excessive circumferential waviness (correct sized ring but locally thick films).

8.3. Piston Bench Test Rig

The bench test apparatus used was originally developed to study the performance of different piston ring and cylinder bore designs during sliding motion. A force transducer measured the push/pull force required to move the piston through the cylinder. The primary variables examined were friction and wear. However when the test rig was modified for ultrasonic measurements, the force measurements were disabled.

Figure 8.06 shows a schematic of the test rig. Two cylinders are mounted on the bench as shown. Both pistons are driven by means of a connecting rod attached to a crank on a motor. Each piston has two piston rings; one at each end. High pressure oil (Shell Tellus T32) is fed into the cavity between the two rings (as shown in figure 8.07). The oil then passes over the piston rings to the low pressure oil outlets. This configuration ensured that there was no net force in the axial direction.
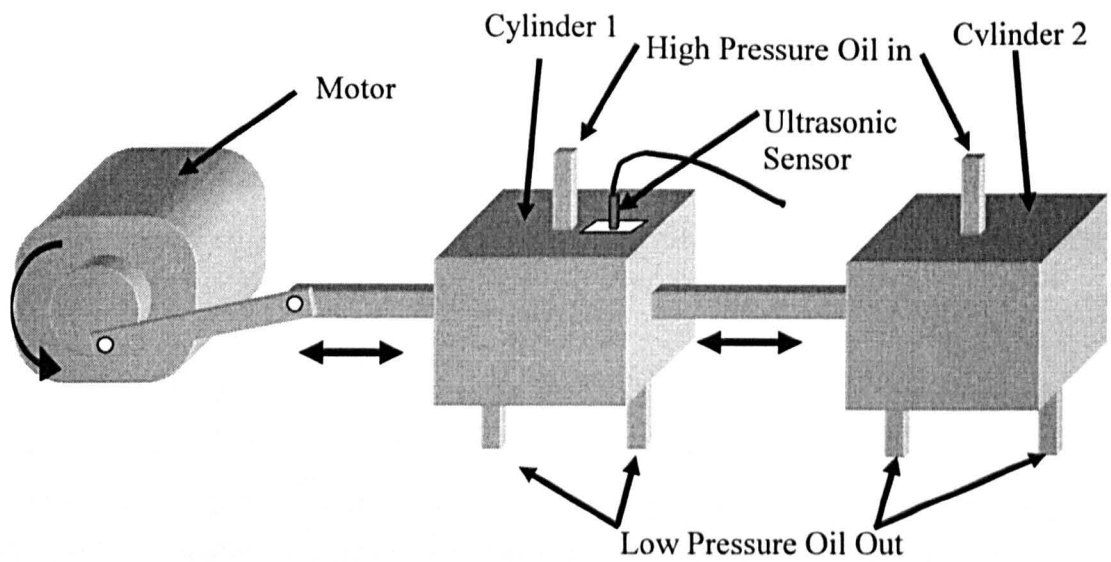
Figure 8.07. Schematic of the test bed showing test cylinder 1 and 2.

Within cylinder 1 and 2 there are non-acting double ended pistons as shown in figure 8.07. A non-acting piston was used to simplify testing whilst replicating operating conditions of 10 to 35 MPa. Piston stroke was 43mm and oil temperature was 50°C.
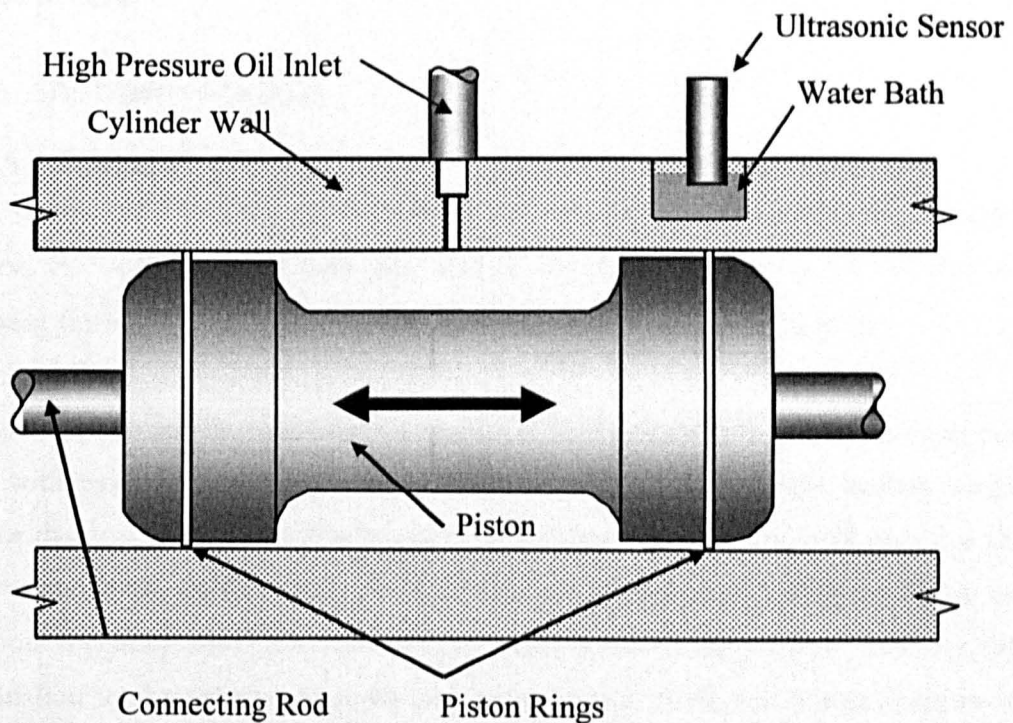
Figure 8.08. Schematic of the non-acting piston used in testing. High pressure fluid is supplied to the centre of the piston stroke and gets forced out in both directions.

125

In the testing, a piston ring made from hardened bearing steel 100 Cr6, was used. The rings were 75mm diameter, 5mm wide and 2mm thick and had a range of profiles including a 'square' ring i.e. there was no change in height across the cross-sectional profile. Typical surface roughness's were in the region 0.2μm Ra. There was also a circumferential clearance that relates the 'roundness' of the cylinder to the ring. It was found that many of the rings that were to be tested had a circumferential variation of up to 20μm.

Several different piston rings were tried in the test rig. This was to try and examine what the effect was on film thickness for a variety of tolerances. Some of these tests did not yield any results due to the local film thickness being larger than the measurable range of the sensor. In other tests where the expected tolerance was within range of the sensor there was still a failure to get data. This was due to circumferential waviness of the ring. Results were obtained when the ring was rotated to provide a 'hump' rather than a 'hollow' at the measurement point. This was less than ideal as the ring rotated during testing. The results presented in this chapter were from a ring that had minimal circumferential waviness and that gave the best results over the range of pressures and speeds possible.

8.4. Instrumentation

8.4.1. Sensor

Due to the small contact width between the cylinder and the piston ring, a focusing sensor was used. A water bath was used to couple the sensor to the cylinder whilst allowing for height adjustment to take account of focusing (see figure 8.08).

The sensor was selected according to equation (4.01) and also based upon experimental tests with sensors of different frequencies. The goal was to select the highest frequency sensor that was possible, as this provides the smallest spot size. A small spot size allows measurement on thinner rings, measurement on thicker rings at higher sliding speed (without triggering) and potential for measurements across ring profiles. However, due to attenuation in the cylinder material (see section 8.4.2) there was a restriction in using higher frequencies.

The sensor that was chosen (a Panametrics 10MHz focusing sensor) was the best sensor to give maximum frequency but minimum attenuation. This sensor had a focal spot size of approximately 920µm on the inside of the cylinder. The sensor had a 75mm focal length in water. The length of the water path between the cylinder wall and the front face of the sensor was calculated using equation (4.02). This ensured that the sensor was in the optimum position to provide a measurement spot that was as small as possible.

It was known that the maximum operating temperature of the test rig would be about 55°C. This was within the operating limits of the sensor (60°C). However, before testing, it was unclear whether the temperature effect would have an adverse effect on the film thickness measurement. This proved not to be the case for the simple reason that the presence of the lubricant film was intermittent (i.e. when the piston ring passed the focal spot (or measurement point) of the sensor as shown in figure 8.12). This provided a pulse from the inner surface of the liner with and without a lubricant film over the course of each stroke. Hence this allowed a reference signal and a measurement signal to be captured every stroke.
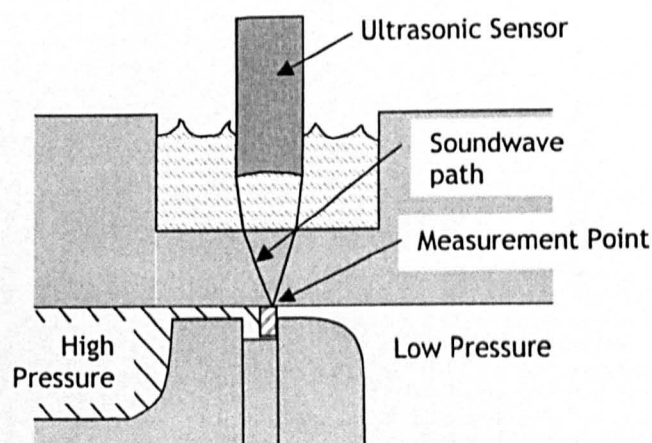
Figure 8.08. Schematic diagram of the sensor location and focusing through a water bath and the cylinder wall

8.4.2. Test Rig Modification

The cylinder that was used in the testing was made from a nodular cast iron. In section 3.3.3 it was shown that the attenuation is linked to the microstructure, and coarse materials, such as the cast iron used in this test, can severely attenuate the ultrasonic signal.

Initial tests were carried out to examine the attenuation of the cylinder material. Sensors of increasing frequency were placed on the liner to investigate transmission of sound. It was found to be very attenuative, so much so that it was not possible to receive a 10MHz signal though the cylinder wall (10MHz was the minimum frequency that could be used in order to produce a small enough focal spot for the piston rings under consideration). To resolve this issue a slot was milled in the cylinder to provide an area with a thinner wall thickness (see figure 8.08). It was found that 4mm was the maximum thickness that a 10MHz focusing sensor could look through and receive a signal suitable for processing.

The sensor was held in a jig that allowed for movement in the vertical direction to adjust for focusing (see section 4.3.1.2). The sensor was mounted vertically above the centreline of the piston and in the middle of the stroke. As can be seen from figure 8.09, this was also the point of highest sliding velocity.
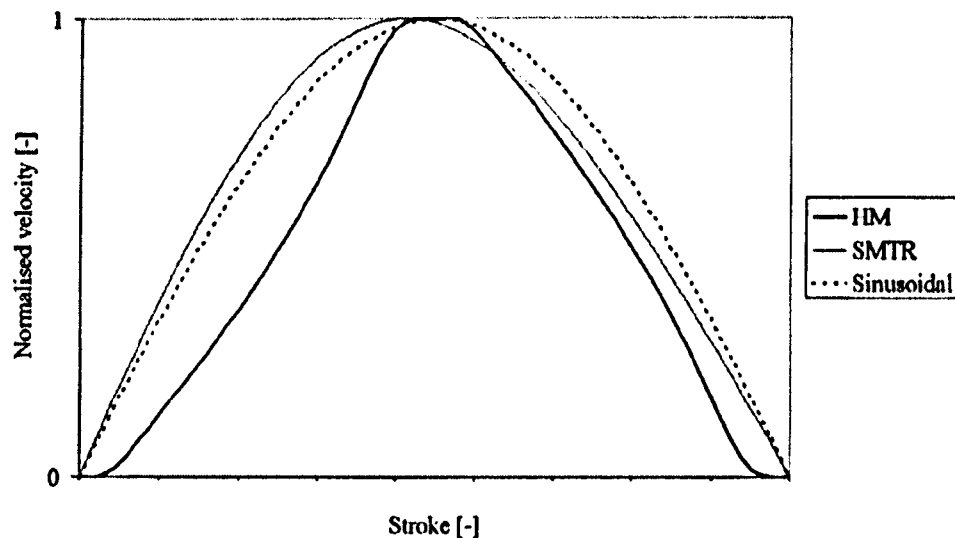
Figure 8.09. Comparison of sliding velocities between a Hydraulic Motor (HM), Sliding Movement Test Rig (SMTR), and pure sinusoidal motion (Skytte af Sätra [2005]).

This was the point that was of most interest from a research point of view, but was the most difficult point from a leakage point of view as explained in section 8.6.

8.5. Lubricant Film Measuring Apparatus

The equipment for measuring the lubricant film thickness in this application is that described in Chapter 5.

8.6. Measurement Procedure

The method of calculating film thickness is the same as that described in section 6.5. The application of that technique presented a major challenge however.

As was noted in section 8.4 the measurement point where the sensor was located coincided with the point of highest sliding velocity. This meant that either the measurement system had to catch data as fast as possible, or the pulser needed to be triggered in order to ensure that at least one measurement was made on the ring. Unfortunately this second option was not available during testing so effort was focused on capturing the data as fast as possible.

In order to capture data as fast as possible, software was written to save the raw data to disk without any on-line calculation of film thickness. Due to software and hardware limitations the maximum speed that data could be captured was approximately 8 Hz (chapter 8 deals with a development in the technique used to measure at a much higher speed, up to 10kHz).

In order to ensure that there were a sufficient number of measurements on the piston ring, the maximum sliding speed was calculated based upon the capture rate of the measurement system, the size of the focal spot of the transducer and the width of the piston ring. This was calculated to be 12mm/s which was significantly lower than the actual maximum operating speed of the test rig.

The test was run at a variety of test conditions and the raw data was collected. This data was then post processed using the software described in section 5.2.4 and shown in Appendix 5.

8.7. Results

Figure 8.09 shows successive pulses captured as the piston ring passed the measurement spot. Each pulse has a similar shape but slightly different amplitudes.
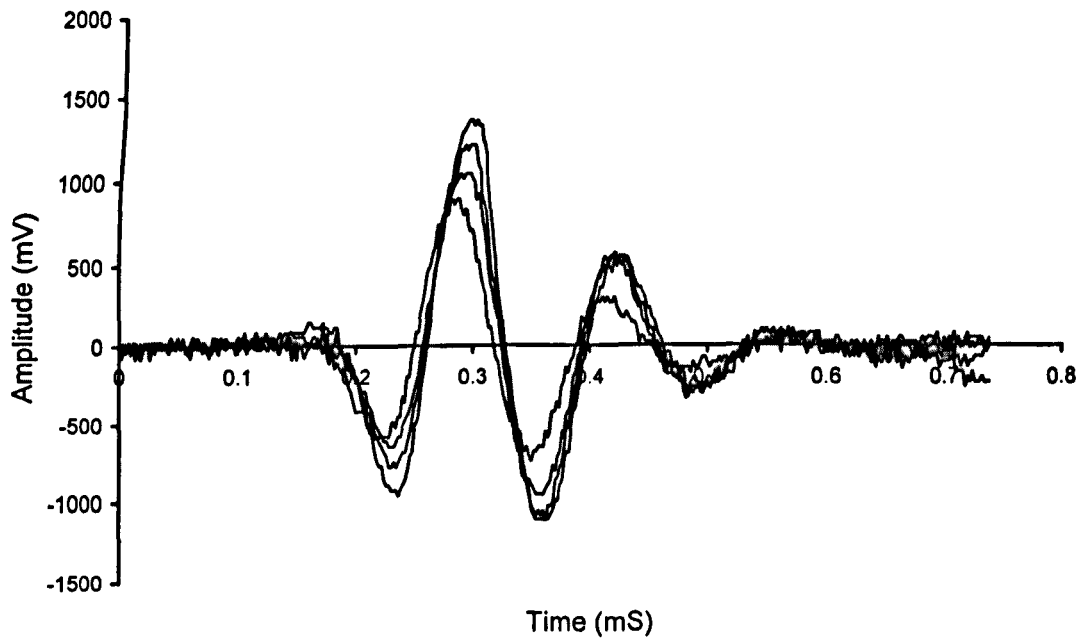
Figure 8.09. A selection of pulses captured as the piston ring passed the measurement area.

Figure 8.10 below shows successive FFT's of the time domain signals. Also shown is the reference where a signal was captured without an oil film.
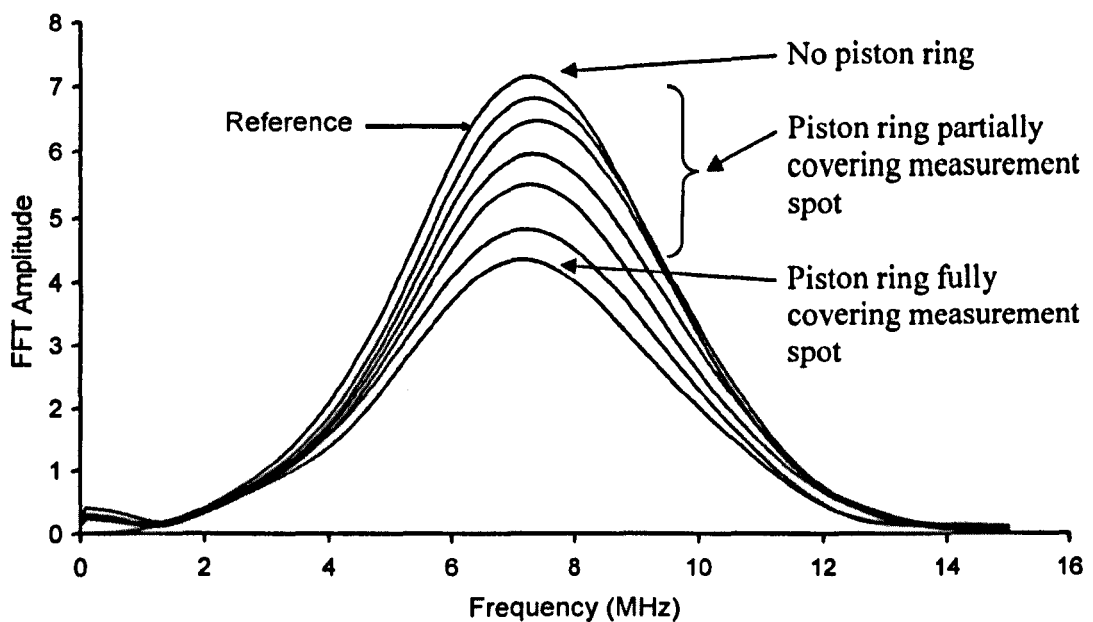
Figure 8.10. A selection of FFT's of pulses captured as the piston ring passed the measurement spot.

Figure 8.11 shows the FFT's from figure 8.10 divided by the reference also shown in figure 8.10.
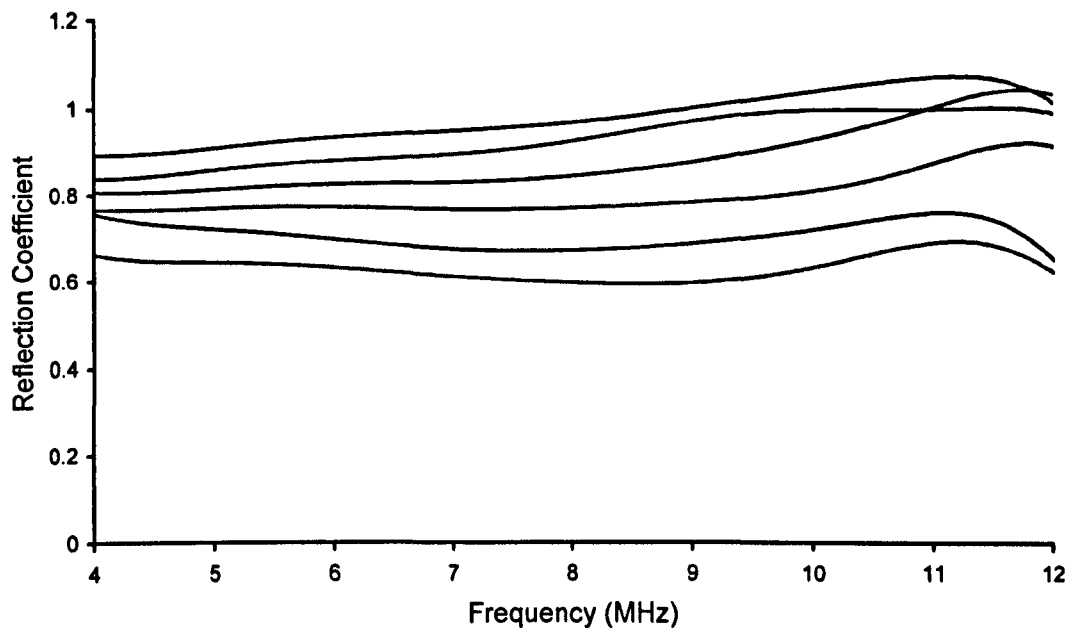
Figure 8.11. A selection of reflection coefficients versus frequency plots as the piston ring passed the measurement spot.

It can be seen that there is a range of reflection coefficients measured from the piston ring passing the measurement point. These reflection coefficients, however, cannot be related to oil film thickness because they do not represent a change in oil film thickness. As the piston ring passes the measurement point the measurement point is partially covered by the ring, covered by the ring and partially covered by the ring as it passes. Figure 8.12 shows the progression of a ring past the measurement point.
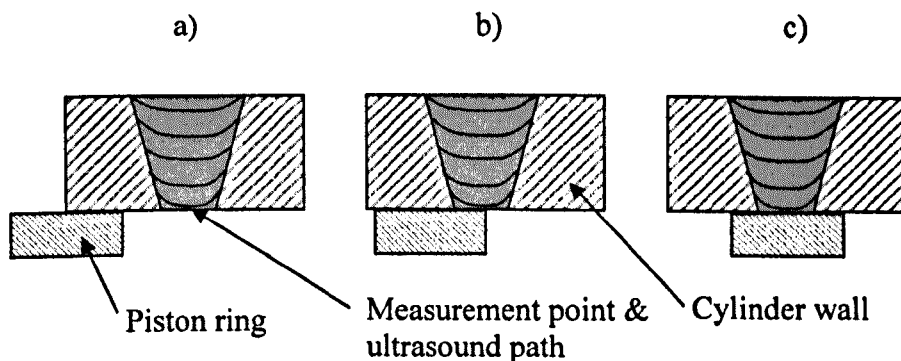
Figure 8.12. Three cases of reflection of an ultrasonic signal a) complete reflection due to steel/air interface, b) partial reflection due to partial air/partial oil film reflection, and c) partial reflection due to the oil film.

131

Thus it will be seen that only when the ring is fully covered can measurements of the oil film thickness be made with confidence. Figure 8.13 shows a series of conditions that pass the measurement point.
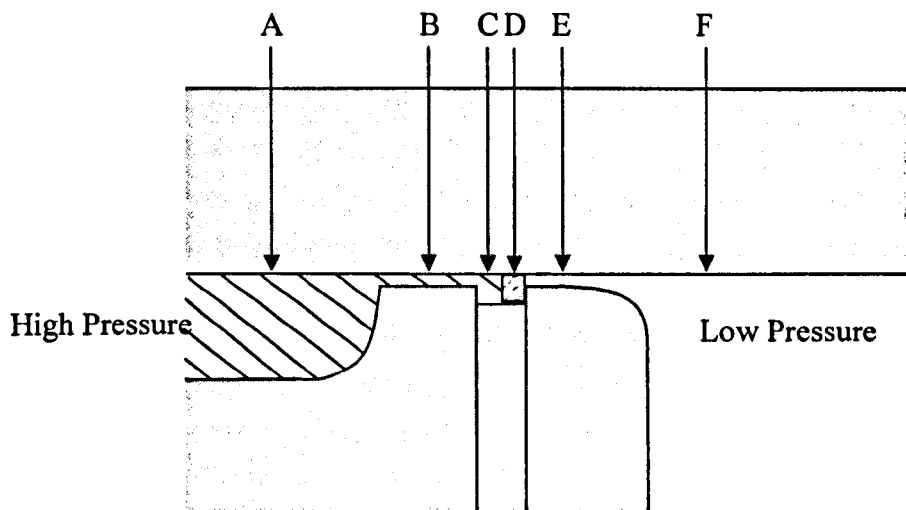
Figure 8.13. Close-up view of the piston profile either side of the piston-ring showing six different conditions, A, B, C, D, E, and F that pass the measurement point.

The conditions shown in figure 8.13 can be seen in the results shown in figure 8.14. At condition D, where the piston ring covers the measurement point, there are a minimum of two measurements. It can also be seen that the measurement is symmetrical about the TDC (top dead centre).
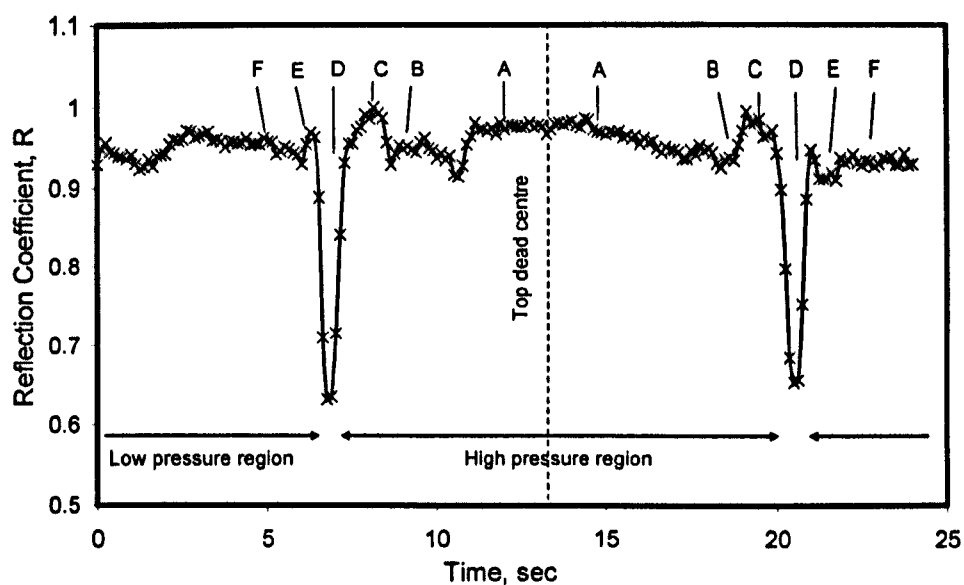
Figure 8.14. Measured reflection coefficients during a complete stroke. Conditions A, B, C, D, E, and F correspond to figure 8.13.

A range of measurements were made at different speeds and pressures. Figure 8.15 shows these results. The measurement points in this graph were taken from the equivalent point D in figure 8.14 for each test condition.
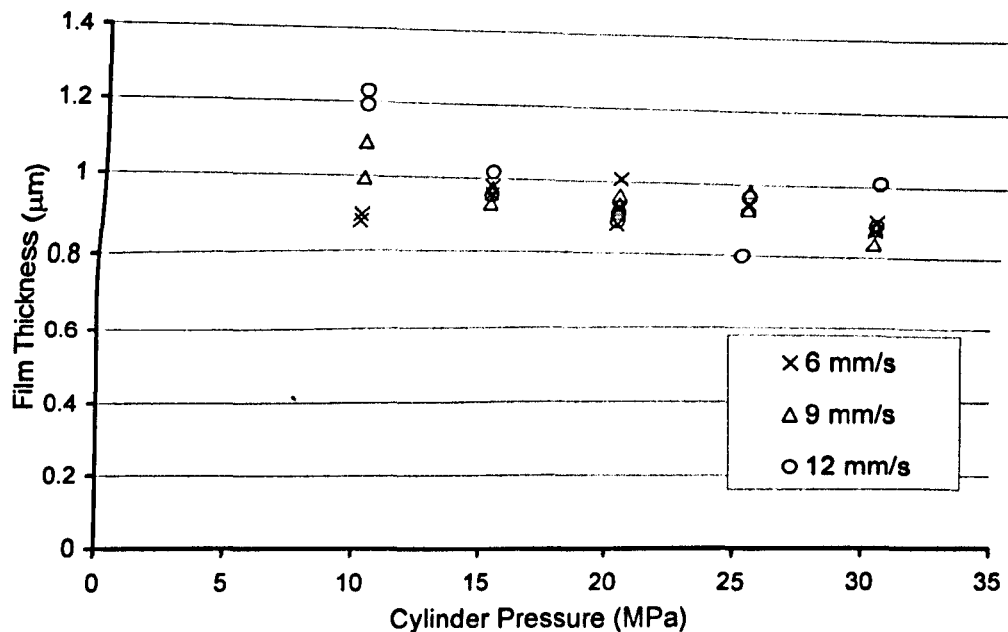
Figure 8.15. Plot of film thickness versus pressure for a range of different speeds.

The range of tests that were conducted was restricted due to two primary factors. Firstly, the maximum pressure tested was limited due to the fact that part of the cylinder wall had been machined away to allow measurement through the cylinder wall. Secondly, the measurement procedure was not highly optimised at the time of testing thus restricting the speed at which data could be captured. This second point seriously limited the range of testing possible.

The results show that there is not a significant change in film thickness with increasing pressure. This is most likely due to the tolerance being the primary control of film thickness over the range of loads and speeds tested. However, there is a thicker film with increasing speed at low cylinder pressures. This is probably due to the formation of hydrodynamic lift at lower pressures. There also seems to be a general trend in figure 8.15 of a lower film thickness with increasing cylinder pressure.

Baba et al [2006], Bolander et al [2004], Sanda et al [1997] all used laser induced fluorescence (LIF) to measure film thicknesses in the range 1 to 40 μm. Furuhama et al [1960] used resistance to measure film thickness in the range 0 to 7 μm. Wakuri et al [1993] used a displacement technique to measure film thickness in the range 5 to 15 μm.

All the above papers report an increase in film thickness with an increase in sliding speed, a decrease in film thickness with an increase in load (pressure). Bolander et al [2004] demonstrated considerable agreement between measured film thickness and predicted film thickness over a range of loads speeds and crank angle. Thus it seems that the results obtained broadly agree with those from literature.

8.8. Conclusions

Non-invasive measurements of film thickness have been successfully made on the film thickness between a piston ring and cylinder. The ultrasonic method has been demonstrated to be a suitable technique for measuring film thicknesses in piston/cylinder interfaces. The technique was developed in the following ways:

- The rate of measurement was increased significantly over previous tests. Whilst the capture rate of 8Hz was not exceedingly fast, it was an improvement on the previous work. Additionally, the necessity for a method of high speed capture was made evident if this work, or work like it was going to be carried out.

- The method of post processing was developed. The technology for acquiring data and then doing CPU intensive processing after experimentation had been completed was introduced. The viability of this approach was confirmed in this study.

- Focusing of the ultrasonic wave. The problems of focusing an ultrasonic sound wave down to a small point were overcome, and the technique was proven to work for small

- Implementing measurements at elevated temperatures. The temperatures encountered during this test setup were not significantly high compared with IC engine cylinder temperatures, but the concept of testing at high temperatures was proven and a technique to calibrate for temperature was developed.

Chapter 9:

Prosthetic Metal-on-Metal Hip Joint Film Measurement

9.1. Introduction

This chapter looks at the application of the ultrasonic technique to the measurement of film thicknesses in a prosthetic hip joint. This research was done in collaboration with the Biomechanics group at the University of Leeds. The background to the use of metal on metal joints is discussed, the experimental set up is described and the hip joint simulator is explained. High speed measurements were required for this application and a method of measuring film thicknesses dynamically at up to 10kHz was developed. This represented a significant enhancement of the technology and its application to dynamic high speed applications. A post processing method was also developed to enable high speed raw data capture. Software was developed and written to automatically post process the raw data and produce film thickness results.

9.2. Background

Artificial hip joints are now widely used to treat damaged hip joints. Traditionally these artificial joints have consisted of the polymer on metal type (a metal stem and head, and a polymer acetablar cup) largely due to the failure of early metal on metal implants (Amstutz et al [1996]). Recently there has been a move within the industry to shift back towards a metal-on-metal type hip joint (both head and cup are metal). This is due to the fact that patients requiring replacement hips are increasingly younger (Liu et al [2006]). Younger patients tend to be more active and loading, impact loads, frequency of

actuation and actuation angle tend to be greater than in older patients. This results in an increase in wear, impact damage and quantity of wear particles in the body. In addition to the joints being implanted in younger patients, patients are also living longer. This requires a joint that can survive harsher conditions for a longer period of time without need for replacement either due to excessive wear, or wear particles causing bone damage. It is believed that metal-on-metal joints are able to satisfy these requirements.

In the 1960's metal-on-metal joints were used as replacements (Amstutz et al [1998]) but it soon became apparent that they were not able to survive the operating conditions. This was due to poor materials, poor manufacturing tolerances, and poor designs (McKellop et al. [1996]). With recent advances in materials, manufacturing processes and design metal-on-metal joints are enjoying rising popularity. Additionally, wear rates of only 2 μm to 20μm per year in metal on metal hip joints is much more favourable than polyethylene on metal joints which have wear rates in the region of 100 μm to 300 μm per year (Liu et al [2006]).

Tribologically speaking, metal on metal (in contact – i.e. zero fluid film) is not a good combination of materials for low friction and wear. Thus in a metal on metal implant the lubrication is crucial to the performance of the joint. Failed lubrication can lead to excessively high friction (indeed joints have been known to lock solid) and an excessive quantity of wear particles.

Lubrication, specifically the lubricant film thickness, is a critical factor to both know and control if metal on metal hip joints are to be successful.

9.3. Measurement of lubricant film thickness in metal-on-metal hip joints.

Attempts have been made to measure the film thickness in metal-on-metal joints (primarily Dowson et al [2000], and Smith et al [2001]) but due to the nature of the joint several techniques are ruled out. Firstly optical techniques are not practical due to the requirement to use optically transparent components. Alternatively the use of an optical 'window' (or optic fibre) disturbs the fluid film and produces false measurements. Secondly, local capacitive techniques do not work for the reason mentioned above: the requirement for a sensor to be placed adjacent to the fluid film. Thirdly resistive

techniques (or overall capacitive techniques) give a measurement of the entire lubricant film averaged over the lubricating area. Practically speaking resistive measurements tend to give an on/off, contact/separation, measurement rather than film thickness (see Dowson et al [2000], and Smith et al [2001]).

Ultrasonic reflection is a potential method for the measurement of fluid film thickness in artificial joints.

9.4. Experimental Set-up

Measurement of fluid film thickness in an artificial hip joint was conducted at Leeds University in the Department of Mechanical Engineering. The following points detail the experimental set-up of the tests.

9.4.1. Hip Joint

The hip joint is a 54mm diameter metal on metal type manufactured by DePuy limited (similar to that shown in figure 9.01). It is manufactured from Cobalt-Chrome steel (Young's modulus 210GPa, poisson's ratio 0.3). The average roughness of the head was measured at 0.010μm Ra. The average roughness of the cup was measured at 0.007μm Ra. The average waviness of the head was measured at 0.1323μm Wa. The average waviness of the cup was measured at 0.4636 μm Wa. The cup has a thickness of approximately 4.5mm. The head has a thickness varying from 1mm at the edge to 3.5mm at the centre. The diametrical clearance of the joint tested was 100μm.
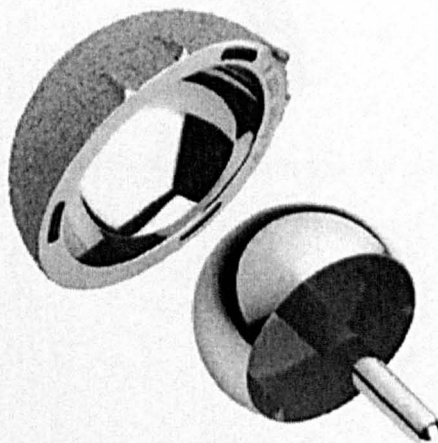
Figure 9.01. Metal on metal type hip joint[1]

---

[1] Image taken from http://www.keepmeactive.com/images/Cormetheadandcup.jpg on 12/05/07

9.4.2. Adhesive

Due to the low temperature nature of the testing (testing stayed at room temperature), there were not many constraints placed on the type of adhesive used. A high temperature cyanocryalate (Resist 200 from Holdtite Ltd) was used due to its high strength, stability and fast cure time.

9.4.3. Sensor

A single 7.1mm diameter, 0.2mm thick piezo sensor was used (supplied by Morgan Electro-Ceramics). Due to the fact that piezo materials are very heat sensitive and are easily damaged if too much heat is applied, a low temperature solder was used in conjunction with a temperature controlled soldering iron (limited to 225°C). Soldering was done prior to bonding to ensure a small thermal mass and allow a good soldered joint with the wire.

The sensor was bonded onto a flat that was ground on the back of the cup as shown in figure 9.02 and 9.03 below. This positioned the sensor at the vertical top of the cup, the expected position of minimum film thickness. However, Walker et al (1971) reported that in ten joints removed from patients, there was no wear in the polar region of the joint indicating that the thickest film was that the polar region.
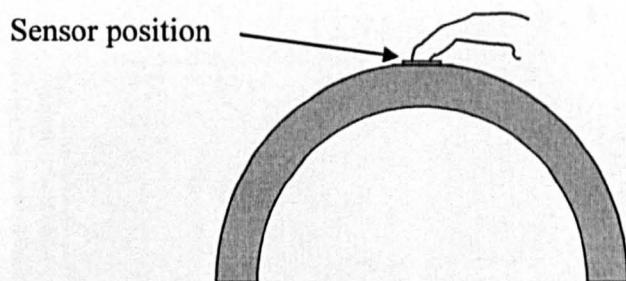
Sensor position

Figure 9.02. Section through the cup showing the position of the sensor
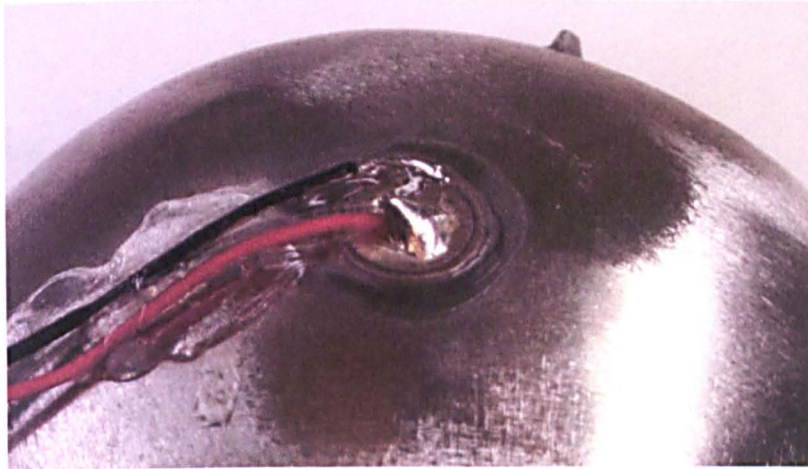
Figure 9.03. Photo of the sensor bonded to the back of the cup.

9.4.4. Friction Simulator

The equipment used for testing the artificial hip joint was a Prosim friction simulator, manufactured by Simulation Solutions UK Ltd. The friction simulator is designed to replicate the operating conditions that an artificial hip joint experiences in the body. Experimental variables such as load (both dynamic and static), frequency (number of actuation cycles per second), and actuation angle were adjustable. Figures 9.04 and 9.05 below show test rig photographs and schematic respectively.
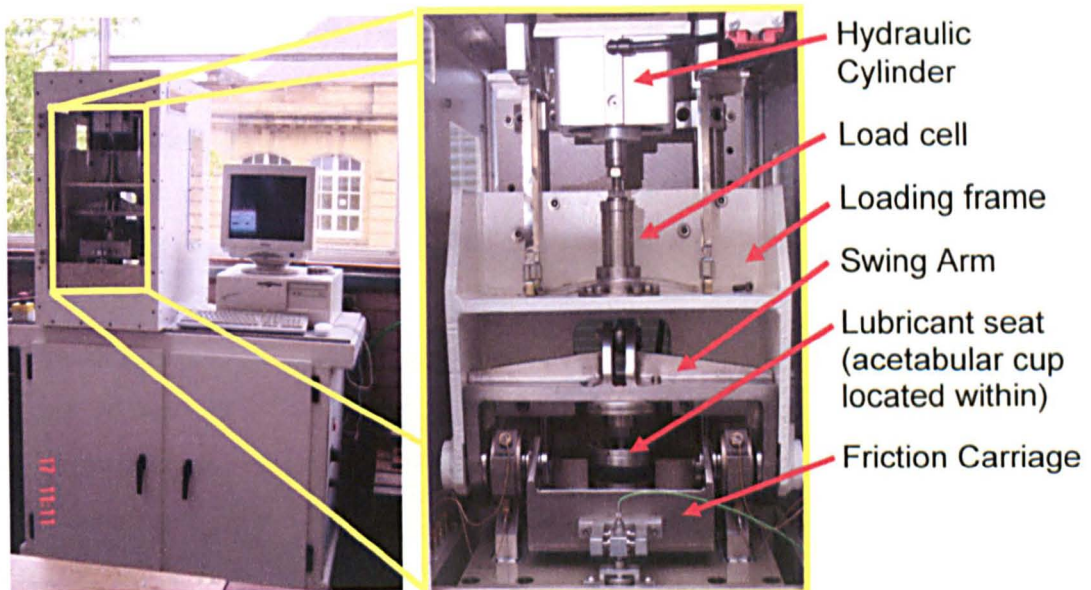
Figure 9.04. The ProSim Artificial Hip Joint Friction Simulator used in experiments.
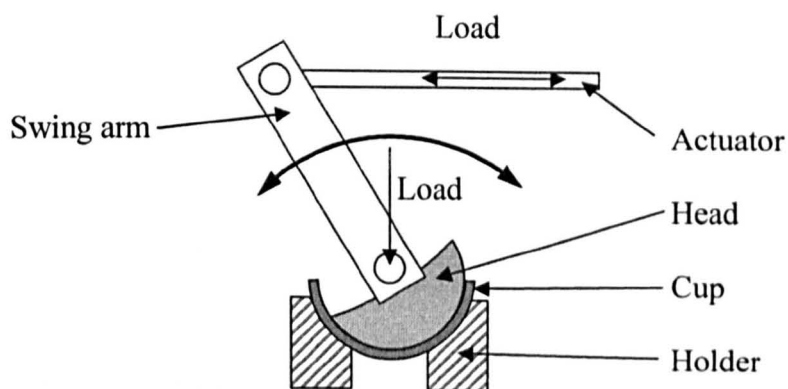
Figure 9.05. Schematic of test rig shown in figure 9.04.

9.4.5. Lubricant

The joint was tested with water and varying percentages of bovine serum (ranging from 100% water to 100% bovine serum). Bovine serum was used to try and replicate as accurately as possible the real-world conditions that the joint was going to experience. The bovine serum was tested for its density using a pipette and high resolution scales. The speed of sound was measured in a chamber similar to that shown in figure 6.09. The density was measured at 1480 m/s and the density was measured at 998 kg/m^3.

9.4.6. Data Capture

The actuation angle used in the test was $\pm25°$ from vertical or in other words 50° per half cycle and thus an actuation of 100° per complete cycle. In order to measure the film thickness at many points over the cycle (at a minimum of one measurement per degree) the data had to be captured at high speed, saved and post-processed. A LeCroy Waverunner Lt342 was used to capture and digitise the data from the pulser. The data requirements were considerable: 1 cycle per second consisting of 100 measurements, with each measurement consisting of 1002 data points, totalling 100,200 data points per second. In order to accomplish this, a segmenting function on the oscilloscope was used. The segmenting function only captures a pre-defined length of data at a pre-defined time from the trigger. Thus it only captures and digitises the relevant data while discarding the rest (see figure 9.07). The data was stored in the oscilloscope's internal memory which was 200k data points. Thus two complete cycles of the test rig were able to be captured with the test rig running at 1Hz. This data was then downloaded to the PC over GPIB while the next set of data was being captured.

9.4.7. Pulser Repetition Rate

The pulser/receiver used was a UPR manufactured by NDT Solutions Ltd as described in section 5.11. The pulse repetition rate (i.e. the number of pulses sent out and received per second) was set to 0.1kHz which was the lowest setting available. This repetition rate controlled the capture rate of the oscilloscope (the oscilloscope was set to trigger from the external trigger provided by the UPR). The pulser was set to pulse at 10V with a receiver gain of 30dB.

9.5. Signal Processing

This section goes step by step through the signal processing of the data captured from the oscilloscope.

9.5.1. Post processing software

The software developed for post processing the data is described in section 5.2.4 and a schematic is shown in figure 5.09. An example of the software is shown in appendix 5.

9.5.2. Segmented Reflection Measurements

Reflected pulses were captured using the segmenting procedure as described in section 9.46. Figures 9.06 and 9.07 below show an example of segments captured during a test where the film thickness decreased. The usefulness of the segmenting becomes clear in the fact that only the data of interest is captured (for example, compare with figure 6.05).
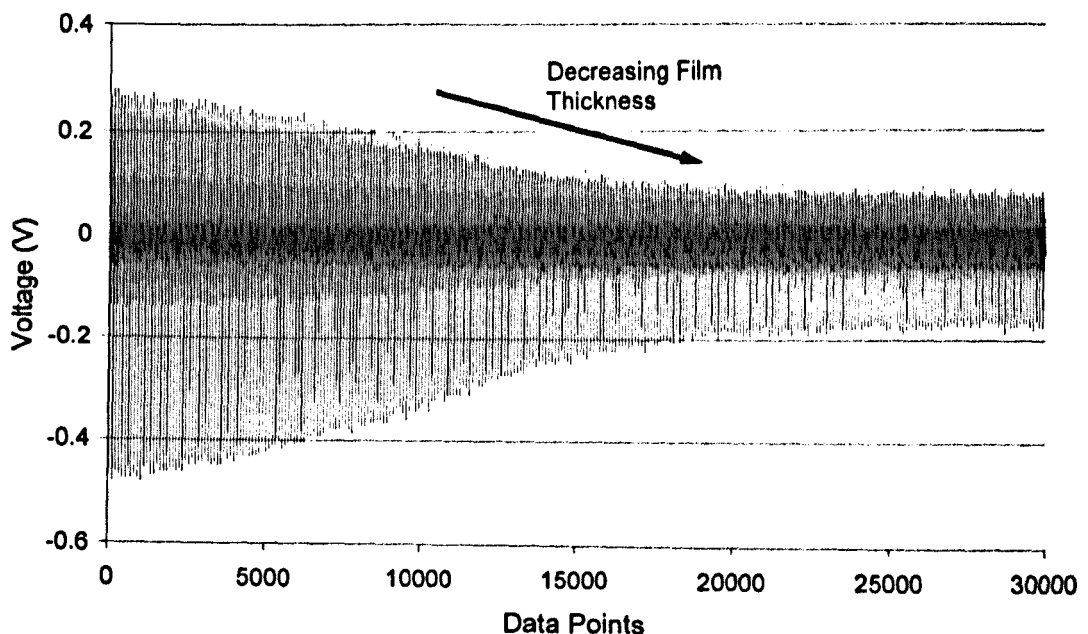
Figure 9.06. Voltage Vs Data Points of 300 sequential segments captured during a test showing a decrease in film thickness.
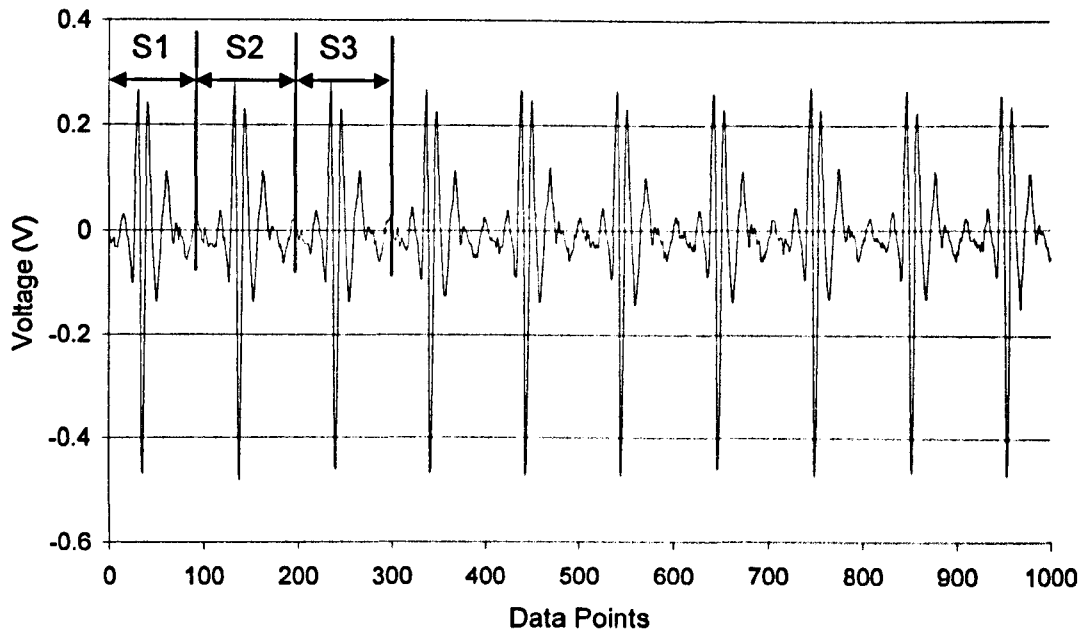
Figure 9.07. Voltage Vs Data Points of the first 10 segments from figure 9.06. The first three segments are highlighted S1, S2, and S3.

9.5.3. Film Thickness Calculation

The data shown in figures 9.06 and 9.07 were post processed, the steps of which are shown below in figures 9.08 to 9.12. Figure 9.08 below shows a selection of pulses overlaid on each other demonstrating the effect of film thickness on the time domain pulse. These pulses were then converted to the frequency domain as shown in figure 9.09.
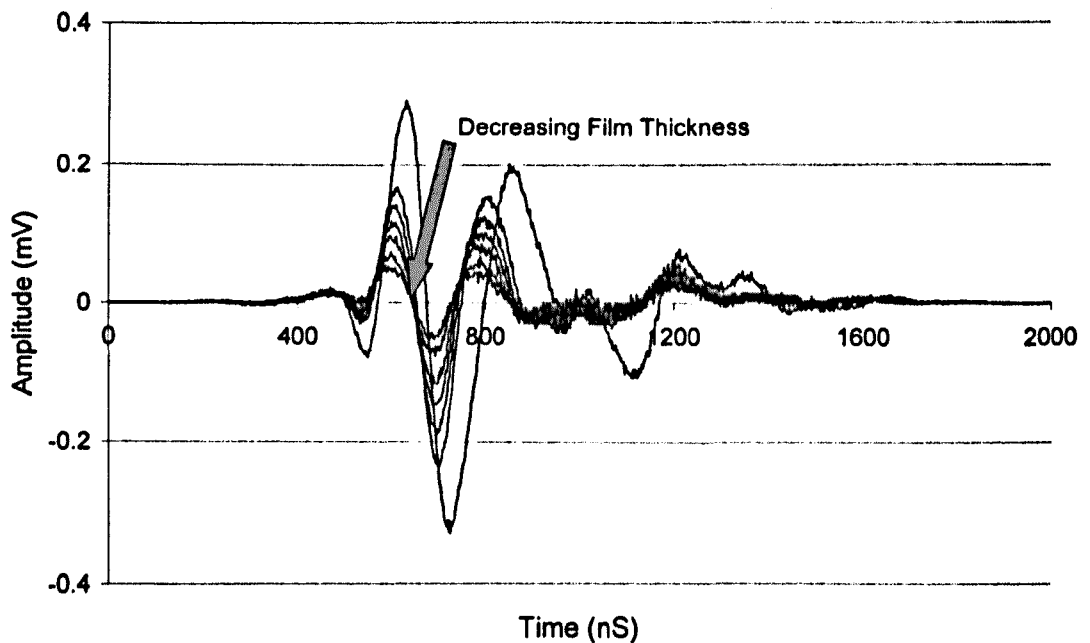
Figure 9.08. Amplitude Vs Time of selected pulses from testing over laid on one another.

142

The effect on the amplitude in the frequency domain with decreasing film thickness can be clearly seen below. The bandwidth shown in figure 9.09 below is the frequency range where the measurement remained stable without being affected by noise.
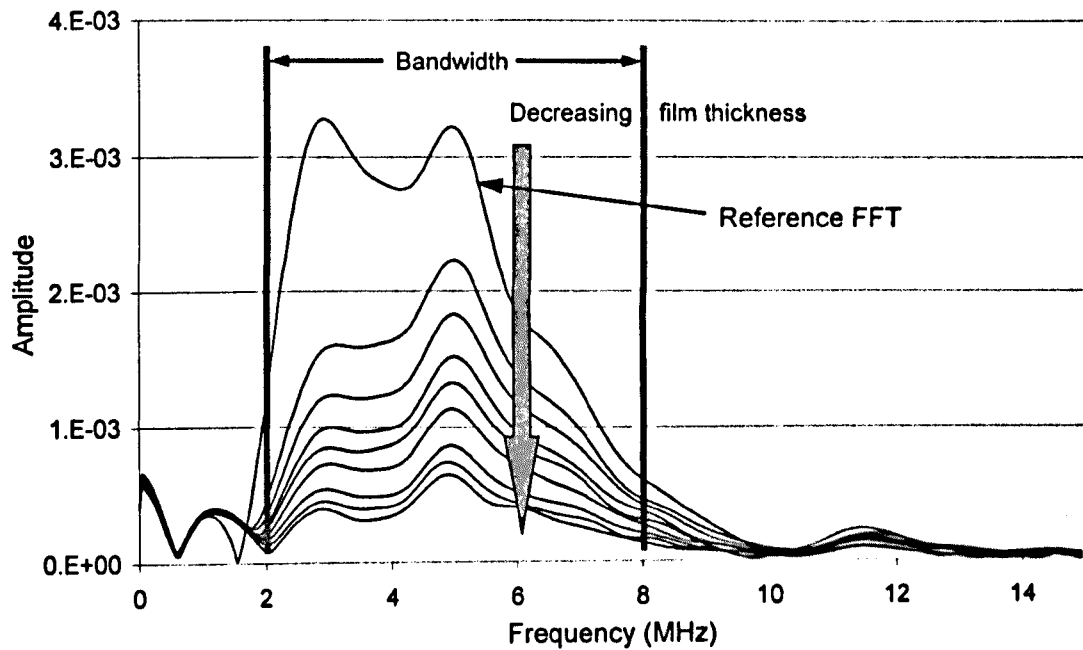
Figure 9.09. Amplitude Vs frequency of selected pulses from testing (fft's of pulses shown in figure 9.08).

Once the FFT's are computed, they are then divided by the reference signal. This gives a plot of reflection coefficient vs frequency as shown in figure 9.10 below. It can be seen that the reflection coefficient increases with frequency within the measurement bandwidth. It can also be seen that outside the measurement bandwidth the reflection coefficient becomes meaningless. This is due to the fact that one very small number is being divided by another very small number and electrical noise or signal fluctuation can have dramatic effects on the results.
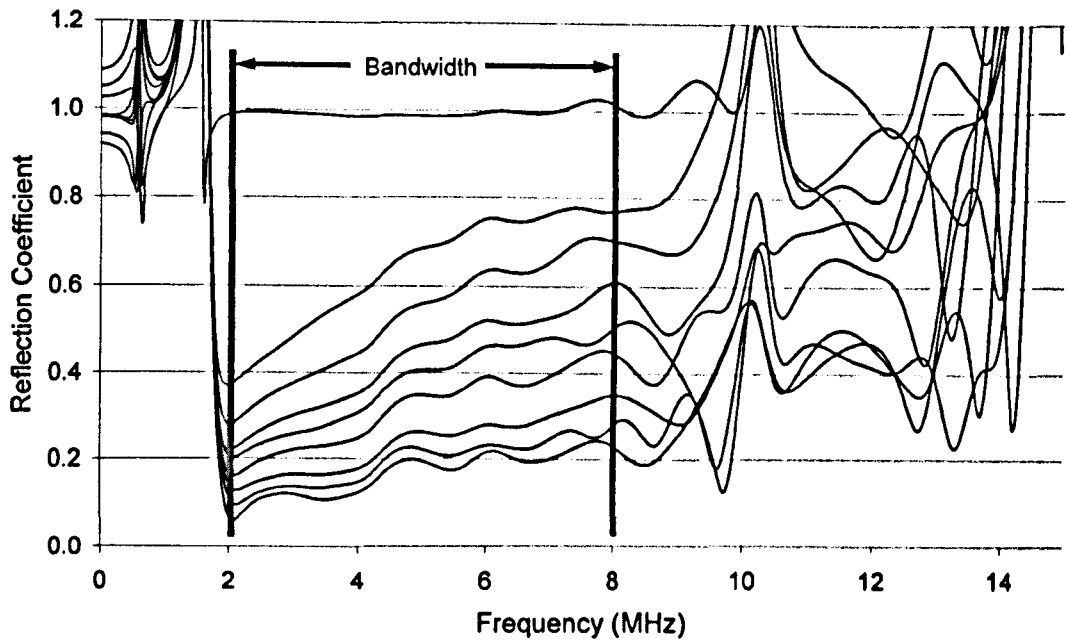
Figure 9.10. Reflection Coefficient Vs Frequency of selected pulses from testing (fft's of figure 9.09 divided by the FFT of the reference shown in figure 9.09).

Once the reflection coefficient is computed the film thickness can be calculated. Figures 9.11 and 9.12 below show the result of this calculation. It can be seen that the average film thickness does not vary with frequency within the bandwidth. Outside the bandwidth there is considerable variation in results.
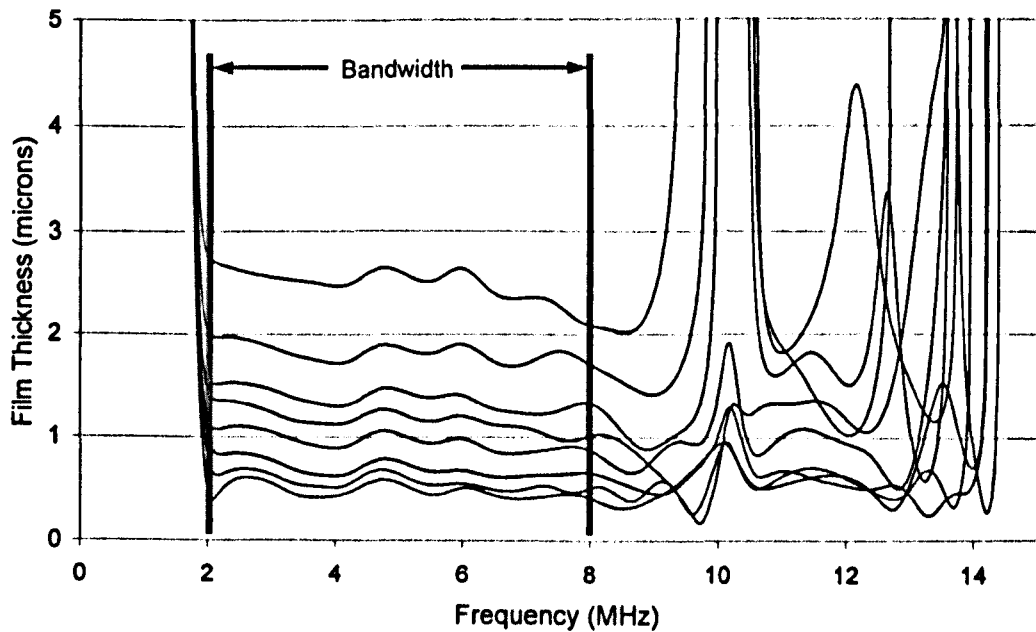
Figure 9.11. Film Thickness Vs Frequency for selected pulses from testing (reflection coefficients from figure 9.10 put through equation 3.20)
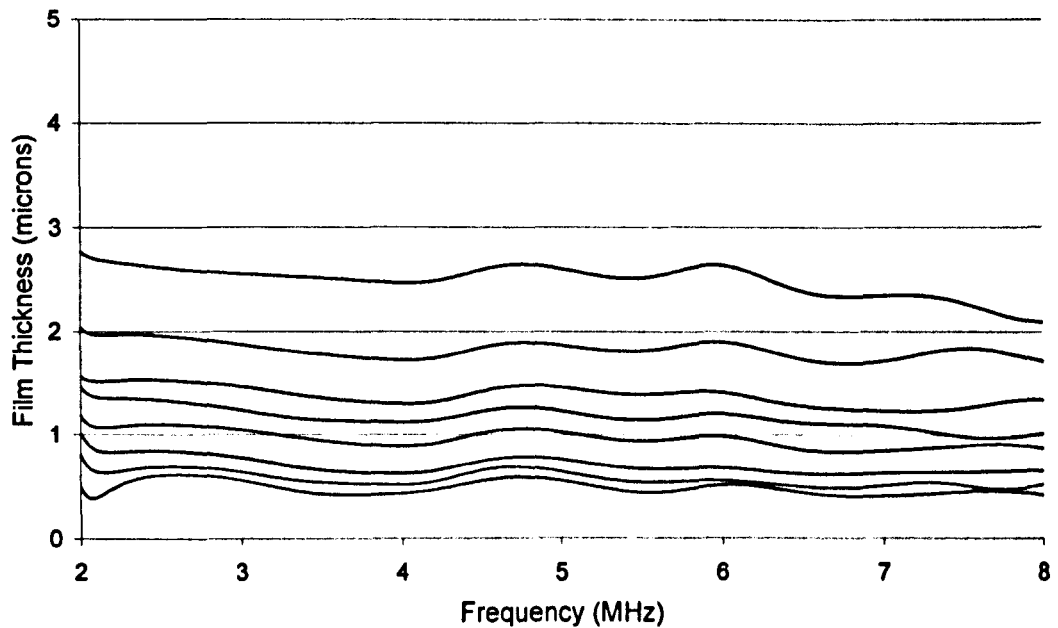
Figure 9.12. Film Thickness Vs Frequency for selected pulses from testing. This figure only shows the film thickness from within the bandwidth shown in figure 9.11.

9.6. Film Thickness Results

Several test sequences were conducted to examine the effect of various variables on the film thickness. All the data was captured and processed using the method outlined in section 9.5.

9.6.1.1. Measurement Over One Complete Cycle

Figure 9.13 below shows the film thickness measured over one cycle. The minimum film measured is approximately 0.45μm. It can be seen that there is some considerable variation in the film thickness due to the loading conditions and experimental set up. Figure 9.14 shows the loading and gait cycle of the testing machine.
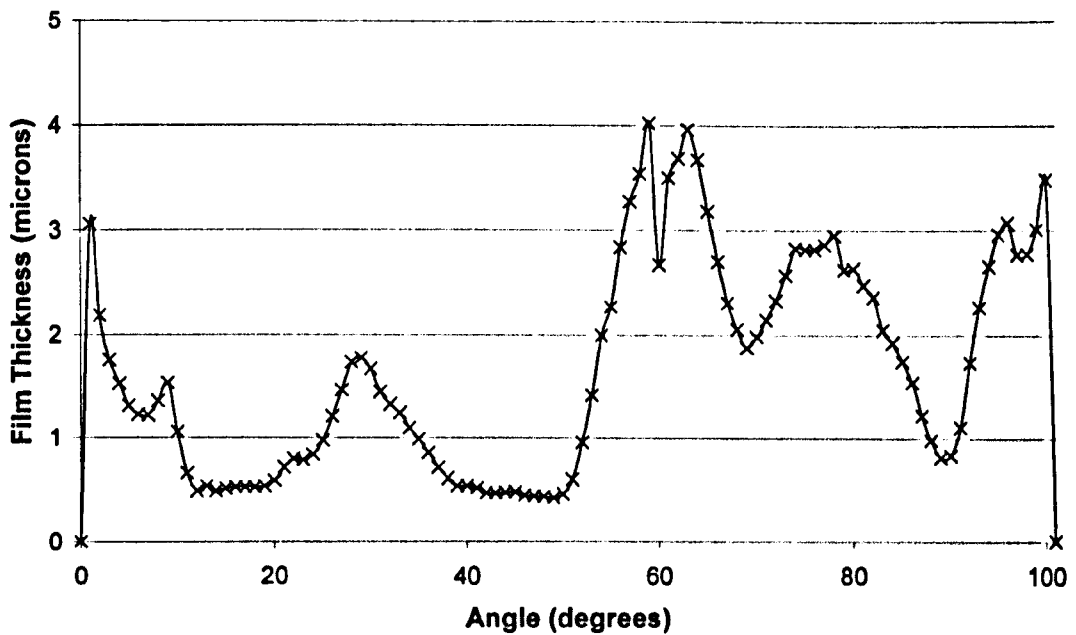
Figure 9.13. Film thickness Vs angular position for one complete cycle.
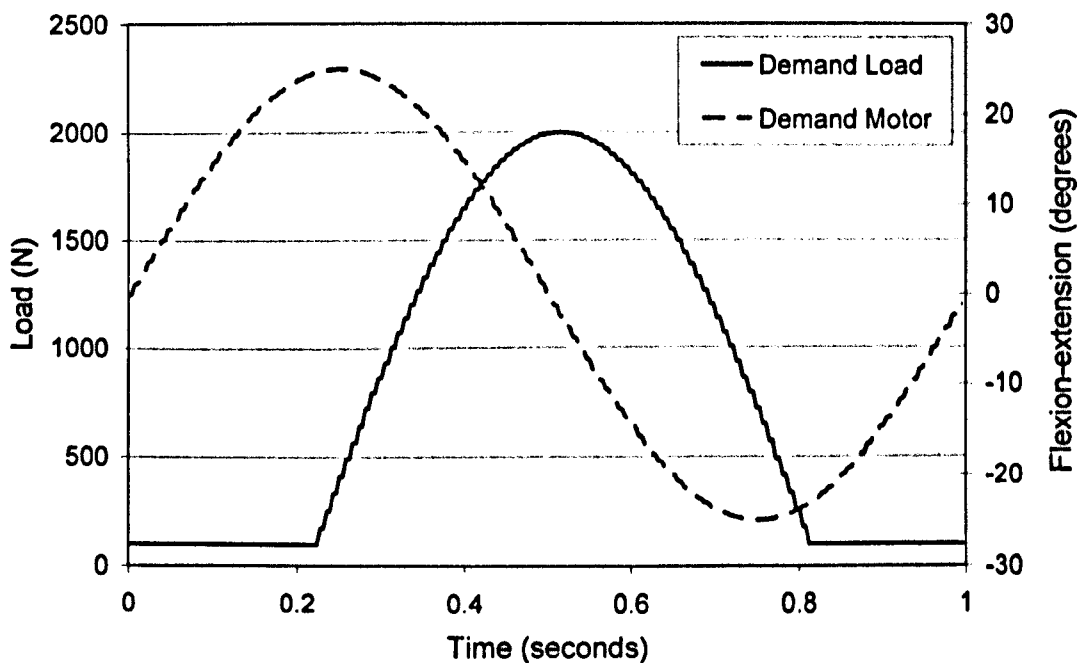
Figure 9.14. Loading curve and gait cycle of test rig.

9.6.1.2. Static Loading with a Range of Lubricants

Tests were conducted using a static vertical load to examine the effect of viscosity on film thickness over time on a squeeze film. Several different viscosity lubricants were tested, specifically 100% water, 75% water 25% bovine serum, and 100% bovine serum. The results of these tests are shown in figure 9.15. The film thickness was measured 5

minutes after the load was applied. As expected the film thickness decreased with an increase in applied load.
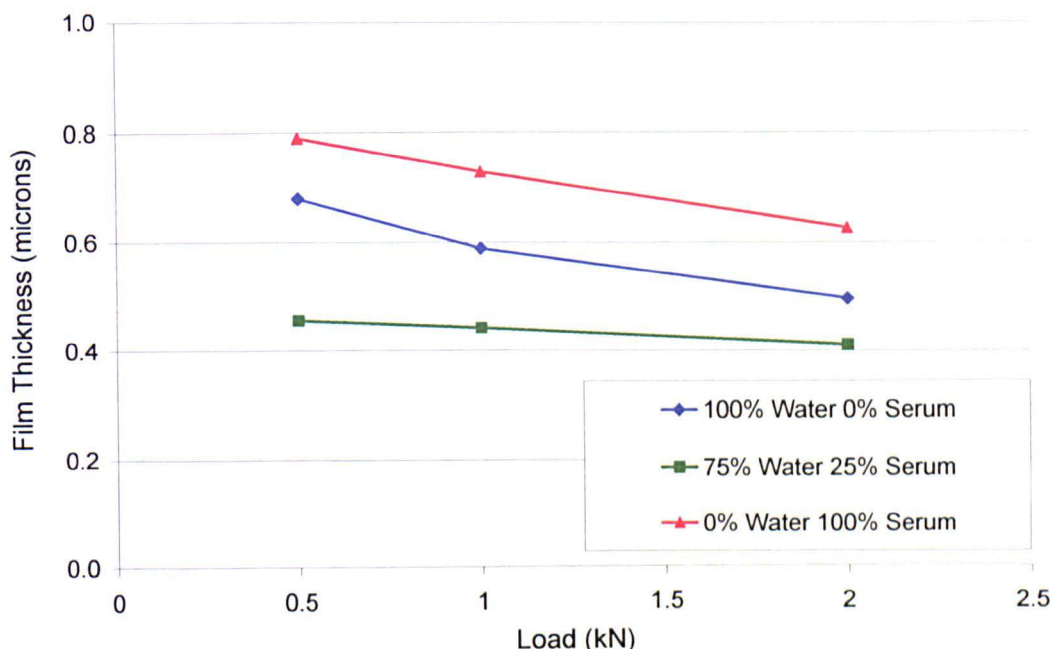
Figure 9.15. Film thickness Vs Load for static test.

Although the film thickness does decrease with time for all three lubricants, the order that they appear does not seem to correspond to expected theory (higher viscosity lubricant such as 100% serum should produce a thicker film for longer as the lubricant is squeezed out slower than a less viscous lubricant such as water). There are a couple of reasons that may explain this behaviour:

- During testing, when the lubricant had been placed in the cup, the head was brought down into the cup. Sometimes this movement was sharp and the impact of the head in the cup produced a visible splash. Other times it was much more gradual. This may mean that there have been less lubricant in the cup at the start of the test using 75% water and 25% serum.

- It may be that the 75% water and 25% serum was not well mixed and the more viscous serum may have attached itself to the cleaned metallic parts leaving the unmixed water sandwiched in between. This then may have produced a path of less resistance for the water to squeeze out.

9.6.1.3. Friction and Film Thickness

The friction coefficient was measured during the tests. Figure 9.16 below shows the measured friction coefficient against the film thickness for three lubricants. It can be seen

147

that as the film thickness gets thinner the friction factor increases. This is due to increased asperity contact.
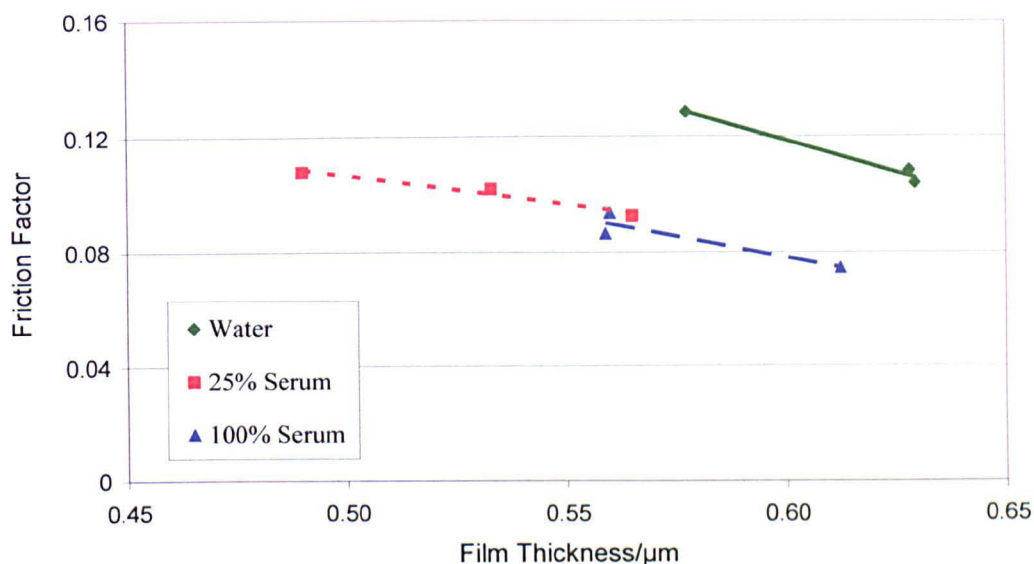
Figure 9.16. Friction Vs film thickness for three different lubricants.

It will be noticed that the friction factor is higher in the test with water compared to the tests with serum even though there is a thicker film separating the components. This is most likely due to proteins from the serum building up on the surfaces of the component and providing some boundary lubrication at very thin films.

9.7. Discussion

Measuring the fluid film thickness in an artificial hip joint has been done using ultrasonic reflection. During this testing several issues were raised that have merit in discussing.

9.7.1. Comparison with Calculated Film Thicknesses.

The measured film thicknesses were compared with a computational model by a colleague at Leeds University (for examples of these models see Chan et al. [1999], Liu et al [2006], Williams et al [2006]) as shown in Table 9.1 below. It will be seen that the measured films are far thicker than that predicted by the computational model. The reason for this is that the computational model that was used assumed perfectly spherical interfaces and perfect actuation and loading. The results are clearly in error as the predicted film is thinner than either of the measured surface roughness's as mentioned in section 9.4.1. Real world imperfections have had, in this case, significant effects on the film thickness.

Lubricant	Load	Predicted Film (μm)	Measured Film (μm)
Water	0.5kN	0.004	0.680
	1kN	0.003	0.589
	2kN	0.002	0.496
25% Serum	0.5kN	0.004	0.455
	1kN	0.003	0.442
	2kN	0.002	0.410
100% Serum	0.5kN	0.005	0.790
	1kN	0.004	0.730
	2kN	0.003	0.627

Table 9.1. Predicted and measured films for a range of lubricants and loading conditions.

9.7.2. Comparison with Published Data

Udofia et al [2003] reported calculated film thicknesses in the region 0.25 μm to 1μm for a range of lubricants with varying viscosities. This compares well with ultrasonic measurements made. Additionally, Dowson et al [2000] reported high resistance during parts of a walking cycle for a range of different lubricants. This seemed to indicate full film lubrication in certain parts of the cycle. Again, this would seem to contradict the computational models mentioned above.

9.7.3. Joint Surface Roughness and Form

Figures 9.17 and 9.18 show measurements from a similar hip joint to that used in this study. Both graphs have had the diameter subtracted from the measured form to give a flat line for a perfectly round object. In both figures the surface waviness deviation can be seen as an approximately sinusoidal line. The average waviness' are 0.46μm and 0.15μm respectively. This explains why there is considerable variation in the film thickness over the cycle as the relative roughness's of the joints interact with each other.

Modified Profile — Claire 272 - 1 - W/10x2.5mm/G/LS Arc — 12/06/2006 11:43:20
Claire 272 - 28.1mm/Admin/FTSS S5 3D — 12/06/2006 11:41:51

Radius	27.2725	mm										
Wa	0.4663	µm	Wq	0.5222	µm							
Wsk	0.0245		Wku	1.6137								
Wp	0.2789	µm	Wv	0.1842	µm							
WLo	24.9998	mm	Wt	1.6237	µm	Wmr(c)	57.32	% Height (mean)	0.000	µm		
Wlq	15359.31	µm	Wdq	0.01	°	WHSC	1	peaks Height (mean)	0.000	µm		
Wda	0.01	°	Wz	0.4631	µm	Wdc	1.6237	µm mr1%	0.0	% mr2%	100.0	%
Ws	0.00	µm	WSm	17663.50	µm	Wmr	50.00	% offset	0.000	µm mr%	50.00	%
Wln	25.0000	mm	Wc	1.6237	µm	WVo	0.0284	vol offset	0.000	µm mr%	50.00	%
						WPc	0.4	pks/cm Height (mean)	0.000	µm bandwidth	0.00	µm

Figure 9.17. 28 mm long waviness profile across the pole of a metal cup.

Modified Profile — Claire 269 - 1 - W/37x0.8mm/G/LS Arc — 12/06/2006 11:16:39
Claire 269 - 29.1mm/Admin/FTSS S5 3D — 12/06/2006 11:14:29

Radius	27.2512	mm										
Wa	0.1532	µm	Wq	0.1766	µm							
Wsk	0.2196		Wku	1.9001								
Wp	0.0283	µm	Wv	0.0381	µm							
WLo	26.5998	mm	Wt	0.7010	µm	Wmr(c)	43.71	% Height (mean)	0.000	µm		
Wlq	7550.54	µm	Wdq	0.01	°	WHSC	1	peaks Height (mean)	0.000	µm		
Wda	0.01	°	Wz	0.0863	µm	Wdc	0.7010	µm mr1%	0.0	% mr2%	100.0	%
Ws	1224.48	µm	WSm	20461.75	µm	Wmr	50.00	% offset	0.000	µm mr%	50.00	%
Wln	29.6000	mm	Wc	0.7010	µm	WVo	0.0054	vol offset	0.000	µm mr%	50.00	%
						WPc	0.3	pks/cm Height (mean)	0.000	µm bandwidth	0.00	µm

Figure 9.18. 28 mm waviness profile across the pole of a metal head.

9.7.4. Contact and Film Thickness

With a decrease in film thickness the likelihood of the surfaces coming into contact increases. Where there is a surface waviness this becomes almost a certainty once the film thickness decreases to a similar level as the amplitude of the waviness. As friction is directly related to contact, friction measurements are a good indication of what is

happening in an artificial hip joint, hence the propensity to use this as a research tool in the design of these joints.

Only liquid layers have been considered in this work and so it is worth asking what happens when there is a mixed interface – solid/solid contact and solid/liquid/solid lubrication. Reddyhoff [2006] reported on the effect on the ultrasonic measurement of solid/solid contact. It was shown that the effect of solid/solid contact on the measurement only becomes significant when there is significant amounts of solid/solid contact within the measurement area. For a polished steel ball (R_a = 0.01μm) against a polished steel disk (R_a = 0.12μm) there was only an effect of approximately 10% on the film thickness at a film thickness of approximately 0.12μm.

9.8. Conclusions

Non invasive measurements of fluid film thickness in a metal on metal type hip joint have been made for the first time. The ultrasonic technique was developed to take into account the special challenges that metal on metal hip joints posed:

- High speed measurements were extended further from the work on piston rings. Capture rates up to 10 kHz were made possible using the segmenting approach to data capture. Post processing minimized the CPU requirements while saving data by keeping signal processing until after testing was finished.

- Measurements in the range 0.2 – 8μm were recorded. This proved the technique for application in components where the films are sub-micron.

- The trends in the measured film thicknesses correlate to measurements of friction. The film thicknesses were larger than expected from the theory but can be understood in terms of the waviness of the ball and cup of the joint.

- From the data obtained it seems that the surface film of proteins is important in the lubrication of metal-on-metal hip joints. This film helps in boundary lubrication where asperities come into contact.

- Surface waviness, form and roughness are very important when they are of the same order as the films in the component.

Chapter 10:

Future Work

This chapter describes possible further areas for study, both in the applications studied in this thesis but also in the wider industrial environment. These suggestions can be summarised as:

- Improvements in the generic method.

- Enhancements to the work done here.

- New areas of application.

10.1 Generic Developments

Several generic improvements to the application of the technique will be suggested here.

- Investigation of adhesives. As adhesives are heated they start to soften. This reduces the response of sensor and changes the amount of energy transmitted into and received from a component. The work conducted in this thesis did not experience particularly high temperatures, but some real world applications can have very high temperatures. The adhesive type, thickness, thermal performance and long term stability should be further investigated to identify both more suitable materials and to define the effect of these variables on long term performance.

- Piezo materials. There is a wide range of piezo materials available, some of which have, for example, excellent thermal performance (some can go up to 500°C). In this work the general piezo material Navy IV was used. There may be

considerable advantage in identifying other piezo materials that show a minimal change in physical and electrical characteristics with temperature.

- Sensor size and shape. The sensors used in these studies were off the shelf sensors that were deemed suitable for the task in hand. There may be considerable advantage in using different sensor shapes, different electrode patterns, multiple electrodes to produce sensor arrays etc. For example, Silk [1984] describes a sensor with a varying thickness for producing an exceptionally broadband acoustic response.

- Piezo coatings. There is considerable potential in some of the piezo electric coatings that it is now possible to coat components in (for example see Lee [2004]). Intellifast GmbH manufacture a piezo coating on bolt heads for measurement of length as an indication of tension within the bolt. This technology has many advantages, in particular – high temperature (proven up to 300°C), perfect bond between piezo material and component, ability to sputter complex electrode patterns for novel sensor patterning, high frequencies for thin film work, and small focal spot for used in concentrated contacts.

- Other processing methods. The work described here only considered the amplitude of the FFT. It is also possible to use the phase of the FFT to measure film thickness. This would allow for measurements on acoustically adverse material combinations (e.g. measuring lubricant films in polymer bearings running against a steel counterface). Additionally it would give a second measurement that could be used to reduce the error in the amplitude measurement.

10.2. Improvements to Existing Measurement Applications

10.2.1. Journal Bearings

Whilst the measurement of film thickness using ultrasound has been demonstrated in this work, further work should be done on the practical application of the technology. In particular

- Sensor development. It has proven difficult to find suitable sensors for measuring real world film thicknesses. This is due to a combination of the fact that each sensor has a range of measurable film thicknesses. In order to use the spring model in journal bearings with film thicknesses in the region of 25-40μm, a sensor with a bandwidth of 0.5-2 MHz would be required. In practice it is

difficult to get sensors that have this kind of bandwidth that are suitable for application in real engineering components. This is due to the fact that a sensor with a resonating frequency of 0.5MHz has a thickness of 4mm. In order to prevent bending modes from being excited in the sensor the diameter needs to be at least 5 times the thickness (preferably 10 times), hence requiring a sensor of 20mm diameter minimum.

- Multiple sensors. Multiple sensors would allow measurements to be made in a journal that had a wide range of film thicknesses (e.g. in the main bearing on a crankshaft of a large marine diesel engine the film can fluctuate between 5µm and 500µm). Each sensor has a lower 'window' in the spring model regime (see figure 6.03) and a window in the resonant dip regime with a 'blind spot' in between the two 'windows'. By using multiple sensors around the circumference films can always be measured and results extrapolated where individual sensors are operating in the 'blind spot'.

- Cavitation. The onset of cavitation was discovered in this work (see section 7.33). As the ultrasonic technique relies on the acoustic properties of the fluid film, any cavitation will change these properties. By using multiple sensors this change could be quantified by interpolating between measurements in the non-cavitating and cavitating region.

10.2.2. Piston Rings

The following could be explored further:

- Piston Rings in Combustion Engines. It would be of interest to continue the work into the field of combustion engines. Effects of combustion pressure, lubricant viscosity, temperature, speed and materials could be explored.

- Sensor on a Ring. By putting a sensor on a ring (either through bonding or a piezo coating) the film thickness over an entire cycle could be mapped out.

- Long Term Testing. By measuring the film thickness over a long period of time any running in effects could be explored.

- A faster capture time to allow higher sliding speeds to be measured. The author has, since this work was completed, developed a high speed method (see chapter 8) of data capture (see also Dwyer-Joyce et al [2006]) and also an ultra-high speed method – up to 200kHz.

- A less nodular cast iron to reduce attenuation. The upper pressure that this could be tested at was limited due to extensive machining to allow the ultrasonic signal to travel through the piston wall. A less attenuative cast iron would allow less machining and thus higher pressures.

- A higher frequency. The measurement spot size is dependent on the frequency of the transducer. Thus a higher frequency transducer has a smaller spot size. This work would benefit from a smaller measurement spot to investigate the profile of the piston ring as it passed. This will depend on the previous two points being implemented.

- Measure of leakage across the piston ring would be useful to correlate film thickness measurements to actual leakage rates.

- The effect on film thickness of using different lubricants with different viscosities.

10.2.3. Artificial Hip Joints

There are three main topics that could be further explored in artificial hip joints.

- Long Term Testing. The work conducted in this thesis was a proof of concept study, primarily to develop the ultrasonic measurement technique. There is a considerable amount of potential research on the back of this initial investigation. In particular it would be very useful to conduct tests over an extended period of time to investigate and quantify running in effects.

- 3-D Mapping of Film Thickness. As the was only one sensor used in testing the hip joint is was difficult to establish what the effect of the testing machine was on the film thickness measurements. By mapping the film thickness over the entire area of the joint it would be possible to see both the test machine effects and also any geometry effects. 3-D mapping of the joint could be achieved by using multiple sensors.

- Investigation of Clearance. There seems to be considerable disagreement between hip joint manufacturers as to the best clearance between the femoral head and cup. Using ultrasound on a range of joints with different clearances would provide valuable information on this topic.

- Sensor size – it would be worth investigating the use of smaller sensors. The sensors used in this study were 7.1mm diameter and thus the measurement that

was taken was over this area. Smaller sensors would allow the effect of spatial averaging to be investigated

- Sensor Position – the position of the sensor in this study was at the top of the cup, the position of minimum film thickness. Future studies should examine placing the sensor/sensors at different positions on the cup.

- Sensor Frequency – the sensor in this study had a centre frequency of 10MHz. future studies could investigate using higher frequency sensors to examine the lower film thicknesses.

10.3. Potential Areas of Application

10.3.1. Thin Layers

- Any thin layer embedded between two materials can, in theory, be measured using ultrasonic reflection. Applications such as the properties and thickness of material coatings, paper in paper mills, and the manufacture of aluminium foil.

- Additionally, free surface films (e.g. a thin layer of oil on steel) on surfaces of components can be measured. Applications could include thickness of paint on a surface, the thickness of the layer of cooling oil on the inside of jet engines, thin layers of flowing liquid over a surface.

10.3.2. Machine Components

The following areas would benefit from application of this technology:

- Thrust Pad Bearings. Many of the developments to journal bearings have direct application in thrust pad bearings. One application where the measurement of film thickness could have particular benefit is in the use of actively tilting thrust pad bearings. By use of an active control of pad tilt, combined with a measurement of film thickness the bearings could be controlled to suit desired operating conditions. Other areas to be investigated are cavitation, dynamic effects on the lubricant film, and two-phase flow in the bearing.

- Mechanical seals have not been explored in this thesis but present a real opportunity for this technology to provide a condition monitoring solution. Mechanical seals suffer from not having many technologies to monitor them and yet are critical to many processes. Effect of pressure, speed, materials, temperature, lubricant on film thickness could all be explored. Development of integrated sensors into seals would provide a platform to build on.

- EHL contacts in rolling element bearings. There is potential in this technology for non-invasive condition monitoring of rolling element bearings using this technology. Key challenges are: focusing the sound onto the contact spot, applying sensors in a non-invasive manner (i.e. without modification of bearing or housing), acoustic properties of the lubricant, high frequency hardware.

- Gear teeth. This also is classed as EHL, but the challenges are different. The primary difficulties in this application are mounting the sensor so that it can receive a reflection from the lubricant film, and measurement of the film thickness while the gear teeth are moving.

- Cam/Tappet interface in an IC engine. Like EHL in rolling element bearings and gear teeth, this application would require a highly focused sound wave onto the line contact.

- Extrusion lubrication. This technique could be applied to monitoring the lubrication used in some extrusion applications such as UPVC used in the manufacture of window frames. It may be a challenge mounting a sensor in the die to allow for measurement.

Chapter 11:

Conclusions

This chapter details the conclusions that can be drawn from this work on the development of a technique for measuring lubricant film thickness using ultrasonic reflection.

11.1. Background

Existing condition monitoring and film thickness measurement technologies were surveyed. The approaches to both are diverse and varied as are the applications where they are implemented.

It was seen that condition monitoring of bearings and the like required a robust method and system for application in industrial environments. It was also noted that most of the approaches to condition monitoring are based on indirect methods of detection – shaft displacement, temperature, vibration, acoustic emissions etc. These methods of condition monitoring have been implemented in a minority of safety critical, large, high cost applications. Whilst these methods do provide some information, they do not monitor the health of the weakest link in the system – the lubricant film thickness.

The methods of film thickness measurement that were surveyed in the chapter have not, almost without exception, been implemented in condition monitoring applications in the industrial environment. This is because of two reasons: either the film measurement technique cannot be applied to real components (as in the case of the optical methods where components are not optically translucent) or the method has been shown to not

be robust enough for the industrial environment (as in the case of electrical techniques that suffer from issues of electrical isolation and drift of the electrical properties of the system).

It was seen that there is a lack of technology for non-invasive measuring of lubricant film thickness in real engineering components in an industrial environment.

The theory behind ultrasound was examined and some of the basic physical concepts were introduced. The propagation of ultrasound through a material was described and the various modes and forms that the ultrasonic vibration can take were mentioned. The focus of the study was on the propagation of longitudinal (or pressure) waves. The various material parameters were described and the effect of material properties on the transmission of ultrasound was examined.

The ultrasonic theory was then developed from the reflection of sound at a simple interface to an interface where there is a thin layer of liquid. The equations 3.06-3.22 showed the relationship between the reflection of an ultrasonic wave to the acoustic properties and thickness of a thin layer.

Three models were put forward for calculating film thickness. Firstly, where $h >> \lambda$ the technique simply measures the time between successive pulses. Secondly, where $h = \lambda$ there is a resonant dip in the received ultrasonic frequency spectrum that can be related to film thickness. Thirdly, where $h << \lambda$ the spring model was described where the frequency dependent response from the lubricant film is converted to a frequency independent film thickness. A comparison was carried out showing the differences between the various models and their measurement limits.

NDT sensors were described in detail with consideration giving to coupling, focusing, temperature effects and frequency response. Various equations were described that were used for the selection of the correct sensor for a particular application. The hardware was described in detail with an explanation of methods of pulsing and their advantages and disadvantages. The method of operation of the UPR was described. Finally some space was given to considering digitisation and the computer system that provided the signal processing.

11.2. System Development

The generic system was developed for the measurement of fluid film thickness. The specific details of the hardware components that were brought together were given with some explanation on why specific parts were chosen.

An important discovery over the course of the research was the use of low frequencies to measure a wide range of films. This is described in section 5.1.3.1. This discovery paved the way for the application of this technology in some applications that were previously not possible due to requirement for excessively high frequencies. This also had the effect of reducing the specifications on the hardware end associated with lower frequencies.

The most significant development in sensors was the use of piezo elements rather than NDT sensors. This development opened up further opportunities along with reducing costs. The testing conducted on the prosthetic hip joint in chapter 9 is an example of where it would have been very difficult to use an NDT sensor. The use of a piezo element presented this testing opportunity.

The software described in section 5.2 and shown in Appendices 2-8 was written to provide a platform for developing the ultrasonic method and applying it to new applications. The modelling software provided a valuable resource for understanding what was expected to happen in the experimental work.

The measurement of material properties was described with methodologies to circumvent problems such as excessive attenuation. The practical issue of capturing reference pulses was discussed.

Another major accomplishment in this work was the methods for calibration in situations where there was an adverse temperature effect. Four methods were put forward for how to take account of the amplitude change in pulsing and receiving properties of the sensor. The first of these methods worked for thick films operating in the resonant dip model range of film thicknesses. The second relied on changes in the film thickness, in particular the film being much thicker than what the sensor could measure, to provide an indication of the temperature effect. The third and fourth method was applicable in situations where there is no change in the film thickness, or the film

thickness is always within the sensor 'window'. This last method used geometric effects or multiple layers to create a second pulse from which calibration could be taken.

Verification and validation of the ultrasonic measurements was carried out in two test rigs. In the first, measurements of the film between two glass sheets were measured via a focusing transducer in an immersion scanning tank. The two glass sheets were separated by a known thickness at one end to provide a tapered film thickness. The film thicknesses results and the predicted results compared very well. In the second experiment, a transducer mounted in a journal bearing was rotated around part of the journal and measurements of the annular gap compared to theoretical annular gap geometry. Once again the results compared very favourably. Additionally the predicted minimum film from Sommerfeld theory was shown to compare well with the position of minimum film measured ultrasonically.

11.3. Experimental Work

11.3.1. Journal Bearings

The ultrasonic technique has been applied to two journal bearings. The first test rig at the University of Sheffield allowed the technology to be trialled. The test rig allowed for measurements to be taken around the circumference of the journal. The application of low frequency sensors was first applied in this test rig to measure film thicknesses in the range 5-25μm. Load and speed was varied to produce a range of results for different test conditions. The results from the test rig compared well with Sommerfeld theory. The measurements around the circumference of the journal also compared well with theoretical film thicknesses. Cavitation was detected in the diverging part of the bearing.

The second test rig was the location of the first application of this technology in an industrial setting. Film thicknesses were measured over a wide range of loads and speeds. Temperature effects on the sensor were discovered and the method outlined in section 6.3.2 was employed to take account of the temperature effects. The results from the test rig were compared with a 1D and 2D computational model. There was good agreement between the predicted and measured film thickness.

161

11.3.2. Piston Ring

The ultrasonic method was applied to the film thickness between a piston ring and a cylinder from a hydraulic motor in a test rig at KTH University, Stockholm, Sweden. Focusing of ultrasound was employed to produce a small measurement point that could measure film thickness as the piston ring passed. Attenuation of the cylinder material was found to be a problem and machining took place to provide a thinner section for the ultrasound to pass through. High speed film measurements were required in order to capture film measurements from the ring. Higher speed data capture was used (not significantly high, however at only 8Hz). The technique for post processing was implemented in order to save data and removed CPU intensive processing from the software capturing the data.

Results obtained from the test rig (and failed tests due to thick films) seemed to indicate that the initial clearance between the piston ring and the cylinder was the dominating factor in film thickness as opposed to pressure and/or sliding speed. The results obtained, however, do show a relationship between sliding speed and film thickness. At lower pressures there is a noticeable increase in film thickness.

11.3.3. Prosthetic Hip Joint

Non invasive measurements of fluid film thickness in a metal on metal type hip joint have been made. Small piezo sensors were employed to measure the film thickness in the joint whilst it was articulated and loaded in a test rig. Very high speed measurements were employed to capture data (up to 10kHz), with data being written to disk at approximately 10MB/s. Much thinner films (in the range 0.2-8µm) were measured than in the previous applications. The results were compared friction measurement and show a correlation between thinner films and higher friction coefficients. Results were compared to predicted film thicknesses in the literature. There was agreement between the published predicted films and the films measured. However, the results were also compared with a FEM computational model, but disagreed considerably. This disagreement between experiment and theory was shown to be feasible when the waviness measurements were considered.

References:

Abdel-Latif, L. A., Peeken, A., and Benner, J. (1985). "Thermodynamic analysis of thrust-bearing with circular pads running on bubbly oil." Transactions of the ASME. Journal of Tribology. **107**: 527-37.

Akihama, K., Fujikawa, T., and Hattori, Y. (1998). "Laser-induced fluorescence imaging of NO in a port-fuel-injected stratified-charge SI engine - correlations between NO formation region and stratified fuel distribution. " Proceedings of the 1998 SAE International Spring Fuels & Lubricants Meeting & Exposition, May 4-6 1998, Dearborn, MI, USA, SAE, Warrendale, PA, USA.

Allan, T. (1971). "The effect of deformation on the behaviour of hydrodynamic journal bearings." Tribology **4**(3): 164-165.

Amstutz, H. C., and Grigoris, P. (1996). "Metal on metal bearings in hip arthroplasty." Clinical Orthopaedics and related research. **329S**: S11-S34.

Amstutz, H.C., Grigoris, P., and Dorey, F.J., (1998). "Evolution and future of surface replacement of the hip." Journal of Orthopaedic Science. **3**(3): 169-186

An, Q., and Priest, M.(2001). "Study on the influences of bubbly oil on the cavitation erosion in journal bearings of engines." Jixie Gongcheng Xuebao/Chinese Journal of Mechanical Engineering. **4**: 378-380.

Applied Measurements Ltd. (2005). Accessed at http://www.lvdt.co.uk/pdf/AML-M.pdf on 2 June 2005.

Arakawa, T. (1983). "A study on the transmission and reflection of an ultrasonic beam at machined surfaces pressed against each other." Materials Evaluation. **41**: 714-719.

Astridge, K. G., and Longfield, M. D. (1967). "Capacitance measurement and oil film thickness in a large radius and ring machine." Proc. Inst. Mech. Eng. **182**: 89-96

Baba, Y., Taneichi, Y., Ishima, T., and Obokata, T. (2006). "Fundamental study on lubricant oil film behaviour by LIF and PIV." Trans. JSME. **72**(716): 1001-1006.

Bently, (2005). Bently Nevada. Accessed at http://www.bently.com/articles/ apnotes/an044.asp#fig2 on 02 June 2005.

Bolander, N. W., Steenwyk, B. D., Kumar, A.., and Sadeghi, F. (2004). "Film thickness and friction measurement of piston ring cylinder liner contact with corresponding modelling including mixed lubrication. " Proc. ICEF ASME 2004 fall technical conference, October 24-27, Long Beach, California USA. ICEF2004-903.

Booser, E.R., Ryman, F.D., and Linkinhoker, C.L. (1995) "Golden Oldies: Maximum temperature for Hydrodynamic Bearings under Steady Load." Lubrication Engineering. **51**(1): 61-68.

Butcher, A. E. (1967-68). "Developments in the measurement of oil-film thickness in dynamically loaded bearings." Proceedings of the Institution of Mechanical Engineers. **192**: 105-108.

Cameron, A. (1966). The principles of lubrication. London, Longmans.

Cameron, A., and Gohar, R. (1966). "Theoretical and experimental studies of the oil film in lubricated point contact." Proceedings of the Royal Society of London. **A291**: 520-536.

Cameron, R. (1967-68). "Measurement of oil film thickness between rolling discs by by a variable-magnetic-reluctance technique." Proceedings of the Institution of Mechanical Engineers. **182**: 59-61.

Chamniprasart, K., Al-Sharif, A., Rajagopal, A.R., and Szeri, A.Z. (1993). "Lubrication with binary mixtures: bubbly oil." Transaction of the ASME. Journal of Tribology. **115**: 253-60.

Chan, F.W., Bobyn, J.D., Medley, J.B., Krygier, J.J., and Tanzer, M. (1999). "The Otto Aufranc Award – Wear and lubrication of metal-on-metal hip implants." Clinical Orthopaedics & Related Research. **369**: 10-24.

Chu, P. S. Y., and Cameron, A. (1967). "Flow of electric current through lubricated contacts." ASLE Transactions. **10**: 226-234.

Chun, S. M., and Ha, D.H. (2001). "Study on mixing flow effects in a high-speed journal bearing." Tribology International. **34**(6): 397-405.

Chun, S. M. (2002). "A parametric study on bubbly lubrication of high-speed journal bearings." Tribology International. **35**(1): 1-13.

Chun, S. M. (2004). "Thermohydrodynamic lubrication analysis of high-speed journal bearing considering variable density and variable specific heat." Tribology International. **37**(5): 405-413.

Constantinescu, V. N. (1965). "Theory of turbulent lubrication." Proceedings of International Symposium on Lubrication and Wear, Univeristy of Houston, TX Berkeley, CA, USA. MrCurtnhan Publishing Co.

Constantinescu, V. N. (1965). "Basic relationships in turbulent lubrication and extension to include thermal effects." Transactions of the ASME. Journal of Lubrication Technology. **95**: 147-54.

Constantinescu, V. N., and Galetuse, S. (1974). "On the possibilities of improving the accuracy of the evaluation of inertia forces in laminar and turbulent films." Transactions of the ASME. Journal of Lubrication Technology. **96**(1): 69-79.

Constantinescu, V. N., Smith, R. N., and Galetuse, S. (1980). "Influence of inertia forces in film rupture in laminar and turbulent lubrication." ASLE Transactions **23**(1): 61-69.

Davies, A (Ed.). (1998). "Handbook of Condition Monitoring: Techniques and Methodology". Springer Press. P304. ISBN: 978-0-412-61320-3.

Dowson, D., McNie, C. M., and Goldsmith, A. A. J. (2000). "Direct experimental evidence of lubrication in a metal-on-metal total hip replacement tested in a joint simulator." Proc. Instn Mech. Engrs, Part C, Journal of Mechanical Engineering Science. **214**(C1): 75- 86.

Drinkwater, B. W., Dwyer-Joyce, R. S., and Cawley, P. (1994). "Study of the transmission of ultrasound across real rough solid-solid interfaces." Proceedings of the 1994 IEEE Ultrasonics Symposium. Part 2 (of 3), Nov 1-4 1994, Cannes, Fr, IEEE, Piscataway, NJ, USA.

Drinkwater, B. W., Dwyer-Joyce, R. S., and Cawley, P. (1996). "A study of interaction between ultrasound and a partially contacting solid-solid interface." Proceedings of the Royal Society of London. **452**: 2613-2628.

Drinkwater, B. W., Dwyer-Joyce, R. S., and Cawley, P. (1997). "Study of the transmission of ultrasound across solid-rubber interfaces." Journal of the Acoustical Society of America **101**(2): 970.

Dwyer-Joyce, R. S., Drinkwater, B.W., and Quinn, A.M. (2001). "The use of ultrasound in the investigation of rough surface interfaces." Journal of Tribology. **123**(1): 8- 16.

Dwyer-Joyce, R. S., Drinkwater, B. W., and Donohoe, C. J. (2002). "The measurement of lubricant-film thickness using ultrasound." Proceedings of the Royal Society of London. A 459: 957-976.

Dwyer-Joyce, R.S., Reddyhoff, T., and Drinkwater, B. (2003). "Operating Limits for Acoustic Measurement of Rolling Bearing Oil Film Thickness." STLE Tribology Transactions.47(3): 366-375.

Dwyer-Joyce, R.S., Harper, P., and Drinkwater, B. (2003). "A Method for the Measurement of Hydrodynamic Oil Films Using Ultrasonic Reflection." Tribology Letters. 17: 337-348.

Dwyer-Joyce, R.S., Green, D.A., Balakrishnan, S., Harper, P., Lewis, R., King, P., and Rahnejat, H. (2006). "The Measurement of Liner-Piston Skirt Oil Film Thickness by Ultrasonic Means." SAE Paper 2006-01-0648 (presented at the Society of Automotive Engineers International Congress, Detroit, April 4-6 2006), in SP 2013:127-132 (ISBN 13 978 076801 748 9), in press Transactions of the SAE.

Dyson, A. (1966). "Investigation of the discharge voltage method of measuring the thickness of oil films formed in disc machine under condition of elastohydrodynamic lubrication." Proceedings of the Institution of Mechanical Engineers. 181: 633-646.

El-Butch, A. M. A. (2002). "The effect of bubbly oil on the THD lubrication of tilting pad journal bearings subjected to rotating unbalance load." Meccanica 36(6): 717-729.

El-Sisi, S. I., and Shawki, G. S. A. (1960). "Measurement of oil-film thickness between disks by electrical conductivity." Trans. ASME J. Basic Eng. 82: 12–18

Ettles, C. M., Knox, R. T., Ferguson, J. H., and Horner, D. (2003). "Test results for PTFE-faced thrust pads, with direct comparison against Babbitt-faced pads and correlation with analysis." Trans. ASME. J Tribology. 125:814-823.

Filipczynski, L., Pawlowski, Z., Wher, J. (1966). "Ultrasonic Methods of Testing Materials." Butterworths, P1.

FLIR Systems, (2005). Accessed at http://www.flirthermography.com/ success/ ir_image/1096/industry _id/1001/ on 02 Jun. 2005.

Ford, R.A.J., and Ford, C.A. (1978). "Laser-based fluorescence techniques for measuring thin liquid films." Wear 51: 289-297.

Furey, M. J. (1961). "Metallic contact and friction between sliding surfaces." ASLE Transactions 4: 1-11.

Furuhama, S. and Sumi, T.A. (1961). "A Dynamic Theory of Piston-Ring Lubrication: Measureemnt of Oil Film Thickness." Bull. JSME, 4: 744-752.

Gardiner, D. J., Baird, E., Gorvin, A. C., and Marshall, W. E. (1984). "RAMAN spectra of fluids in elastohydrodynamics contacts." Proceedings of the 9th AIRAPT International High Pressure Conference. Part 2: Fluids, Engineering, and Safety., Albany, NY, USA, North-Holland, New York, NY, USA.

Garner, D.R. and Leopard, A.J. (2005). "Temperature Measurements in Fluid Film Bearings". Accessed at http://magnetic.waukbearing.com/download_library on 02 June 2005.

Ghosh, M. K., and Nagraj, A. (2004). "Rotordynamic characteristics of a multilobe hybrid journal bearing in turbulent lubrication." Proceedings of the Institution of Mechanical Engineers. 218: 61-67.

Glavatskikh, S.B., and Larrson, D. (2000). "Oil film thickness measurement by means of an optic lever technique." Lubrication Science. 13(1): 309-316.

Glavatskikh, S. B., Uusitalo, O., and Spohn, D. J. (2001). "Simultaneous monitoring of oil thickness and temperature in fluid film bearings." Tribology International. 34: 853-857.

Gohar, R., and Cameron, A. (1963). "Optical measurement of oil film thickness under elastohydrodynamic lubrication." Nature. 200: 458-459.

Goodman, M. A. (2004). "Condition-based Lubrication Using Ultrasound Technology:" NORIA Website. [online]. Available from: http://www.noria.com/learning_center/category_article.asp?articleid=535&relatedbookgroup=Lubrication. Accessed 24th March 2004.

Gustafson, R.E. (1967). "Behaviour of a pivoted-pad thrust bearing during start-up." Trans. ASME, Journal of Lubrication Technology: 134-142.

Hamilton, G. M., and Moore, S. L. (1967). "A modified gauge for investigating an elastohydrodynamic contact." Proc. Inst. Mech. Eng. 182: 251–257.

Hashimoto, H., and Wada, S. (1988). "Turbulent lubrication theory considering the surface roughness effects (1st report, modified turbulent lubrication equation)." Nippon Kikai Gakkai Ronbunshu, C Hen/Transactions of the Japan Society of Mechanical Engineers, Part C 54(508): 3056-3064.

Hayward, A. T. J. (1961). "The viscosity of bubbly oil." Fluid Report N0. 99. Glasgow, UK, National Engineering Lab.

Harker, R. G. And Hansen, J.S. (1985). "Rolling Element Bearing Monitoring Using High Gain Eddy Current Transducers." J. eng. gas turbine power. **107**(1): 160-164

Hidrovo, C. H., and Hart, D. P. (2001). "Emission reabsorption laser induced fluorescence (ERLIF) film thickness measurement." Ins. Phys., Meas. Sci and Tech. **12**: 467-477.

Hidrovo, C. H., and Hart, D. P. (2002). "2D thickness and temperature mapping of fluids by means of a two-dye laser induced fluorescence ratiometric scheme." Journal of Flow Visualization and Image Processing. **9**(2-3): 171-191.

Higgison, G. R., and Reed, S. (1967-68). "An optical method of measuring film thickness." Report 5, Proc. IMechE **182**: 56-58.

Hobel, M., and Haffner, K. (1999). "An on-line monitoring system for oil-film, pressure and temperature distributions in large-scale hydro-generator bearings." Measuring Science Technology. **10**: 393-402.

Hodgson, K., Dwyer-Joyce, R.S., and Drinkwater, B.W. (2000). "Ultrasound as an experimental tool for investigating engineering contacts." Tribologia- Finnish Journal of Tribology. **19**(4): 9-17.

Hohn, B-R., Michaelis, K., and Kopatsch, F. (2001). "Determination of film thickness, pressure and temperature in elastohydrodynamic lubrication in the past 20 years in Germany." Proc. Instn. Mech. Engrs., Part J. **215**:235-242.

Hopf, G., and Schuler, D. (1989). "Investigations on large turbine bearings working under transitional conditions between laminar and turbulent flow." Trans. ASME J Tribology. **111**: 628–634.

Horner, D. (2003). Personal communication between D. Horner, Michell Bearings Ltd and Phil Harper.

Hoult, D. P., and Takiguchi, M. (1991). "Calibration of the laser fluorescence technique compared with quantum theory." Tribology Transactions. **34**(3): 440-444.

Hoyt-Darchem, (2005). Accessed at http://www.hoyt-darchem.demon.co.uk/ babbitt.html on 14 June 2005.

Irani, K., Pekkari, M., and Angstrom, H-E. (1997). "Oil film thickness measurement in the middle main bearing of a six-cylinder supercharged 9 litre diesel engine using capacitive transducers." Wear. **207**: 29-33.

Johnston, G. J., Wayte, R., and Spikes, H.A. (1991). "Measurement and study of very thin lubricant films in concentrated contacts." Tribology Transactions. **34**(2): 187-194.

Jubault, I., Mansot, J.L., Vergne, P., and Mazuyer, D. (2002). "In-situ pressure measurements using Raman microspectroscopy in a rolling elastohydrodynamic contact." Journal of Tribology. 124(1): 114-120.

Kendall, K. and Tabor, D. (1971). "An ultrasonic study of the area of contact between stationary and sliding surfaces," Proc. R. Soc. Lond. A 323: 321-340.

Khonsari, M. M., Booser, E. R. (2001). "Applied Tribology: Bearing Design and Lubrication." Wiley-Interscience Publication. 225-228.

Kim, K. W., Tanaka, M. and Hori, Y. (1995). "An experimental study on the thermohydrodynamic lubrication of tilted pad thrust bearings." Japanese Journal of Tribology, 40(1):1-13.

Kino, G. S. (1987). "Acoustic Waves." Prentice-Hall. P197.

Kingsbury, Inc. (2005). Electrical Pitting of a Tilting Pad Journal Bearing. Accessed at http://www.kingsbury.com/pdfs/universe_brochure.pdf on 06/07/05

Kirk, M. T. (1962). "Hydrodynamic lubrication of 'Perspex'." Nature. 194: 965-966.

Kluber Lubrication (2004). "Protection lubricant supply as spray." http://www.manufacturingtalk.com/news/klu/klu123.html. Accessed 18th December 2007.

Krautkramer, J., and Krautkramer, H. (1975). "Ultrasonic testing of materials." New York, Springer-Verlag.

Krolikowski, J., and Szczepek, J. (1991). "Prediction of contact parameters using ultrasonic methods." Wear 148: 181-195.

Lane, T. B., and Hughes, J. R. (1952). "A study on oil film formation in gears by electrical resistance measurements." British Journal of Applied Physics. 3: 315.

Lansdown, A. R. (1996). "Lubrication and lubricatin selection: A pratical guide." London, Mechanical Engineering Publication (MEP).

Lee, B., C. (2003). Personal communication between B. C. Lee and Phil Harper.

Lee, C. K., Cochran, S., Abrar, A., Kirk, K. J., and Placido, F. (2004) "Thick aluminium nitride films deposited by room-temperature sputtering for ultrasonic applications." Ultrasonics 42: 485–490.

Liu, F., Jin, Z. M., Hirt, F., Rieker, C., Roberts, P., and Grigoris, P. (2006). "Transient elastohydrodynamic lubrication analysis of metal-on-metal hip implant under simulated walking conditions." Journal of Biomechanics. 39: 905-914.

Lux, J. P., and Hoult, D.P. (1991). "Lubricant film thickness measurements in a diesel engine piston ring zone." Lubrication Engineering. 47(5): 353-364.

MacConochie, I. O., and Cameron, A. (1960). "The measurement of oil film thickness in gear teeth." Transactions of the ASME. Journal of Basic Engineering. **82D**: 29-34.

Machine Design (2005). Accessed at http://www.machinedesign.com/ASP/strArticleID/56800/strSite/MDSite/viewSelectedArticle.asp on 14 June 2005.

Maday, C. J., (2002). "The Foundation of the Sommerfeld Transformation." Trans. ASME, Journal of Tribology. **124**: 645-646.

Mann, U. (2005). "Schmierfilmbildung in elastohydrodynamisch en Kontakten, Einfluß verschiedener Grundole und Viskositats-Index-Verbesserer." Dissertation, Technische Universitat, Munchen.

Martin, F.A. (1998). "Oil Flow in a Plain Steadily Loaded Journal Bearing: Realistic Predictions using Rapid Techniques." Proc IMechE, Part J, Journal of Engineering Tribology. **212**(4):413-425.

Mason, W., P. (1948). "Electromechanical Transducers and Wave Filters." Princeton, NJ:Van Nostrand.

McKellop, H., Park, S.H., Chiesa, R., Doorn, P., Lu, B., Normand, P., Grigoris, P., and Amstutz, H.. (1996). "In vivio wear of 3 types of metal on metal hip prostheses during 2 decades of use." Clinical Orthopaedics & Related Research. **329S**: 128-140.

Miettinen, J. (2000). "Condition Monitoring of Grease Lubricated Rolling Bearings by Acoustic Emission Measurements." Thesis submitted for the degree of Doctor of Technology, Tampere University of Technology. 6/11/00. Accessed at http://www.acutest.fi/docs/THESIS.PDF on 02 Jun. 2005.

Morando, L. E. (1996). "Technology Overview: Shock Pulse Method." Technology Showcase: Integrated Monitoring, Diagnostics and Failure Prevention. Proceedings of a Joint Conference, Mobile, Alabama, April 22-26, 1996. Accessed at http://handle.dtic.mil/100.2/ADP010177 on the 16/03/08.

MTI Inc. (2005). Accessed at http://www.mtiinstruments.com/gaging/products/microtrak-2.html on 02 Jun. 2005.

New, N. H. (1974). "Experimental comparison of flooded, directed, and inlet orifice type of lubrication for a tilting pad thrust bearing." Trans. ASME. Journal of Lubrication Technology. **96**: 22-27.

Ng, C. W., and Pan, C.H.T. (1965). "A linearized turbulent lubrication theory." Transactions of the ASME. Journal of Basic Engineering. **87**: 675-88.

Nieman, G., and Gartner, F. (1965). "Distribution of hydrodynamic pressure on counterformal line contacts." ASLE Transactions. 8: 235-249.

Panametrics (2006). "Ultrasonic Transducers Technical Notes". Technical Notes - Olympus NDT Inc., 48 Woerd Avenue, Waltham MA 02453, USA.

Pialucha, T. (1992). "The reflection coefficient from interface layers in NDT of adhesive joints. " Thesis submitted for the degree of doctor of Philosophy at Imperial College, London, UK. A copy of this thesis was accessed at http://www.imperial.ac.uk/ndt/public/publications/pdf/pialucha-1992-reflection-thesis.pdf on 08 June 2005.

Pialucha, T., and Cawley, P. (1994). "The detection of embedded layers using normal incidence ultrasound." Ultrasonics. 32: 431-440.

Poppinga, R. (1941). "Indication of lubricating film destruction by measurement of the electrical transmission resistance between piston ring and cylinder." Dtsch. Kraftf.-Forsch., Ht. 54, Berlin; VDI-Verlag.

Povey, M. J. W. (1997). "Ultrasonic technique for fluid characterization." San Diego, Academic Press.

Rapposelli, E., Falorni, R., and d'Agostino, L. (2002). "Two-phase flow and inertial effects on the rotordynamic forces in whirling journal bearings." Proceedings of the 2002 ASME Joint U.S.-European Fluids Engineering Conference, Jul 14-18 2002, Montreal, Que., United States, American Society of Mechanical Engineers.

Raimondi, A.A. and Boyd, J. (1958) "A solution for the finite journal bearing and its application to analysis and design –I, -II, and -III." ASLE Trans. 1(1), I: 159-174, II: 175-193, III: 194-209.

Read, L.J., and Flack, R.D. (1987). "Temperature, pressure and film thickness measurements for an offset half bearing." Wear 117:197-210.

Reddyhoff, T. (2006). "Ultrasonic Measurement Techniques for Lubricant Films." PhD Thesis, University of Sheffield, Department of Mechanical Engineering.

Richardson, D. E., and Borman, G.L. (1991). "Using fiber optics and laser fluorescence for measuring thin oil films with application to engines". International Fuels and Lubricants Meeting and Exposition, Oct 7-10 1991, Toronto, Ontario, Canada, Published by SAE, Warrendale, PA, USA.

Safar, Z., and Szeri, A. Z. (1974). "Thermodynamic lubrication in laminar and turbulent regimes." Transaction of the ASME. Journal of Lubrication Technology 96: 48-57.

Sartorius, (2005). http://www.sartorius.com/index.php?id=851. Accessed on 02 Jun. 2005.

Sanda, S., Murakami, M., Noda, T., and Konomi, T. (1997). "Analysis of lubrication of a piston ring package." Trans. JSME. 40(3):478-486.

Scruby, C.B. (1987). "Instrument Science and Technology. An Introduction to Acoustic Emission." Journal of Physics E, Scientific Instruments. 20(8): 946-953.

Shaw, B. T., Hoult, D. P., and Wong, V.W. (1992). "Development of engine lubricant film thickness diagnostics using fiber optics and laser fluorescence. " International Congress and Exposition, Feb 24-28 1992, Detroit, MI, USA, Publ by SAE, Warrendale, PA, USA.

Sherrington, I., and Smith, E. H. (1985). "Experimental methods for measuring the oil film thickness between the piston rings and cylinder wall of internal combustion engines." Trib. Int. 18: 315 - 320.

Silk, M. G. (1984). "Ultrasonic transducers for nondestructive testing. " Bristol, Hilger.

Siripongse, C., Rogers, P.R., and Cameron, A. (1958). "Thin film lubrication." Lubrication Engineering. 186: 146-147.

Sjödin U. I. and Olofsson U. L-O., (2003), "Initial sliding wear on piston rings in a hydraulic motor." Wear. 254: 1208-1215.

Sjödin U. I., and Olofsson U. L-O. (2003). "Experimental study of wear interaction between piston ring and piston groove in a radial piston hydraulic motor." Metrology and Properties of Engineering Surfaces, Halmstad, Sweden Sept 10-11.

Skytte af Sätra, U. (2005). "Wear of piston rings in hydrostatic transmissions." http://urn.kb.se/resolve?urn=urn:nbn:se:kth:diva-432 (2008-01-29)

Smart, A. E., and Ford, R. A. J. (1974). "Measurement of thin liquid films by a fluorescence technique." Wear. 29: 41-47.

Smith, E. H. (1980). "The influence of surface tension on bearings lubricated with bubbly liquids." Trans.ASME. Journal of Lubrication Technology. 102: 91-6.

Smith, S. L., Dowson, D. and Goldsmith, A. A. J. (2001). "The effect of diametral clearance, motion and loading cycles upon lubrication of metal-on-metal total hip replacements." Proc Instn Mech Engrs, Part C. 15: 1-5.

Sommerfeld, A. (1904). "Zur Hdrodynamischen Theorie der Schmiermittel-Reibung." Z. Math. Physik. 50: 97-155.

Sommerfeld, A. (1942). "Mechanics (Translated from 4th German edition by Martin O. Stern).", Academic Press.

Spikes, H. A. (1999). "Thin films in elastohydrodynamic lubrication: The contribution of experiment." Proceedings of the Institution of Mechanical Engineers. **213**: 335-352.

Tallian, T. E., Mc Cool, J.J., and Sibley, L.B. (1965). "Partial hydrodynamic lubrication in rolling contact." Proceedings of Elastohydrodynamic Lubrication Conference,, Leeds, England, 21 September, 1965.

Tanaka, M., Hori, Y. and Ebinume, R. (1985). "Measurement of the film thickness and temperature profiles in a tilting pad thrust bearing." Proc. JSLE International Conference, Tokyo, Japan: 553-558.

Tattersall, H. G. (1973). "The ultrasonic pulse-echo technique as applied to adhesion testing." Journal of Applied Physics. **6**: 819-832.

Taylor, C. M. (1969-70). "Turbulent lubrication theory applied to fluid film bearing desing." Proceedings of the Institution of Mechanical Engineers. **184**: 40-47.

Tonnensen, J., and Hansen, P.K. (1981). "Some experiments on the steady state characteristics of a cylindrical fluid film bearing considering thermal effects." ASME Journal of Lubrication Technology. **103**:107-114.

Udofia, I.J., and Jin, Z.M. (2003). "Elastohydrodynamic Lubrication analysis of metal-on-metal hip-resurfacing prostheses." Journal of Biomechanics. **36**: 537-544.

Wakuri, Y., Ono, S., Soejima, M., and Masuda, K. (1981). "Oil-film Behaviour of Reciprocating Slider with Circular Profile (Optical Measurement of Oil-film Separation Boundary). " Bulletin of JSME. **24**(194):1462-1469.

Wakuri, Y., Hamatake, T., Soejima, M., and Kitahara. (1993). "Lubrication of Piston Ring Pack." Trans. JSME. **59**(561):1504-1511.

Walker, P.S., and Gold, B. L. (1971). "The tribology (friction, lubrication and wear) of all-metal artificial hip joints." Wear. **17**: 285-299

Wilcock, D. F. (1950). "Turbulence in high speed journal bearing." Transactions of the ASME. **72**: 852-34.

Wilcock, D. F., and Pinkus, O. (1984). "Effects of turbulence and viscosity variation on the dynamic coefficients of fluid film journal bearings." Proceedings of the ASME/ASLE Joint Lubrication Conference., San Diego, CA, USA, ASME, New York, NY, USA.

William, J. A. (1994). "Engineering tribology." New York, Oxford University Press.

Willis, T., and Seth, B. (1975). "Gap geometry measurements in oil-filled gaps using laser diffraction techniques." ASLE Proceedings 1975, for 30th ASLE Annual Meeting, May 5-8 1975, Atlanta, Ga.

Wittig, S., Glahn, A., and Himmelsbach, J. (1994). "Influence of high rotational speeds on heat transfer and oil film thickness in aero-engine bearing chambers." Transactions of the ASME. Journal of Engineering for Gas Turbines and Power 116(2): 395-401.

Zhang, J., Drinkwater, B., W., and Dwyer-Joyce, R. S. (2007). "Ultrasonic oil-film thickness measurement: An angular spectrum approach to assess performance limits." Journal of the Acoustical Society of America 121(5) : 2612-2620.

Appendix 1:

List of Papers

This is a list of papers that have been published by the author on the measurement of film thicknesses using ultrasonic reflection.

Papers Submitted

[1]   Reddyhoff, T., Dwyer-Joyce, R.S., and Harper, P., (2006) '*A New Approach for the Measurement of Film Thickness in Liquid Face Seals*', submitted to Tribology Transactions.

Papers in Print

[2]   Reddyhoff, T., Dwyer-Joyce, R.S., and Harper, P., (2006), '*Ultrasonic Measurement of Film Thickness in Mechanical Seals*', Sealing Technology, Volume 2006, Issue 7, July 2006, pp. 7-11.

[3]   Dwyer-Joyce, R.S., Green, D.A., Balakrishnan, S., Harper, P., Lewis, R., King, P., Rahnejat, H., 2006, '*The Measurement of Liner-Piston Skirt Oil Film Thickness by Ultrasonic Means*', SAE Paper 2006-01-0648 (presented at the Society of Automotive Engineers International Congress, Detroit, April 4-6 2006), in SP 2013, pp127-132 (ISBN 13 978 076801 748 9), in press Transactions of the SAE.

[4]   Dwyer-Joyce, R.S., Harper, P., and Drinkwater, B., (2004), '*A Method for the Measurement of Hydrodynamic Oil Films Using Ultrasonic Reflection*', Tribology Letters, Vol. 17, pp. 337-348.

[5]   P. Harper, R.S. Dwyer-Joyce, U. Sjödin, U. Olofsson, (2005) '*Evaluation of an Ultrasonic Method for Measurement of Oil Film Thickness in a Hydraulic Motor Piston Ring*',

Proceedings of the 31th Leeds-Lyon Symposium on Tribology, "Life Cycle Tribology", eds. D.Dowson, M.Priest, G.Dalmaz, A.A.Lubrecht, Elsevier Tribology Series No. 48, pp. 305-312, (ISBN 0-444-51687-5).

[6]   Harper, P., Dwyer-Joyce, R. S., (2004), *Measuring Oil Film Thickness with Ultrasound*, Lubrication Excellence Conference Proceedings, March 23rd-25th, pp 425-428.

[7]   Drinkwater, B. W., Dwyer-Joyce, R. S., and Harper, P., (2004), *On-Line Measurement of Lubricant Film Thickness Using Ultrasonic Reflection Coefficients*, AIP Conference Proceedings, February 26, Volume 700, Issue 1, pp. 984-991

[8]   Dwyer-Joyce, R.S., Harper, P., and Drinkwater, B., (2004), *Evaluation of an ultrasonic oil film measurement technique for PTFE faced thrust pad bearings*, Proceedings of the ASME/STLE International Joint Tribology Conference, IJTC 2004, 2004, p 697-710.

[9]   Harper, P., Hollingsworth, B., Dwyer-Joyce, R.S., and Drinkwater, B.W., (2004), *Journal Bearing Oil Film Measurement Using Ultrasonic Reflection*, Proceedings of the 29th Leeds-Lyon Symposium on Tribology, Elsevier Tribology Series No. 41, pp. 469-476, (ISBN 0-444-51243-8).

[10] Dwyer-Joyce, R.S., Harper, P., and Drinkwater, B., (2003), *Oil Film Measurement in PTFE Faced Thrust Pad Bearings for Hydrogenerator Applications*, Proc IMechE part A, Journal of Power & Energy, Vol. 220, pp. 619 – 628.
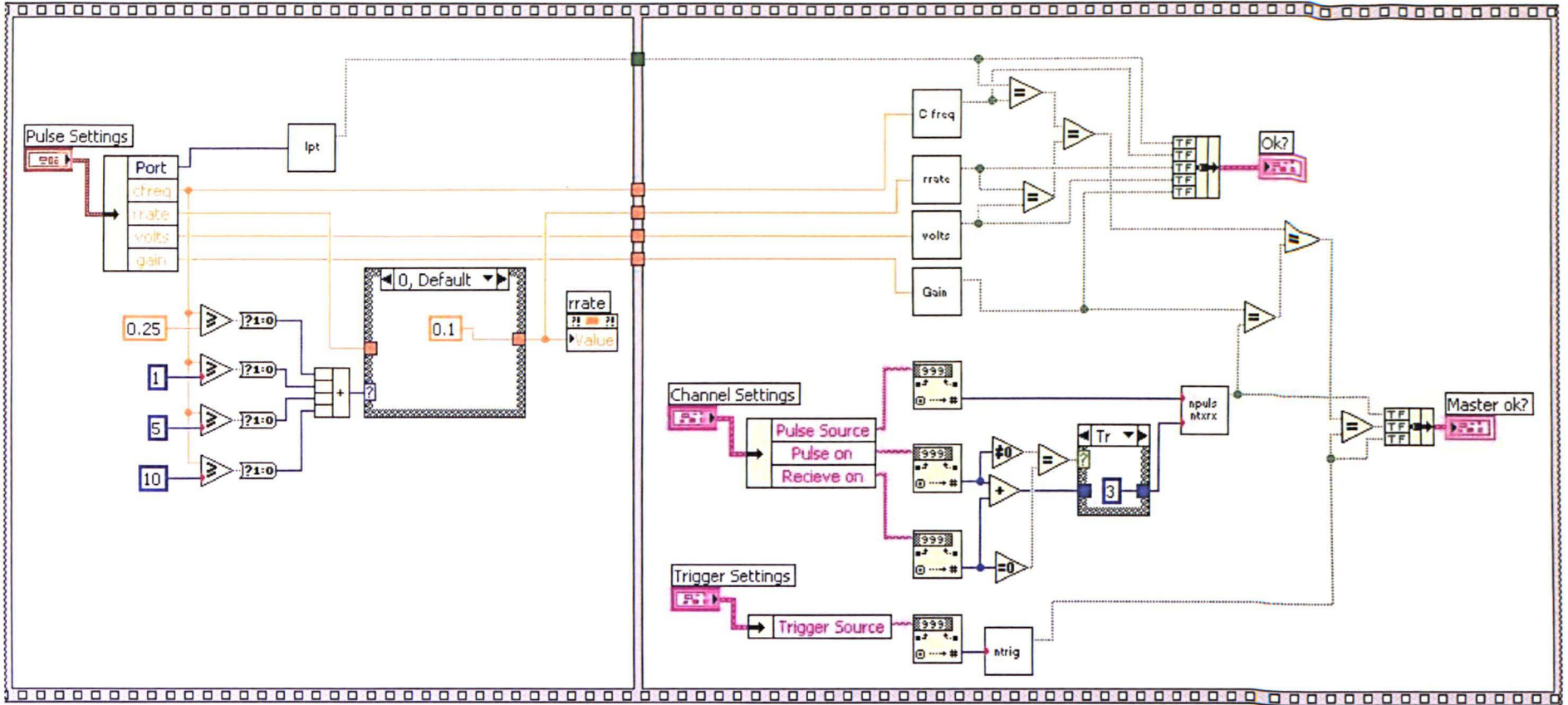
Appendix 2:
Tachometer Driver

The figure below shows a screen grab of the software for controlling the Laser
Tachometer over the serial RS232 port.
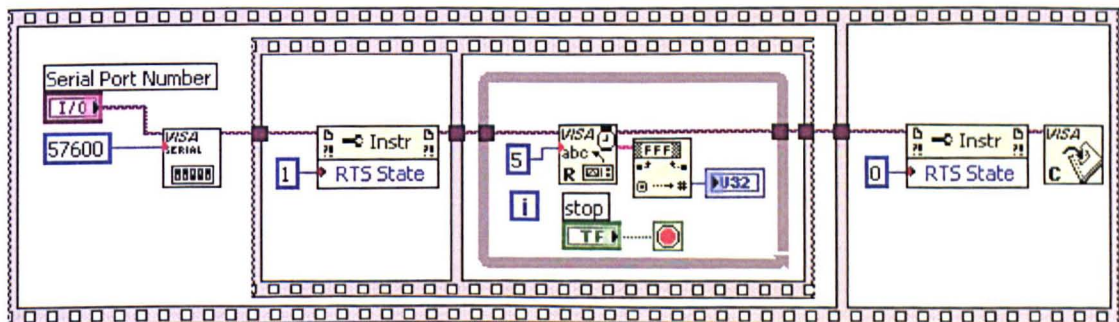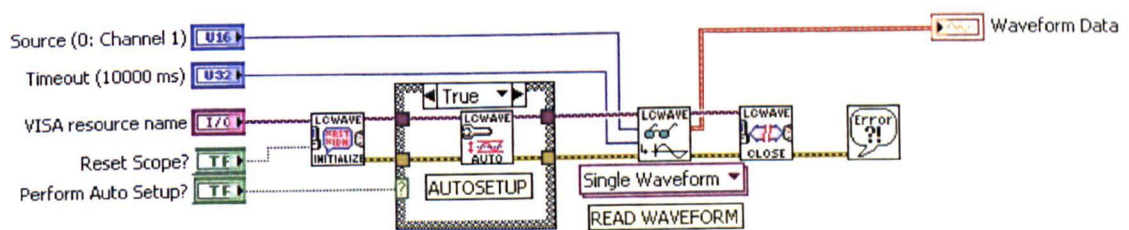
Appendix 3:
UPR Control Software

The following page shows a screen grab of the software for controlling the UPR via a dll across the parallel port.
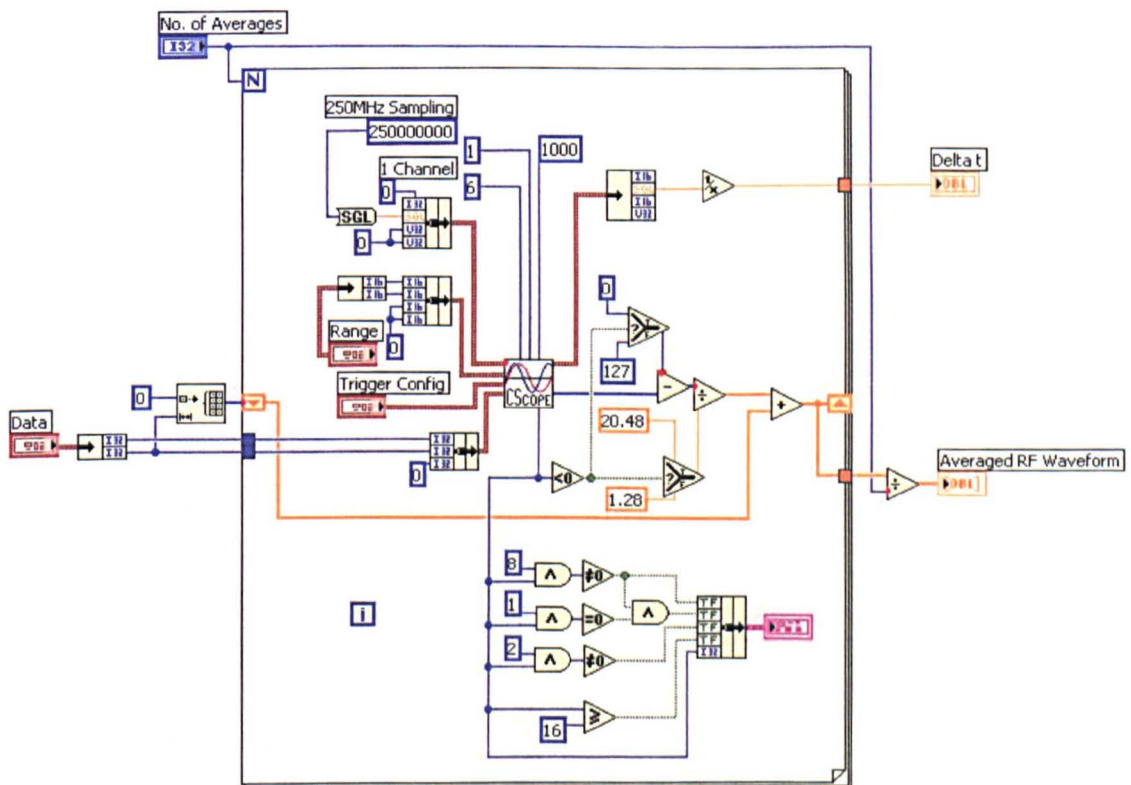
Appendix 4:
Oscilloscope Control Software

The figure below show a screen grab of the software for controlling and downloading data from the oscilloscope.

Appendix 5:
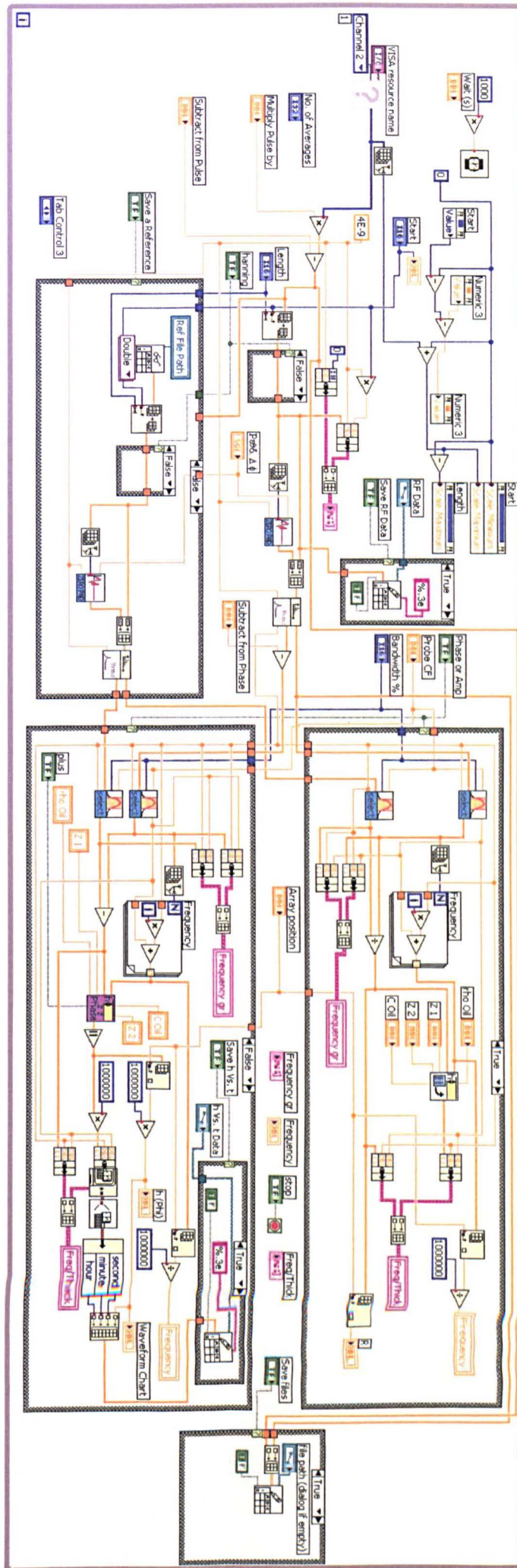
Gage Control Software

The figure below shows the software for controlling the Gage PCI card and acquiring data from it.

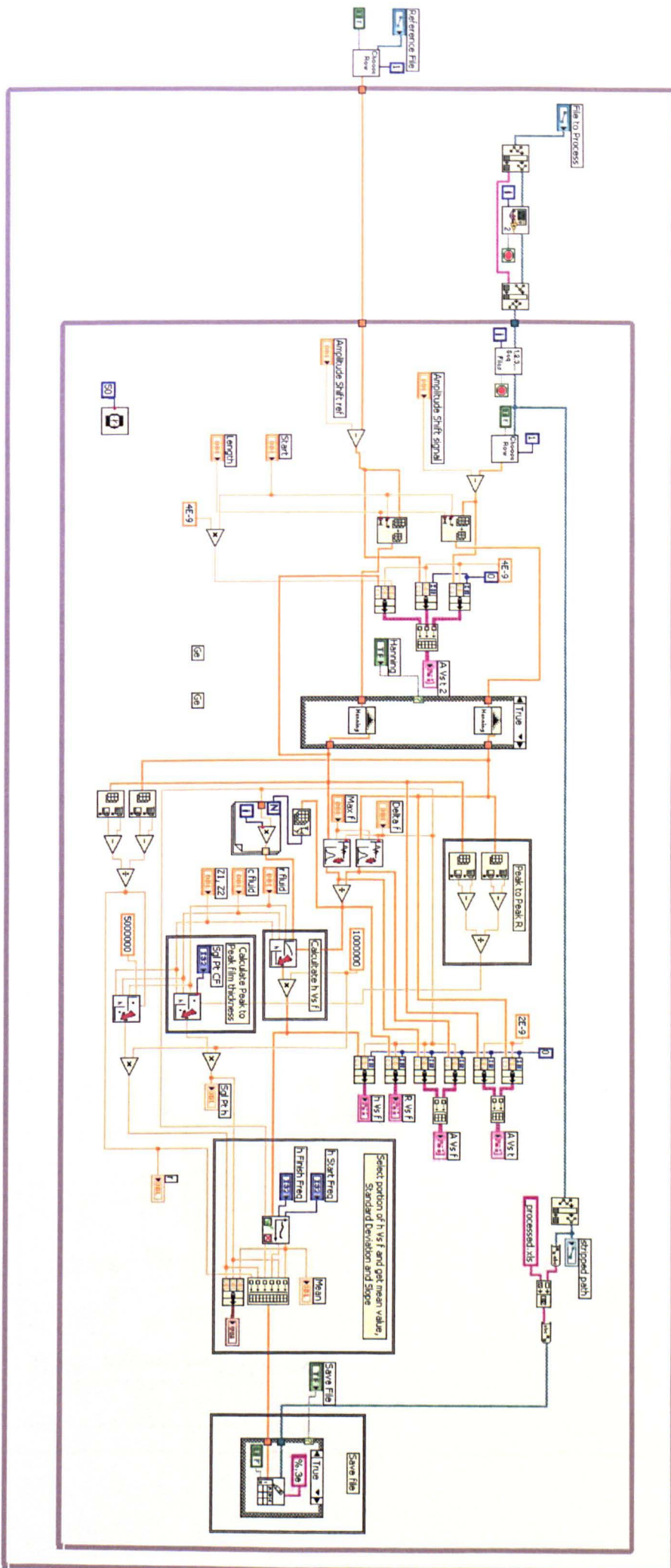# Appendix 6:

Online Film Thickness Software

The following page shows a screen grab of the online film thickness software. The waveform is captured from the oscilloscope and the film thickness calculated.

Appendix 7:

Post-Processing Film Thickness Software

The following page shows a screen grab of the automated post-processing data. The software is able to process all the files in a specified folder.

185

Appendix 8:
Film Thickness Modelling Software

This is a screen grab of the block diagram of the software for modelling the response of an ultrasonic wave to a thin embedded layer.